9950-720

DOE/JPL-955567-82/8
Distribution Category UC-63

PHASE II PROGRAM RESULTS PERIODIC REPORT SUPPLEMENT

on the

DESIGN, ANALYSIS, AND TEST VERIFICATION OF ADVANCED ENCAPSULATION SYSTEMS

For period ending

1 October 1981

Contract 955567

Prepared by:

Alec Garcia
Chuck Minning

Approved by:

Nick Mardesich
Group Manager
Product Development
Advanced Programs

SPECTROLAB, INC.
12500 Gladstone Avenue
Sylmar, California 91342

June 1982

The JPL Flat-Plate Solar Array Project is sponsored by the U.S. Department of Energy and forms part of the Solar Photovoltaic Conversion Program to initiate a major effort toward the development of low-cost solar arrays. This work was performed for the Jet Propulsion Laboratory, California Institute of Technology by agreement betseen NASA and DOE.

ACKNOWLEDGEMENT

The work presented in this report is the result of the joint effort of numerous individuals at both Spectrolab and Hughes Aircraft Company. Members of the team and their respective areas of technical responsibility were as follows:

- +R. T. Breen - Assembly of Thermal Test Apparatus Thermal, Thermal Test Supervisor
- +Dr. J. F. Coakley - Thermal, Optical Analysis
- +L. B. Duncan - Structural Analysis
- *A. Garcia III - Photovoltaic Consultant, Program Management
- +D. M. Gillaspy - Test Coordination and Performance, Design of Structural Deflection Test Fixture
- +R. H. Kiewert - Design of Structural Deflection Test Fixture
- +F. G. McKinney - Test Coordination
- +Dr. C. P. Minning - Electrical Analysis, Program Management
- *Dr. W. E. Taylor - Photovoltaic Consultant, Program Management
- +L. E. Vaughn - Strain Gage Selection, Structural Test Supervisor

* - Spectrolab

+ - Hughes Aircraft Company

PREFACE

This report documents the second phase of a three-phase program that is a joint effort by Spectrolab and Hughes Aircraft Company. In Phase 1 an analytical model was developed which enabled the prediction of performance of various encapsulation designs. Models relating to the thermal, optical, structural, and electrical performance were developed. Using this analytical method the most cost effective module design can be found.

The objective of the second phase was to verify the models by testing modules and coupons. The models may then be modified as necessary to bring predicted and empirically found results into agreement. Additionally, full-size modules of the most cost effective design will be built and put through the JPL qualification test sequence.

During the third phase Spectrolab will finalize the low cost design and deliver the design to JPL.

Phase two testing is reported in this document. Full size modules have not yet been built.

CONTENTS

CONTENTS (Continued)

CONTENTS (Concluded)

LIST OF ILLUSTRATIONS

LIST OF ILLUSTRATIONS (Concluded)

LIST OF TABLES

LIST OF TABLES (Concluded)

1.0 SUMMARY

The test data reported herein and the correlations of these data with the optical, electrical isolation, structural, and thermal models developed during Phase 1 of the program [3]* led to the following conclusions regarding analytical model verification and module performance:

1. Optical Test

   - The utility of the optical model has been verified. This model was used to predict cell electrical power output within 25 percent of the measured power output.
   - The optical model underpredicted cell power output for both xenon and tungsten illumination sources. This error was probably due to the assumption of a perfectly smooth surface for an etched cell. As a result, the reflectance at the cell/pottant interface was overestimated.
   - There was better agreement between test data and analytical prediction for the xenon source than for the tungsten source.
   - Agreement between test data and analytical predictions was best for AR-coated and/or texturized cells.

2. Electrical Isolation Test

   - The utility of the series capacitance model has been verified. This model was able to predict breakdown voltages between the maximum and minimum breakdown voltages measured during the test.
   - The model overpredicts the dependence of encapsulation system breakdown voltage on pottant thickness.
   - All electrical failures occurred at the edges of the simulated solar cells in the test specimens. No failures could be attributed to the presence of bubbles in the pottant.
   - Inclusion of Craneglas in the pottant slightly increases the electrical isolation capability of the encapsulation system.

3. Thermal Structural Test

   - Data from this test were of limited value due to instrumentation problems and failure to achieve steady-state conditions.
   - Strain attenuation in EVA was observed (as predicted) but quantitative correlation was not possible. EVA was a poor choice of pottant for verification of the analytical model. A limited retest is recommended with a pottant modulus of elasticity greater than 2×10^4 psi.

4. Structural Deflection Test

   - The utility of the structural deflection model has been verified. Deflections measured at the center of each module agreed to within 10 percent of the predicted deflections for all but the steel substrate module. Measured cell stresses agreed to within 10 percent of the predicted cell stresses for plain wood substrate modules.

* Numbers in brackets designate references at the end of this report.

- Measured cell stresses were approximately 50 percent lower than those predicted for both glass superstrate and steel substrate modules. The structural "membrane effect" in the module load-bearing member, which was not taken into account in the model, is thought to be responsible for these results. Further consultation with JPL structural analysts is recommended to confirm this hypothesis.
- No cells were cracked during performance of the test.
- Ribbed wood substrate modules require careful design to minimize stress concentrations at the rib ends. One way to overcome this stress concentration problem is to support the rib ends as well as the module edges.

5. Thermal Test

- The thermal model overpredicts cell temperature somewhat. This overprediction was due mainly to uncertainties in the air flow pattern around the test modules, uncertainties in the distribution of incident radiant energy flux in the plain of the modules, a suspected lateral temperature gradient in the glass front panel of the test set-up, and uncertainties in the assumed value of emissivity of the test chamber walls. Agreement between predictions and test data was best for those situations where the module had a high emissivity back cover.
- Cell temperature is not significantly affected by pottant thickness.
- The predicted trend of decreasing cell temperature with increasing module backside emissivity was confirmed.
- Insulation of the backsides of the test modules lead to cell temperature increases ranging from 4.3°C to 15°C.

2.0 INTRODUCTION

2.1 OVERVIEW

This report contains information on a series of tests performed in support of Spectrolab Letter Contract 79PMY263-6321/88774. These tests were part of a larger program concerned with the development of analytical tools for performing tradeoffs in the thermal, optical, structural, and electrical isolation design of encapsulation systems for flat-plate photovoltaic modules. The analytical methodology and computer programs were developed during Phase 1 of the program and are described in reference 3. Test verification of the analytical methodology was the objective of Phase 2 of the program and is the subject of this report.

The role of the encapsulation system in a photovoltaic module is to package, protect, and support the solar cells and electrical interconnects of the module. Construction elements of a typical encapsulation system for the accomplishment of these goals are illustrated in Figure 2-1. As might be expected, the design of encapsulation systems requires tradeoffs between conflicting design requirements. For example, structural requirements favor a thick layer of pottant between the front cover and cells of a glass superstrate module; on the other hand, optical and thermal requirements favor a thin pottant layer for this type of module. In the past, design tradeoffs to satisfy these requirements have been carried out in a cut-and-dry fashion with resultant heavy investments in time and money. Development of analytical tools for the rational design of these construction elements was the objective of Phase 1 of the program.

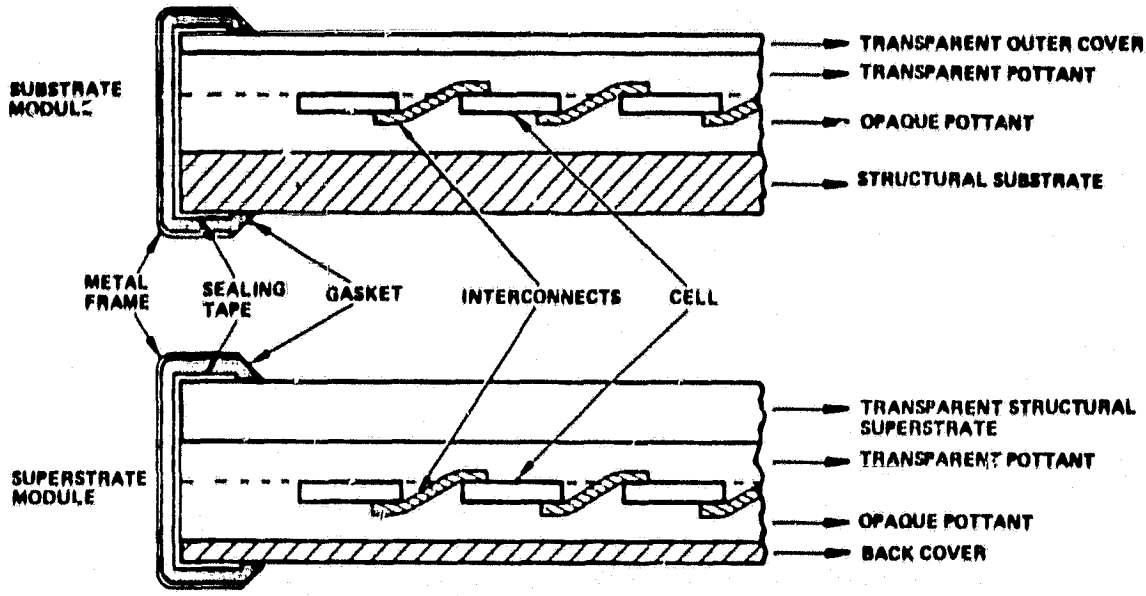

Figure 2-1. Construction elements of photovoltaic modules.

Two types of modules were investigated during both phases of the program:

1. A superstrate module in which structural support is provided by a transparent load-bearing member on the sun side of the cells
2. A substrate module in which structural support is provided by an opaque backing material behind (i.e. on the anti-sun side) the cells.

The arrangement of construction elements for each module type is illustrated in Figure 2-1. Structural support for the cells is provided by the structural substrate in a substrate module and by the transparent superstrate in a superstrate module. The pottant protects the cells and the cell interconnects from the environment. The transparent superstrate in a superstrate module and the transparent front cover in a substrate module help protect the pottant by screening out some of the ultraviolet radiation in the solar spectrum. The superstrate and front cover also provide protection against soiling and abrasive action by wind-blown sand and dirt. Sealing tape around the edges of the module prevents moisture infiltration into the pottant. The gasket cushions the module against shock due to rough handling and also permits the module to expand and contract during the daily heating and cooling cycle. The back cover on a superstrate module protects the pottant from the environment and, in certain cases, enhances module cooling. The edge frame is used to attach the module to an array. Placement of a module in a typical array field is illustrated in Figure 2-2.

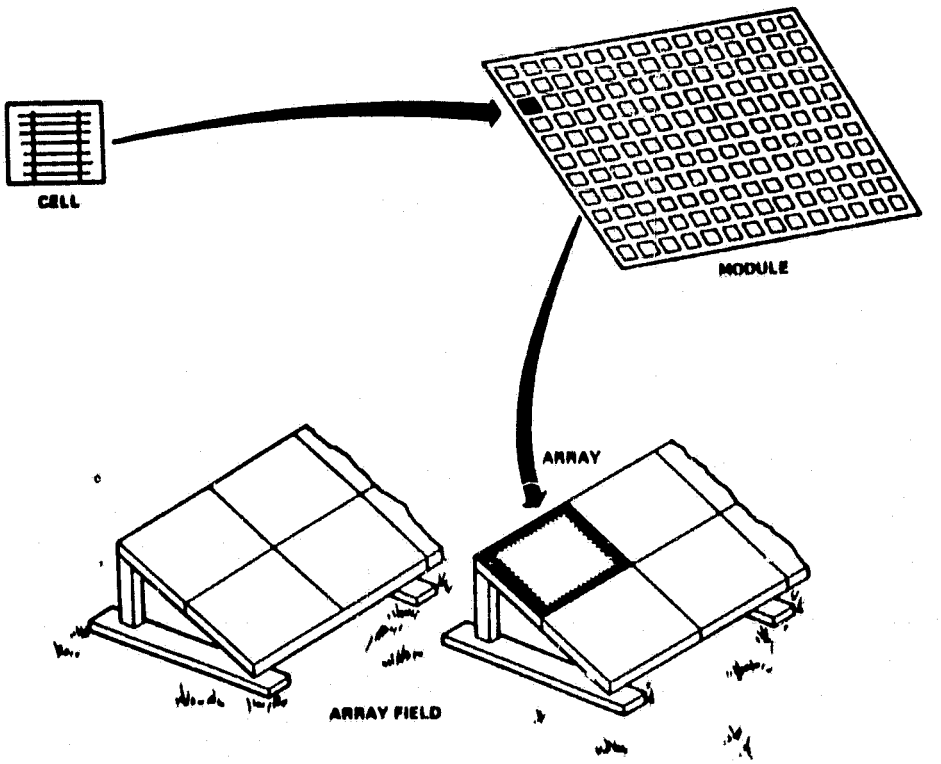

Figure 2-2. Module placement in an array field.

The analyses performed during Phase 1 were for a 1.2-meter square module using 10.2 cm (4-inch) square, 0.254 mm (0.010 inch) thick cells spaced 1.3 mm apart, as shown in Figure 2-3. Most of the analyses were performed for environments specified in references 7 and 8 (i.e. LSA module qualification requirements). For example, sizing of the structural support member of a

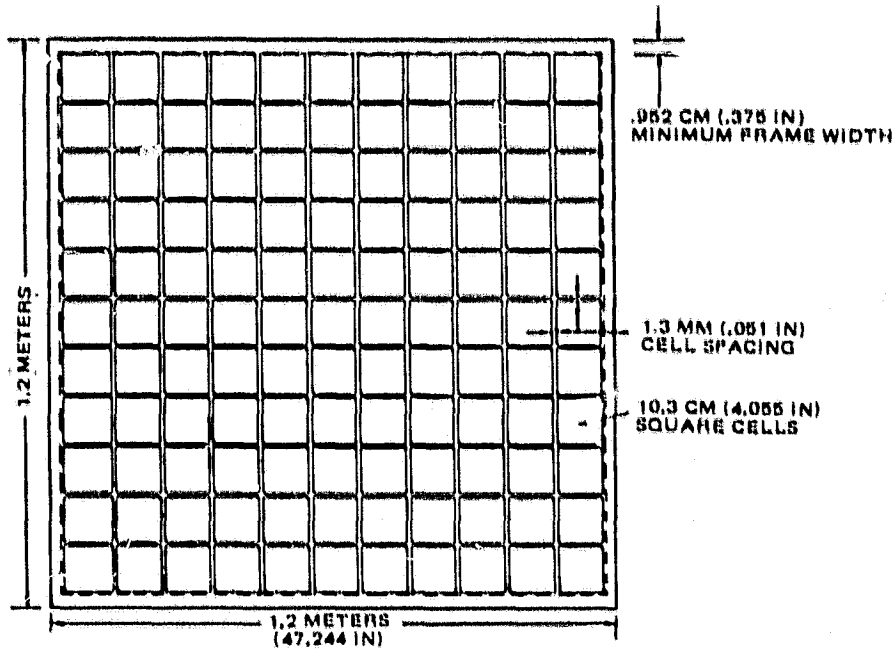

Figure 2-3. Plan view of module showing cell arrangement.

module was determined for a uniform, normal pressure load of 50 psf. This load corresponds to the pressure difference generated between the front and back surface of a module by a 100 mph wind. Thermal and optical calculations were performed for a wind velocity of 1 meter/sec parallel to the ground and for a module tilt (relative to the local horizontal) of 37 degrees.

2.2 SCOPE

Originally, Phase 2 was to consist of three distinct segments, as outlined in the Phase 2 Test Plan [9]: (1) verification tests, (2) overstress tests, and (3) qualification tests. The qualification tests were to be performed on full-scale (1.2 meter × 1.2 meter) modules with a full complement of 121 electrically-connected photovoltaic cells. Smaller specimens were to be used for the verification and overstress tests. In June 1981, JPL assumed responsibility for performance of the qualification tests; hence material on qualification tests is not contained in this report.

2.2.1 Verification Test

The goal of the verification tests was to establish confidence in the analytical design methodologies developed during Phase 1 and to modify the analytical models wherever test data warranted such action. These tests were performed on specimens designed to permit the experimental measurement of important parameters such as cell temperature, cell stress, stress in the load-bearing member of a module, and electrical breakdown voltage. For these tests, environmental conditions were chosen to approximate, as closely as possible, the environmental conditions analyzed in Phase 1.

Five separate and independent tests comprised the verification test segment of the test plan. These tests were

1. Optical test
2. Electrical isolation test
3. Thermal structural test
4. Structural deflection test
5. Thermal test

Details of each test and data analyses are presented in Sections 3 through 7 of this report.

2.2.2 Overstress Test

Overstress tests are those tests where the test specimens are subjected to an environment in excess of that for which the encapsulation system was designed. The purpose of these tests was to precipitate failures in the test specimens that ordinarily would not appear during short-term qualification tests but might occur during long-time field exposure.

In this program, overstress tests were treated as an extension of the thermal structural and structural deflection verification tests. In the thermal structural tests, the appropriate specimens were subjected to environment temperatures below the glass transition temperature of the pottant. In the structural deflection tests, the appropriate specimens were subjected to an increasing normal pressure load until catastrophic failure occurred or the load capacity of the test apparatus was reached.

2.3 TEST CRITERIA

This test program did not require a pass/fail criterion. However, from past experience and in the light of unknown factors described in Section 7 of reference 3, the following margins apply when comparing test data with pretest predictions:

Data Item	Criteria
Cell Temperature	±10 percent of predicted value
Module Deflection	±10 percent of predicted value
Stress	±25 percent of predicted value
Power Output (Optical, Thermal Tests)	±25 percent of predicted value

2.4 RESPONSIBLE ENGINEERING AUTHORITY

Each test was performed under the direction of a responsible engineering authority (REA), who was responsible for all pretest preparations (including inputs to the test plan), pretest predictions, test monitoring, and post-test analysis. The REAs were:

Test	REA
Optical	J.F. Coakley (Hughes)
Electrical Isolation	A. Garcia (Spectrolab) C.P. Minning (Hughes)
Structural Deflection	L.B. Duncan (Hughes)
Thermal Structural	L.B. Duncan (Hughes)
Thermal	J.F. Coakley (Hughes)

2.5 TEST LOCATIONS

The verification and overstress tests were performed at the following locations:

Test	Location
Optical	Spectrolab (Foothill Facility) 12865 Foothill Blvd. Sylmar, CA 91342
Electrical Isolation	Spectrolab (Foothill Facility)
Thermal Structural	Hughes Aircraft Co. (Rodeo Rd. Facility) 5901 Rodeo Blvd. Culver City, CA 90230
Structural Deflection	Hughes Aircraft Co. (Rodeo Rd. Facility)
Thermal	Hughes Aircraft Co. Bldg. R2 (Bally Chamber) 2060 E. Imperial Hwy. El Segundo, CA 90245

3.0 OPTICAL TEST

3.1 TEST OBJECTIVE

The objective of the optical verification test was to validate the optical analysis methodology developed during Phase 1 of the program. The verification process consisted of measuring the electrical power produced by several encapsulated cells and then comparing these measurements with the electric power outputs predicted (by the optical model) for these cells.

3.2 TEST SPECIMENS

Thirteen two-cell coupons, as designated in Table 3-1, were used as test specimens in the optical tests. The geometric layouts and dimensions of these specimens are illustrated in Figure 3-1. The total thickness of each specimen was measured at several locations inside the perimeter of each cell, and test predictions were based on the average of these measured thicknesses. The back side of each cell was left bare so that good thermal contact could be made between the cell and the holding fixture. Test coupons OC-6 through OC-13 were fabricated in the configurations shown in Figures 3-1f through 3-1m; each cell in these coupons was then cut out (before testing) to eliminate excess encapsulant around the edges of the cells.

This series of coupons was selected to verify the accuracy of the model as well as the ability of the model to predict trends (i.e., changes in cell power output resulting from changes in the optical parameters of the encapsulation system). These trends can be evaluated by comparing the electrical outputs measured for each coupon. Such trends include:

1. Relative performance of single crystal silicon and polycrystalline silicon cells
2. Effect of glass iron content for glass superstrate modules
3. Effect of Craneglas in pottant on cell electrical output
4. Effect of stipple-out versus stipple-in configuration for glass superstrate modules
5. Relative performance of Korad and Tedlar as front cover materials for substrate modules
6. Relative performance of texurized and non-texturized cells
7. Effect of AR-coating on electrical output of texturized cells
8. Effect of pottant thickness on cell electrical output
9. Relative performance of AR-coated and non AR-coated cells.

3.3 TEST SET-UP

Placement of a test coupon in the holding fixture of an illumination source is shown in Figure 3-2. An actual coupon in the fixture is shown in Figure 3-3. Both tungsten and xenon illumination sources were used in these tests, and the holding fixtures were slightly different for these two pieces of equipment.

Nameplate data for the equipment used in this test are found in Appendix A.

TABLE 3–1. OPTICAL TEST SPECIMENS

Coupon Number	OC-1	OC-2	OC-3	OC-4	OC-5	OC-6	OC-7	OC-8	OC-9	OC-10	OC-11	OC-12	OC-13
Front Cover	Low-Iron Glass Stipple-In	Low-Iron Glass Stipple-In	High-Iron Glass	Low-Iron Glass Stipple-In	Low-Iron Glass Stipple-Out	Korad	Tedlar	Tedlar	Tedlar	Tedlar	Tedlar	Tedlar	Tedlar
Pottant*	EVA	EVA	EVA	EVA/CG	EVA/CG	EVA	EVA	EVA/CG	EVA/CG	EVA/CG	EVA	EVA	EVA/CG
Pottant Thickness	11 mil	6 mil	14 mil	13 mil	22 mil	18 mil	18 mil	19 mil	18 mil	18 mil	55 mil	17 mil	21 mil
Cell Type**	SC-2 in Sq	PC-2 in X 4 in	SC-2 in Sq	SC-2 in Sq	SC-2 in Sq	SC-2 in Sq	SC-2 in Sq	SC-2 in Sq	SC-2 in Sq (AR)	SC-2 in D (Text)	SC-2 in Sq	SC-2 in Sq (AR)	SC-2 in D (AR Text)

*EVA - Ethylene vinyl acetate
EVA/CG - Ethyle vinyl acetate with Cracoglas
**SC - Single crystal silicon
PC - Polycrystalline silicon
AR - Cell with antireflection coating
Text - Cell with texturized surface

ORIGINAL PAGE IS
OF POOR QUALITY

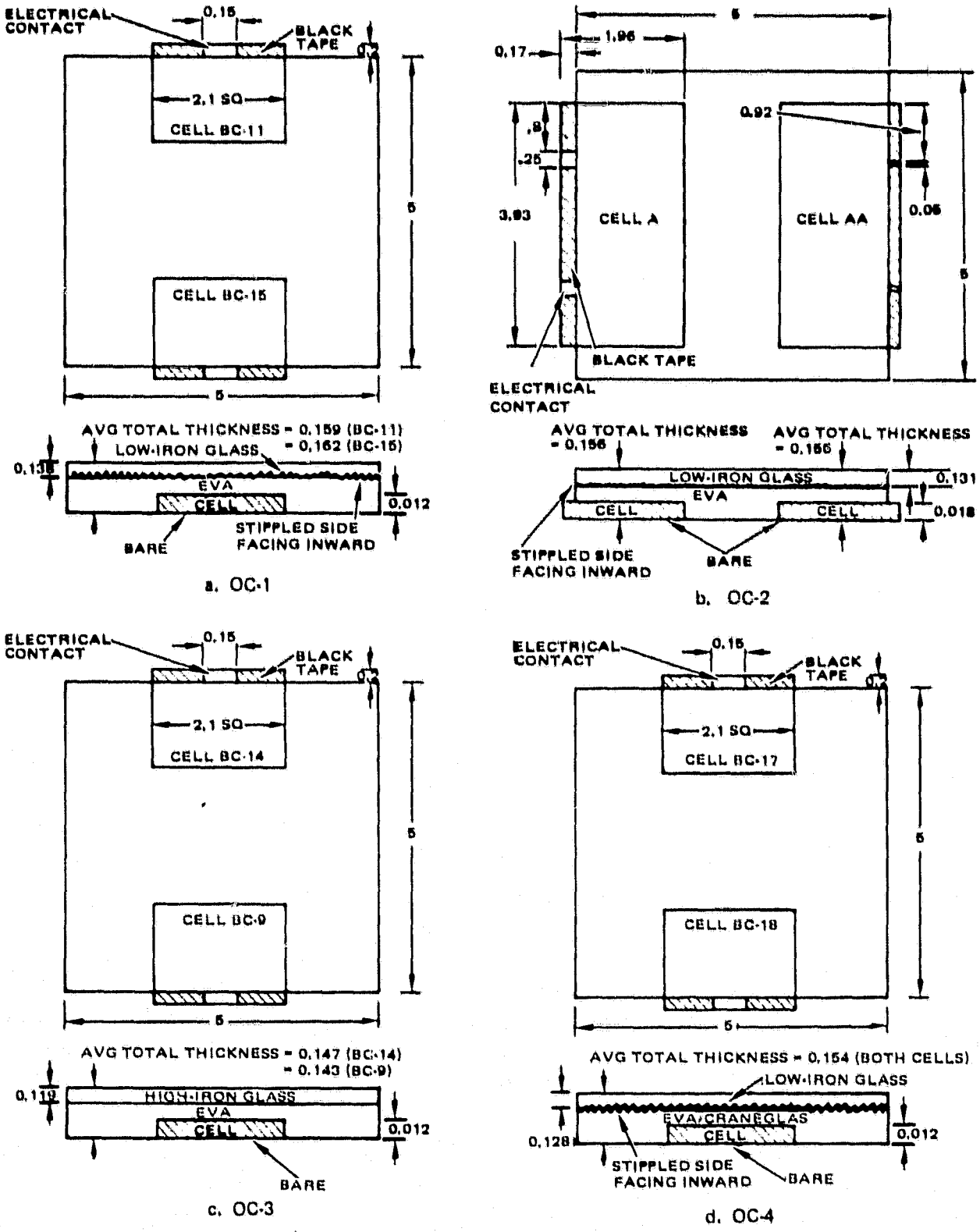

Figure 3-1. Optical test coupons; all dimensions in inches.

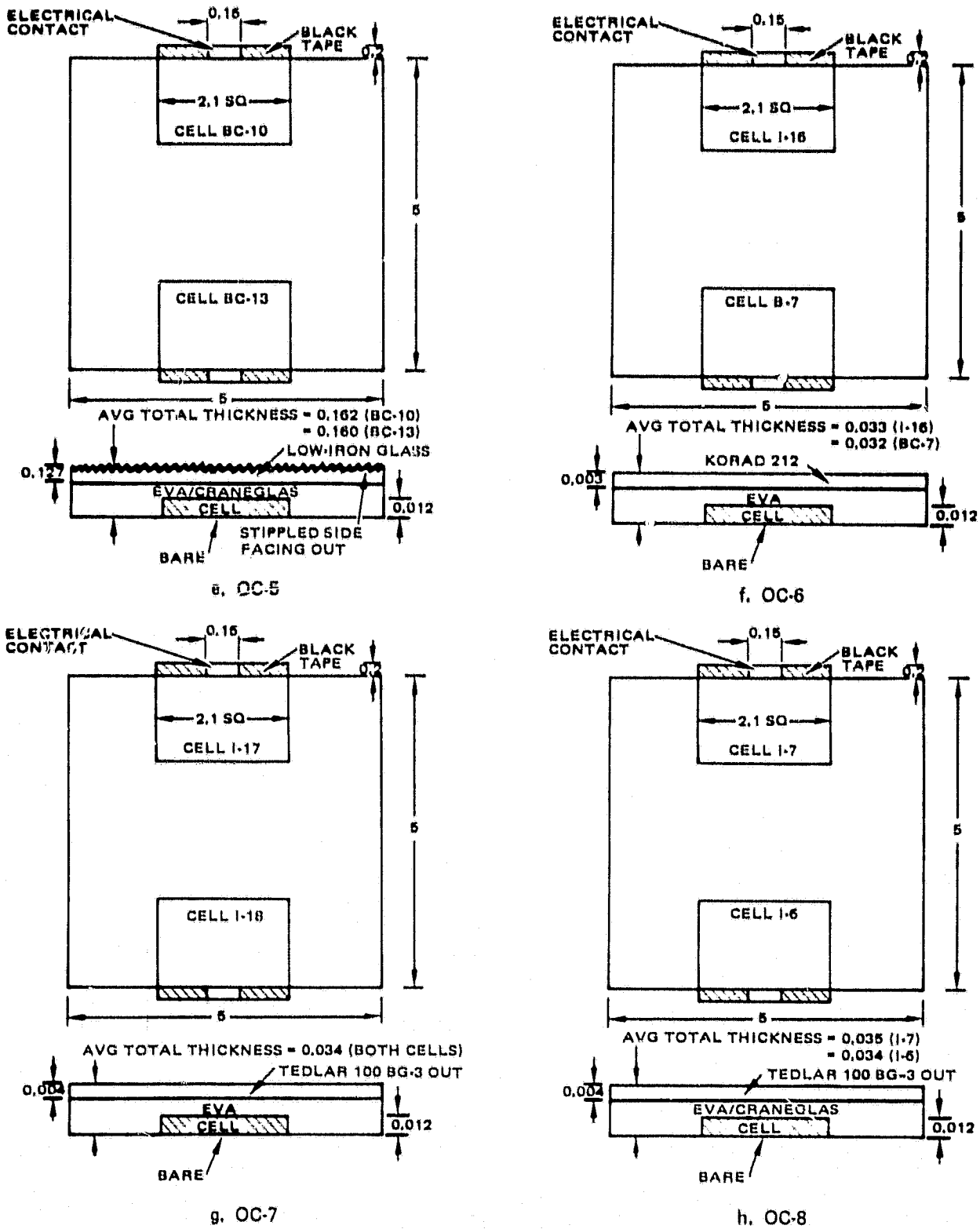

Figure 3-1 (continued). Optical test coupons.

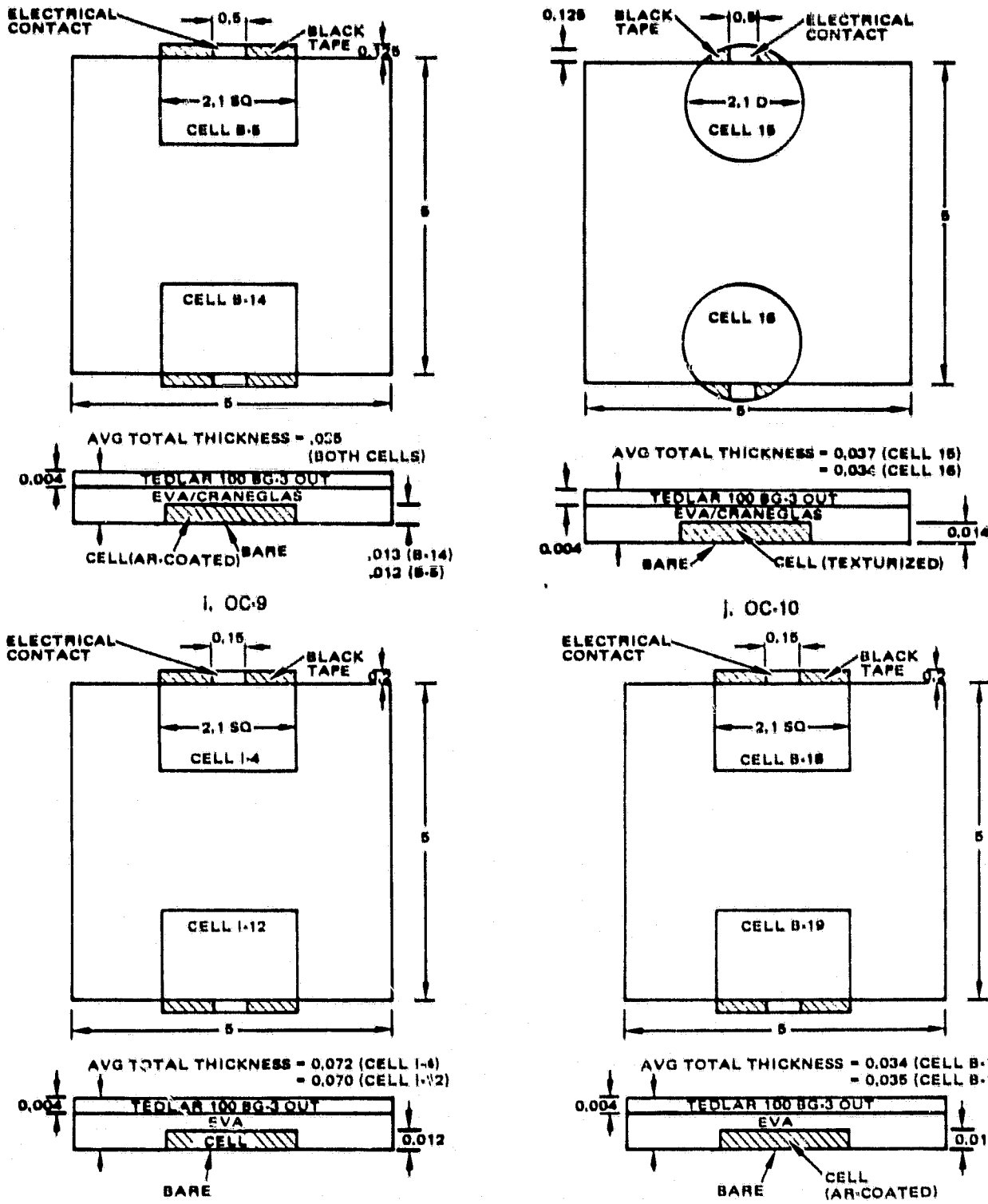

i. OC-9

j. OC-10

k. OC-11

l. OC-12

Figure 3-1 (continued). Optical test coupons.

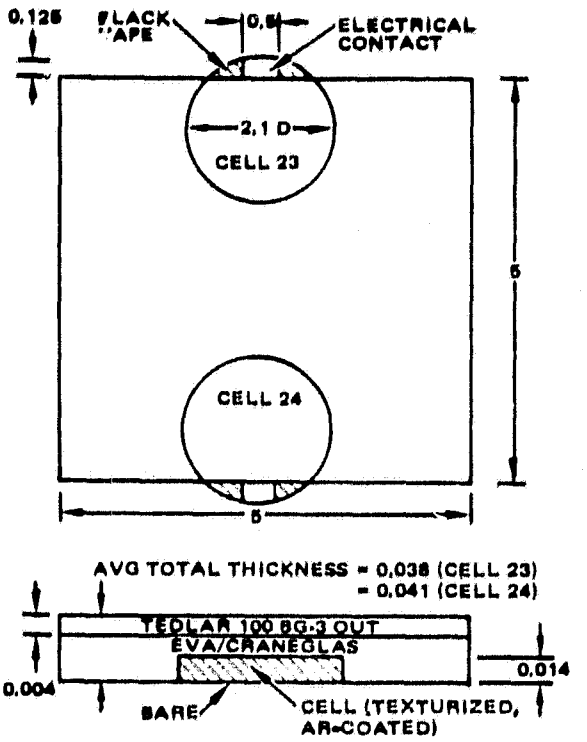

m. OC-13

Figure 3-1 (continued). Optical test coupons.

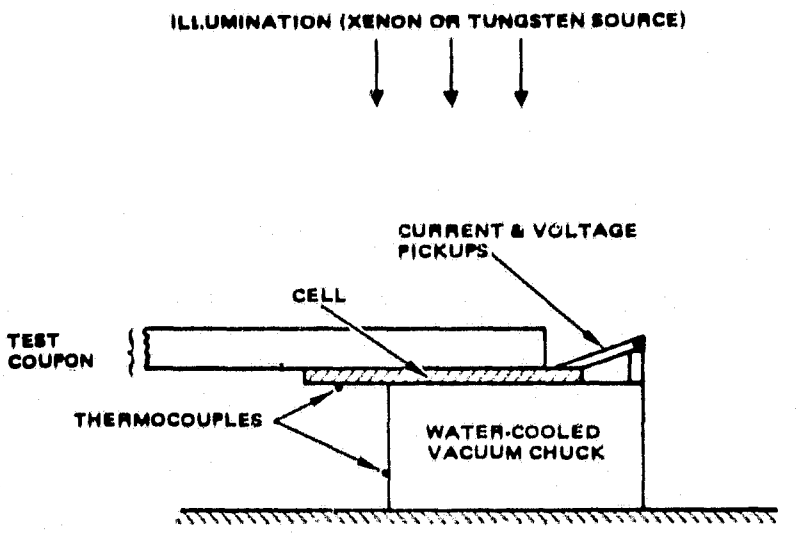

Figure 3-2. Placement of optical test coupon in fixture of illumination source.

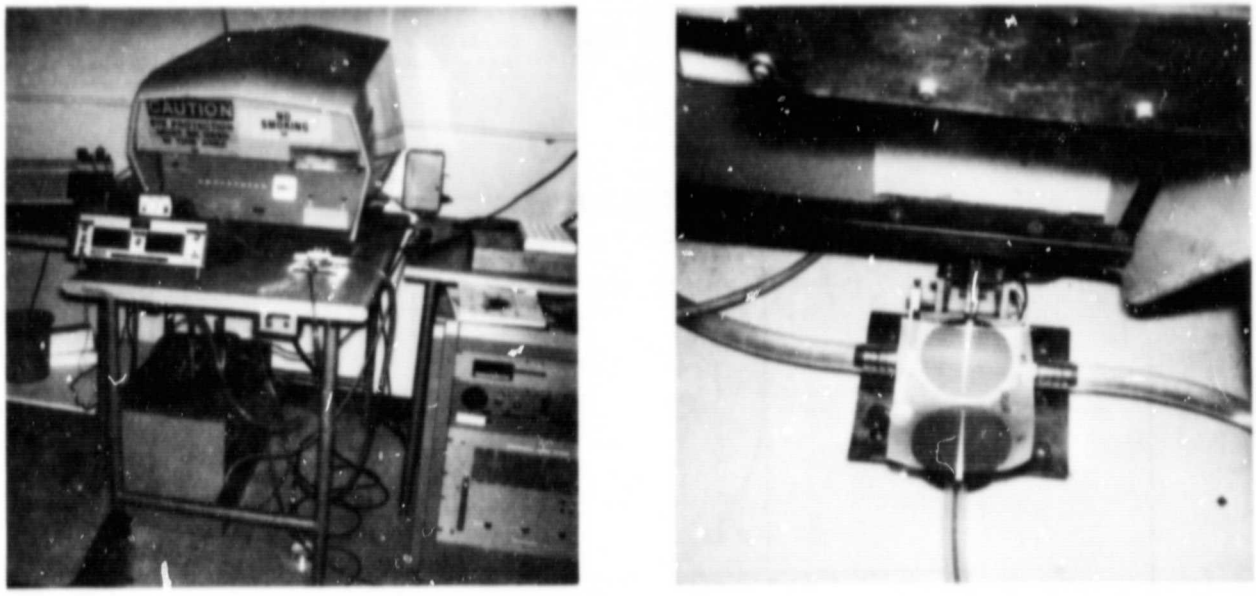

a. Lab setup

b. Close up

Figure 3–3. Coupon no. OC–10 in xenon illumination source.

3.4 TEST CONDITIONS

The optical tests were performed at near-ambient temperature conditions. The temperatures of the cooling fixtures ranged between 28° and 29°C, and measured cell temperatures ranged between 29° and 35°C.

The radiant energy flux of the illumination sources was set by means of standard photovoltaic cells. The standard cells, as well as the procedure for setting the fluxes, are described in Appendix A. Radiant energy fluxes were set at 0.135 W/cm^2 and 0.100 W/cm^2 for the xenon and tungsten sources respectively. A pyranometer (see item 2, Table A–4, Appendix A) was used to check these flux settings. The standard cell and the pyranometer readings were in agreement for the xenon source, but not for the tungsten source. The pyranometer indicated that the total radiant energy flux was 0.22 W/cm^2 for the tungsten source. These results were expected since most of the energy in the xenon spectrum falls within the response range of the cells, whereas most of the energy in the tungsten spectrum does not. Beam uniformity is shown in Figure 3–4 for the xenon source. Information on beam uniformity for the tungsten source was not available, but the uniformity of this source was thought to be less than that of the xenon source.

The following parameters were measured for all cells and both illumination sources:

1. Open-circuit voltage before encapsulation
2. Open-circuit voltage after encapsulation
3. Short-circuit current before encapsulation
4. Short-circuit current after encapsulation
5. Cell current at 500 mV before encapsulation
6. Cell current at 500 mV after encapsulation

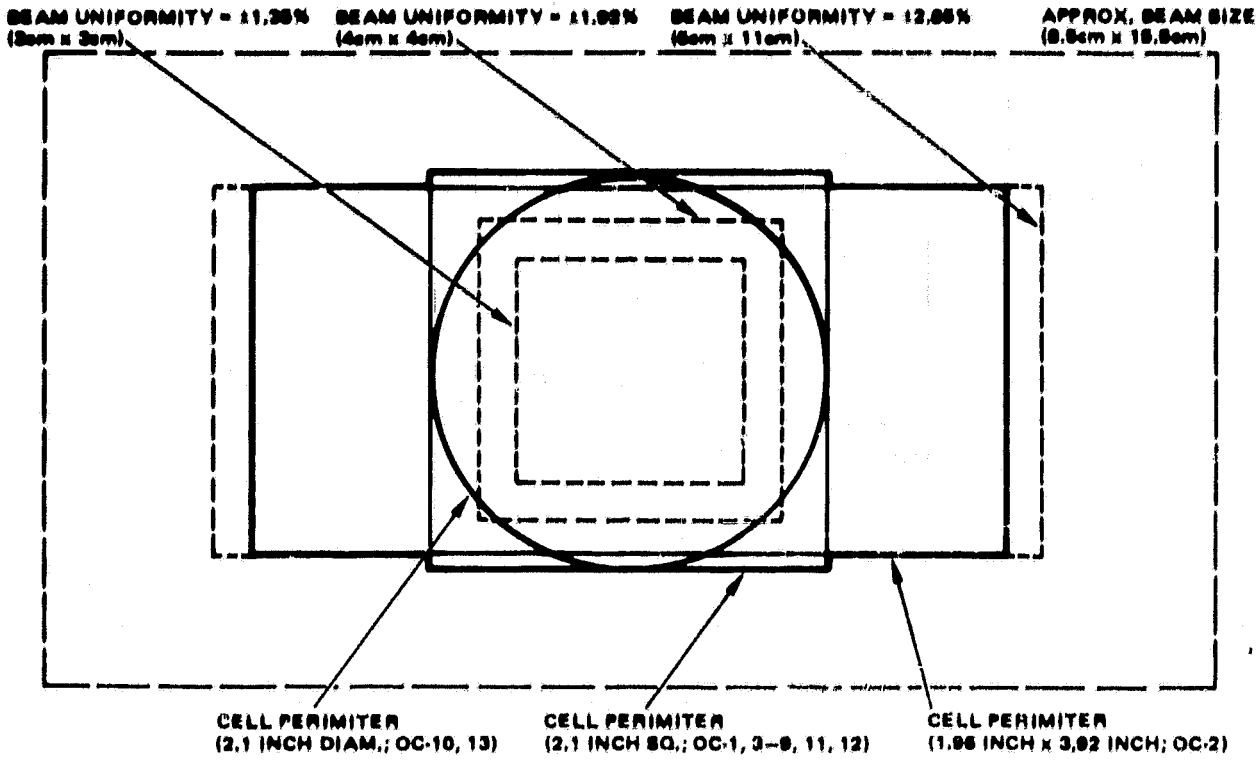

Figure 3-4. Uniformity of xenon source beam and outlines of test coupon cells.

3.5 DATA ANALYSIS

3.5.1 Test Data Summary

Measured values of the short circuit current (I_{sc}), current at 500 mV (I_{500}), and open circuit voltage (V_{oc}) for each cell are listed in Table B-1 of Appendix B. These parameters were measured in both the tungsten and xenon light sources before and after encapsulation of each cell in its respective coupon. The ratios of electric current (I_{sc} and I_{500}) measured after encapsulation divided by electric current measured before encapsulation are also listed in Table B-1. Since the current ratios form the basis for subsequent discussion of the test data, these ratios are listed in Table 3-2 as well. The maximum electrical power produced by each cell can be approximated by multiplying I_{500} by 0.5 volts.

In all cases, values of V_{oc}, I_{sc}, and I_{500} measured for the xenon source were greater than those measured for the tungsten source. This result was expected since the xenon source provided more available energy, at wavelengths coincident with the spectral response (i.e., power conversion efficiency versus wavelength) of silicon, for conversion to electricity. As shown in Figure 3-5, approximately 87 percent of the energy from the xenon source is available at wavelengths less than 1.2 μm. Conversely, only 35 percent of the energy from the tungsten source is available at wavelengths less than 1.2 μm.

For coupons OC-1 through OC-8 and OC-11, I_{sc} and I_{500} were generally greater for encapsulated cells than for bare (i.e. unencapsulated) cells. These parameters remained essentially unchanged or decreased slightly after encapsulation for AR-coated and/or texturized cells (OC-9, 10, 12, 13). These results were expected since encapsulation makes bare silicon cells less

TABLE 3-2. OPTICAL TEST RESULTS

Coupon	Coupon Description	Cell Number	Xenon		Tungsten	
			I_{sc} Ratio	I_{500} Ratio	I_{sc} Ratio	I_{500} Ratio
OC-1	Low-iron glass (stipple in) 11 mil EVA single crystal cell	BC-11 BC-15	1.21 1.31	0.83 1.24	1.38 1.47	0.93 1.44
OC-2	Low-iron glass (stipple in) 6 mil EVA polycrystalline cell	A AA	1.22 1.25	1.28 1.40	1.21 1.19	1.24 1.27
OC-3	High-iron glass 14 mil EVA single crystal cell	EC-14 BC-9	1.13 1.16	1.21 1.14	1.23 1.24	1.12 1.17
OC-4	Low-iron glass (stipple in) 13 mil EVA/Craneglas single crystal cell	BC-17 BC-18	1.32 1.28	1.30 1.23	1.44 1.44	1.42 1.36
OC-5	Low-iron glass (stipple out) 22 mil EVA/Craneglas single crystal cell	BC-10 BC-13	1.30 1.31	1.28 1.29	1.49 1.46	1.44 1.44
OC-6	Korad 18 mil EVA single crystal cell	I-16 B-7	1.23 1.10	1.23 1.27	1.21 1.07	1.21 1.03
OC-7	Tedlar 18 mil EVA single crystal cell	I-17 I-18	1.22 1.22	1.18 1.16	1.35 1.36	1.39 1.36
OC-8	Tedlar 19 mil EVA/Craneglas single crystal cell	I-7 I-6	1.22 1.23	1.33 1.21	1.42 1.41	1.39 1.40
OC-9	Tedlar 18 mil EVA/Craneglas single crystal cell (AR-coated)	B-5 B-14	1.00 0.99	0.98 1.01	1.01 1.02	0.96 0.98
OC-10	Tedlar 18 mil EVA/Craneglas single crystal cell (texturized)	No. 15 No. 16	1.05 1.05	1.03 1.02	1.05 1.04	1.05 1.02
OC-11	Tedlar 55 mil EVA single crystal cell	I-4 I-12	1.25 1.22	1.24 1.21	1.43 1.42	1.45 1.47
OC-12	Tedlar 17 mil EVA single crystal cell (AR-coated)	B-18 B-19	0.93 0.95	0.91 0.93	0.97 0.98	0.92 0.93
OC-13	Tedlar 21 mil EVA/Craneglas single crystal cell (AR-coated, texturized)	No. 23 No. 24	0.98 0.99	0.97 0.94	0.98 0.99	0.92 0.89

Notes:

1. I_{sc} = short-circuit current, ma
2. I_{500} = cell current at 500 mv, ma
3. Current ratios refer to current measured after encapsulation divided by current measured before encapsulation.

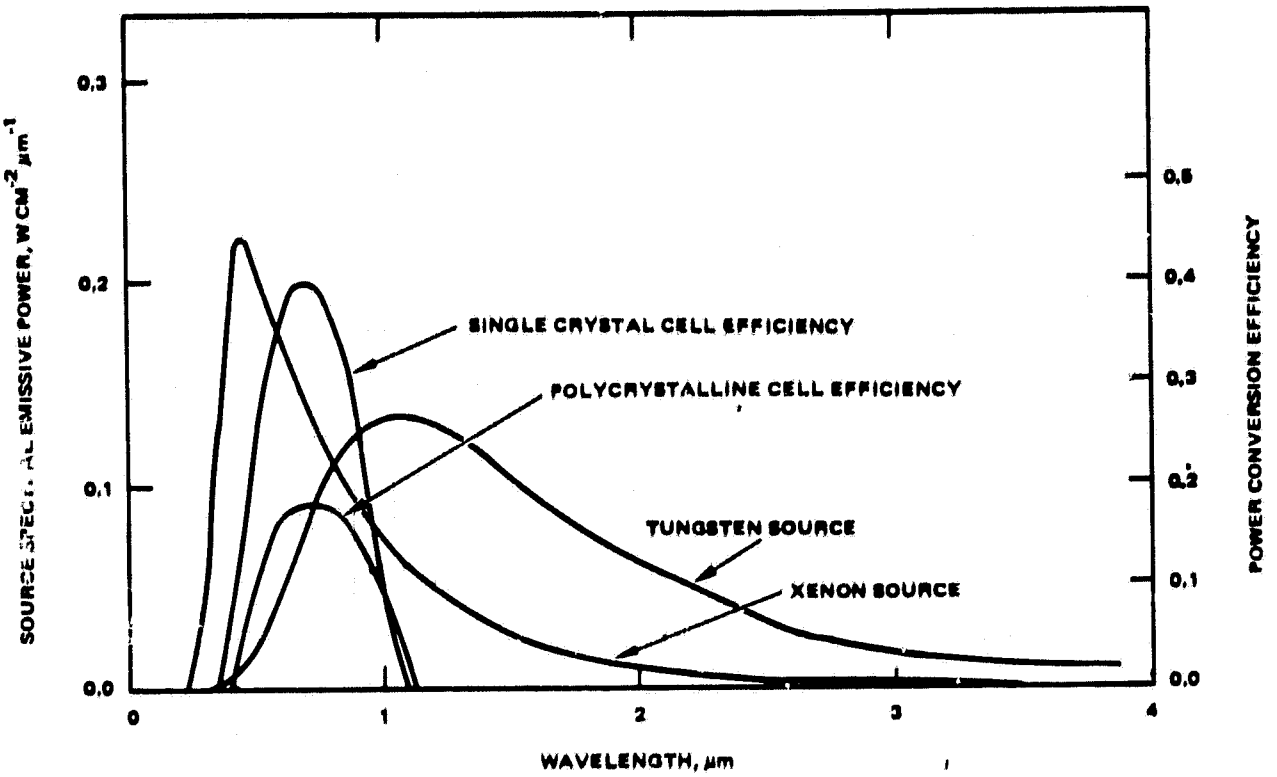

Figure 3-5. Spectral distribution of xenon and tungsten radiant energy fluxes and spectral power conversion efficiencies of silicon solar cells.

reflective, thus permitting more of the incident radiant energy to be converted to electricity. Since the AR-coated and texturized cells reflect little of the incident radiant energy, encapsulation of these cells has little or a slightly detrimental effect (due to absorption of the incident radiation in the encapsulation layers) on cell electrical output. Cell BC-11 of coupon OC-1 was cracked during measurement of the current at 500 mV, which resulted in low values of I_{500} for both light sources.

3.5.2 Description of Analytical Model

The three layer model developed in Section 5.3.2 of reference 3 is used as the basis for correlating analysis with test data. This model, shown in Figure 3-6, is an idealized representation of radiant energy propagation through the front cover and pottant layers on the sun side of a photovoltaic cell. In addition to determining the maximum electric power generated by the cell,

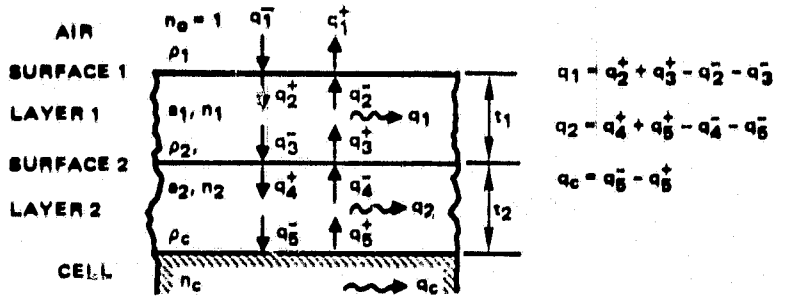

Figure 3-6. Optical model.

this model is also used to determine the radiant energy absorbed as heat in the cell and the layers of the encapsulation system. The radiant energy flux incident on a surface is indicated by a superscript minus (−) and the radiant energy flux leaving a surface is indicated by a superscript plus (+). Details for calculation of these fluxes are found in reference 3. The relations between the fluxes and the total radiant energy absorbed by the cell (q_c) and the radiant energy absorbed as heat in the layers of the encapsulation system (q_1 and q_2) are shown in Figure 3-6. At present, this model does not calculate electric current and voltage.

The major parameters in this model are

1. Front cover absorption coefficient, a_1
2. Pottant absorption coefficient, a_2
3. Front cover index of refraction, n_1
4. Pottant index of refraction, n_2
5. Cell index of refraction, n_c
6. Reflectivity at interface between cell and pottant, ρ_c
7. Reflectivity at interface between pottant and front cover, ρ_2
8. Reflectivity at interface between air and front cover, ρ_1
9. Front cover thickness, t_1
10. Pottant thickness, t_2
11. Spectral power conversion efficiency of the cell, C_λ

Items 1 and 2 are wavelength dependent. Items 6, 7, and 8 are wavelength dependent if anti-reflection (AR) coatings are present on either the cell, the front cover, or both the cell and front cover. The Fresnel equation (eq. 5-10, reference 3) for normal incidence was used to calculate the reflectivities of non AR-coated and non-texturized surfaces. Equation (5-22) of this reference* was used to calculate the reflectivities of encapsulated, texturized silicon cells ($\rho = 0.0096$) and stippled glass ($\rho = 0.05$ facing in, $\rho = 0.048$ facing out). The reflectivities of AR-coated cells were calculated by means of eqs. (5-11, 12 and 13) of reference 3. For this test, all AR-coatings were assumed to be SiO (index of refraction = 1.95) and optimized for an air/silicon interface with a minimum reflectivity at 0.6 μm.

The other required information for the model includes the spectrum of the illumination source and the spectral power-conversion efficiency of the cell. The spectra of the xenon and tungsten sources are shown in Figure 3-5. The spectral power conversion efficiency of the cell, C_λ, is not an easily measured parameter, and values of this parameter could not be found in the literature. However, curves of short-circuit current versus wavelength were readily available. These curves are determined for an incident radiant energy flux that is invariant with wavelength, and the results are reported in units of milliamps per milliwatt per cm^2 of incident radiant energy [6,12]. Relative response curves (i.e. the short circuit current measured at wavelength λ divided by the maximum value of the short-circuit current for all λ) of typical single crystal and polycrystalline silicon cells are shown in Figure 3-7.

A typical current versus voltage curve for a single-crystal silicon cell is shown in Figure 3-8. The maximum electric power generated by these cells occurs at approximately 0.5 volts. The curves of I_{sc} versus λ and I_{500} versus λ are assumed to be identical. Since the maximum power is given approximately by $P_{max} \cong 0.5\ I_{500}$, the relative response curve can presumably be used in place of the spectral power conversion efficiency.

* Note that this expression should read as $\rho_T = 0.05 + 0.95\ \rho^2$

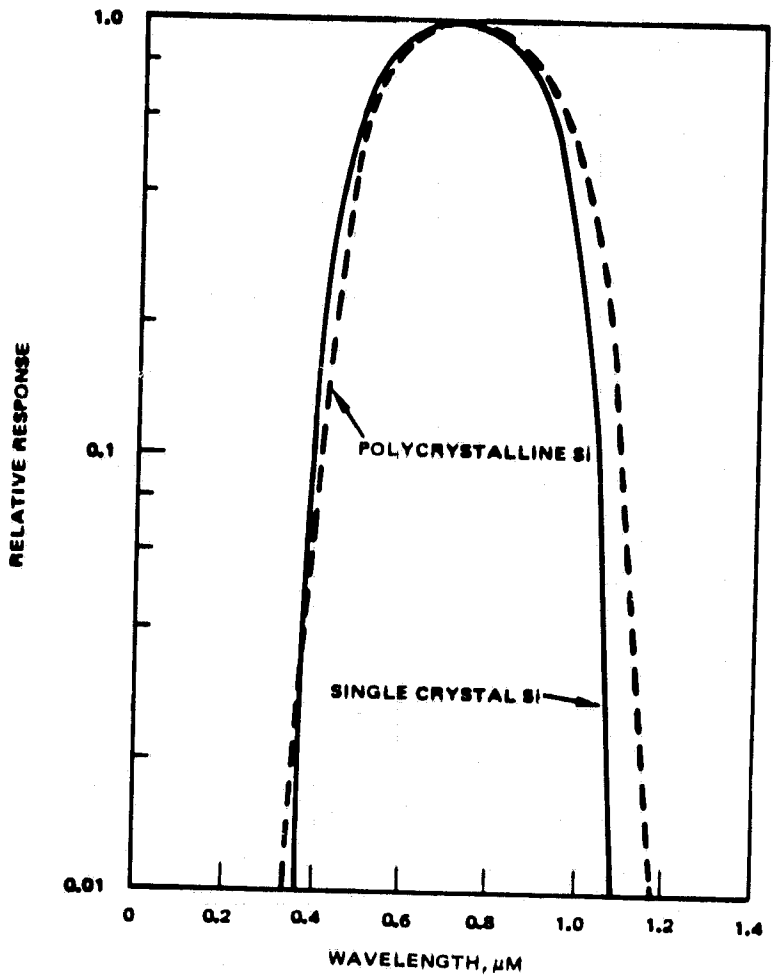

Figure 3-7. Relative response curves for single crystal and polycrystalline silicon solar cells.

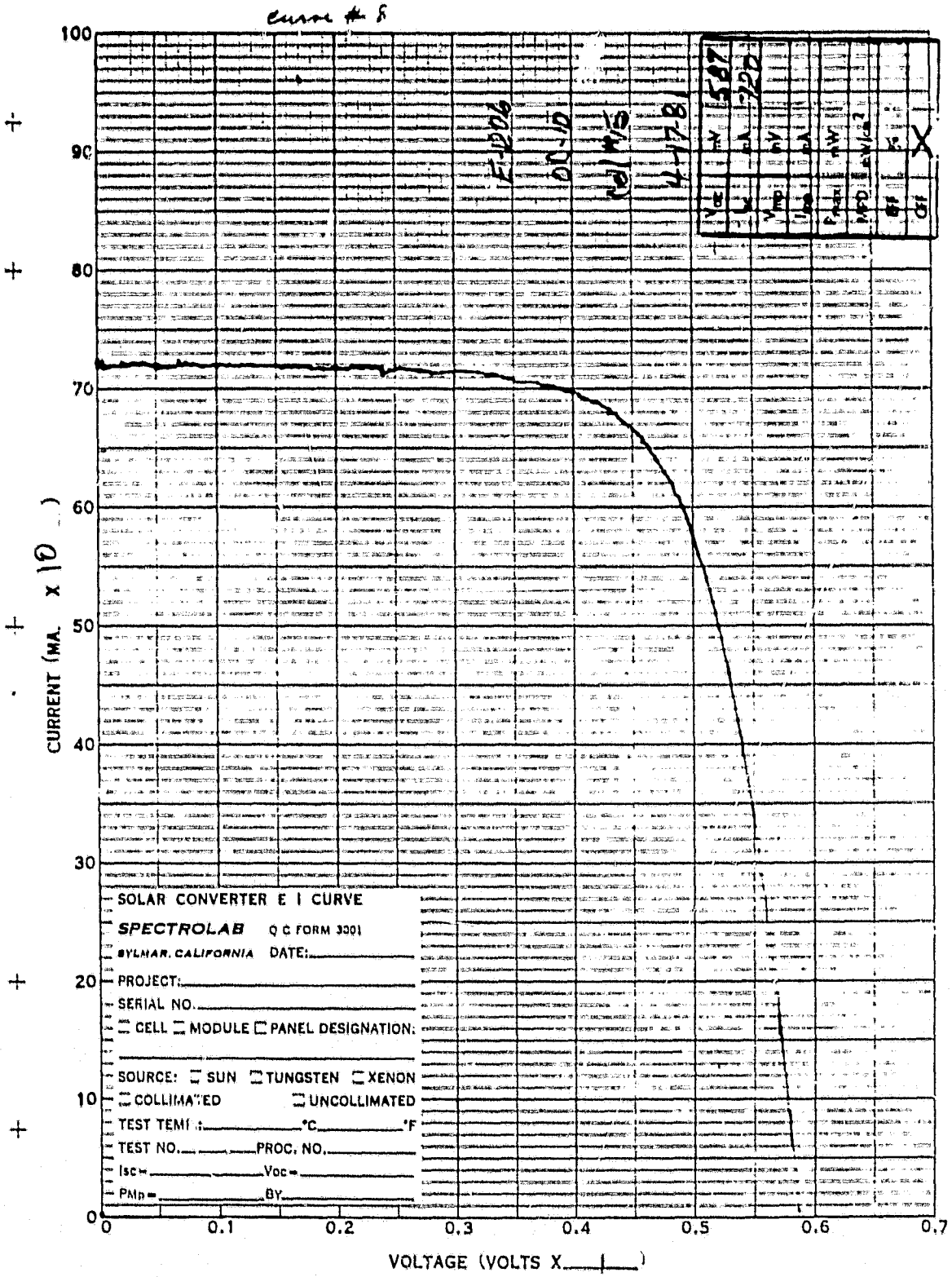

Figure 3-8. Typical current versus voltage curve for an encapsulated, single-crystal silicon cell.

3.5.3 Calculation Details

The basic approach used in the optical model is to divide the illumination spectrum into a number of equal-energy intervals. Twenty equal-energy intervals were used in this correlation analysis; corresponding to these energy intervals are twenty wavelength bands of unequal size. The electric power generated by the cell is determined by means of the following relation

$$P = A_c \sum_{i=1}^{20} C_{\lambda i} q_{ci} \tag{3-1}$$

where:

A_c = area of cell, cm^2

$C_{\lambda i}$ = power conversion efficiency for energy interval i

q_{ci} = radiant energy flux in interval i absorbed by cell, $watt/cm^2$

The power conversion efficiency, $C_{\lambda i}$, is evaluated at the midpoint of each wavelength band. Values of q_1, q_2, and q_c are calculated for each energy interval.

Power conversion efficiencies varied somewhat between cells used in the test. To account for these variations, the maximum value of the spectral power conversion efficiency for an unencapsulated cell used in the test was adjusted in the following manner:

$$C_{max}{}^a = C_{max}{}^t \frac{\eta_a}{\eta_t} \tag{3-2}$$

where:

$C_{max}{}^a$ = maximum value of spectral power conversion efficiency for cell to be tested

$C_{max}{}^t$ = maximum value of spectral power conversion efficiency for typical cell

η_a = overall power conversion efficiency of actual cell

η_t = overall power conversion efficiency of typical cell

Here, η is defined as

$$\eta = \frac{P}{A_c q_c} \tag{3-3}$$

Values of $C_{max}{}^t$ and η_t used in this analysis are listed in Table 3-3. The power conversion efficiency at any wavelength is then found by multiplying $C_{max}{}^a$ by the relative response shown in Figure 3-7.

TABLE 3-3. VALUES OF $C_{max}{}^t$ AND η_t FOR "TYPICAL" SINGLE CRYSTAL AND POLYCRYSTALLINE SILICON CELLS

Cell Type	$C_{max}{}^t$	η_t
Single crystal	0.395	0.0831
Polycrystalline	0.183	0.06

The overall power conversion efficiency of an actual cell, η_a, was determined by means of the following relation for non-texturized and non AR-coated cells

$$\eta_a = \frac{0.5\ I_{500}}{(1 - \rho_c)\ A_c\ q_i^-} \tag{3-4}$$

where:

I_{500} = cell current measured at 0.5 volts, amps

ρ_c = reflectivity of cell surface

q_i^- = incident radiant energy flux on cell surface, watt/cm^2

Since the reflectivity of AR-coated surfaces is wavelength dependent, the following modified form of Equation (3-4) was used to calculate η_a for coupons OC-9, 12, and 13:

$$\eta_a = \frac{0.5\ I_{500}}{A_c \sum_{i=1}^{20} (1 - \rho_{ci})\ q_{1i}^-} \tag{3-5}$$

where ρ_{ci} and q_{1i}^- correspond to the reflectivity evaluated at the midpoint of wavelength band i and the incident radiant energy in that band respectively.

The active areas of the cells were 24.9 cm^2 for the 2.1-inch square cells, 46.5 cm^2 for the two-inch × four-inch cells, and 18.8 cm^2 for the two-inch diameter cells. These areas allow for cell surface blockage by the black tape and metallization.

Values of ρ_c and relative cell efficiency ($= C_\lambda / C_{max}$) are listed in Tables 3-4 and 3-5 for unencapsulated and encapsulated cells, respectively. This information is tabulated for each of the equal energy intervals for the xenon and tungsten sources. Values of η_a for each cell used in the test are listed in Table 3-6.

One prediction was made for each coupon to minimize computer time and labor. Average cover layer and pottant thicknesses used in these calculations are listed in Table 3-7. The power efficiencies used in the calculations corresponded to the average power efficiencies of the cell pairs used in each coupon.

3.5.4 Results

The measured and predicted electric power produced by the encapsulated cells are compared in Tables 3-8 and 3-9. Also included are measured and predicted ratios of cell output power after encapsulation to cell output power measured before encapsulation. The average electric power for the two cells of each coupon and the predicted electric power based on average properties (i.e. cell efficiency and encapsulation layer thicknesses) for each coupon are tabulated. These results are shown for both illumination sources.

In all cases, the average electric power predicted by the model was less than the average measured power. Agreement was best for the xenon source; the average discrepancy (as percentage of the measured value) was −7.4 percent for xenon and −13.1 percent for tungsten. The absolute values of the discrepancy ranged from −2.2 to −15.1 percent for xenon and from −1.2 to −24.3 percent for tungsten. Agreement between measured and predicted power output was best for AR-coated and texturized cells; this agreement was best for the tungsten source.

TABLE 3–4. WAVELENGTH BANDS FOR ILLUMINATION SOURCES, CELL RELATIVE EFFICIENCIES, AND REFLECTIVITIES OF UNENCAPSULATED AR–COATED CELLS

	Xenon Source						Tungsten Source					
	Wavelength Band		Cell Relative Efficiency		Reflectivity		Wavelength Band		Cell Relative Efficiency		Reflectivity	
Energy Interval	Endpoints	Midpoint	SC	PC	AR-Coated Only	AR-Coated & Texturized	Endpoints	Midpoint	SC	PC	AR-Coated Only	AR-Coated & Texturized
1	0.201, 0.368	0.284	0	0	0.288	0.129	0.3 , 0.7	0.50	0.633	0.546	0.093	0.058
2	0.368, 0.404	0.386	0.058	0.044	0.28	0.125	0.7 , 0.83	0.76	0.987	0.984	0.025	0.051
3	0.404, 0.444	0.424	0.228	0.109	0.216	0.094	0.83, 0.91	0.86	0.823	0.885	0.065	0.054
4	0.444, 0.462	0.458	0.380	0.279	0.166	0.076	0.91, 0.99	0.95	0.506	0.650	0.102	0.060
5	0.462, 0.502	0.482	0.532	0.437	0.119	0.064	0.99, 1.09	1.03	0.147	0.311	0.132	0.067
6	0.502, 0.544	0.523	0.722	0.656	0.065	0.054	1.09, 1.17	1.12	0	0.071	0.158	0.074
7	0.544, 0.568	0.552	0.810	0.770	0.037	0.051	1.17, 1.25	1.20	0	0	0.178	0.080
8	0.568, 0.594	0.581	0.861	0.836	0.017	0.050	1.25, 1.34	1.29	0	0	0.198	0.087
9	0.594, 0.648	0.621	0.924	0.934	0.003	0.05	1.34, 1.43	1.38	0	0	0.214	0.094
10	0.648, 0.674	0.661	0.962	0.978	0.0004	0.05	1.43, 1.54	1.47	0	0	0.228	0.099
11	0.674, 0.748	0.711	1.0	1.0	0.009	0.05	1.54, 1.65	1.58	0	0	0.242	0.105
12	0.748, 0.774	0.761	0.987	0.984	0.025	0.051	1.65, 1.77	1.70	0	0	0.254	0.111
13	0.774, 0.868	0.821	0.924	0.940	0.049	0.052	1.77, 1.91	1.83	0	0	0.264	0.116
14	0.868, 0.914	0.891	0.734	0.825	0.078	0.056	1.91, 2.08	1.99	0	0	0.275	0.122
15	0.914, 1.028	0.971	0.418	0.590	0.110	0.061	2.08, 2.29	2.17	0	0	0.284	0.127
16	1.028, 1.112	1.07	0.048	0.191	0.143	0.070	2.29, 2.55	2.41	0	0	0.293	0.132
17	1.112, 1.248	1.18	0	0	0.174	0.079	2.55, 2.91	2.72	0	0	0.302	0.137
18	1.248, 1.412	1.33	0	0	0.206	0.090	2.91, 3.47	3.18	0	0	0.310	0.141
19	1.412, 1.688	1.55	0	0	0.238	0.104	3.47, 4.6	4.02	0	0	0.319	0.147
20	1.688, 3.192	2.44	0	0	0.294	0.132	4.6 , 18.2	11.4	0	0	0.331	0.154

Notes:

1. SC = single crystal silicon
   PC = polycrystalline silicon
2. Reflectivity of AR-coated only cells is applicable to coupons OC–9 and OC–12
3. Reflectivity of AR-coated and texturized cells is applicable to coupon OC–13.
4. Reflectivity of non AR-coated and non-texturized silicon = 0.333
5. Reflectivity of non AR-coated texturized silicon = 0.155

TABLE 3–5. WAVELENGTH BANDS FOR ILLUMINATION SOURCES, CELL RELATIVE EFFICIENCIES, AND REFLECTIVITIES OF ENCAPSULATED AR–COATED CELLS

	Xenon Source						Tungsten Source					
	Wavelength Band		Cell Relative Efficiency		Reflectivity		Wavelength Band		Cell Relative Efficiency		Reflectivity	
Energy Interval	Endpoints	Midpoint	SC	PC	AR-Coated Only	AR-Coated & Texturized	Endpoints	Midpoint	SC	PC	AR-Coated Only	AR-Coated & Texturized
1	0.201, 0.368	0.284	0	0	0.177	0.080	0.3 , 0.7	0.50	0.633	0.546	0.069	0.055
2	0.368, 0.404	0.386	0.058	0.044	0.172	0.078	0.7 , 0.83	0.76	0.987	0.984	0.036	0.051
3	0.404, 0.444	0.424	0.228	0.109	0.134	0.067	0.83, 0.91	0.86	0.823	0.885	0.055	0.053
4	0.444, 0.462	0.458	0.380	0.279	0.106	0.061	0.91, 0.99	0.95	0.506	0.650	0.073	0.055
5	0.462, 0.502	0.482	0.532	0.437	0.082	0.056	0.99, 1.09	1.03	0.147	0.311	0.088	0.057
6	0.502, 0.544	0.523	0.722	0.656	0.055	0.053	1.09, 1.17	1.12	0	0.071	0.102	0.060
7	0.544, 0.568	0.552	0.810	0.770	0.041	0.052	1.17, 1.25	1.20	0	0	0.113	0.062
8	0.568, 0.594	0.581	0.861	0.836	0.032	0.051	1.25, 1.34	1.29	0	0	0.124	0.065
9	0.594, 0.648	0.621	0.924	0.934	0.026	0.051	1.34, 1.43	1.38	0	0	0.133	0.067
10	0.648, 0.674	0.661	0.962	0.978	0.025	0.051	1.43, 1.54	1.47	0	0	0.141	0.069
11	0.674, 0.748	0.711	1.0	1.0	0.029	0.051	1.54, 1.65	1.58	0	0	0.149	0.071
12	0.748, 0.774	0.761	0.987	0.984	0.036	0.051	1.65, 1.77	1.70	0	0	0.156	0.073
13	0.774, 0.868	0.821	0.924	0.940	0.047	0.052	1.77, 1.91	1.83	0	0	0.163	0.075
14	0.868, 0.914	0.891	0.734	0.825	0.061	0.054	1.91, 2.08	1.99	0	0	0.169	0.077
15	0.914, 1.028	0.971	0.418	0.590	0.077	0.056	2.08, 2.29	2.17	0	0	0.175	0.079
16	1.028, 1.112	1.07	0.048	0.191	0.094	0.058	2.29, 2.55	2.41	0	0	0.181	0.081
17	1.112, 1.248	1.18	0	0	0.110	0.062	2.55, 2.91	2.72	0	0	0.186	0.083
18	1.248, 1.412	1.33	0	0	0.128	0.066	2.91, 3.47	3.18	0	0	0.191	0.085
19	1.412, 1.688	1.55	0	0	0.147	0.071	3.47, 4.6	4.02	0	0	0.197	0.087
20	1.688, 3.192	2.44	0	0	0.181	0.081	4.6 , 18.2	11.4	0	0	0.205	0.090

Notes.

1. SC = single crystal silicon
   PC = polycrystalline silicon
2. Reflectivity of AR-coated only cells is applicable to coupons OC–9 and OC–12
3. Reflectivity of AR-coated and texturized cells is applicable to coupon OC–13.
4. Reflectivity of non AR-coated and non-texturized silicon = 0.206
5. Reflectivity of non AR-coated texturized silicon = 0.090

TABLE 3-6. POWER CONVERSION EFFICIENCY (η_a) OF BARE CELLS BEFORE INCORPORATION IN TEST COUPONS

Coupon	Cell No.	Xenon Light Source			Tungsten Light Source		
		I_{500}, A	Power, W	η_a	I_{500}, A	Power, W	η_a
OC-1	BC-11	0.561	0.280	0.125	0.450	0.225	0.063
	BC-15	0.577	0.288	0.128	0.454	0.227	0.063
OC-2	A	0.506	0.253	0.060	0.367	0.184	0.027
	AA	0.464	0.232	0.055	0.345	0.172	0.025
OC-3	BC-14	0.536	0.268	0.120	0.469	0.234	0.065
	BC-9	0.577	0.288	0.128	0.466	0.233	0.065
OC-4	BC-17	0.577	0.288	0.128	0.472	0.236	0.066
	BC-18	0.536	0.268	0.120	0.431	0.216	0.060
OC-5	BC-10	0.574	0.287	0.128	0.460	0.230	0.064
	BC-13	0.564	0.282	0.126	0.464	0.232	0.065
OC-6	I-16	0.550	0.275	0.123	0.502	0.251	0.070
	B-7	0.603	0.302	0.135	0.577	0.288	0.080
OC-7	I-17	0.552	0.276	0.123	0.440	0.220	0.061
	I-18	0.553	0.277	0.124	0.435	0.218	0.059
OC-8	I-7	0.508	0.254	0.113	0.446	0.223	0.062
	I-6	0.556	0.278	0.124	0.435	0.218	0.061
OC-9	B-5	0.762	0.381	0.124	0.692	0.346	0.073
	B-14	0.780	0.390	0.127	0.705	0.352	0.074
OC-10	No. 15	0.578	0.289	0.125	0.511	0.256	0.068
	No. 16	0.569	0.285	0.123	0.503	0.252	0.067
OC-11	I-4	0.511	0.256	0.114	0.411	0.206	0.056
	I-12	0.542	0.271	0.121	0.423	0.212	0.058
OC-12	B-18	0.786	0.393	0.128	0.710	0.355	0.075
	B-19	0.770	0.385	0.126	0.694	0.347	0.073
OC-13	No. 23	0.570	0.285	0.119	0.505	0.252	0.066
	No. 24	0.609	0.305	0.128	0.550	0.275	0.071

TABLE 3–7. AVERAGE COVER LAYER AND POTTANT THICKNESSES

Coupon	Cover Layer Thickness, inch	Pottant Thickness, inch
OC-1	0.138	0.011
OC-2	0.131	0.006
OC-3	0.119	0.014
OC-4	0.128	0.013
OC-5	0.127	0.022
OC-6	0.003	0.018
OC-7	0.004	0.018
OC-8	0.004	0.019
OC-9	0.004	0.018
OC-10	0.004	0.018
OC-11	0.004	0.055
OC-12	0.004	0.017
OC-13	0.004	0.021

TABLE 3-8. COMPARISON OF MEASURED AND PREDICTED ELECTRIC POWER OUTPUT FOR XENON ILLUMINATION SOURCE

Coupon	Coupon Description	Average Power (Measured)*			Average Power (Calculated)	
		Unencapsulated, W	Encapsulated, W	Ratio**	Encapsulated, W	Ratio†
OC-1	Low-iron glass (stipple in) 11 mil EVA single crystal cell	0.288 (cell BC-15 only)	0.358 (cell BC-15 only)	1.24	0.328	1.14
OC-2	Low-iron glass (stipple in) 6 mil EVA polycrystalline cell	0.242	0.325	1.34	0.276	1.14
OC-3	High-iron glass 14 mil EVA single crystal cell	0.278	0.326	1.17	0.3	1.08
OC-4	Low-iron glass (stipple in) 13 mil EVA/Craneglas single crystal cell	0.278	0.352	1.27	0.312	1.12
OC-5	Low-iron glass (stipple out) 22 mil EVA/Craneglas single crystal cell	0.284	0.366	1.29	0.314	1.11
OC-6	Korad 18 mil EVA single crystal cell	0.288	0.360	1.25	0.311	1.08
OC-7	Tedlar 18 mil EVA single crystal cell	0.276	0.324	1.17	0.308	1.12
OC-8	Tedlar 19 mil EVA/Craneglas single crystal cell	0.266	0.337	1.27	0.293	1.10
OC-9	Tedlar 18 mil EVA/Craneglas single crystal cell (AR-coated)	0.386	0.383	0.99	0.365	0.95
OC-10	Tedlar 18 mil EVA/Craneglas single crystal cell (texturized)	0.287	0.294	1.02	0.273	0.95
OC-11	Tedlar 55 mil EVA single crystal cell	0.264	0.335	1.27	0.305	1.16
OC-12	Tedlar 17 mil EVA single crystal cell (AR-coated)	0.389	0.358	0.92	0.350	0.90
OC-13	Tedlar 21 mil EVA/Craneglas single crystal cell (AR-coated, texturized)	0.295	0.281	0.95	0.260	0.88

*Average for two cells of each coupon

**Ratio = power measured after encapsulation divided by power measured before encapsulation

†Ratio = power predicted for cell after encapsulation divided by power measured before encapsulation

TABLE 3-9. COMPARISON OF MEASURED AND PREDICTED ELECTRIC POWER OUTPUT FOR TUNGSTEN ILLUMINATION SOURCE

Coupon	Coupon Description	Average Power (Measured)*			Average Power (Calculated)	
		Unencapsulated, W	Encapsulated, W	Ratio**	Encapsulated, W	Ratio†
OC-1	Low-iron glass (stipple in) 11 mil EVA single crystal cell	0.227 (cell BC-15 only)	0.326 (cell BC-15 only)	1.44	0.257	1.13
OC-2	Low-iron glass (stipple in) 6 mil EVA polycrystalline cell	0.179	0.224	1.25	0.202	1.13
OC-3	High-iron glass 14 mil EVA single crystal cell	0.234	0.268	1.14	0.235	1.00
OC-4	Low-iron glass (stipple in) 13 mil EVA/Craneglas single crystal cell	0.226	0.314	1.39	0.255	1.13
OC-5	Low-iron glass (stipple out) 22 mil EVA/Craneglas single crystal cell	0.231	0.333	1.44	0.252	1.09
OC-6	Korad 18 mil EVA single crystal cell	0.270	0.300	1.11	0.285	1.06
OC-7	Tedlar 18 mil EVA single crystal cell	0.219	0.302	1.38	0.245	1.12
OC-8	Tedlar 19 mil EVA/Craneglas single crystal cell	0.221	0.308	1.39	0.243	1.10
OC-9	Tedlar 18 mil EVA/Craneglas single crystal cell (AR-coated)	0.350	0.339	0.97	0.343	0.98
OC-10	Tedlar 18 mil EVA/Craneglas single crystal cell (texturized)	0.254	0.262	1.03	0.245	0.96
OC-11	Tedlar 55 mil EVA single crystal cell	0.217	0.315	1.45	0.241	1.11
OC-12	Tedlar 17 mil EVA single crystal cell (AR-coated)	0.351	0.325	0.93	0.329	0.94
OC-13	Tedlar 21 mil EVA/Craneglas single crystal cell (AR-coated, texturized)	0.264	0.239	0.90	0.225	0.85

*Average for two cells of each coupon

**Ratio = power measured after encapsulation divided by power measured before encapsulation

†Ratio = power predicted for cell after encapsulation divided by power measured before encapsulation

Since the beams of both illumination sources were not perfectly collimated, it was suspected that radiant energy reflected off those parts of the encapsulation system not covering the cell might give rise to a "light-concentrating" effect (i.e. the zero-depth concentrator phenomenon) and thus be a source of discrepancy between measured and predicted cell output power. To test this hypothesis, cardboard frames were cut such that only the cell of a coupon was illuminated. I_{sc} was measured with and without the frame for each source. The current measured with the frame divided by the current measured without the frame is called the framing factor. Multiplying the average measured power in Tables 3-8 and 3-9 by the appropriate framing factors yields somewhat better agreement between predicted and measured cell power; these results are shown in Tables 3-10 and 3-11. These results indicate that "light concentration" within the encapsulation system was responsible for a no more than 2 percent increase in measured power output.

TABLE 3-10. COMPARISON OF MEASURED (WITH FRAME) AND PREDICTED ELECTRIC POWER OUTPUT FOR XENON ILLUMINATION SOURCE

Coupon	Coupon Description	Framing Factor	Average Power, Watts		
			Measured		Calculated
			Without Frame	With Frame	
OC-1	Low-iron glass (stipple in) 11 mil EVA single crystal cell	0.985	0.358	0.353	0.328
OC-3	High-iron glass 14 mil EVA single crystal cell	0.988	0.326	0.322	0.3
OC-4	Low-iron glass (stipple in) 13 mil EVA/Craneglas single crystal cell	0.97	0.352	0.341	0.312
OC-5	Low-iron glass (stipple out) 22 mil EVA/Craneglas single crystal cell	0.98	0.366	0.359	0.314
OC-6	Korad 18 mil EVA single crystal cell	1.0	0.360	0.360	0.311
OC-8	Tedlar 19 mil EVA single crystal cell	0.996	0.337	0.336	0.293
OC-10	Tedlar 18 mil EVA/Craneglas single crystal cell (texturized)	0.995	0.294	0.293	0.273
OC-11	Tedlar 55 mil EVA single crystal cell (AR-coated)	0.97	0.335	0.325	0.305
OC-12	Tedlar 17 mil EVA single crystal cell (AR-coated)	0.997	0.358	0.357	0.350
OC-13	Tedlar 21 mil EVA/Craneglas single crystal cell (AR-coated, texturized)	0.989	0.281	0.278	0.260

TABLE 3-11. COMPARISON OF MEASURED (WITH FRAME) AND PREDICTED ELECTRIC POWER OUTPUT FOR TUNGSTEN ILLUMINATION SOURCE

Coupon	Coupon Description	Framing Factor	Average Power, Watts		
			Measured		Calculated
			Without Frame	With Frame	
OC-1	Low-iron glass (stipple in) 11 mil EVA single crystal cell	0.986	0.326	0.321	0.257
OC-3	High-iron glass 14 mil EVA single crystal cell	0.991	0.268	0.266	0.235
OC-4	Low-iron glass (stipple in) 13 mil EVA/Craneglas single crystal cell	0.982	0.314	0.308	0.255
OC-5	Low-iron glass (stipple out) 22 mil EVA/Craneglas single crystal cell	0.976	0.333	0.325	0.252
OC-6	Korad 18 mil EVA single crystal cell	1.0	0.300	0.300	0.285
OC-8	Tedlar 19 mil EVA single crystal cell	0.988	0.308	0.304	0.243
OC-10	Tedlar 18 mil EVA/Craneglas single crystal cell (texturized)	0.997	0.262	0.261	0.245
OC-11	Tedlar 55 mil EVA single crystal cell (AR-coated)	0.983	0.315	0.310	0.241
OC-12	Tedlar 17 mil EVA single crystal cell (AR-coated)	0.997	0.325	0.324	0.329
OC-13	Tedlar 21 mil EVA/Craneglas single crystal cell (AR-coated, texturized)	0.824	0.239	0.197	0.225

3.6 DISCUSSION

The results in Tables 3-8 and 3-9 clearly show that the optical model underpredicts the output power from encapsulated cells. The fact that agreement between test and prediction is best for AR-coated and texturized cells coupled with the fact that etched cells were used in the coupons indicates that use of the Fresnel equation yielded too high a value for the reflectivity of the cell surfaces. Use of a lower value of reflectivity in the optical model would yield substantially better agreement between measured and predicted cell output power.

Other possible contributing factors to the discrepancy between prediction and measurement are non-uniform flux in illumination sources and non-uniform pottant thickness above the cells. The importance of these factors was not determined.

Part of the discrepancy for the tungsten source can be found in the calculation method. Use of equal-energy intervals gives rise to poor resolution of the cell response for this source. A larger number of intervals would overcome this problem.

Since the efficiencies of the cells varied so much between coupons, it is best to use the power ratios listed in Tables 3-8 and 3-9 to discern trends. A comparison between ratios for coupons OC-1 and OC-4 indicates that the presence or absence of Craneglas in the pottant has little influence on cell power output. A comparison of ratios for coupons OC-4 and OC-5 shows that outward-facing or inward-facing stippling of low-iron glass superstrates has little influence on cell power output. The negative effects of iron-content in glass superstrates can be seen by comparing ratios for coupons OC-1 and OC-3. A comparison of ratios for coupons OC-7 and OC-11 shows that a three-fold increase in pottant thickness yields only a slight change in cell power output.

In summary, the test results have demonstrated the utility of the optical model to predict cell power output for a broad spectrum of optical parameters characteristic of encapsulation systems. The model consistently underpredicts cell output power, but this problem can be rectified by using more precisely known values of optical properties, such as reflectivity at the cell surface.

4.0 ELECTRICAL ISOLATION TEST

4.1 TEST OBJECTIVE

A major design requirement for any photovoltaic module is that the encapsulation system be able to withstand at least 3000 volts DC before electrical breakdown. Thus, the objective of the electrical verification test was to assess the validity of the electrical isolation model used to determine material thicknesses of the encapsulation system to satisfy this requirement. To accomplish this objective, the breakdown voltage was measured for specially-designed coupons that employed simulated solar cells and different encapsulation schemes. Specific items to be investigated were

1. Effect of Craneglas on breakdown voltage
2. Effect of pottant thickness on breakdown voltage
3. Electrical isolation capability of wood substrates.

4.2 TEST SPECIMENS

Four types of coupons (listed in Table 4-1) were used as test specimens. The geometric layouts and dimensions of the different coupon types are illustrated in Figure 4-1. Approximately 25 of each coupon type were tested to electrical breakdown (failure) of the encapsulation system. This quantity was deemed sufficient to permit a preliminary statistical analysis of the results.

TABLE 4-1. SPECIMENS FOR ELECTRICAL ISOLATION VERIFICATION TESTS

Type	Front Side	Back Side
A	0.004 in. Tedlar, 0.018 in. EVA	0.018 in. EVA/CG, 0.001 in. Alum. Polyester
B	0.001 in. Tedlar, 0.018 in. EVA	0.036 in. EVA/CG, 0.001 in. Alum. Polyester
C	0.001 in. Tedlar, 0.018 in. EVA	0.018 in. EVA/CG, 0.125 in. Wood Product
D	0.001 in. Tedlar, 0.036 in. EVA/CG	0.036 in. EVA/CG, 0.125 in. Wood Product

Wood Product = Duron (U.S. Gypsum Co.)
EVA = Ethylene Vinyl Acetate
EVA/CG = Ethylene Vinyl Acetate with Craneglas
Alum. Polyester = Aluminized Polyester

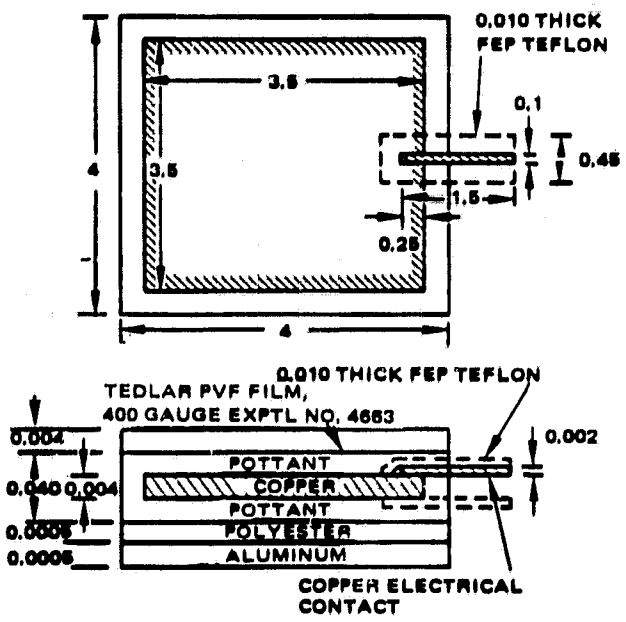

a. Type A

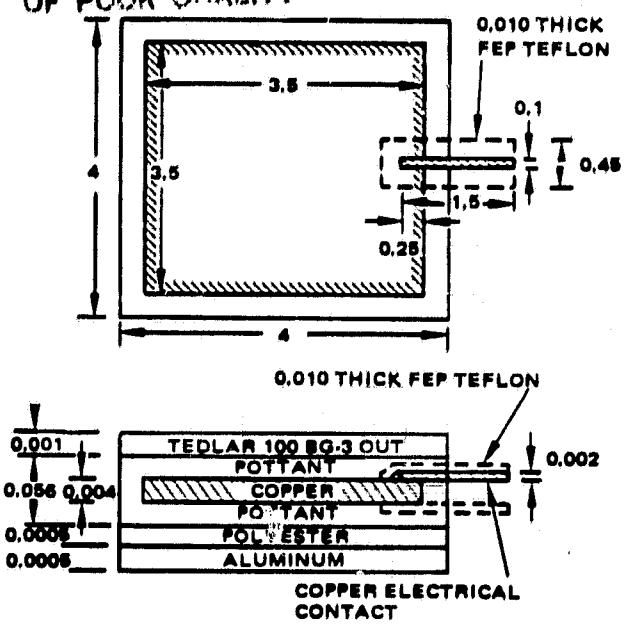

b. Type B

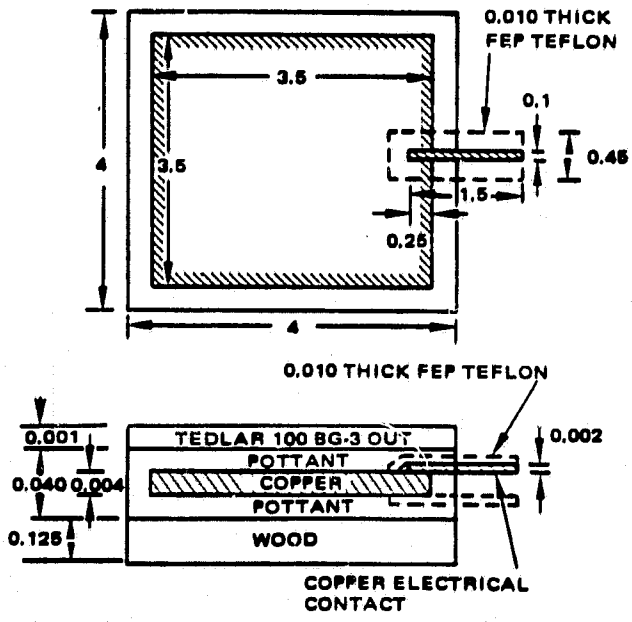

c. Type C

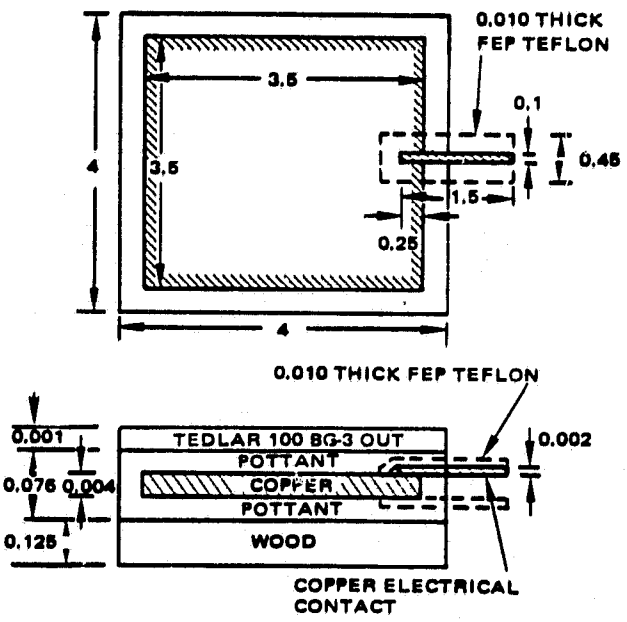

d. Type D

Figure 4-1. Electrical isolation test coupons; dimensions in inches.

4.3 TEST SET-UP

A hipot tester was used to determine the breakdown voltage of the encapsulation system on both the front and back sides of each specimen. The test set-up is illustrated in Figure 4-2. Test coupons were placed on the 3 × 3 × 1/2 inch aluminum block so that the block was centered over the copper electrode (i.e. the simulated solar cell). The edges of the aluminum block were rounded, which, combined with the central placement of the block over the copper electrode, served to minimize edge effects. The aluminum block was connected to ground, and an electrical potential was applied to the copper electrode (via the copper contact) by means of the hipot tester.

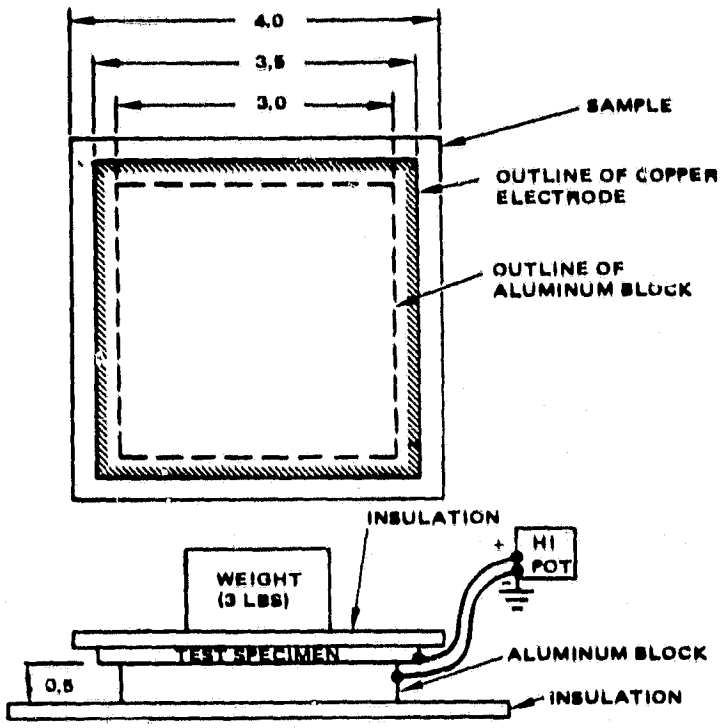

Figure 4-2. Test set-up for electrical isolation tests; dimensions in inches.

4.4 TEST CONDITIONS

The test coupons were conditioned at 72°F and 50 percent relative humidity for a minimum of 24 hours before test. The coupons were placed in the apparatus shown in Figure 4-2 and tested to failure immediately upon removal from the controlled temperature and humidity environment. Two tests were performed on each coupon (one for each side).

During a test, the applied voltage was increased in 500-volt increments from zero volts to breakdown. The leakage current was measured at each voltage setting. A leakage current in excess of 5 mA was taken as the criterion for electrical breakdown of the encapsulation system.

4.5 DATA ANALYSIS

4.5.1 Test Data Summary

Results of the electrical isolation test are listed in Tables B-3 through B-6 of Appendix B. For purposes of analysis, the key results (maximum breakdown voltage, minimum breakdown voltage, and average breakdown voltage for each coupon type) are listed in Table 4-2.

TABLE 4-2. SUMMARY OF ELECTRICAL ISOLATION TEST DATA

Coupon Type	Side	Breakdown Voltage, kV		
		Maximum	Minimum	Average
A	Front	19	10	15.6
	Back	11	1	6.8
B	Front	19	12	15.2
	Back	13	5	8.6
C	Front	21	5	13.2
	Back	25	8	22.3
D	Front (with Craneglas)	25	12	18.1
	Front (without Craneglas)	23	10	15.8
	Back	25	22	24

The LSA electrical isolation requirement of ≥3000 volts DC was met in nearly every case. Only four of coupon type A (back side) failed to meet this requirement. Voltage breakdown did not occur in the back side of four type C coupons, in the front side of one type D coupon, and in the back side of ten type D coupons.

On the average, the breakdown voltages for the test specimens were in excess of 6000 volts. This result was expected, as explained below.

4.5.2 Correlation with Analytical Model

The series capacitance model (see reference 3, Section 4.2.2) is used as the basis of correlating analysis with test data. This model is illustrated in Figure 4-3 for each of the test specimens. For ease of discussion, EVA and EVA containing Craneglas will be referred to as the pottant; Tedlar, wood product, and aluminized polyester film will be referred to as covers.

When an electrical potential difference is applied across the encapsulation system, electric fields are generated within the pottant and cover layers. As the applied voltage is increased, these electric fields increase until the electric field in one of the layers exceeds the dielectric strength of the material. At this point, the layer breaks down electrically (in effect, becoming a conductor), and the entire potential difference (voltage) is thus imposed across the second layer. This sudden increase in voltage leads to a sharp increase in the electric field in the second layer. If the dielectric strength of the second layer is exceeded, complete breakdown of the encapsulation system occurs. If the dielectric strength of the second layer is not exceeded, the external voltage must be increased further to cause breakdown.

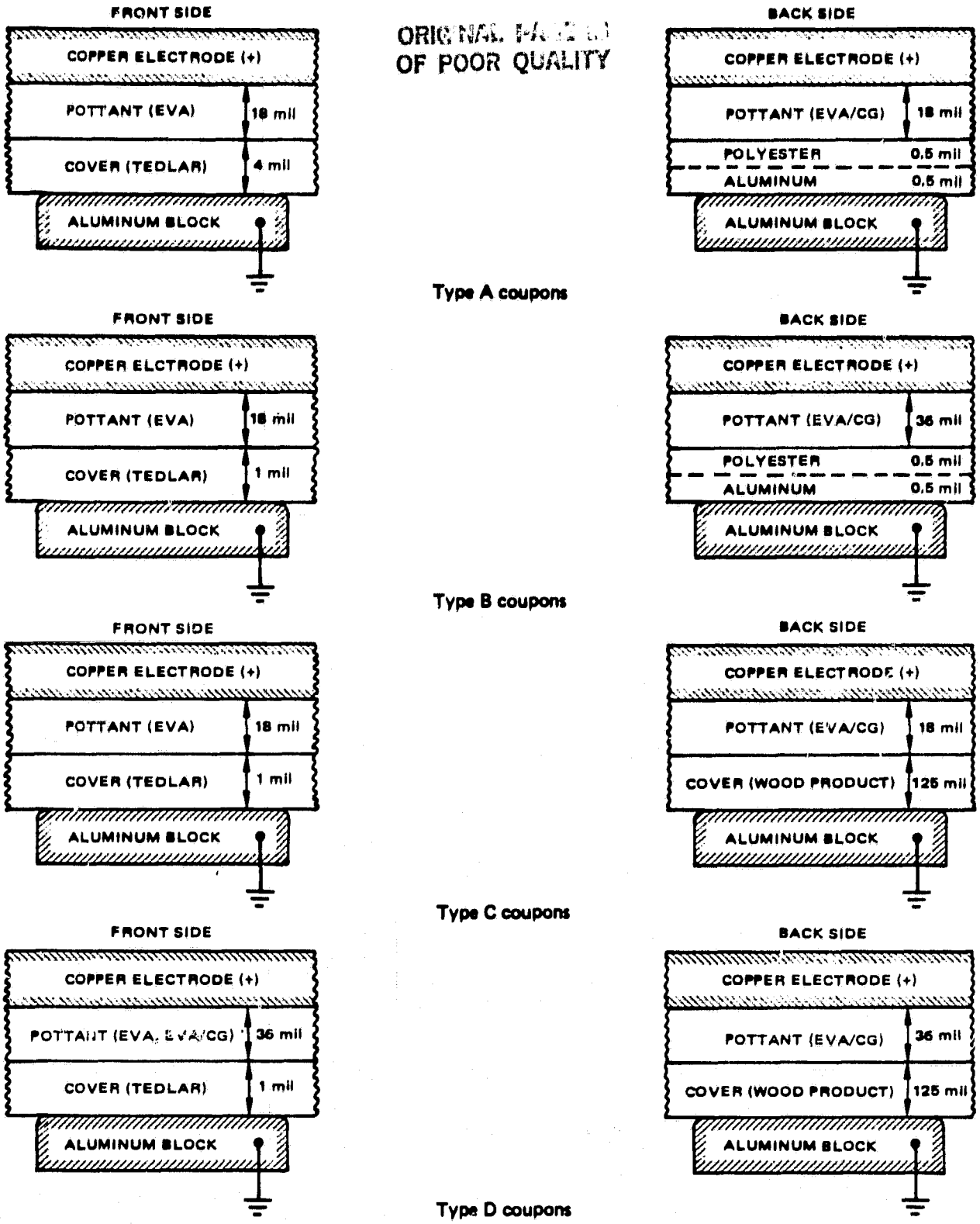

Figure 4-3. Series-capacitance analytical models for electrical isolation test specimens.

The series capacitance model is a simple one-dimensional idealization of the encapsulation system in which the internal electric field is assumed to be uniform in each layer. For the cover and pottant layers, this model yields the following relations for the corresponding electric fields:

$$E_c = \frac{V_o}{t_c + \left(\frac{\gamma_c}{\gamma_p}\right) t_p} \tag{4-1}$$

$$E_p = \frac{V_o}{\left(\frac{\gamma_p}{\gamma_c}\right) t_c + t_p} \tag{4-2}$$

where:

E_c = electric field in the cover layer, volt/mil
E_p = electric field in the pottant layer, volt/mil
V_o = electrical potential across encapsulation system, volt
t_c = cover layer thickness, mil
t_p = pottant thickness, mil
γ_p = pottant dielectric constant
γ_c = cover layer dielectric constant

Values of dielectric constant and dielectric strength are listed in Table 4–3 for the materials used in the test coupons. The properties of EVA and EVA/Craneglas are assumed to be identical. These properties were obtained from several literature sources, and the environmental conditions (i.e. temperature and humidity among others) varied from source to source. Hence, the best that can be predicted is a maximum and a minimum breakdown voltage for the two sides of each coupon type.

TABLE 4–3. ELECTRICAL PROPERTIES FOR EVA, TEDLAR, AND WOOD

Material	Dielectric Constant	Dielectric Strength, volt/mil
EVA	2.7–3.2	620
Tedlar	7.4–9.9	1700–3500
Wood Product	2.1	175

For ease of discussion, the simplest situations (coupon A back side and coupon B back side) will be dealt with first. In these cases, the 0.0005 inch thick layer of polyester is assumed to contribute nothing to the electrical isolation capability of the encapsulation system. Therefore, the entire potential difference is presumably imposed across the pottant (EVA). Here, the maximum potential difference that can be withstood by the pottant is

$$V_o = S_p t_p \tag{4-3}$$

where S_p is the dielectric strength of the pottant. The corresponding values of V_o at breakdown are then found to be:

$$V_o = 620 \times 18 = 11{,}160 \text{ volt (Type A, back side)}$$

$$V_o = 620 \times 36 = 22{,}320 \text{ volt (Type B, back side)}$$

Analysis of the back sides of coupons C and D is somewhat more involved. Here, the values of γ_p/γ_c vary from a minimum of 1.286 (= 2.7/2.1) to a maximum of 1.523 (= 3.2/2.1). In both coupon types, the maximum potential difference that can be withstood by the wood is 21875 volt (= 175 × 125). The maximum potential differences that can be withstood by the EVA in coupons C and D are 11160 volts (= 620 × 18) and 22320 volts (= 620 × 36), respectively.

The predicted, maximum breakdown voltage is found by substituting $\gamma_p/\gamma_c = 1.286$, $t_p = 18$, and $t_c = 125$ into equations 4-1 and 4-2 to yield

$$E_p = \frac{V_o}{1.286 \times 125 + 18} = \frac{V_o}{178.8} \tag{4-4}$$

$$E_c = \frac{V_o}{125 + (18/1.286)} = \frac{V_o}{139} \tag{4-5}$$

for coupon type C. Now breakdown in a material occurs when the electric field in that material exceeds the dielectric strength. Substitution of $S_p = 620$ volt/mil for E_p and $S_c = 175$ volt/mil for E_c into the above equations then yields two relations to evaluate the value of V_o at which breakdown begins. It is clear that when $V_o \geq 24325$ volt, the wood breaks down electrically and this voltage is then imposed across the EVA. Since this potential is greater than the maximum that can be withstood by the EVA (an 18-mil layer of EVA can withstand 11,160 volts), the entire encapsulation system fails electrically. The predicted, minimum breakdown voltage is found in a similar manner by substituting $\gamma_p/\gamma_c = 1.523$ into Equations (4-1) and (4-2)

$$E_p = \frac{V_o}{208.4} \tag{4-6}$$

$$E_c = \frac{V_o}{136.8} \tag{4-7}$$

For this case, wood fails electrically when $V_o \geq 23943$ volts; this potential cannot be withstood by the EVA, and therefore the entire encapsulation system fails electrically. Thus, the maximum and minimum predicted breakdown voltages for the back side of a type C coupon are 24325 volts and 23943 volts, respectively. Using a similar line of reasoning, the predicted maximum and minimum breakdown voltages for the back side of a type D coupon are 26775 volts and 26008 volts, respectively.

The front sides of the coupons are the most complex situations to analyze because of the wide range in properties for Tedlar and EVA. Here, values of γ_p/γ_c range from 0.273 (= 2.7/9.9) to 0.432 (= 3.2/7.4). The minimum and maximum potential differences that can be withstood by a 0.001-inch thick layer of Tedlar (coupon types B, C, and D) are 1700 volts and 3500 volts, respectively; for a 0.004-inch thick layer these minimum and maximum values increase to 6800 volts and 14000 volts, respectively.

For coupon type A, the minimum value of V_o at which the pottant breaks down is found by substituting the minimum value of γ_p/γ_c (= 0.273) into Equations (4–1) and (4–2)

$$E_p = \frac{V_o}{19.1} \tag{4–8}$$

$$E_c = \frac{V_o}{70} \tag{4–9}$$

Setting $E_p = S_p = 620$ in Equation (4–8), the minimum value of V_o at which breakdown occurs in the pottant is 11,837 volts. The value of E_c in the Tedlar cover just before the onset of breakdown in the pottant is found by substitution of V_o determined from Equation (4–8) into Equation (4–9); this value of E_c is 169 volt/mil, which is well below the minimum dielectric strength for Tedlar. However, once breakdown occurs in the pottant, the entire 11837-volt potential difference is imposed across the Tedlar and the corresponding value of E_c is found by substituting $V_o = 11837$ into Equation (4–9) to yield $E_c = 2959$ volt/mil, which is above the minimum breakdown voltage for Tedlar. Therefore, the predicted minimum value of V_o at which breakdown is expected to occur in the front side of coupon type A is 11837 volts.

The maximum value of V_o which the encapsulation system is expected to withstand is found by substituting the maximum value of $\gamma_p\gamma_c$ (= 0.432) into Equations (4–1) and (4–2) to give

$$E_p = \frac{V_o}{19.7} \tag{4–10}$$

$$E_c = \frac{V_o}{45.6} \tag{4–11}$$

Setting $E_p = S_p = 620$ in Equation (4–10) yields $V_o = 12231$ volts; this is the applied voltage at which breakdown is predicted to occur in the pottant for $\gamma_p/\gamma_c = 0.432$. Substitution of this value of V_o into Equation (4–11) yields $E_c = 3058$ volt/mil, which is less than the maximum dielectric strength of Tedlar. Therefore, it is possible that breakdown can occur in the pottant while the encapsulation system remains electrically intact because the entire voltage can be withstood by the Tedlar. As mentioned previously, V_o must exceed 14000 volts before the 0.001-inch thick Tedlar cover will fail electrically. Thus, the front side encapsulation system of coupon type A can withstand a maximum potential difference of 14000 volts.

A similar line of reasoning is used to evaluate the minimum and maximum values of V_o for the front side of coupon types B, C, and D. The predicted and measured values of V_o at breakdown are compared in Table 4–4.

TABLE 4–4. COMPARISON OF PREDICTED AND MEASURED VALUES OF V_o AT BREAKDOWN

Coupon Type	Side	Description	V_o at Breakdown, kV			
			Measured		Predicted	
			Max	Min	Max	Min
A	Front	4 mil Tedlar, 18 mil EVA/CG*	19	10	14	11.8
	Back	18 mil EVA/CG, 1 mil Al Polyester*	11	1	11.2	11.2
B	Front	1 mil Tedlar, 18 mil EVA/CG	19	12	11.4	11.3
	Back	36 mil EVA/CG, 1 mil Al Polyester	13	5	22.3	22.3
C	Front	1 mil Tedlar, 18 mil EVA	21	5	11.4	11.3
	Back	18 mil EVA/CG, 125 mil wood	25	8	24.3	23.9
D1	Front	1 mil Tedlar, 36 mil EVA/CG	25	12	22.6	22.5
	Back	36 mil EVA/CG, 125 mil wood	25	21	26.8	26.0
D2	Front	1 mil Tedlar, 36 mil EVA	23	10	22.6	22.5
	Back	36 mil EVA/CG, 125 mil wood	25	22	26.8	26.0

* EVA/CG = EVA with Craneglas
Al Polyester = Aluminized Polyester

4.6 DISCUSSION

The range of predicted and measured values of V_o for each coupon is plotted in Figures 4–4 and 4–5. As shown in these figures, all coupons except four samples of coupon A backside passed the LSA 3000 volt breakdown requirement.

The ranges of measured breakdown voltages were far greater than those predicted by substitution of material properties with known uncertainties in their values into the series capacitance model. The predicted breakdown voltage for the backsides of the four coupon types all fell in the high end of the range of measured breakdown voltages or outside the range altogether. In general, the predictions fell within the range of measured breakdown voltages. For those cases where the predictions fell outside the the ranges of the test results, only the predictions for the backside of coupon type B were substantially (i.e. more than 2000 volts) outside the ranges of the test results.

Predictions for encapsulation schemes with thin (i.e. 18 mils) pottant layers fell in the middle to low end of the ranges of measured breakdown voltage. The two exceptions to this observation are the backside of coupon type A and the backside of coupon type C. There is no readily apparent explanation for the backside of coupon type A. On the other hand, wood is part of the encapsulation scheme on the backside of coupon type C, and all encapsulation schemes with wood have predicted breakdown voltages either slightly above or in the high end of the ranges of measured breakdown voltages.

A comparison of the test results for the front sides of coupon types A and B indicates that, for an 18 mil layer of EVA, the thickness of the front cover does not significantly influence the breakdown voltage of the encapsulation system. For both cases, the model predicted breakdown voltages in the low end of the ranges of test results and also predicted a slight decrease in breakdown voltage as the front cover thickness was decreased.

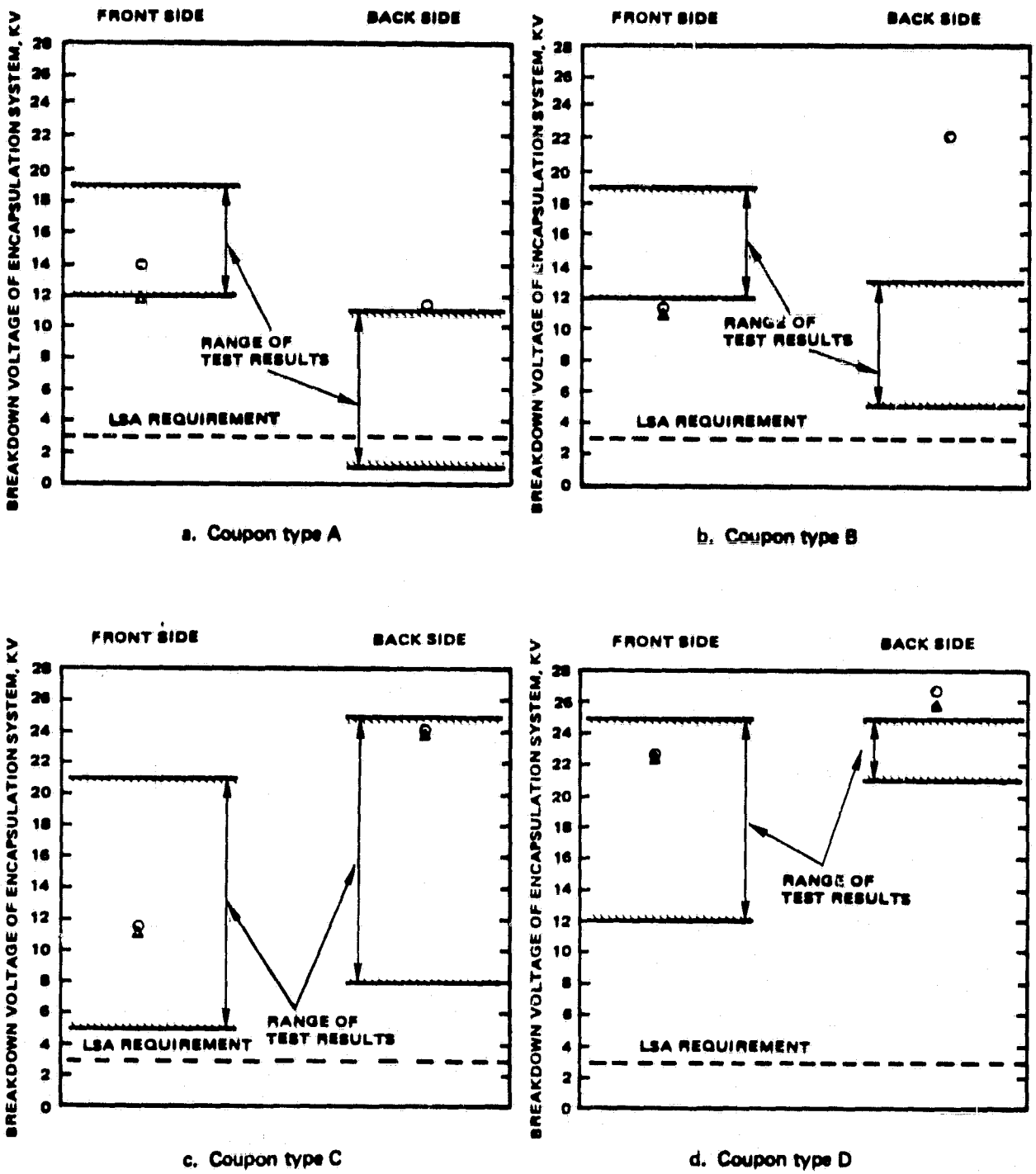

Figure 4-4. Comparison of measured and predicted values of breakdown voltage for coupon types A, B, C and D (O—predicted maximum breakdown voltage, Δ—predicted minimum breakdown voltage).

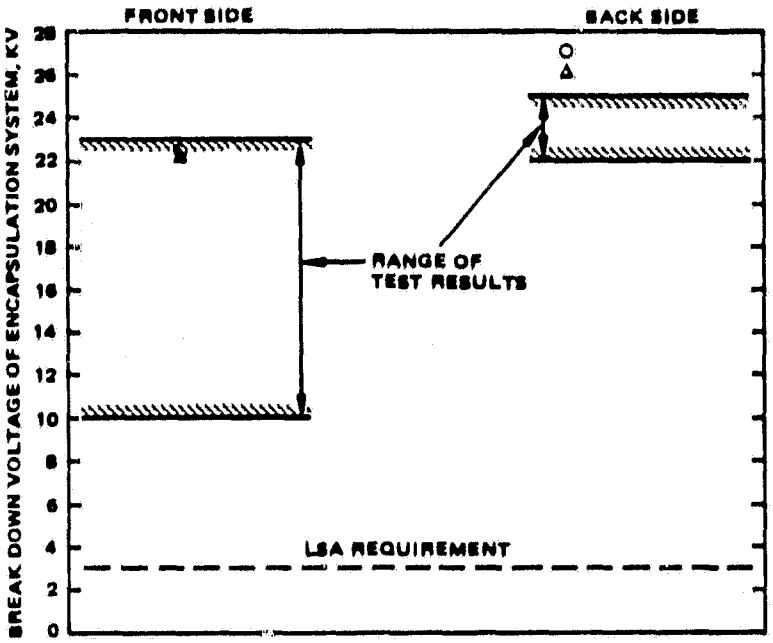

Figure 4-5. Comparison of measured and predicted values of breakdown voltage for coupon type D without Craneglas in frontside pottant layer (O—predicted maximum breakdown voltage, Δ—predicted minimum breakdown voltage).

Comparing the measured breakdown voltages for the frontsides of coupon types C and D, and the backsides of coupons A, B, C, and D indicates that doubling the pottant thickness does not double the measured breakdown voltage. The maximum measured breakdown voltage did not seem to be strongly dependent upon pottant thickness, but the minimum measured breakdown voltage did increase somewhat with increased pottant thickness. Thus, it appears that the model overpredicts the change in breakdown voltage with changes in pottant thickness. Since the dielectric strength of a material is inversely proportional to the square root of the material thickness [1], this result was not unexpected. However, lack of sufficient data at the time of this test made it impossible to evaluate this effect on the prediction of breakdown voltage.

The results for coupon type D indicate that the inclusion of Craneglas in the pottant slightly increases the electrical isolation capability of the encapsulation system.

Post failure inspection of the coupons indicated that failures always occurred at the edges of the simulated solar cells. Even though bubbles were purposely allowed to form in the pottant layers above some of the simulated cells, no failures could be attributed to the presence of the bubbles. In addition, no special attention was paid to eliminating burrs at the cell edges.

In summary, the test results have demonstrated the utility of the analytical model to predict breakdown voltages in the ranges of breakdown voltages measured for several different encapsulation schemes. The model overpredicts the changes in breakdown voltage with pottant thickness, but this can probably be rectified by modifying the model to account for the dependence of pottant dielectric strength on thickness.

5.0 THERMAL STRUCTURAL TEST

5.1 TEST OBJECTIVE

The objective of the thermal structural test was to verify the analytical models used to predict solar cell stress due to temperature excursions. The verification process consisted of measuring the temperatures and mechanical strains in the cell and in the load-bearing member for a variety of encapsulation schemes and then comparing the measured strains with predicted strains for the following parameters:

1. Thermal expansion coefficient of load-bearing member
2. Pottant thickness
3. Pottant modulus of elasticity.

5.2 TEST SPECIMENS

Twelve, one-cell coupons listed in Table 5-1 were used as test specimens for these tests. Two strain gages and two 30 gage copper/constantan thermocouples, one each on the cell and on the load bearing member, were attached to the coupons to measure strain and temperature. Etched, polycrystalline silicon wafers were used instead of finished photovoltaic cells. In addition, a bare polycrystalline silicon cell (3.93 inches square), a piece of low-iron glass (5.0 inches square), a piece of mild steel (5.0 inches square), and a piece of aluminum (5.0 inches square) were instrumented with strain gages and thermocouples to provide calibrations for the strain gages mounted on the coupons. A two-component epoxy phenolic adhesive (MB-610; Saber Enterprises, Long Beach, CA) was used to bond the strain gages to the test coupons. Curing of the adhesive was performed for one hour at 150°C and then for two hours at 160°C. The geometric layouts and the constituent material thicknesses of the coupons are illustrated in Figure 5-1.

Three different pottants were used in the fabrication of the coupons:

1 EVA (ethylene vinyl acetate)—supplied by Springborn Laboratories (Enfield, CT)
2. RTV-615 (a silicone rubber)—purchased from General Electric, Inc. (Waterford, NY)
3. Z-2341 (Polyurethane)—supplied by Development Associates (North Kingston, RI).

EVA was used in three coupons (TSC-1, 6, and 8), RTV-615 was used in five coupons (TSC-2, 3, 7, 9, and 10), and polyurethane was used in four coupons (TSC-4, 5, 11, and 12). In coupons TSC-2, 3, 4, 5, 7, 9, 10, 11, and 12, thin silicon spacers (fabricated from reject solar cells) were placed between the cell and the load-bearing member in an attempt to control pottant thickness during the fabrication process.

5.3 TEST SET-UP

A small oven was used to provide the controlled thermal environment for the test specimens. This oven provides both low (i.e. below ambient) and high temperature (i.e. above ambient) test conditions. Due to the small size of the oven, only three specimens could be tested simultaneously. A copper/constantan thermocouple was used to monitor the air temperature inside the oven.

TABLE 5-1. THERMAL STRUCTURAL VERIFICATION TEST SPECIMENS

Coupon No.	TSC-1	TSC-2	TSC-3	TSC-4	TSC-5	TSC-6	TSC-7	TSC-8	TSC-9	TSC-10	TSC-11	TSC-12
Load Bearing Member	Low-Iron Glass	Low-Iron Glass	Low-Iron Glass	Low-Iron Glass	Low-Iron Glass	Aluminum	Aluminum	Mild Steel	Mild Steel	Mild Steel	Mild Steel	Mild Steel
Pottant	EVA*	Silicone	Silicone	Polyurethane	Polyurethane	EVA	Silicone	EVA	Silicone	Silicone	Polyurethane	Polyurethane
Avg. Pottant Thickness, mil	16	6	12	5	16	15	8	19	5	11	11	15

*EVA = ethylene vinyl acetate

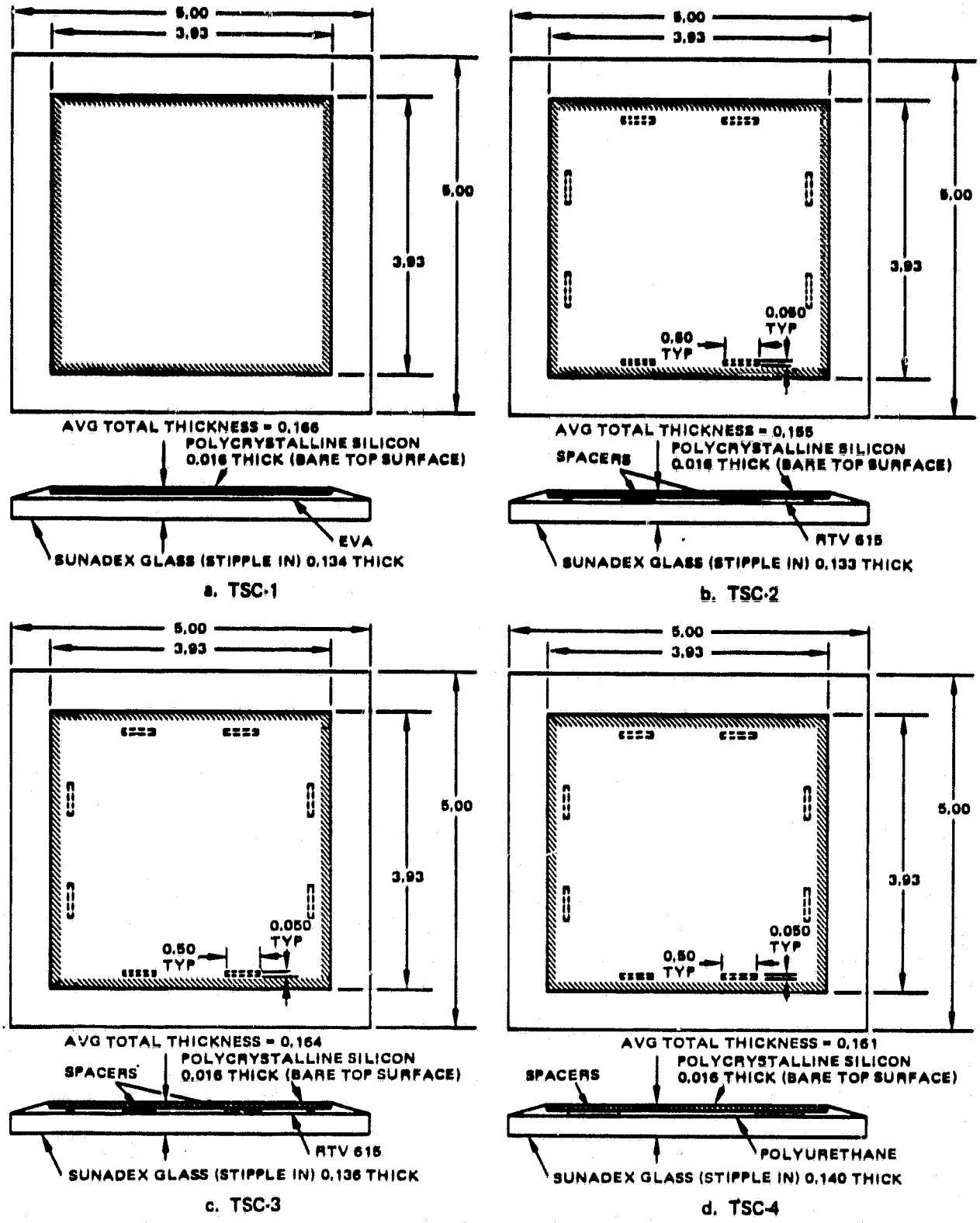

Figure 5-1. Thermal structural test coupons; dimensions in inches.

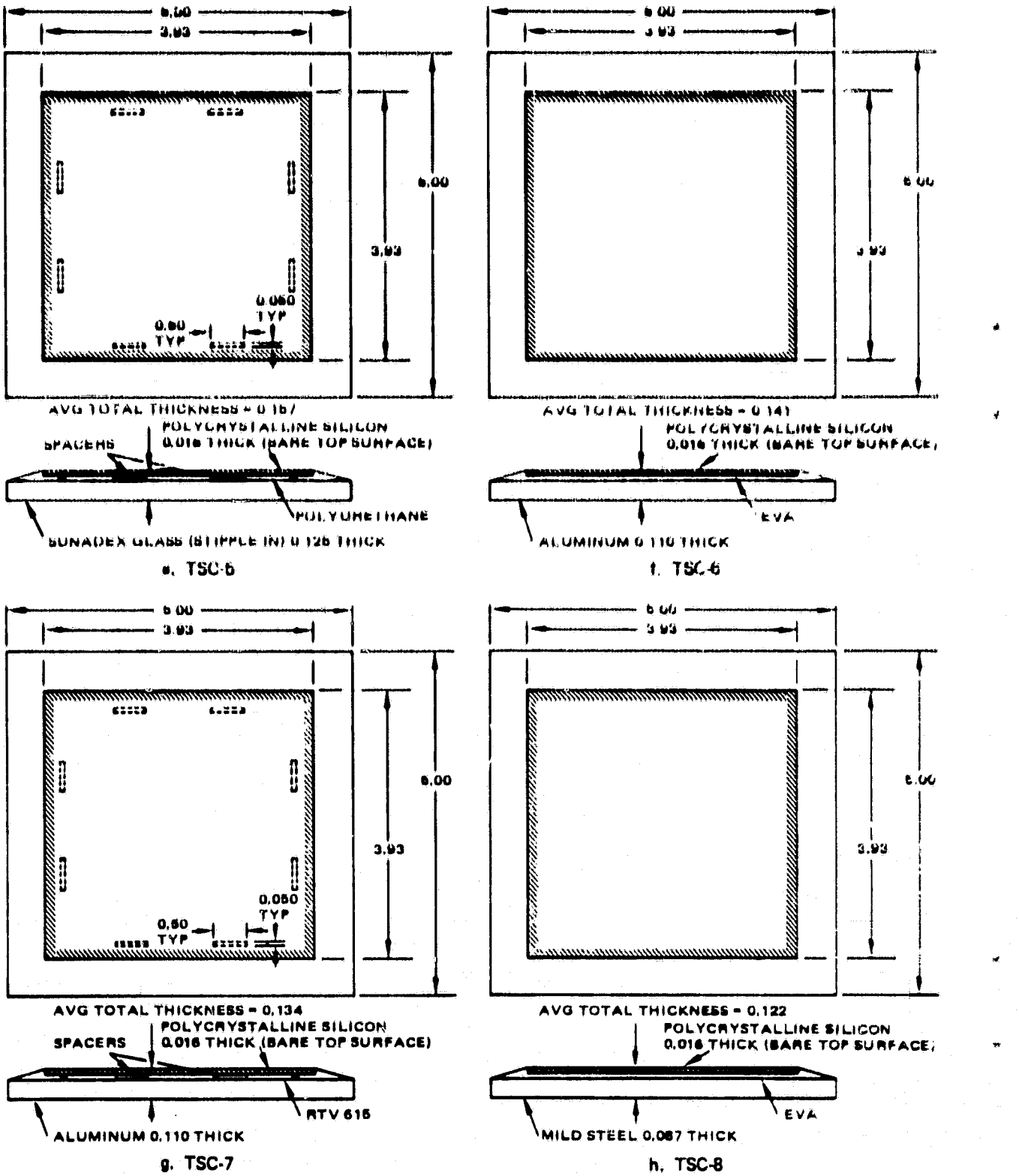

Figure 5-1. Thermal structural test coupons (continued).

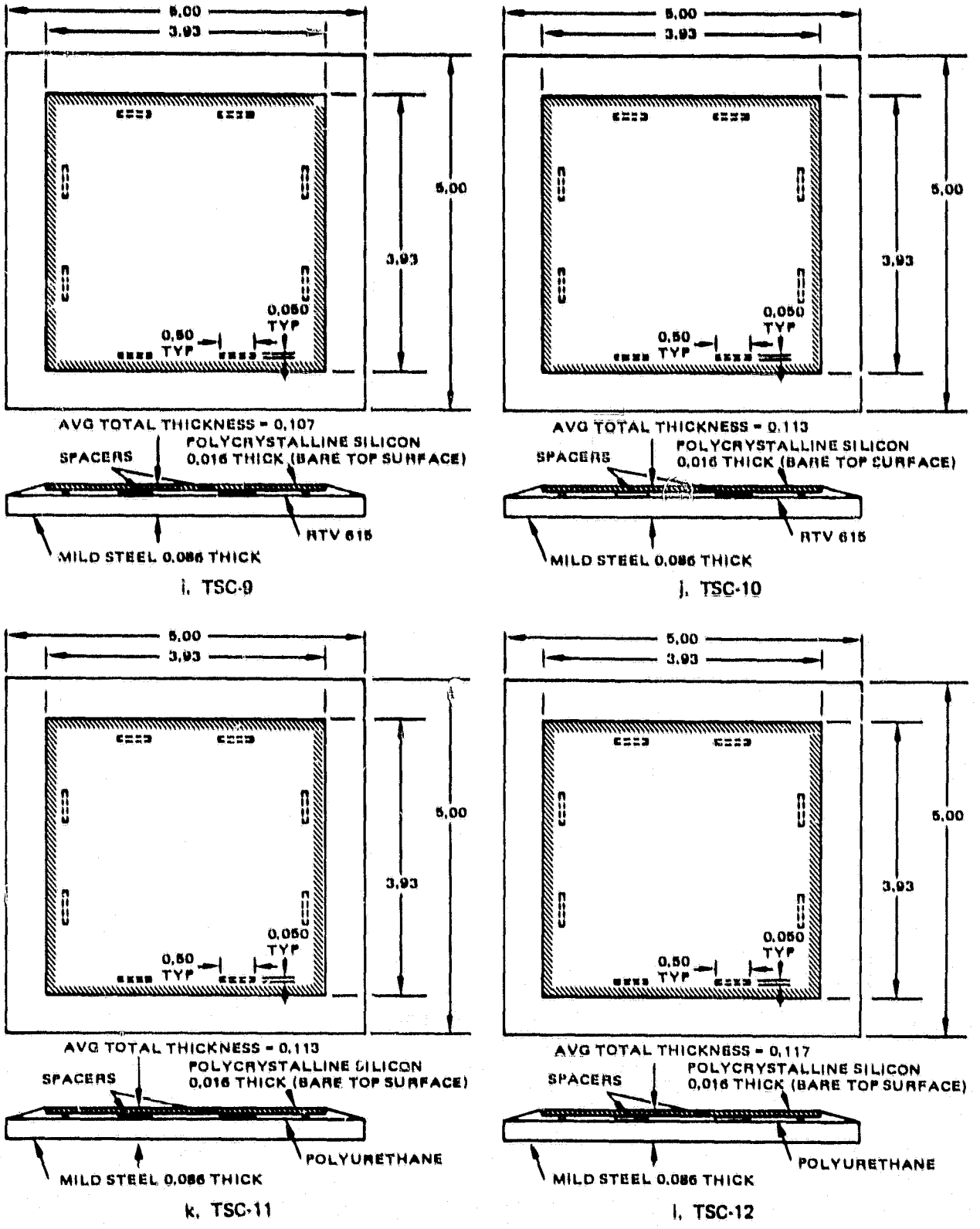

Figure 5-1. Thermal structural test coupons (continued).

Test instrumentation is illustrated in Figure 5-2. The strain indicator (shown as item 10 in Figure 5-2) converted the resistance readings (ohms) from the strain gages to units of strain (microinches per inch). A potentiometer was used to measure the millivolt readings from the thermocouples; these readings were manually converted to temperature by consulting a voltage versus temperature table for copper/constantan thermocouples.

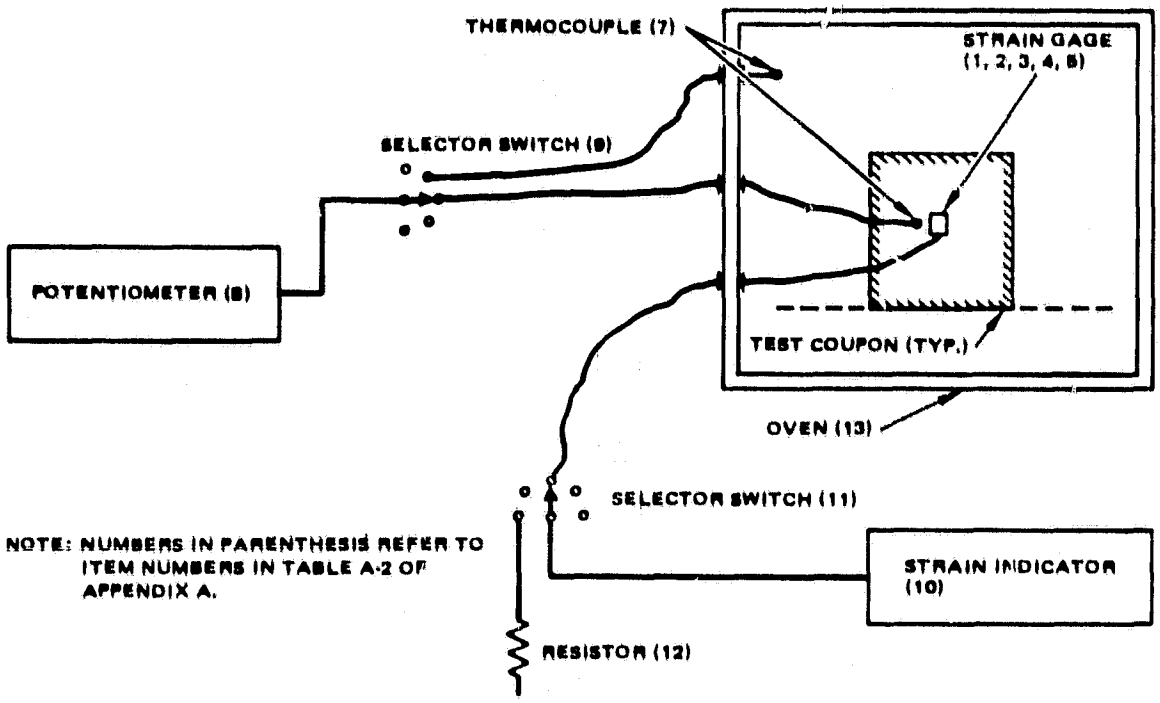

Figure 5-2. Instrumentation for thermal structural test.

Placement of three typical test coupons in the oven is illustrated in Figure 5-3, and the oven and supporting instrumentation are illustrated in Figure 5-4. Instrumentation nameplate data are found in Table A-2 of Appendix A.

5.4 TEST CONDITIONS

5.4.1 Normal Test Sequence

In the first series of measurements, coupons TSC-2, 3, 4, 5, 7 , 9, 10, 11, and 12 were subjected to an environment where the air temperature in the oven was cycled through the following sequence:

$$\text{ambient} \rightarrow 40^\circ\text{C} \rightarrow 60 \rightarrow 80 \rightarrow 100 \rightarrow 80 \rightarrow 60 \rightarrow 40 \rightarrow 20 \rightarrow 0 \rightarrow -20 \rightarrow -40 \rightarrow -20 \rightarrow 0^\circ\text{C} \rightarrow \text{ambient}$$

The temperature at each step was maintained for approximately five minutes to ensure temperature equalization between the test specimens and the air circulating in the oven.

Strain measurements were first obtained for the plain glass, silicon, aluminum, and steel specimens. These "apparent strain" measurements were used as a reference for subsequent strain measurements obtained with the test coupons.

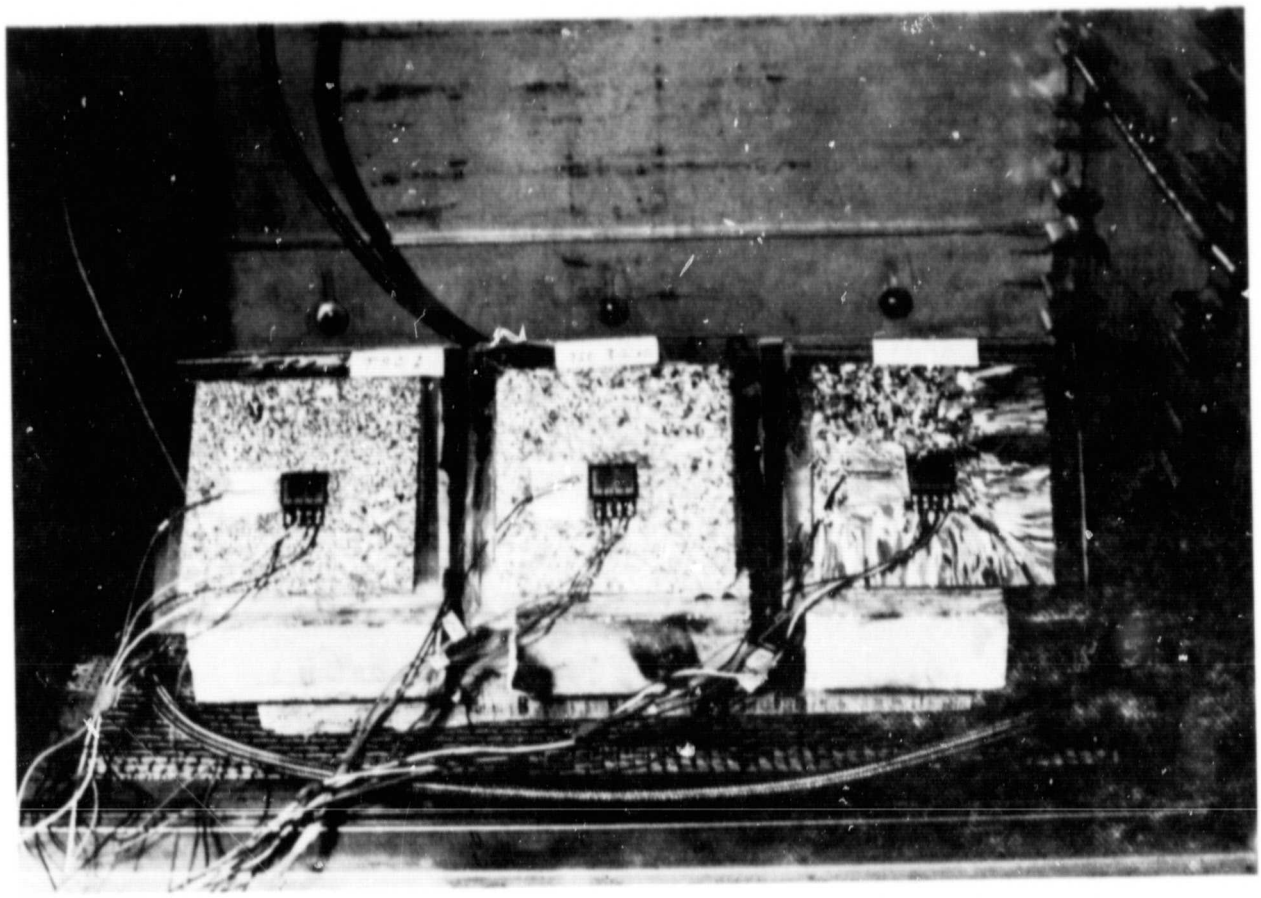

Figure 5-3. Three typical test coupons placed in oven for thermal structural test.

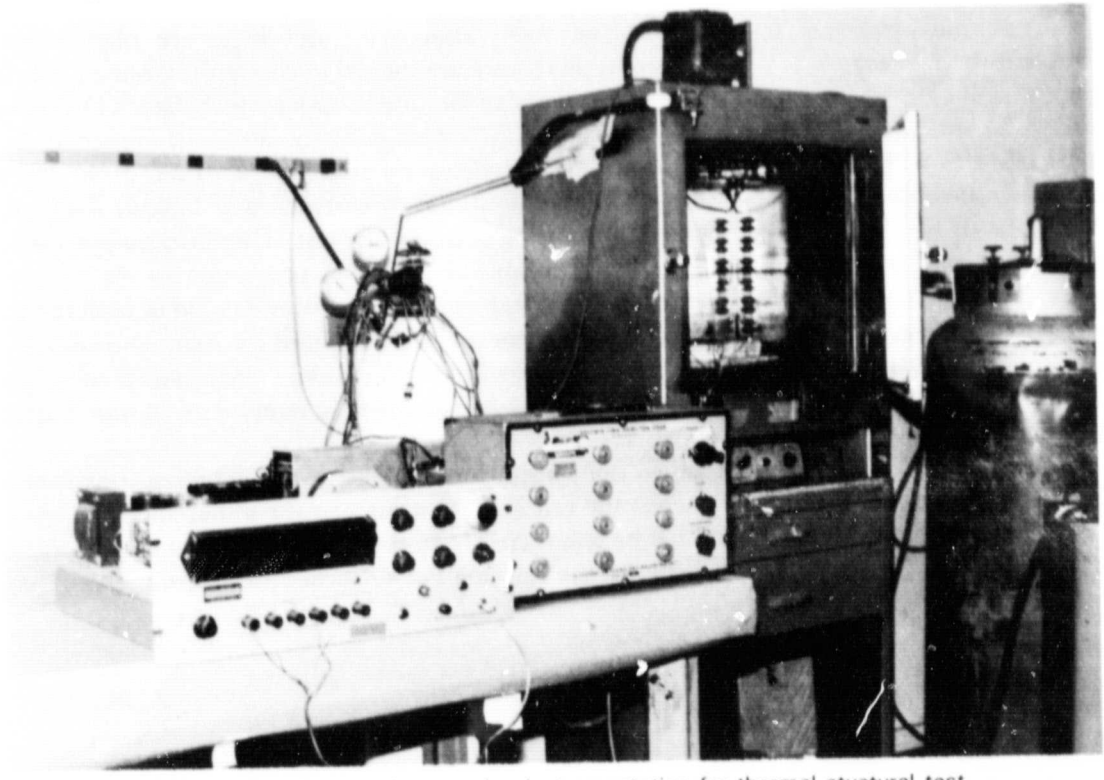

Figure 5-4. Oven and supporting instrumentation for thermal stuctural test.

5.4.2 Overstress Test Sequence

In this series of measurements, coupons TSC-1, 6, and 8 were subjected to an environment where the air temperature in the oven was cycled through the following temperature sequence:

ambient → 40°C → 60 → 80 → 100 → 120 → 140 → 120 → 100 → 80 → 60 → 40 → 20 → 0
→ −20 → −40 → −60 → −40 → −20 → 0°C → ambient

The temperature at each step in this sequence was maintained for approximately 5 minutes to ensure temperature equalization between test specimens and the air circulating in the oven. The lowest temperature of this sequence is approximately 20°C below the glass transition temperature of ethylene vinyl acetate (EVA).

As in the normal test sequence, the "apparent strain" measurements were obtained before obtaining strain measurements with the test coupons.

5.5 DATA ANALYSIS

5.5.1 Apparent Strain Data

When strain gage is bounded to a panel which undergoes a temperature excursion, a strain is induced in the gage even when the panel undergoes free expansion or contraction. Ideally, there should be no mechanical strain when the thermal expansion of the panel material is unrestrained. This "apparent strain" is caused by the different thermal expansion coefficients (i.e. "thermal mismatch") of the gage, the adhesive, and the panel material. The apparent strain is highly non-linear with respect to temperature and must be determined for each gage/panel combination at every temperature of interest. Strain gages are selectively matched to the panel material to minimize the apparent strain. However, the apparent strain is zero (i.e. zeroed out by the strain indicator; see Figure 5-2) only at a single, arbitrary temperature (ambient temperature for this test).

Strain measurements for plain silicon, steel, aluminum, and glass are plotted against temperature in Figure 5-5. Also plotted in this figure are the strain curves provided by the strain gage manufacturer. The following conclusions can be drawn from these data: (1) measured strains for the plain specimens are non-linear with respect to temperature, as expected; (2) the measured strains differ significantly from the manufacturer's data; (3) the strains in the two axes differ significantly for each biaxial strain gage; and (4) the measured strains indicate the presence of significant hysteresis during the heating/cooling cycles of the test. The different strains along orthogonal axes may be due to thermal orthotropy (i.e. different properties for the two orthogonal directions) of the strain gages, of the coupon materials, or a combination of both the strain gages and coupon materials. The strain measurements were averaged for each temperature and subsequently adjusted such that the average measured strain versus temperature curve passes thru zero at 25°C. The adjusted strain for a plain specimen is referred to as the "apparent strain".

When a test coupon is subjected to temperature excursions, the resultant strains consist of those due to thermal mismatch between the cell and substrate and the apparent strain. At each temperature, the apparent strain must be subtracted from the measured strain to determine the strains due only to the mismatch between the cell and the substrate materials.

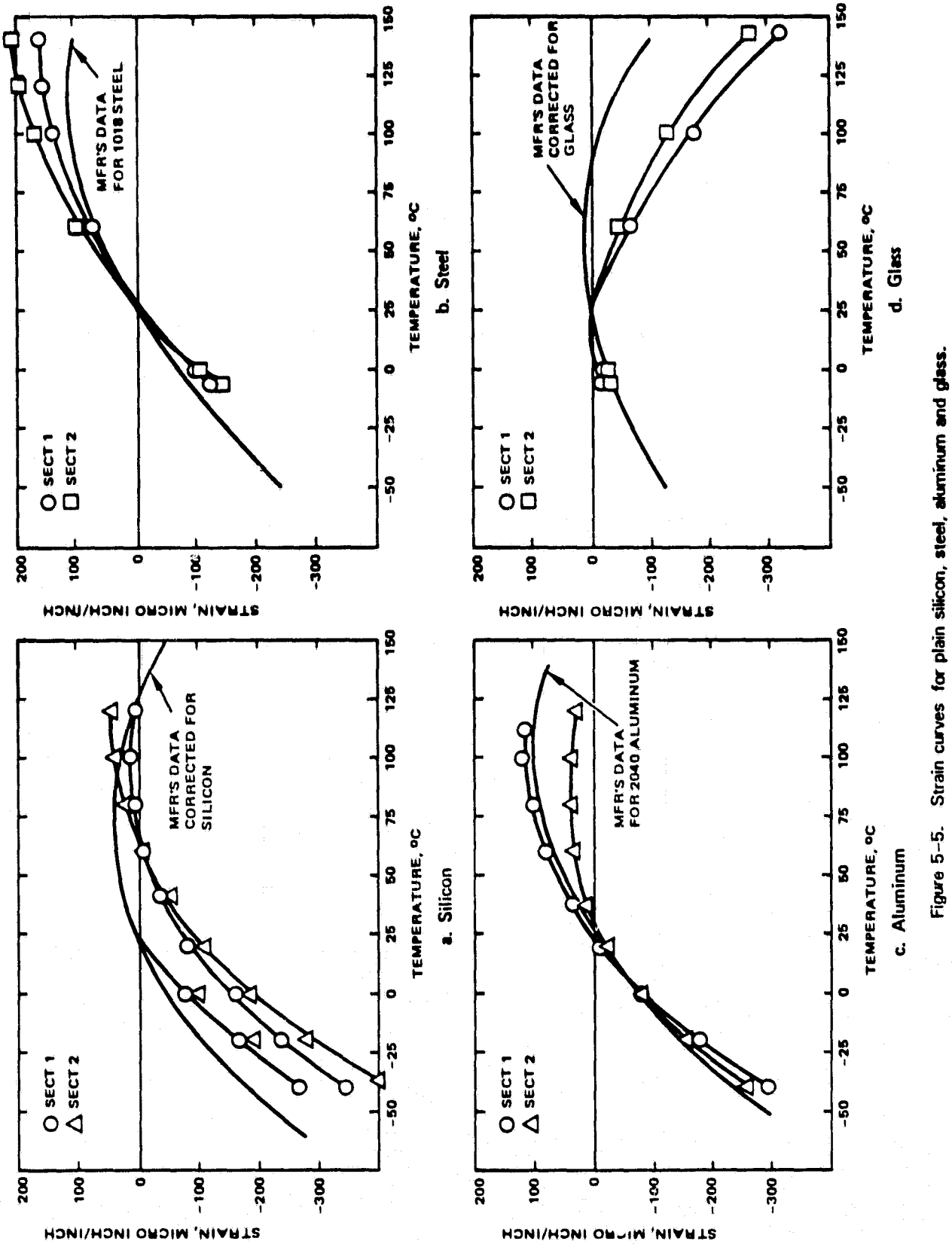

Figure 5-5. Strain curves for plain silicon, steel, aluminum and glass.

5.5.2 Test Coupon Data

Measured cell strains for test coupons with EVA, silicone, and polyurethane pottants are listed in Tables 5-2, 5-3, and 5-4 respectively. The biaxial strains measured by each strain gage were recorded on separate channels of the strain indicator, designated as sections 1 and 2. These data include apparent strains of the coupon materials, and for convenience the apparent strains for silicon at each temperature are listed in the tables. As with the plain silicon, aluminum, glass, and steel specimens, the strains measured on the coupons were adjusted to give zero strain at ambient temperature.

TABLE 5-2. MEASURED STRAINS IN SILICON CELLS FOR COUPONS WITH EVA

Temperature, °C	Measured Strain, μin/inch							
	Plain Silicon		Alum. Substrate		Glass Substrate		Steel Substrate	
	Sec. 1	Sec. 2	Sec. 1	Sec. 2	Sec. 1	Sec. 2	Sec. 1	Sec. 2
−40	−275	−320	−403	−334	−241	−301	−350	−308
−20	−165	−190	−196	−156	−120	−145	−195	−189
0	−75	−100	−97	−74	−55	−63	−110	−118
20	0	0	0	0	0	0	0	0
40	10	25	48	50	10	26	55	69
60	20	40	44	56	15	47	66	89
80	20	50	24	57	4	49	62	85
100	10	50	10	54	−18	33	73	98
Structural Index = $\alpha_{substrate}$ $(E/t)_{pottant}$			1240		460		453	
Pottant Thickness, mil			15		16		19	
Coupon ID			TSC-6		TSC-1		TSC-8	

The coupons are rank ordered with respect to a structural index, which is listed at the bottom of each column in the tables. This structural index, which is the product of the substrate* thermal expansion coefficient (α) and pottant modulus of elasticity (E) divided by the pottant thickness (t), indicates the expected ranking of each coupon with respect to cell strain. A high value of structural index indicates a high expected value for cell strain, etc. Room temperature material properties were used to determine the indices. Note that cell strain is not linear with respect to structural index; the indices are useful only to rank order the coupons with respect to cell strain.

*The term substrate as used here means a flat panel of the same material used in the load-bearing member of a module.

TABLE 5–3. MEASURED STRAINS IN SILICON CELLS FOR COUPONS WITH SILICONE

Temperature, °C	Measured Strain, μin/inch											
	Plain Silicon		Alum. Substrate		Steel Substrate		Glass Substrate		Steel Substrate		Glass Substrate	
	Sec. 1	Sec. 2	Sec. 1	Sec. 2	Sec. 1	Sec. 2	Sec. 1	Sec. 2	Sec. 1	Sec. 2	Sec. 1	Sec. 2
−40	−275	−320	−248	−285	−274	−312	−342	−347	−299	−301	−203	−252
−20	−165	−190	−145	−172	−165	−195	−194	−197	−190	−202	−108	−139
0	−75	−100	−60	−83	−70	−120	−96	−94	−95	−100	−60	−78
20	0	0	0	0	0	0	0	0	0	0	0	0
40	10	25	36	69	45	34	45	55	42	52	16	21
60	20	40	50	85	40	56	75	103	48	58	12	40
80	20	50	26	99	25	53	86	129	33	51	−14	45
100	10	50	12	101	13	58	110	170	28	64	−28	32
Structural Index = $\alpha_{substrate}(E/t)_{pottant}$			1544		1080		828		486		395	
Pottant Thickness, mil			8		5		6		11		12	
Coupon ID			TSC-7		TSC-9		TSC-2		TSC-10		TSC-3	

TABLE 5–4. MEASURED STRAINS IN SILICON CELLS FOR COUPONS WITH POLYURETHANE

Temperature, °C	Measured Strain, μin/inch									
	Plain Silicon		Glass Substrate		Steel Substrate		Steel Substrate		Glass Substrate	
	Sec. 1	Sec. 2	Sec. 1	Sec. 2	Sec. 1	Sec. 2	Sec. 1	Sec. 2	Sec. 1	Sec. 2
−40	−275	−320	NA	NA	−455	−442	NA	NA	NA	NA
−20	−165	−190	NA	NA	−273	−273	NA	NA	NA	NA
0	−75	−100	−65	−76	−100	−100	−65	−86	−60	−67
20	0	0	0	0	0	0	0	0	0	0
40	10	25	14	36	36	30	9	47	38	37
60	20	40	22	39	29	55	11	59	40	52
80	20	50	13	48	13	56	−16	77	37	56
100	10	50	−6	39	1	58	−37	67	43	50
Structural Index = $\alpha_{substrate}(E/t)_{pottant}$			1021		486		356		285	
Pottant Thickness, mil			4		11		12		5	
Coupon ID			TSC-4		TSC-11		TSC-12		TSC-5	

The coupon strains are generally comparable in magnitude to the apparent strains. This means that the apparent strains are large compared to the strains resulting from the thermal mismatch between the cells, pottants, and substrates. In some cases the coupon strains are less than the apparent strains in absolute value. This result appears to contradict the expectation that a cell is in compression for temperatures below ambient (negative temperature excursions) and in tension for temperatures above ambient (positive temperature excursions). For example, in Table 5-2 the strain in section 2 of coupon TSC-8 is -308 μin/in at $-40°$C. The apparent strain at $-40°$C is -320 μin/in, which implies that the cell is in tension. A possible explanation for this discrepancy is that the apparent strain is different for each silicon cell and thus different for each coupon.

Another factor to consider is the accuracy of the strain gages and the measurement system. Metal foil, resistance-type strain gages are usually accurate to within $\pm$ 1 μinch/inch. When the entire strain measurement system, including gages, wires, amplifiers, and indicators is taken into account, the accuracy is estimated to be within ± 5 percent of the measured value. Thus for a measured strain of 300 μinch/inch, the estimated measurement error is ± 15 μinch/inch.

5.5.3 Comparison of Test Results with Analytical Predictions

In Phase 1 of the program, the effects of different pottant and substrate combinations on cell stress were studied analytically by means of finite element models [3]. These models assumed temperature-invariant material properties and a *linear* relationship between stress and strain. The key results of the studies are

1. The silicon cell is strained when there is a mismatch between the cell and the substrate thermal expansion coefficients. The cell is in compression for negative temperature excursions and in tension for positive temperature excursions.
2. For the same pottant parameters (i.e. thickness and modulus of elasticity) the cell is most strained by an aluminum substrate, less so by a steel substrate, and least strained by a glass substrate.
3. The cell strain is attenuated when the pottant is designed to accommodate the thermal mismatch between the cell and the substrate. In effect, when the pottant is made more flexible by decreasing the modulus of elasticity (or increasing pottant thickness in some cases), the cell strain decreases. Conversely, as the pottant is made stiffer by increasing the modulus of elasticity (or decreasing the thickness in some cases), the cell strain increases.

To eliminate the influence of material property uncertainties, comparisons are made between coupons with the same substrate and pottant materials. Also the properties at $-40°$C are probably the most reliable for predicting cell strain, because the pottants are stiffer at that temperature than at higher temperatures. Therefore, the cell strain due to thermal mismatch between cell, pottant, and substrate should be highest at that temperature. At elevated temperatures, the pottant moduli decrease, and the resultant cell strains decreased accordingly.

In Table 5-2, which lists the results for coupons with EVA, none of the coupons have the same substrate material. However, coupon TSC-6 (aluminum substrate) was expected to have the highest cell strain, and this is so indicated by the data for $-40°$C. On the other hand, coupon TSC-8 (steel substrate) exhibits higher cell strains at higher temperatures, assuming that the silicon cells for both coupons have the same apparent strain versus temperature relationship.

In Table 5-3, comparisons can be drawn between the steel substrate coupons, TSC-9 and TSC-10, and between the glass substrate coupons TSC-2 and TSC-3. TSC-9 was expected to exhibit a higher cell strain than TSC-10; however, at −40°C the cell strains are about the same. As predicted, TSC-2 exhibits a higher cell strain than TSC-3. TSC-7, which has an aluminum substrate, was expected to exhibit higher cell strains than the other coupons with silicone pottant. However, the results indicate that the cell strain is relatively low in TSC-7.

In Table 5-4, which is for coupons with polyurethane pottant, meaningful comparisons cannot be made because cell strains were measured for only one coupon at −40°C.

Analytical predictions were made for coupons TSC-1, 2, 7, and 9 using material properties evaluated at room temperature. The analytical predictions, the corresponding test results, and the structural indices are shown in Table 5-5. These results were determined by subtracting the apparent strains from the coupon strains and then averaging the results for sections 1 and 2 of the strain gages. The structural index ranking is consistent with the analytical predictions, and there is good agreement between analysis and test data for TSC-2. There is poor agreement between analysis and test data for coupons TSC-1, 7, and 9.

TABLE 5-5. THERMAL STRUCTURAL TEST RESULTS AND ANLYSIS PRECITIONS

Test Specimen	Description	Analytical Stress, psi at −40°C	Predicted** Strain, μin/in at −40°C	Measured Strain, μin/in at −40°C	S.I.*
TSC-1	Glass/EVA	−462	−27	+27	460
TSC-2	Glass/Silicone	−762	−45	−47	828
TSC-7	Alum./Silicone	−3156	−186	+31	1544
TSC-9	Steel/Silicone	−1110	−65	+5	1080

* S.I. = Structural Index = $\alpha_{substrate}\,(E/t)_{pottant}$

** Material properties evaluated at room temperature

A cell strain of −186 μinch/inch was predicted for coupon TSC-7. The expected value of measured strain at −40°C (including apparent strain) was about 500 μinch/inch. The maximum measurement inaccuracy was therefore expected to be about 25 μinch/inch. However, since the measured coupon strain was about half the expected value, it is concluded that some factor, which remains unknown at present, other than the accuracy of measurement system must be influencing the test results.

5.6 DISCUSSION

Some correlation was seen between the test results and the trends predicted by analysis. In general, there was poor agreement between analysis and test. The factors which probably contributed most this lack of correlation were: (1) the large values of apparent strain compared to strain resulting from thermal mismatch, and (2) the accuracy of the strain measurement system. In some cases, the large apparent strains gave rise to expected cell strains (i.e. those strains due to thermal mismatch) comparable in magnitude to the inaccuracy of the measurement system. However, in the case of coupon TSC-7 (an aluminum substrate coupon), the expected strains were large but were twice the value of the measured strains; both the expected and measured strains were large compared to the inaccuracy of the measurement system.

Uncertainties in material properties also contributed to the discrepancies between analysis and test data. Properties that require verification are the thermal expansion coefficient of polycrystalline silicon and pottant modulus of elasticity versus temperature.

The trends predicted by the analytical model appear to be reasonable and conservative, but the test results are inconclusive with respect to verification of the analytical model. A limited retest with a "stiff" pottant is recommended; the modulus of this pottant should be greater than 10^4 psi.

6.0 STRUCTURAL DEFLECTION TEST

6.1 TEST OBJECTIVE

The objective of the structural deflection test was to verify the analytical models used to predict solar cell stress, load-bearing layer stress, and module deflection that result from a uniform pressure load on the module surface. The verification process consisted of measuring module deflection, stress in the solar cell, and stress in the load-bearing member for the following parameters:

1. Pottant thickness
2. Ribbed versus unribbed wood substrates
3. Pottant modulus of elasticity
4. Normal pressure load
5. Cell location
6. Load-bearing member material and thickness.

6.2 TEST SPECIMENS

Nine three-cell modules listed in Table 6-1 were used as specimens for these tests. The geometric layouts and the constituent material thicknesses for each module are illustrated in Figure 6-1. Etched, polycrystalline silicon wafers were used rather than finished photovoltaic cells. Three of these unfinished cells were bonded to each test module. A silicone pottant, RTV 615, was used to bond the cells to the load-bearing members of modules SDM-1, SDM-2, and SDM-5 through SDM-9. Polyurethane was used to bond the cells to the load-bearing members of modules SDM-3 and SDM-4. Thin silicon spacers were inserted between the cells and the load-bearing member of each module in an attempt to control pottant thickness during the fabrication process. Two strain gages were associated with each cell position on a module; one strain gage was bonded to the bare surface of the cell, and the other was located opposite the cell and bonded to the anti cell side of the load-bearing member. The wood ribs on modules SDM-7 and SDM-9 were bonded to the wood substrates with structural epoxy (Epiphen ER-825-A, Haven Industries, Inc., Philadelphia, PA).

The thickness of the load-bearing member for several test modules varied considerably, as shown in Figure 6-1. Here, thicknesses measured approximately two inches and 10 inches in from the edges of the module are shown in ellipses.

Edge frame details are shown in Figure 6-2. Due to limited availability of materials, two four-foot lengths of each aluminum extrusion shown in this figure were used to protect the edges of a module during test.

6.3 TEST SET-UP

The fixture used to support a module during this test is shown in Figure 6-3. This fixture is about 48 inches square in horizontal cross-section and was fabricated from a surplus trash container. A four-foot square test module rests on four steel angle bars, which are bolted to the inside periphery of the container. A uniform pressure load is applied to the test module by filling the upper portion (i.e. above the test module) with water. The water is contained within a large plastic bag made of 6-mil thick polyethylene. The fixture is pivoted on one edge, and a load cell is

TABLE 6-1. SPECIMENS FOR STRUCTURAL DEFLECTION VERIFICATION TEST

Module No.	SDM-1	SDM-2	SDM-3	SDM-4	SDM-5	SDM-6	SDM-7	SDM-8	SDM-9
Load Bearing Member	Low-iron Glass	Low-iron Glass	Low-iron Glass	Low-iron Glass	Plain Wood Product	Plain Wood Product	Ribbed Wood Product	Mild Steel	Ribbed Wood Product
Pottant	Silicone	Silicone	Polyurethane	Polyurethane	Silicone	Silicone	Silicone	Silicone	Silicone
Pottant Thickness, mil	10	22	6	15	10	18	9	10	21

ORIGINAL PAGE IS
OF POOR QUALITY

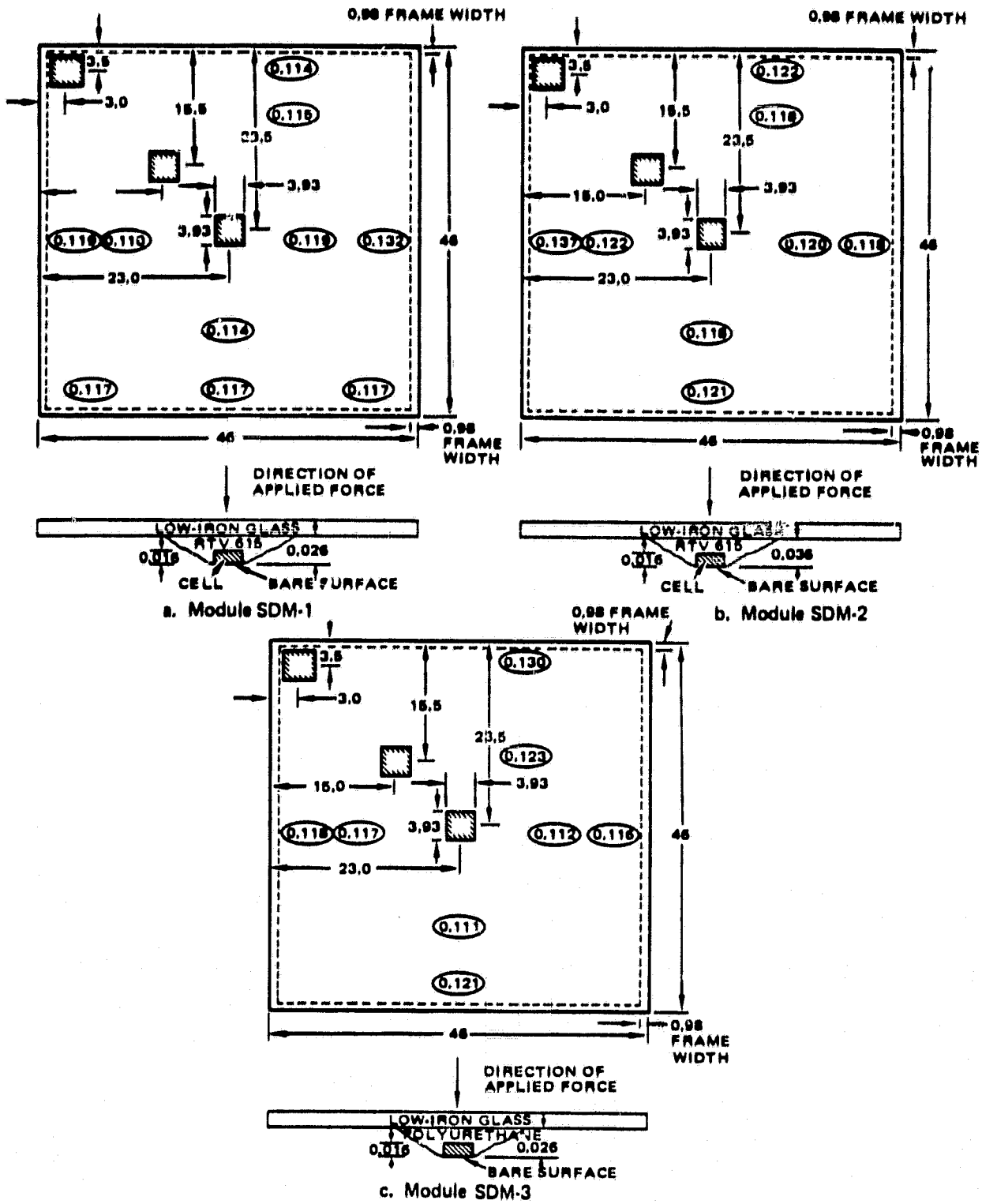

Figure 6-1. Structural deflection test specimens; dimensions in inches and load-bearing member thicknesses shown in ellipses.

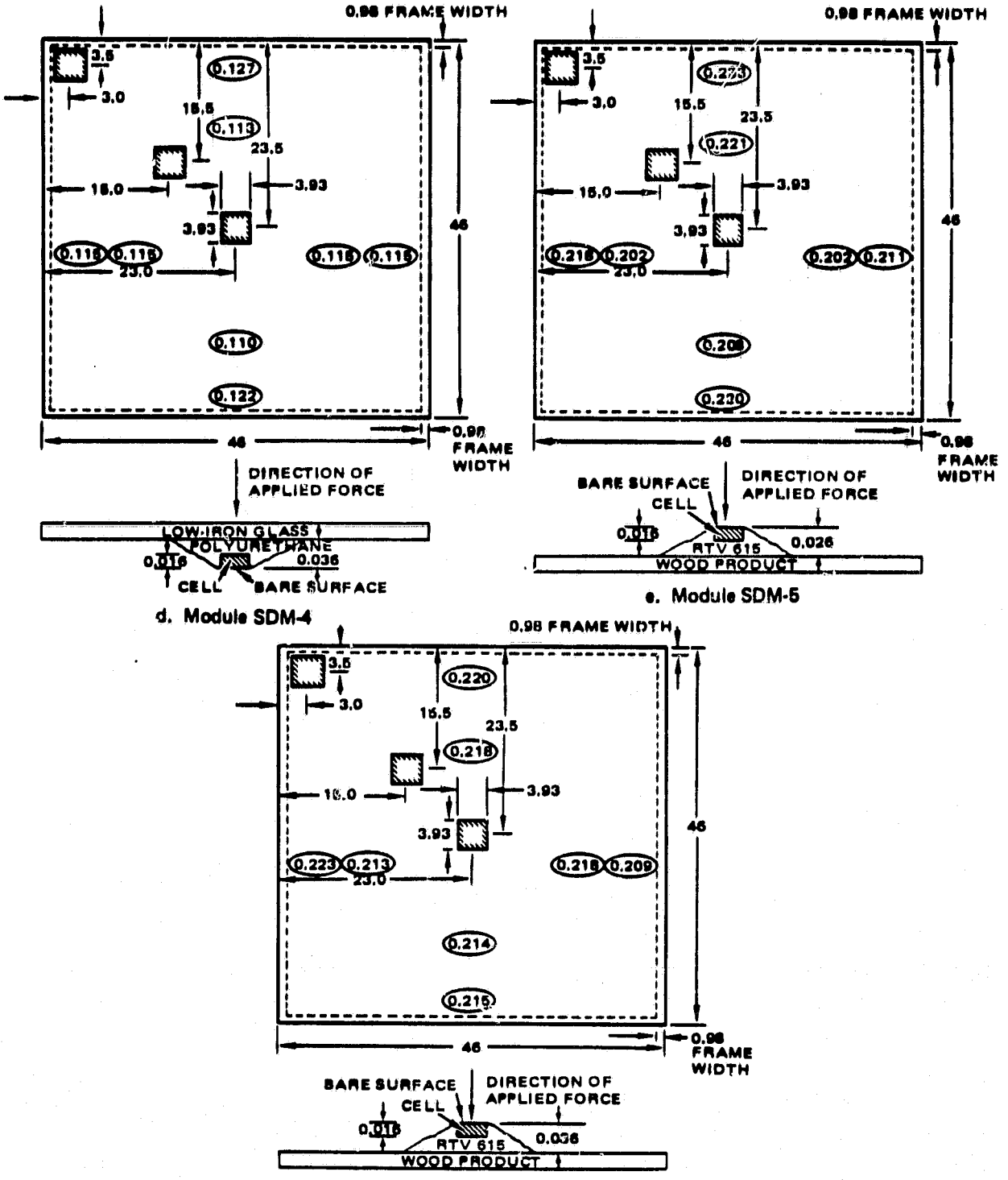

d. Module SDM-4

e. Module SDM-5

f. Module SDM-6

Figure 6-1. Structural deflection test specimens (continued).

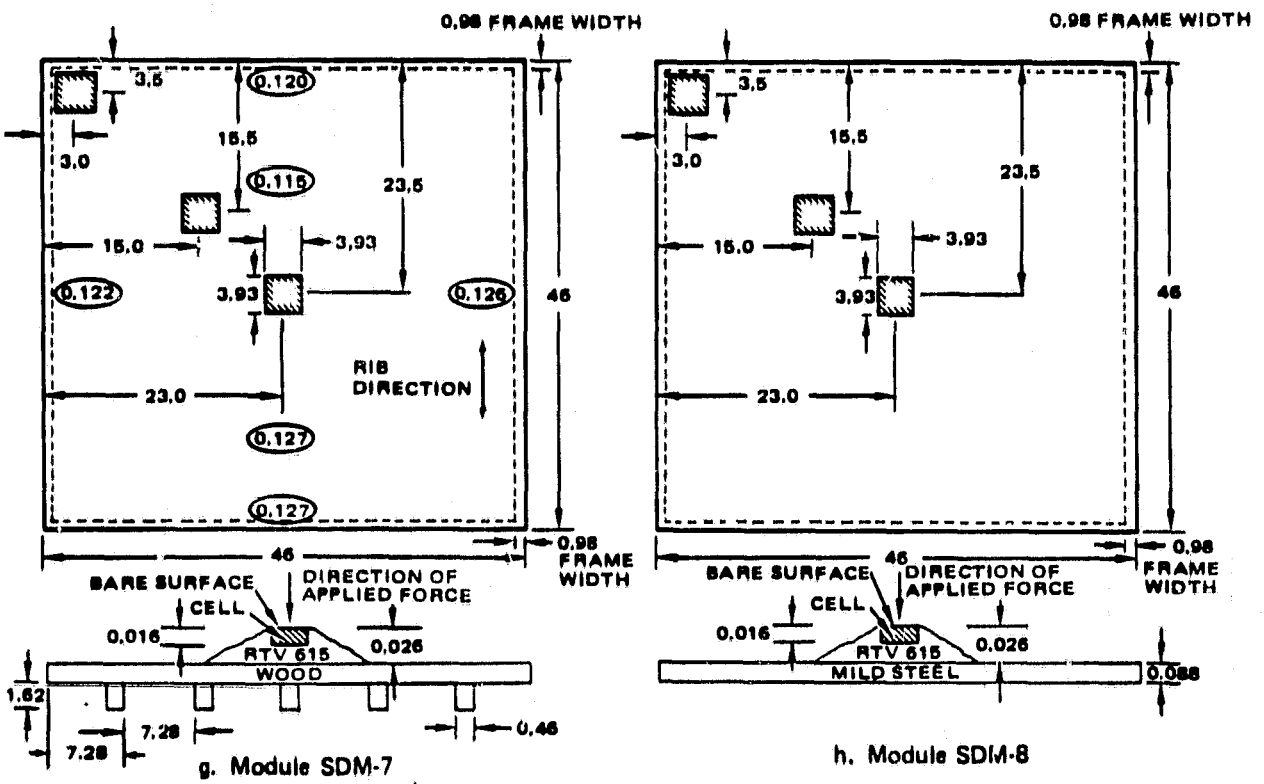

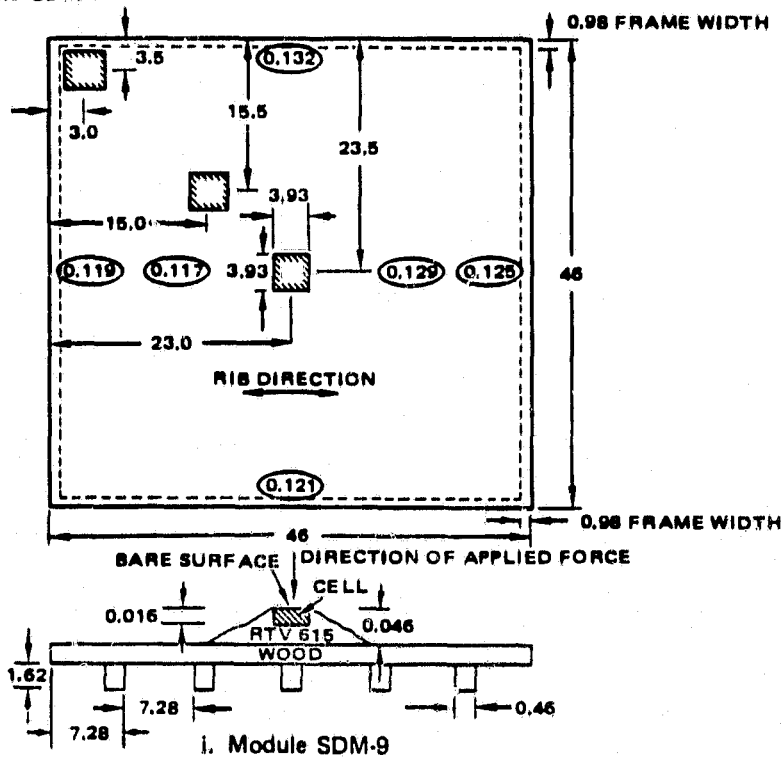

Figure 6-1. Structural deflection test specimens (concluded).

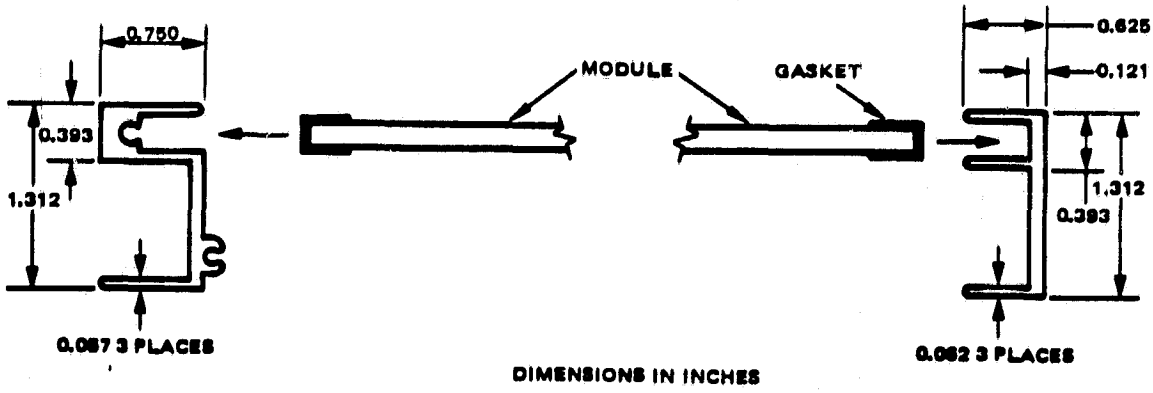

Figure 6-2. Module edge frame details.

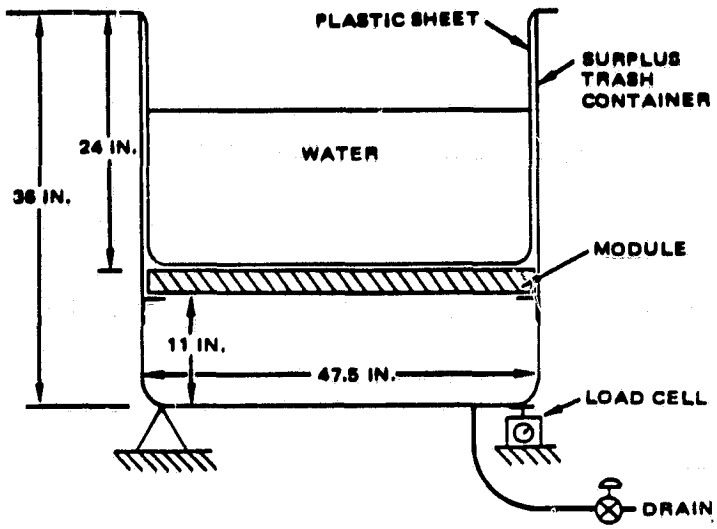

Figure 6-3. Test fixture for structural deflection test.

used to determine the weight of the water, which is directly proportional to the pressure load on the test module, in the apparatus. The fixture with a module in place is shown in Figure 6-4.

Instrumentation of the test apparatus is illustrated in Figure 6-5. The numbers shown in parentheses in this figure refer to equipment item numbers listed in Table A-3 of Appendix A.

Test measurements consisted of total load (i.e. the weight of the water) on the module, module deflection at three locations, and strain gage resistance. Strain gage resistance was converted to units of strain (microinches per inch) by the strain indicator. Load versus deflection curves were generated by the X-Y plotter, which was connected to the load cell and the transducers at the center cell and mid-diagonal cell positions. A dial indicator was used to measure module deflection at the corner cell position. Ports cut into the side of the test fixture permitted access to the transducers and dial indicator.

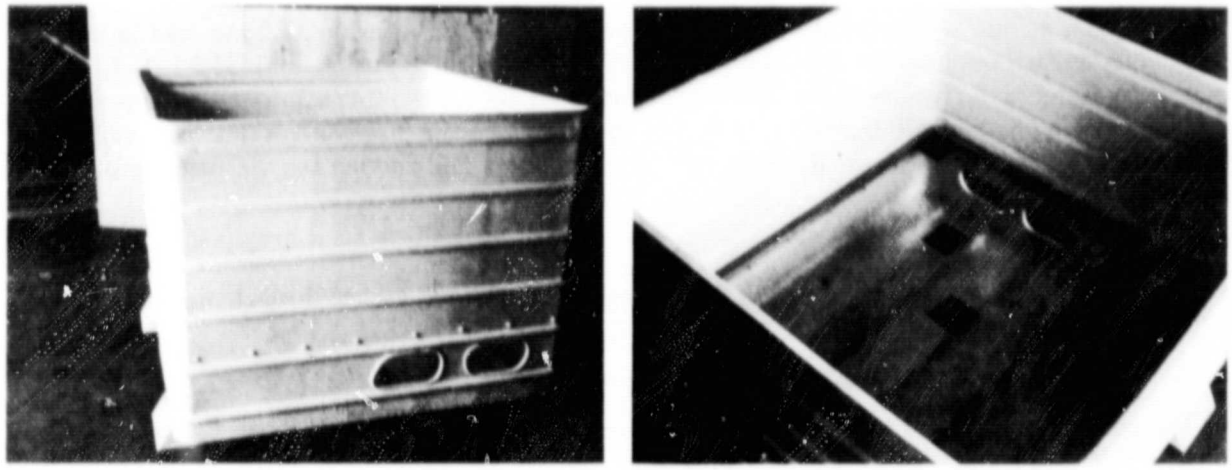

SIDE VIEW SHOWING ACCESS PORTS

MODULE IN PLACE

Figure 6-4. Test fixture for structural deflection test.

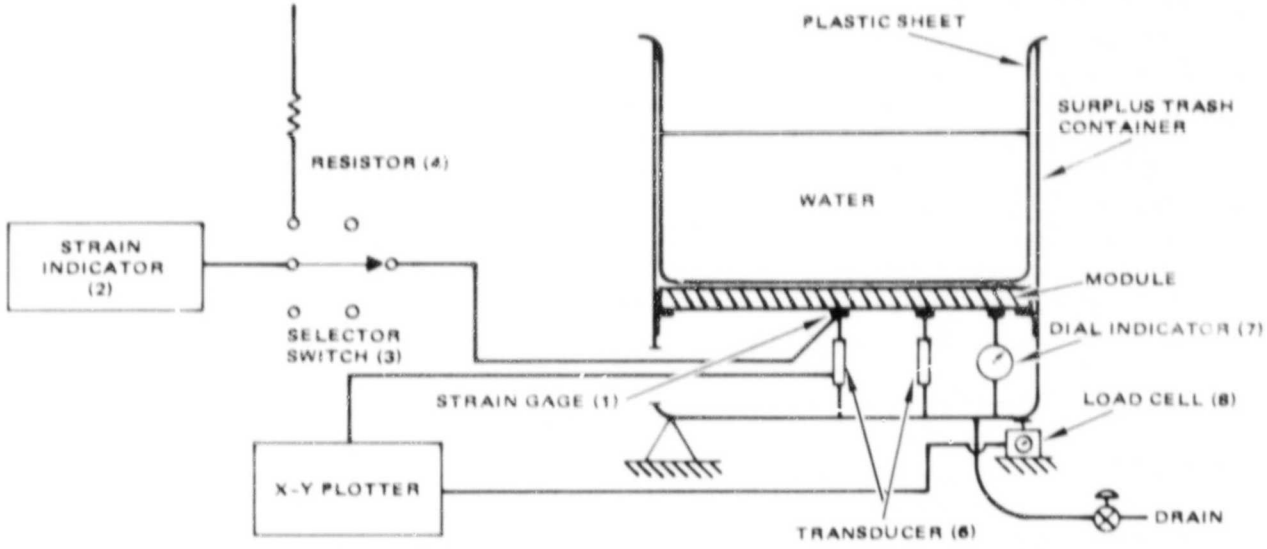

NOTE: NUMBERS IN PARENTHESIS REFER TO ITEM NUMBERS IN TABLE A-3 OF APPENDIX A

Figure 6-5. Instrumentation for structural deflection test.

6.4 TEST CONDITIONS

6.4.1 Normal Test

In the normal test, all modules were cycled through the following pressure sequence

$$0 \rightarrow 10 \rightarrow 20 \rightarrow 30 \rightarrow 40 \rightarrow 50 \rightarrow 40 \rightarrow 30 \rightarrow 20 \rightarrow 10 \rightarrow 0 \text{ psf}$$

Total load, module deflection at the three cell positions, and strain in the cell and load-bearing member at each cell location were measured at each pressure step. For modules SDM-1, 3, and 4, the cells faced the bottom of the test fixture. For modules SDM-5 through SDM-9, tests were performed with the cells facing upward (i.e. the cells were on the water side). For module SDM-2, one test was performed for the cells facing upward, and another test was performed for the cells facing downward.

6.4.2 Overstress Test

In the overstress test, modules SDM-6 and SDM-8 were cycled through the following pressure sequence

$$0 \rightarrow 25 \rightarrow 50 \rightarrow 75 \rightarrow 100 \rightarrow 75 \rightarrow 50 \rightarrow 25 \rightarrow 0 \text{ psf}$$

The cells faced upward during these tests. As in the normal tests, the total load, strains, and deflections were recorded for each pressure step.

6.5 DATA ANALYSIS

6.5.1 Load-Bearing Layer Deflection and Stress

Plots of load versus deflection for the test specimens are shown in Figures B-1 through B-14 of Appendix B. For purposes of discussion, Figures B-7 and B-14 are presented in this section as Figures 6-6 and 6-7, respectively. Strains measured for the cells and load bearing member of each test specimen are listed in Tables B-28 through B-41.

As expected, the ribbed wood modules (SDM-7 and SDM-9) were the only modules that deflected linearly with load; all other modules, including SDM-6 (plain wood), deflected nonlinearly with load. This behavior is shown in Figures 6-6 and 6-7, which are for modules SDM-9 (ribbed wood) and SDM-5 (plain wood), respectively.

The apparent stiffness of the unribbed modules increases as the load and subsequent deflection increase. This behavior is due to "membrane action" (i.e. a spanwise stretching of the modules) and becomes a significant factor when the deflection exceeds one half of the module thickness. This nonlinear behavior causes the load-bearing member deflection and stress for a given load to be less than the deflection and stress predicted by linear theory [13] which does not account for membrane action.

The ribbed wood modules, on the other hand, exhibit linear behavior. This behavior was expected because the module deflections were less than one half of the thickness of an unribbed plate of equivalent stiffness. Note that SDM-7 failed at a load of 30 psf because of local stress concentrations in the module at the ends of the ribs, which were not supported by the test fixture. This failure is discussed in more detail in Section 6.6.

Test data and analytical predictions for module deflection and stress in the load-bearing layer are summarized in Table 6-2. Deflections are listed for the center of each module. The stresses for the glass superstrate modules, SDM-1 through SDM-4, are listed for the top corner surface. The stresses for the other test specimens, which are substrate module designs, are listed for the bottom center surface. These deflection and stress locations were chosen to permit correlation with analysis predictions which were derived from curves developed by JPL [10]. The analysis predictions were based on an unsupported edge distance of 44 inches (the module length of 46 inches minus a one-inch edge interface for the angle bar supports in the test fixture) and the average thicknesses listed in Table 6-2. Thickness for the glass and wood test specimens varied considerably, and at least 10 thickness measurements were taken for each module to obtain the averages listed.

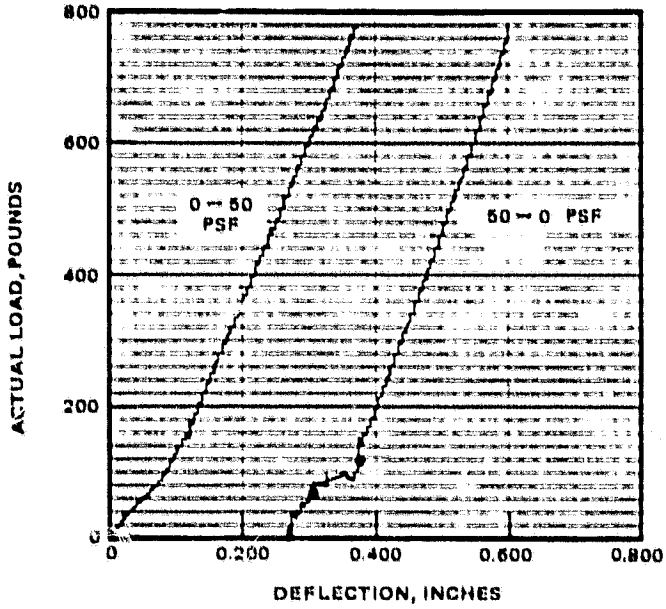

Figure 6-6. Linear load versus deflection curve (module SDM-9, rib ends supported).

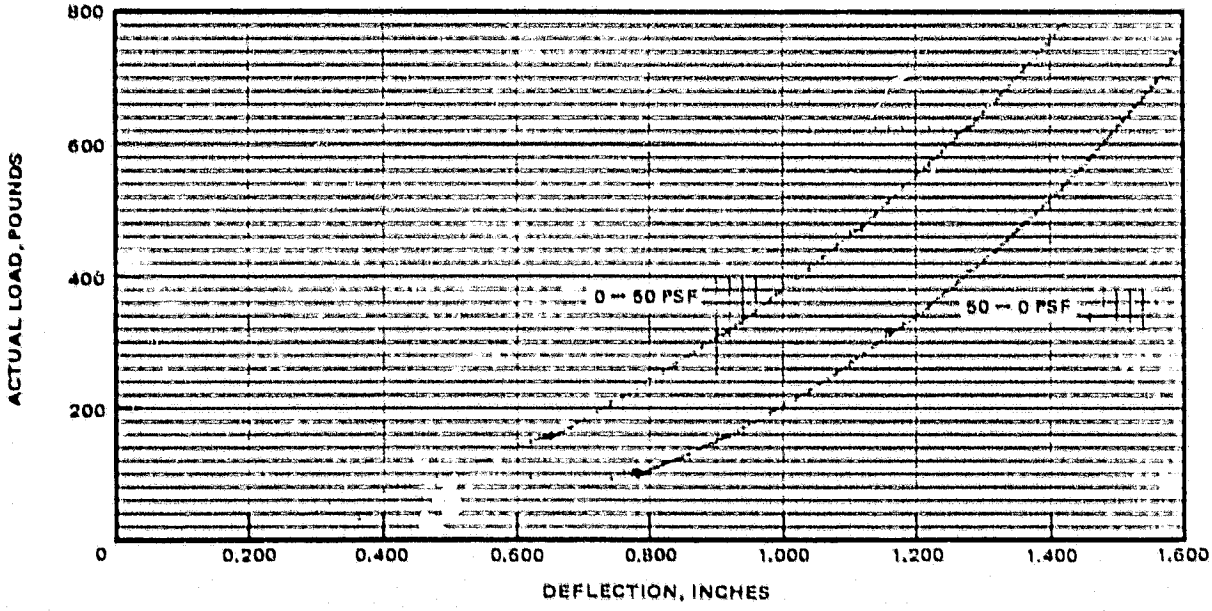

Figure 6-7. Nonlinear load versus deflection curve (module SDM-6, plain wood).

TABLE 6–2. SUMMARY OF TEST RESULTS AND ANALYTICAL PREDICTIONS FOR DEFLECTION AND STRESS IN THE LOAD-BEARING MEMBER OF A MODULE

Test Module	Description	Average Thickness, inches	Deflection,* inches			Stress,** psi		
			Test	Analysis	Δ, Percent	Test	Analysis	Δ, Percent
SDM-1	Glass Superstrate	0.115	0.615	0.67	+8.2	3216	5381	+40.2
2	Glass Superstrate	0.120	0.62	0.65	+4.6	4571	4946	+7.6
3	Glass Superstrate	0.116	0.61	0.67	+8.9	2571	5100	+49.6
4	Glass Superstrate	0.121	0.59	0.65	+9.2	2749	4236	+35.1
5	Plain Wood Substrate	0.208	1.42	1.33	−6.8	817	752	−8.6
6	Plain Wood Substrate	0.216	1.36	1.27	−7.1	766	741	−3.4
7	Ribbed Wood Substrate	0.123	Failure	—	—	—	—	—
8	Steel Substrate	0.088	0.42	0.5	+16.0	2357	4395	+46.4
9	Ribbed Wood Substrate	0.124	0.37	0.36	−2.8	NA	NA	NA

Deflection and stress @ 50 PSF pressure loading.

$$\Delta = \frac{\text{Analysis-Test}}{\text{Analysis}} \times 100$$

*All deflections are for the center cell position

**Stresses for glass superstrate modules are for corner cell position. Stresses for substrate modules are for center cell position.

The test results and analysis predictions for module deflection agree to within 10 percent for all modules except SDM-8, the steel substrate module. The analysis predictions for the glass superstrate modules are high by 4.6 to 9.2 percent. The analysis predictions for the unribbed wood modules, SDM-5 and SDM-6, are low by 6.8 and 7.1 percent, respectively. The best agreement between analysis and test was exhibited by the ribbed wood specimen (SDM-9), which agreed to within 2.8 percent.

The steel substrate module exhibited the greatest discrepancy between analysis and test; the analysis prediction was 16 percent higher than the test result. This result is surprising since the steel module was expected to correlate best with analysis predictions. The thickness of the steel was uniform and the modulus of elasticity of the steel should be about $29\text{–}30 \times 10^6$ psi as listed in the literature.

Stresses were determined by substituting measured strains into the following equations [ref. 2, p. 424]:

$$\sigma_1 = \frac{E}{1 - \nu^2}(\epsilon_1 + \nu\epsilon_2) \tag{6-1}$$

$$\sigma_2 = \frac{E}{1 - \nu^2}(\epsilon_2 + \nu\epsilon_1) \tag{6-2}$$

Here σ_1 and σ_2 are the principal stresses associated with the strains ϵ_1 and ϵ_2 measured along perpendicular axes. Values for Poisson's ratio, ν, were 0.29, 0.30, 0.22, 0.29, and 0.40 for glass, steel, wood, silicon, and pottant, respectively. Poisson's ratio for glass was assumed to equal that of silicon.

The test results and analysis predictions for load bearing layer stress indicate much greater discrepancies than the deflection results. Except for the wood modules, the test results were lower than analysis predictions by 35 to 50 percent. The test results and predictions for SDM-2 agreed to within 7.6 percent. There was good correlation between analysis and test for the wood modules; the analysis predictions were low by 8.6 and 3.4 percent for SDM-5 and SDM-6, respectively.

The relatively poor correlation between analysis and test for the glass superstrate specimens is not surprising. According to the previously cited JPL study [ref. 10], a high stress gradient exists at the corners of the modules where these comparisons were made. The analysis predictions were for the maximum principal stress at the top surface of the glass. It is quite possible that the strain gages were not located at the points of maximum stress. More extensive monitoring of the strain distributions in the vicinity of the corners of the specimens might reveal better correlation.

The stress distributions at the bottom center of the modules, according to the JPL study, are fairly uniform. Therefore, the strain gage location is not as critical for the substrate modules as it is for the glass superstrate modules. Consequently, the substrate specimens should show good agreement between analysis and test. The unribbed wood modules do show good correlation. However, the steel substrate specimen shows a discrepancy of 46 percent. The explanation for this is not apparent.

6.5.2 Solar Cell Stress

The silicon cell strains and maximum principal stresses for a uniform 50 PSF normal load are listed in Table 6-3. For convenience, the module deflections are also listed. The following conclusions can be drawn from the data:

1. Cell stress was highest for the unribbed wood substrate modules.
2. Cell stress was lowest for the glass superstrate modules.

TABLE 6–3. SUMMARY OF MEASURED STRAINS AND PRINCIPAL STRESSES IN SILICON CELLS

Test Module	Load Bearing Layer	Pottant		Measured Strain (μin/in)		Maximum Principal Stress, psi	Maximum Panel Deflection, inches	Comments*
		Material	Thickness, mil	Channel 1	Channel 2			
SDM-1	Glass	Silicone	10	26	25	607	0.62	All cells good
2	Glass	Silicone	22	34	24	770	0.62	Corner cell cracked, others good
3	Glass	Polyurethane	6	8	19	399	0.61	Corner cell suspect
4	Glass	Polyurethane	15	33	20	729	0.59	Corner cell cracked, others good
5	Wood	Silicone	10	73	49	1638	1.42	Corner cell cracked, center cell suspect
6	Wood	Silicone	18	126	124	3036	1.36	Corner cell good, others suspect
8	Steel	Silicone	10	44	35	1018	0.42	All cells good
9	Wood	Silicone	21	12	63	1244	0.37	All cells good

*Cracked cells were damaged during fabrication and handling. No cells were cracked during the test.

3. The cell stress for the steel module was higher than that of the glass modules, although the steel module deflection was less.

4. With the exception of SDM-9, the maximum cell strains and load bearing layer strains occurred at the corner locations. This is a very significant result in that, for modules with nonlinear load versus deflection characteristics, the maximum cell strains occurred at the locations of maximum strains in the load bearing members, rather than in the centers of the modules, where the maximum deflection occurred. In the case of SDM-9, which was the only module with linear load versus deflection characteristics (excluding SDM-7 which failed prematurely), the maximum cell strain also occurred at the location of maximum strain in the load bearing member. However, consistent with linear theory [13], the point of maximum strain and deflection occurred at the center of the load bearing member of SDM-9.

5. The maximum cell stresses at 50 psf loading are well below the 8000 psi allowable stress for silicon established during Phase 1.

These results were consistent with the Phase 1 analysis predictions. It should be noted that no cells were damaged during the tests. However, several cells, such as the corner cells of SDM-3 and SDM-5 were cracked before testing, and the results for these modules should be considered suspect. There also appeared to be a high void fraction in the pottant for the glass superstrate modules. Although it was impossible to inspect the pottant in the steel and wood substrate modules, the void fraction in the pottant was probably high in these modules as well. These factors may explain why the cell stress for SDM-1 was less than that for SDM-2, which contradicts the analytical predictions. A cracked cell may be the reason why the cell stress for SDM-5 is less than that for SDM-6, which, again, is contrary to the analytical predictions.

The test results and analysis predictions for the ratio of load bearing layer strain to cell strain (at 50 psf loading) are summarized in Table 6-4. Test specimens SDM-3 and SDM-5 were not analyzed and are therefore not included in the table. Clearly, the analysis predictions for the superstrate modules (SDM-1, 2, and 4) are low by approximately a factor of two. Analysis

TABLE 6-4. SUMMARY OF TEST RESULTS AND ANALYSIS PREDICTIONS OF THE RATIO OF LOAD BEARING LAYER STRAIN TO CELL STRAIN

Test Module	Ratio of Load Bearing Layer Strain to Silicon Cell Strain		
	Test Results	Analysis Prediction	Δ, Percent
SDM-1	8.8	4.2	−110
2	10.7	4.8	−123
4	10.7	4.8	−123
6	5.4	7.0	+23
8	3.2	3.4	+6
9	6.2	7.0	+11

$$\Delta = \frac{\text{Analysis-Test}}{\text{Analysis}} \times 100$$

predictions for the substrate modules (SDM-6, 8, and 9) are high by 6 to 23 percent. This result suggests that the discrepancies are due to the effects of the membrane effect mentioned earlier and will be discussed in more detail in Section 6.6.2. This hypothesis is supported by test data. The superstrate module SDM-2 was tested with the glass side down as well as with the glass side up. Consistent with analysis predictions, the cell strain changed sign but had approximately the same magnitude in both cases. The average glass strain, however, was $-320\ \mu in/\mu$ with the glass side up and $+133\ \mu in/in$ with the glass side down. This indicates a uniform compression of approximately $-95\ \mu in/in$ superimposed on a bending distribution of approximately $+228\ \mu in/in$. When the SDM-2 measurements were adjusted for the uniform compressive strain, the discrepancy between analysis and test was reduced from -123 percent to -81 percent.

6.6 DISCUSSION

6.6.1 Load-Bearing Layer Deflection and Stress

The following conclusions can be drawn from the test and analysis comparisons made in Section 6.5:

1. Consistent with analysis predictions, all unribbed specimens exhibited nonlinear load versus deflection characteristics and the ribbed specimen exhibited linear characteristics.
2. The maximum deflections ranged from 0.37 inch for the ribbed wood panel to 1.42 inches for the unribbed wood panel. With the exception of the steel panel, the test results and analysis predictions agreed to within 10 percent.
3. The glass superstrate stresses determined by test were about 40 percent lower than the analysis predictions. This result is not surprising since the strain gages were probably not located at the points of the maximum principal stresses to which the test results were compared.
4. The wood substrate stresses compared well with analysis predictions. Here, the strain gages were located at the bottom center of the modules where the stress distribution is very uniform.
5. The steel substrate results do not compare well with analysis predictions. The reasons for the large discrepancies are not apparent.

6.6.2 Solar Cell Stress

The key results for silicon cell stress are

1. No cells were damaged during the test and the maximum principal stresses were well below the 8000 psi allowable stress.
2. In every case, the maximum cell stress occurred at the location of the maximum stress in the load-bearing layer. For the modules with non-linear load versus deflection characteristics, the maximum stress occurred at the corner, rather than at the center, where the deflection was maximum. In the case of the ribbed wood module, the maximum stress in both the cell and the load bearing layer occurred at the center of the module, as expected. This suggests that the maximum cell stress is not directly related to deflection.
3. The analysis predicts a smaller ratio of load-bearing layer strain to cell strain in the case of the superstrate panels. In effect, the analysis predicts higher cell stress than revealed by test. The opposite is true for substrate panels. This discrepancy is probably due to spanwise stretching effects in the load-bearing member.

As explained in the Phase 1 report [3], the relationship between cell strain and load-bearing layer strain for given pottant parameters was determined by means of a two-dimensional finite element analysis. An enforced displacement was applied to the load-bearing layer, and the resulting ratio between cell strain and load-bearing layer strain was determined. Two different enforced displacement functions were applied sequentially to the load-bearing layer. The displacement functions were

a. An out-of-plane displacement which forced the load bearing layer to have a uniform curvature

b. An in-plane stretching of the load bearing layer.

The cell strain was found to be much more sensitive to the out-of-plane displacement function than to the in-plane stretching displacement. Accordingly, the out-of-plane displacement was used to develop the design curves which were presented in the Phase 1 report.

When a module deflects under a pressure load applied to the top surface, bending stresses result. The lower surface of the module is in tension and the top surface is in compression. If the module deflection exceeds about one-half the thickness, spanwise stretching of the module causes a membrane tension stress in the central area of the module. When the edges of the module are not fixed in the in-plane directions, a compressive stress develops around the periphery of the module to equilibrate the membrane stress. This compressive stress at the edges would increase the bending compressive stress at the top surface and decrease the bending tension stress at the bottom surface.

The cell and strain gage locations are shown in Figure 6-1 for both a superstrate and a substrate module. At the corner of the modules, where the maximum cell stresses occurred, the measured compressive stresses at the top surface of the module would be higher than those due to bending alone. The measured tension stresses at the bottom surface of the substrate modules would be lower than those due to bending alone.

The finite element analyses indicated that the cell stress was relatively insensitive to the membrane effects. Thus, for a superstrate module, the ratio of load-bearing-layer stress to cell stress would be larger than analysis predictions, and the opposite would be true for a substrate module. This was indeed demonstrated in the test results.

6.6.3 Failure of Test Specimen SDM-7

The ribbed-wood test specimen, SDM-7, failed at a load of approximately 30 psf. The failure occurred in the load-bearing member at the ends of the ribs, as illustrated in Figure 6-8a. The failure occurred because the ends of the ribs were not supported by the test fixture. The edges of the module were supported by the test fixture, but the ribs terminated just short of the edge support. The location of the resultant stress concentration is shown in Figure 6-8b. In a ribbed module design, the majority of the applied load is transmitted to the edge supports by the ribs. When the ribs are not supported, the load in the ribs must transfer through the panel to the edge support, and a resultant spanwise tension stress is generated through the thickness of the panel. In this case, the resulting failure was delamination of the wood in the spanwise direction, which is a weak direction for the wood product. When the ribs were directly supported by the test fixture, as illustrated in Figure 6-8c, the module sustained 50 psf loading without failure.

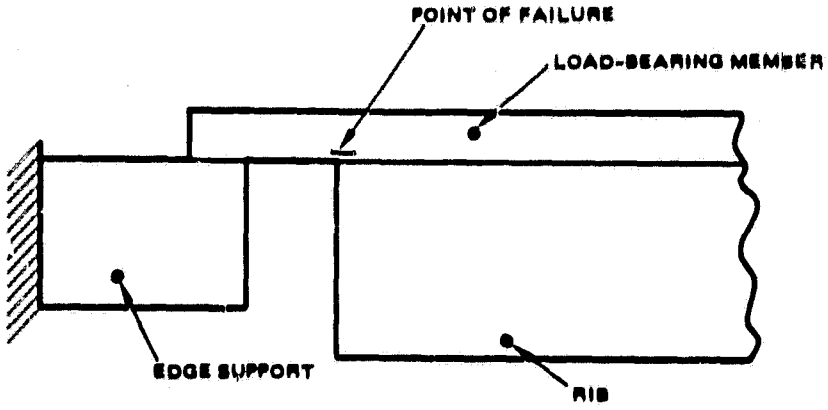

a. Failure Point.

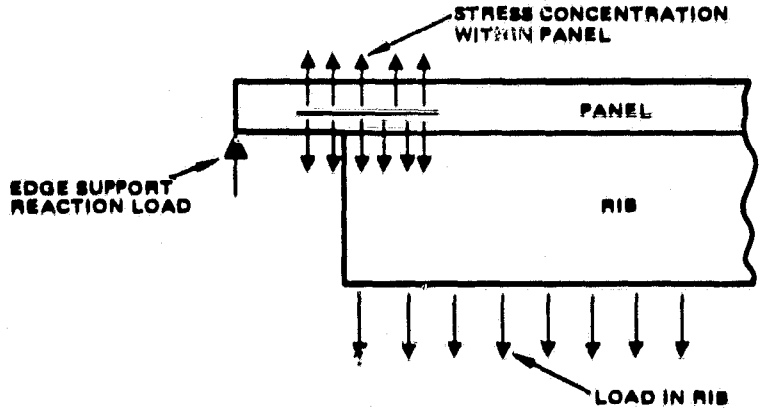

b. Stress concentration in ribbed wood module with unsupported ribs.

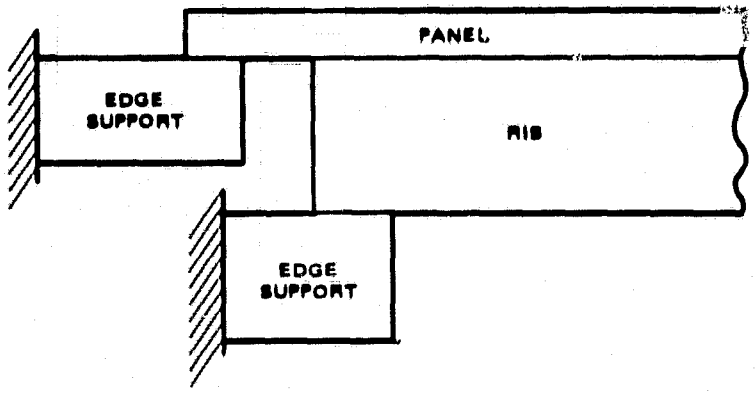

c. Support for ribbed wood module.

Figure 6-8. Failure in test specimen SDM-7.

7.0 THERMAL TEST

7.1 TEST OBJECTIVE

The objective of the thermal test was to verify the analytical methodology and computer algorithms for computing solar cell temperature and electric power output. The main test goal was to confirm the influence of the module backside emissivity on cell temperature and the insensitivity of cell temperature to pottant thickness. The verification process involved measuring steady-state solar cell temperature and power output for a known radiative energy source and other well-defined environmental conditions.

7.2 TEST SPECIMENS

Four minimodules, as designated in Table 7-1, were used in these tests. Nine AR-coated, single-crystal silicon cells were used in each minimodule. These cells were two inches square and were encapsulated with EVA/Craneglas on the sun side and white pigmented EVA/Craneglas on the antisun side. One cell was centrally located in each minimodule and eight cells were symmetrically located around the periphery of the central cell, as shown in Figure 7-1. The cells were connected electrically to an external circuit so that electric power could be withdrawn from the minimodules. The eight peripheral cells were connected in series, but the central cell was connected to a different circuit. This arrangement was chosen to permit a symmetric temperature environment for the cells, while simultaneously permitting measurement of the electrical power produced by the central cell.

TABLE 7-1. THERMAL VERIFICATION TEST SPECIMENS

Module No.	TM-1	TM-2	TM-3	TM-4
Load Bearing Member	Low-Iron Glass	Mild Steel	Wood Product	Wood Product
Top Cover	—	Tedlar	Tedlar	Tedlar
Back Cover	Aluminized Polyester	—	—	—
Pottant Thickness, mil	18	18	18	36

Each minimodule was mounted in an aluminum edge frame. The cross-sectional details of a typical frame were the same as those shown in Figure 6-2 for the structural deflection test specimens.

As shown in Figure 7-2, thermocouples were located on the backside of the center cell of each minimodule. Thermocouples were also located on the back cover of each module and on the backsides of edge cells in modules TM-1, TM-3, and TM-4. In addition, three thermocouples were attached to the edge frame of module TM-1. Thermocouples were attached to the edge cells to provide backup instrumentation in case of thermocouple breakage during module fabrication and during the test. A comparison between center cell and edge cell temperatures also permits an estimate of the lateral temperature gradient in a module. The thermocouple numbers shown in Figure 7-2 correspond to the individual channels of the data acquisition system described in Section 7.3.3. The backside emissivity of each module was changed (by application of black tape to obtain a high emissivity surface or by application of aluminized Mylar tape to obtain a low emissivity surface) during the test.

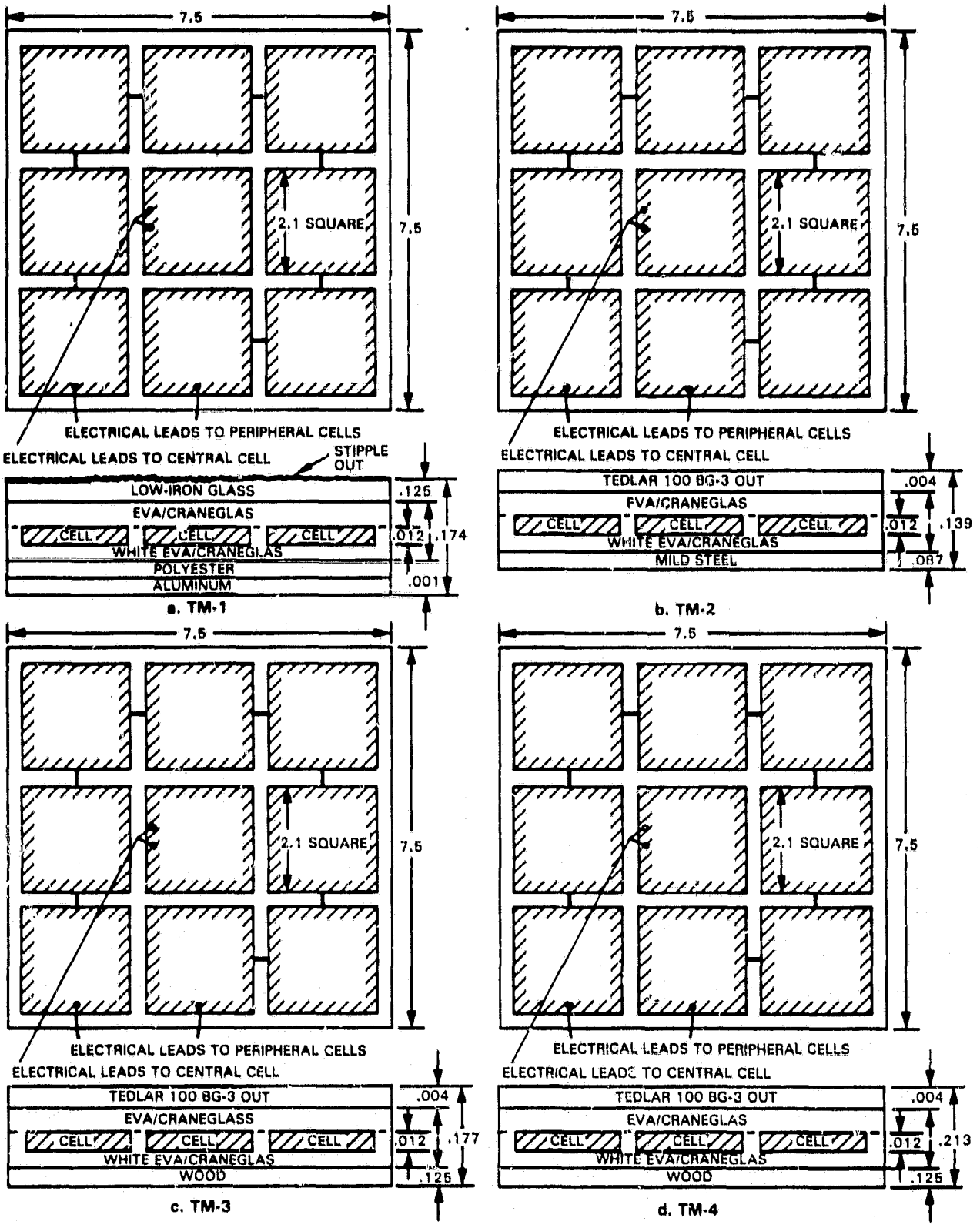

Figure 7-1. Thermal test minimodules; dimensions in inches.

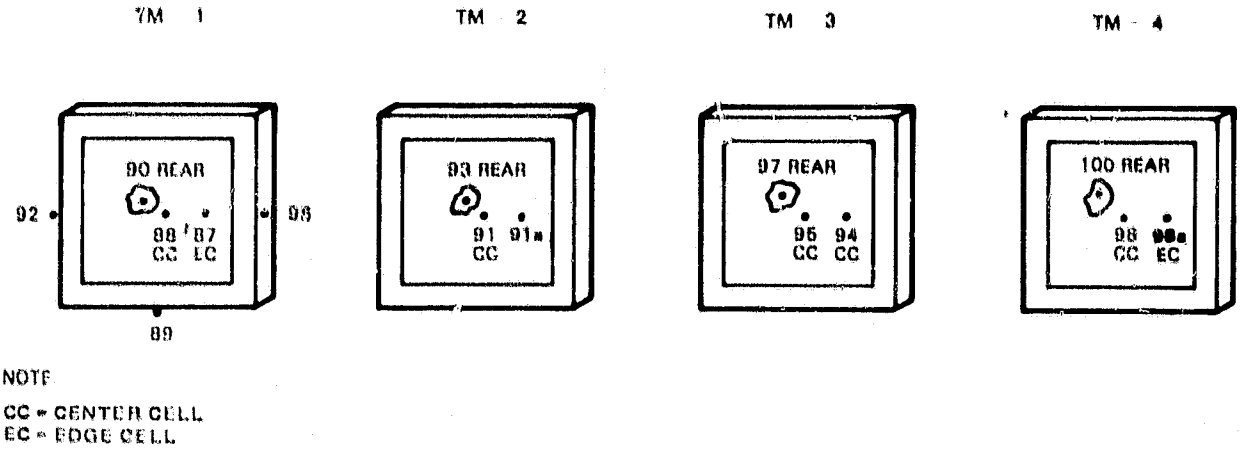

Figure 7-2. Thermocouple locations on test specimens.

7.3 TEST SET-UP

7.3.1 General Considerations

Results of the thermal analysis described in reference 3 indicate that the cell temperature is rather insensitive to pottant thickness and moderately sensitive to module backside emissivity. These results were calculated for an air speed of 1 meter/sec. Recent tests at JPL [4] have shown that cell temperature is very sensitive to wind speed, moderately sensitive to wind direction, and rather insensitive to ambient air temperature.

The operational thermal environment is difficult to simulate in the laboratory. Those items most difficult to simulate are the sky background temperature, the airflow around the module, and the incident solar radiation. For the thermal test described herein, facilities were not conveniently available to provide a controlled air flow around the modules. In addition, no test facility is known to have a capability for simulating the sky background temperature.

Though the operational thermal environment described in reference 3 could not be simulated, the dependence of cell temperature on pottant thickness and module backside emissivity could be verified by a suitably designed test apparatus. Verification of the thermal model would therefore lie in the ability of the model to predict the cell temperature for the thermal conditions existing in the apparatus. Therefore the apparatus was designed to provide: (1) a known convective cooling environment, (2) a known thermal radiation environment, and (3) a radiant energy source of known spectrum and intensity.

7.3.2 Equipment Layout and Instrumentation

The thermal test was performed in the Bally test chamber located at the Hughes facility in El Segundo, California. The dimensions of this chamber (7 feet high × 7 feet wide × 15 feet long) are large enough to accommodate the radiant energy source, test specimens, and dedicated test instrumentation. Enclosure of the entire test set-up provided a thermal radiation background environment with measurable boundary temperatures.

Essential features of the test set-up are illustrated in Figures 7-3 and 7-4. Quartz lamps served as the radiant energy source. These lamps were inserted in three holding fixtures mounted on rails; the rails, in turn, were attached to a moveable cart. The desired radiant energy flux in the plane of the test specimens was achieved by adjusting the distance between the lamps and the modules. Flux uniformity was controlled primarily by the number of lamp bulbs in each fixture.

NOTE:

NUMBERS IN PARENTHESES REFER TO ITEM NUMBERS IN TABLE A-4 OF APPENDIX A

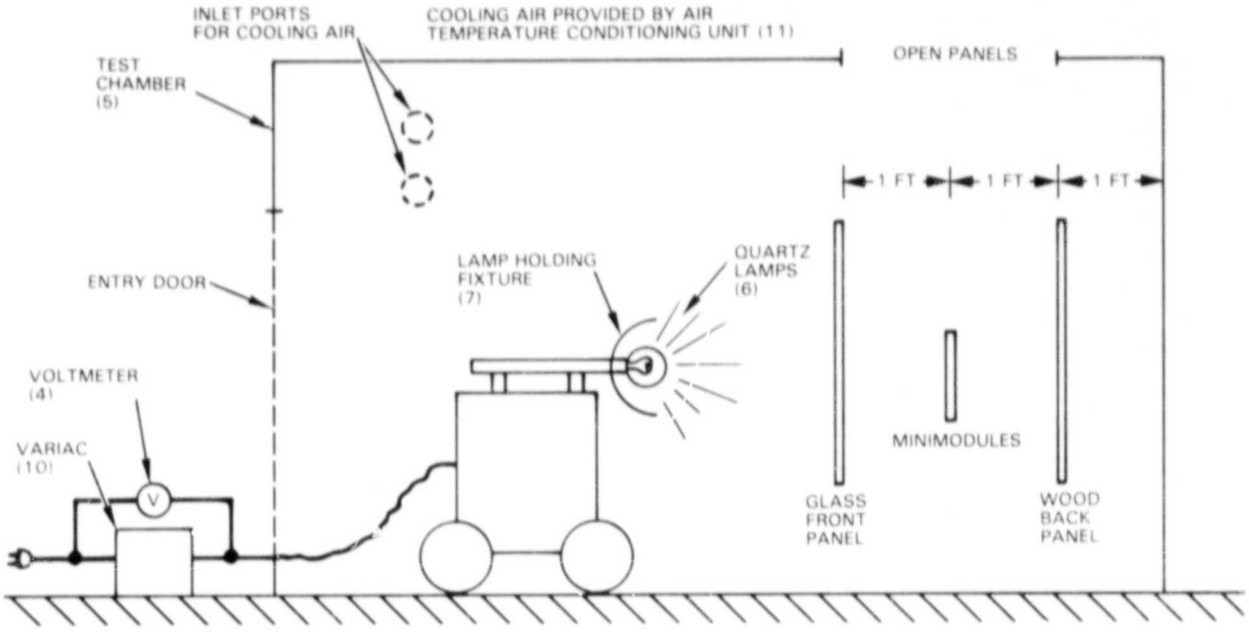

Figure 7-3. Essential features of thermal test set-up.

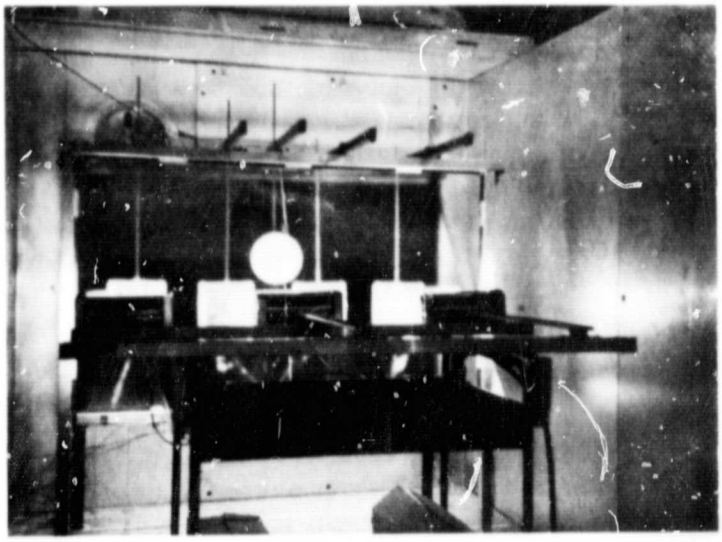

Figure 7-4. Thermal test set-up.

A 3 feet × 5 feet panel of low-iron glass (0.186 inch thick) was placed between the lamps and the test specimens, and a 3 feet × 5 feet black-painted wood panel was placed behind the specimens. This configuration was chosen so that the module radiation environment was controlled primarily by the front and back panels. The glass transmits 91 percent, reflects 7 percent, and absorbs 2 percent of the incident shortwave radiation from the lamps when the lamps are operated at rated voltage (240 volts). The glass is essentially opaque to low-temperature infrared radiation from the test specimens. A separation distance of 12 inches between the test specimens and the front and back panels was chosen to permit convenient access to the test specimens during the test, as well as to permit a low resistance flow path for hot air to exit the chamber. The test specimens were spaced 6 inches apart.

Natural convection, that is, air flow due to temperature gradients, was used as the air cooling mechanism for the test specimens. Conditioned air was introduced through two ports in the chamber wall. A maximum of 810 cfm was available, and flowrate control was achieved by obstructing the inlet ports. An exhaust slot in the chamber roof draws off the stratified hotter air near the roof of the chamber. A hot wire anemometer was used to measure the air velocity and to confirm that essentially natural convective flow condition existed near the modules.

A pyranometer and a pyrheliometer were used to measure the magnitude and uniformity of the radiant energy flux in the plane of the test modules. The pyranometer was placed in a fixed position on the center line of the plane of the test modules; readings from this device were used to set the lamp voltage and distance during all test runs. The pyrheliometer was used to determine flux uniformity; this device was water cooled, mounted on a wand, and inserted through the exhaust slot in the ceiling of the test chamber.

Copper-constantan thermocouples were used to measure temperature. Thermocouples 10 mils in diameter were attached to the cells before encapsulation and attached to the back cover of each module after encapsulation. Thirty gauge thermocouples were attached to the edge frame of module TM-1, the front and back panels, and to the walls of the chamber. Four 30-gauge thermocouples were used to measure air temperature in the vicinity of the test modules, and another was used to measure air temperature below the modules. The locations and identification of those thermocouples associated with the modules are shown in Figure 7-2, and those of the other thermocouples are shown in Figure 7-5.

Other support instrumentation is shown in Figure 7-6. Thermocouple data were transmitted from the test chamber to the test facility control room by the remote data scanner. Information from the remote data scanner was acquired by the test data acquisition system and then subsequently sent to the data logger for immediate viewing on a CRT or to the data manager for subsequent storage and later printout.

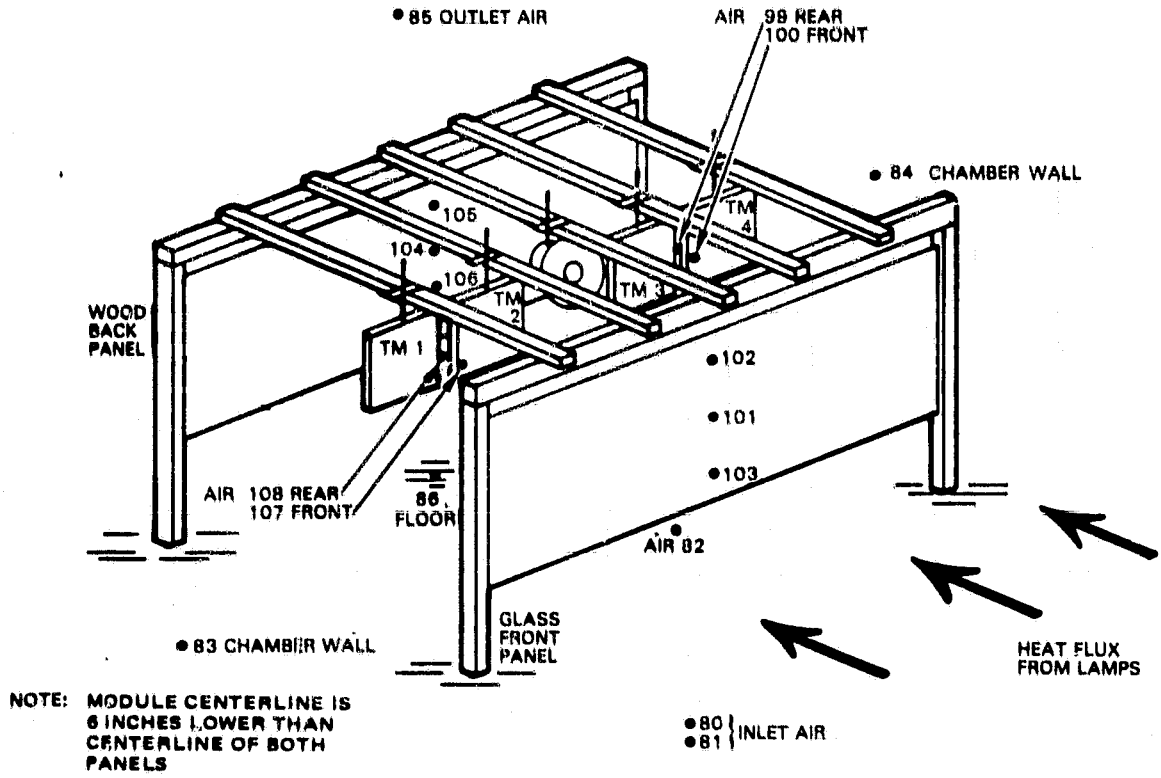

Figure 7-5. Thermocouple locations in test apparatus.

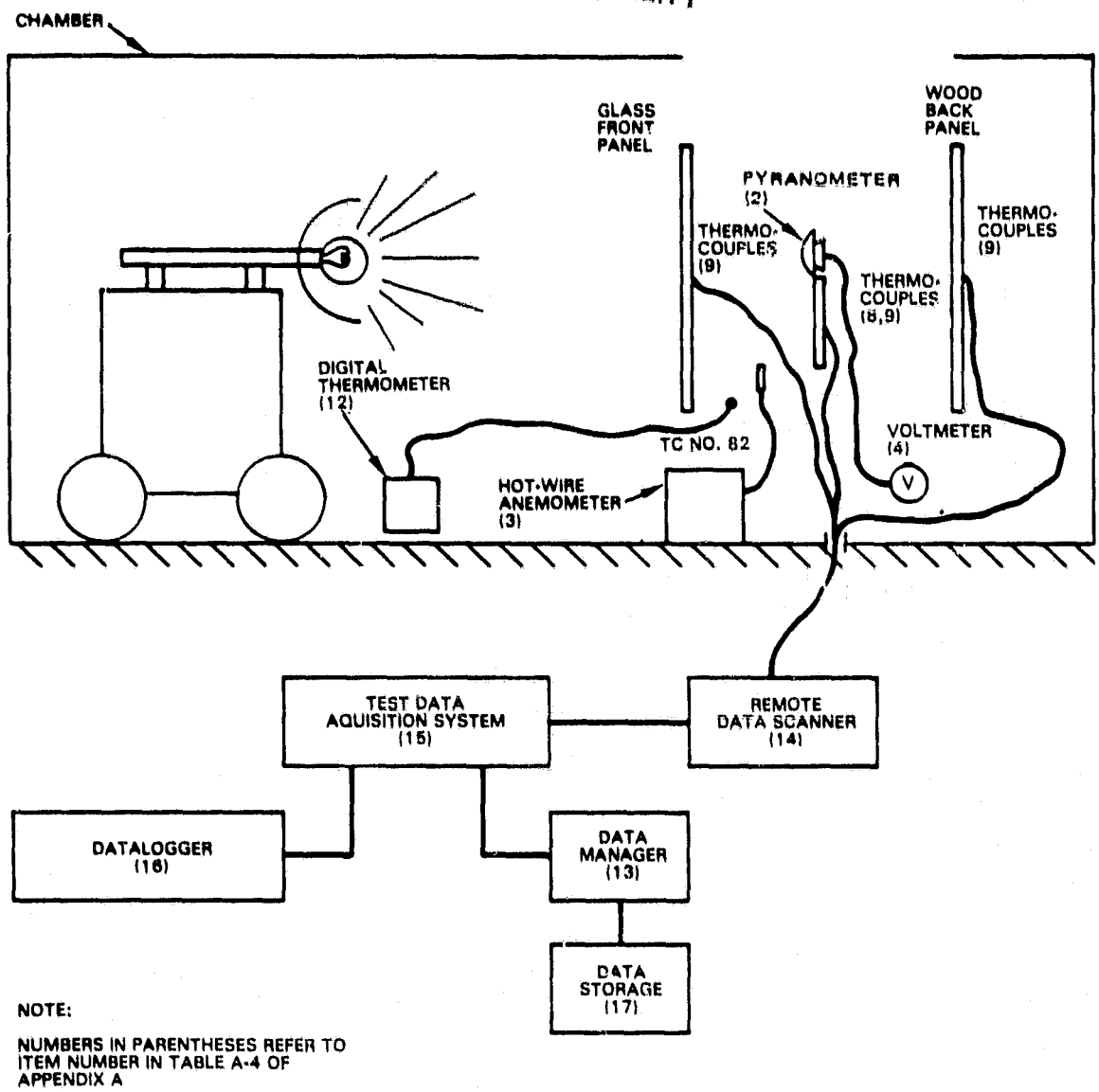

Figure 7-6. Test instrumentation and data management systems for thermal test.

7.4 TEST CONDITIONS

The thermal test consisted of eight test runs in which the incident radiant energy flux and the backside emissivities of the modules were varied for module operation in both the power generation and open circuit modes. At the request of JPL and Spectrolab, an additional test run was performed for modules with insulated backsides. In this run, the backside of each module was covered with one-inch thick polyurethane foam. This test condition is an approximate simulation of a rooftop installation, where airflow past the module backside is expected to be severely restricted. The test conditions are summarized in Table 7-2.

TABLE 7–2. THERMAL TEST PROGRAM

Test Run	Nominal Radiant Energy Flux in Plane of Modules, W/cm^2	Front/Back Emissivity				Comment
		TM1	TM2	TM3	TM4	
1	0.08	0.8/0.04	0.88/0.5	0.88/0.9	0.88/0.9	Open Circuit
2	0.08	0.8/0.04	0.88/0.5	0.88/0.9	0.88/0.9	Power Generation
3	0.114	0.8/0.04	0.88/0.5	0.88/0.9	0.88/0.9	Power Generation
4	0.114	0.8/0.04	0.88/0.5	0.88/0.9	0.88/0.9	Open Circuit
5	0.114	0.8/0.95	0.88/0.95	0.88/0.03	0.88/0.03	Open Circuit
6	0.114	0.8/0.95	0.88/0.95	0.88/0.03	0.88/0.03	Power Generation
7	0.08	0.8/0.95	0.88/0.95	0.88/0.03	0.88/0.03	Power Generation
8	0.08	0.8/0.95	0.88/0.95	0.88/0.03	0.88/0.03	Open Circuit
9	0.08	0.8/0.95	0.88/0.95	0.88/0.03	0.88/0.03	Open Circuit Uninsulated
10	0.08	0.8/NA	0.88/NA	0.88/NA	0.88/NA	Open Circuit Insulated

A nominal radiant energy flux of 0.08 watt/cm^2 was chosen to simulate (as closely as possible) the "nominal thermal environment" used in the definition of the nominal operating cell temperature (NOCT). The higher flux of 0.114 watt/cm^2 was chosen arbitrarily. The procedure for adjusting the lamps is shown in Figure 7–7. The voltage reading on the pyranometer was monitored when adjusting both the lamp voltage and the distance between the modules and lamps. The pyrheliometer was then used to check flux uniformity. The radiant energy flux could be altered by rotating the lamp cart and by changing the number of lamp bulbs.

The procedure followed for each test condition is illustrated in Figure 7–8. Special care was taken to ensure the existence of steady-state for each test run. The ambient air temperature (TC No. 82, see Figure 7–5) was monitored at all times to ensure that the cooling air source for natural convection remained at constant temperature.

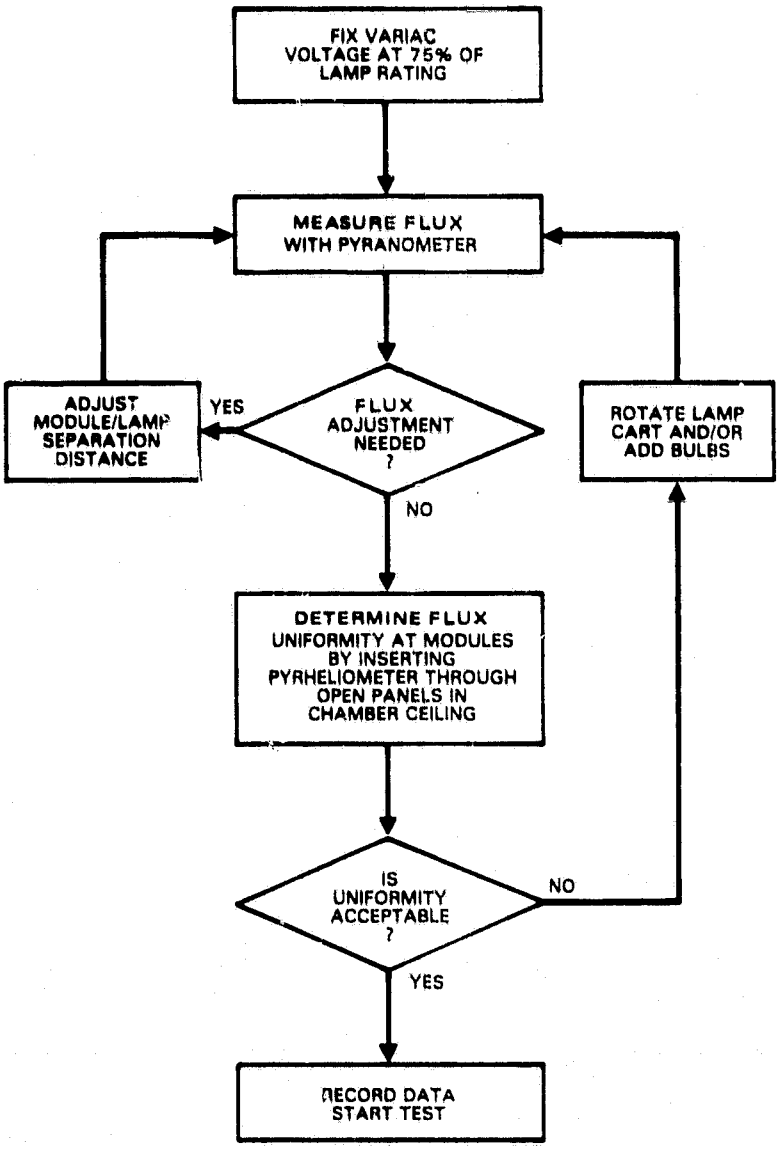

Figure 7-7. Procedure for adjusting lamps.

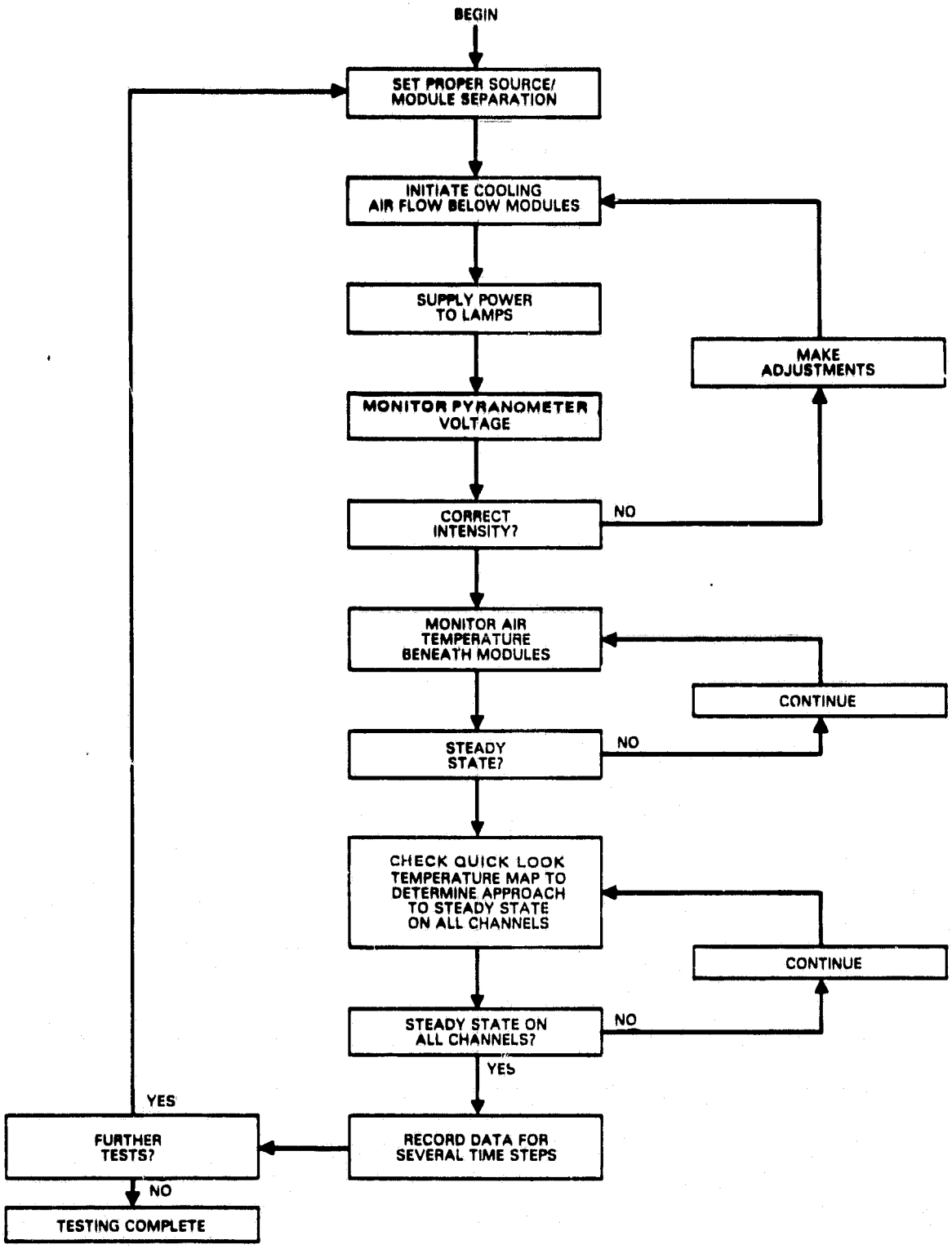

Figure 7-8. Test procedure flow chart.

7.5 DATA ANALYSIS

7.5.1 Test Data Summary

Results of the thermal test are listed in Tables B-43 and B-44 of Appendix B. For the purposes of analysis, the key results (i.e., cell temperature, module backside temperature, air temperature, and radiant energy flux) are listed in Tables 7-3 through 7-6 for modules with uninsulated backsides and in Table 7-7 for modules with insulated backsides.

TABLE 7-3. KEY RESULTS FOR (GLASS SUPERSTRATE) MODULE TM-1

Test Run No.	Backside Emissivity	Radiant Energy Flux, W/cm²		Center Cell Power Output, W	Temperature, °C			
		Nom.	Actual		Air	Center Cell	Edge Cell	Backside
1	0.04	0.08	0.066	0	41.6	69.4	72.1	69.1
2	0.04	0.08	0.066	0.06	41.2	68.4	70.7	68.2
3	0.04	0.114	0.09	0.09	40.9	79.5	83.4	79.1
4	0.04	0.114	0.09	0	41.6	80.6	85.1	80.3
5	0.95	0.114	0.09	0	39.6	78.4	80.1	77.5
6	0.95	0.114	0.09	0.07	40.5	79.4	80.4	78.5
7	0.95	0.08	0.066	0.06	40.1	67.4	68.1	66.8
8	0.95	0.08	0.066	0	39.9	68.1	69.1	67.4

TABLE 7-4. KEY RESULTS FOR (STEEL SUBSTRATE) MODULE TM-2

Test Run No.	Backside Emissivity	Radiant Energy Flux, W/cm²		Center Cell Power Output, W	Temperature, °C			
		Nom.	Actual		Air	Center Cell*	Edge Cell*	Backside
1	0.5	0.08	0.066	0	41.6	63.7	NA	65.1
2	0.5	0.08	0.066	0.06	41.2	67.4	NA	65.3
3	0.5	0.114	0.09	0.09	40.9	72.7	NA	70.8
4	0.5	0.114	0.09	0	41.6	75.6	NA	71.5
5	0.95	0.114	0.09	0	39.6	NA	69.4	70.7
6	0.95	0.114	0.09	0.07	40.5	NA	66.7	71.9
7	0.95	0.08	0.066	0.06	40.1	NA	60.7	64.3
8	0.95	0.08	0.066	0	39.9	NA	64.5	64.8

* Center cell (TC No. 91) thermocouple readings appear questionable. Switched to edge cell (TC No. 91a) after test run No. 4.

TABLE 7–5. KEY RESULTS FOR (WOOD SUBSTRATE) MODULE TM–3

Test Run No.	Backside Emissivity	Radiant Energy Flux, W/cm²		Center Cell Power Output, W	Air	Temperature, °C		
		Nom.	Actual			Center Cell	Edge Cell	Backside
1	0.9	0.08	0.066	0	40.6	74.5	74.5	68.1
2	0.9	0.08	0.066	0.06	40.9	74.5	75.6	68.7
3	0.9	0.114	0.09	0.09	39.9	81.8	84.5	75.6
4	0.9	0.114	0.09	0	40.2	84.3	84.8	77.3
5	0.03	0.114	0.09	0	38.7	84.2	83.9	77.7
6	0.03	0.114	0.09	0.06	40	84.4	85.7	78.2
7	0.03	0.08	0.066	0.06	40	72.7	74.1	68.6
8	0.03	0.08	0.066	0	40.7	74.6	74.1	69.1

TABLE 7–6. KEY RESULTS FOR (WOOD SUBSTRATE) MODULE TM–4

Test Run No.	Backside Emissivity	Radiant Energy Flux, W/cm²		Center Cell Power Output, W	Air	Temperature, °C		
		Nom.	Actual			Center Cell*	Edge Cell*	Backside
1	0.9	0.08	0.066	0	40.6	71.3	NA	66.6
2	0.9	0.08	0.066	0.05	40.9	47.6	NA	67
3	0.9	0.114	0.09	0.11	39.9	61.1	NA	75.7
4	0.9	0.114	0.09	0	40.2	83.1	NA	76.2
5	0.03	0.114	0.09	0	38.7	NA	82.9	80.1
6	0.03	0.114	0.09	0.07	40	NA	84.3	81.1
7	0.03	0.08	0.066	0.02	40	NA	71.2	68.9
8	0.03	0.08	0.066	0	40.7	NA	71.2	69.6

* Center cell thermocouple readings appear questionable. Switched to edge cell (TC No. 98a) after test run No. 4.

TABLE 7-7. KEY RESULTS FOR MODULES WITH INSULATED BACKSIDES

Test Run No.	Radiant Energy Flux, W/cm²		Temperature, °C								Comments
			TM-1 (Glass)				TM-2 (Steel)				
	Nom.	Actual	Air	Center Cell	Edge Cell	Backside	Air	Center Cell	Edge Cell	Backside	
9	0.08	0.066	39.5	66.1	66.4	65.4	39.5	NA	63.4	65.8	Uninsulated Backside
10	0.08	0.066	39.9	77.6	79.0	77.6	39.9	NA	70.2	72.3	Insulated Backside

Test Run No.	Radiant Energy Flux, W/cm²		Temperature, °C								Comments
			TM-3 (Wood)				TM-4 (Wood)				
	Nom.	Actual	Air	Center Cell	Edge Cell	Backside	Air	Center Cell	Edge Cell	Backside	
9	0.08	0.066	39.7	76.1	77.6	71.2	39.7	NA	72.6	70.5	Uninsulated Backside
10	0.08	0.066	40.2	81.7	81.9	79.5	40.2	NA	76.9	77.7	Insulated Backside

7.5.2 Analytical Model

As mentioned in Section 7.3.1, the test chamber environment differed significantly from the terrestrial environment studied in Phase 1 of the program. Consequently, the thermal/optical model described in reference 3 was modified to represent the conditions prevailing in the test chamber.

The thermal model used for the test chamber environment is compared with that used for the terrestrial environment in Figure 7-9. These discrete-element models were used to determine the temperature distribution around a centrally-located cell inside a module. The models differ in four respects: (1) the terrestrial model accounted for the interstitial spacing between the cells whereas the test chamber model did not;* (2) the air cooling in the terrestrial model was by forced convection past a module inclined at 34 degrees to the local horizontal whereas the air cooling in the test chamber model was by buoyancy-driven natural convection past a vertically-mounted module; (3) the terrestrial model used a solar air mass 1.5 spectrum whereas the test chamber model used the spectrum for a quartz lamp; and (4) the ground and sky served as thermal radiation boundaries for the terrestrial model whereas the front and back panels as well as the chamber walls served as thermal radiation boundaries for the test chamber model.

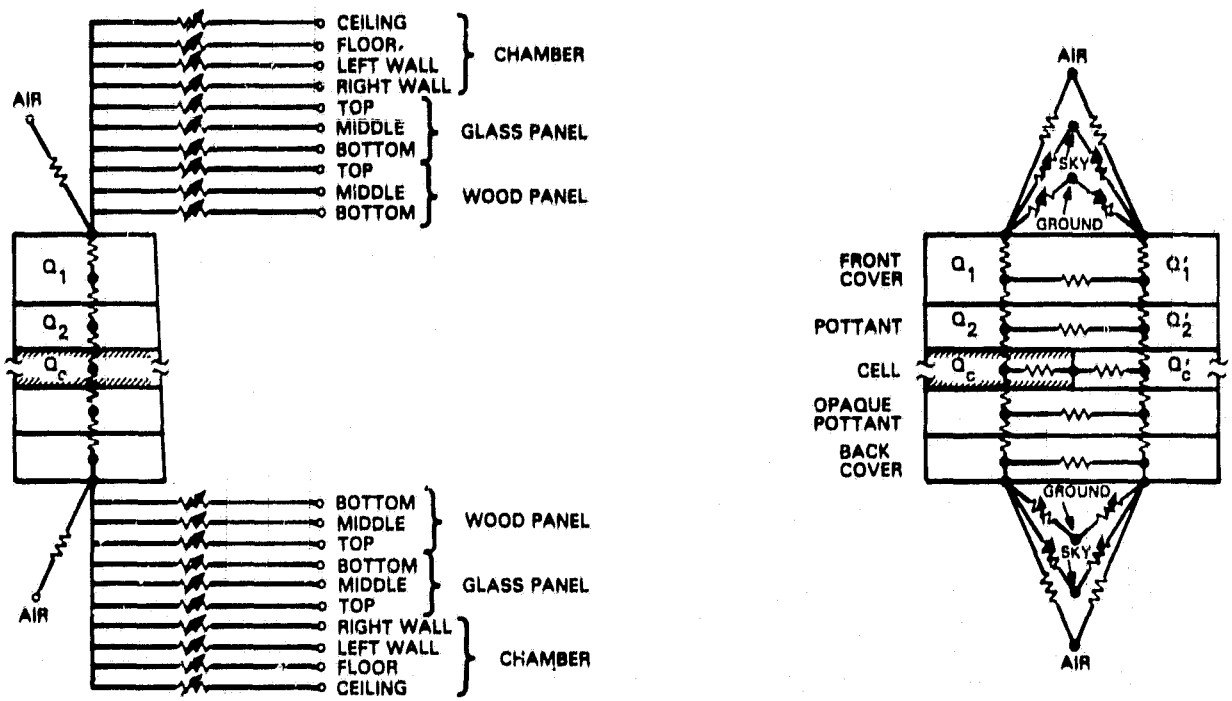

a. MODEL FOR TEST CHAMBER ENVIRONMENT

b. MODEL FOR TERRESTRIAL ENVIRONMENT

Figure 7-9. Thermal models for test chamber and for terrestrial environments.

* For closely-packed rectangular cells, which is the geometry under study here, the presence of the small interstitial space between cells has a negligible effect on cell temperature.

For the test chamber model, the radiant energy absorbed in the layers of the encapsulation system are indicated by Q's in Figure 7-9. Values of Q_1, Q_2, and Q_c were determined by the method outlined in Section 5 of reference 3. Note that since the model for the test chamber environment does not account for the small interstitial spacing between cells, values of Q'_1, Q'_2, and Q'_c were not required for correlating test data.

Temperatures were calculated at a number of points inside and on the surface of the module in both models; these points (nodes) are represented by large black dots in Figure 7-9. The large dots external to the module represent constant temperature boundaries.

The nodes are connected by a network of heat flow paths, which are shown as resistors in Figure 7-9. Each path represents a finite "resistance" to heat flow in the models. As mentioned in Section 6.2.2 of reference 3, absorption-reradiation phenomena in the encapsulation system are ignored, and heat flow inside the module is therefore by conduction only. The conduction resistance between adjacent nodes i and j is given by

$$R_{ij} = \frac{l_{ij}}{kA} \tag{7-1}$$

where l_{ij} is the distance between nodes, k is the thermal conductivity, and A is the cross-sectional area for conductive heat flow.

Air motion (convection) past the module surfaces helps to remove the incident solar radiation absorbed as heat. The thermal resistance to this convective heat flow from the surface to air is given by

$$R_{s\text{-}air} = 1/(hA) \tag{7-2}$$

where h is the convective heat transfer coefficient and A is the cross-sectional area for convective heat flow. The following relation [5] is used to calculate h for natural convection:

$$\frac{hL}{k} = C(GrPr)^m$$

where:

Gr = Grashof number = $\dfrac{g\,\beta\,(T_s - T_{air})\,L^3}{\nu^2}$

Pr = Prandtl number = 0.72 for air

g = gravity = 980 cm/sec^2

β = volumetric thermal expansion coefficient of air, °C^{-1}

L = vertical length of minimodule, cm

T_s = module surface temperature, °C

ν = kinematic viscosity of air, cm^2/sec

$C = 0.59$, $m = 0.25$ } for $GrPr < 10^9$

$C = 0.1$, $m = 0.33$ } for $GrPr > 10^9$

The module surfaces radiate to the ground and sky in the terrestrial environment and to the front and back panels and chamber walls in the test environment. The thermal resistance to radiative heat transfer between a module surface node and a radiation boundary is given by

$$R_{s-b} = (A\sigma \mathscr{F}_{s-b})^{-1} \qquad (7\text{-}4)$$

where σ is the Stefan-Boltzman constant, A is the area for radiative heat flow, and $\mathscr{F}_{s-b}$ is the radiative interchange factor (script-F). The radiative interchange factor is that portion of the radiant energy emitted from surface s that is absorbed at boundary b. Note that the units of Equations (7-1) and (7-2) are °C/w and that the units of Equation (7-4) are $°K^4/w$. The thermal resistances are input to the thermal analyzer program in this way. Further discussion follows later in this section.

The script-F's, which were complex functions of the geometry and surface emissivities of the test set-up, were determined by means of the RENO computer program.* The surface emissivities and the script-F's used in the analyses presented here are listed in Tables 7-8 and 7-9, respectively. Note that the script-F's for test runs 1-4 differed from those for test runs 5-8. This difference was due to the change in module backside emissivities between runs 4 and 5. All surfaces in the test set-up were treated as grey bodies.

TABLE 7-8. SURFACE EMISSIVITIES FOR THERMAL TEST

Surface	Emissivity
Front Glass Panel	0.8
Back Wood Panel (black-painted)	0.9
Chamber Walls (dimpled aluminum)	0.09
Black Tape	0.95
Silver Tape	0.03
Aluminized Mylar	0.04

* The RENO program was originally developed by the Aerojet-General Corporation. Turner Associates, who upgraded the Aerojet software, now maintains exclusive rights to its usage at Hughes under a license agreement.

C-2

TABLE 7–9. RADIATIVE INTERCHANGE FACTORS FOR THERMAL TEST SET–UP

Boundary	Radiative Interchange Factor, $\mathcal{F}$															
	Test Run 1–4								Test Run 5–8							
	TM–1		TM–2		TM–3		TM–4		TM–1		TM–2		TM–3		TM–4	
	Front	Back	Front	Back	Front	Back	Front	Back	Front	Back	Front	Back	Front	Back	Front	Back
Glass Front Panel																
Bottom	0.195	0.001	0.247	0.001	0.234	0.016	0.194	0.015	0.206	0.016	0.252	0.018	0.237	0.001	0.210	0.001
Center	0.19	0.001	0.231	0.008	0.229	0.014	0.217	0.017	0.177	0.019	0.219	0.019	0.241	0.001	0.223	0.001
Top	0.048	0.001	0.063	0.008	0.076	0.014	0.064	0.019	0.052	0.018	0.065	0.016	0.059	0.001	0.064	0.001
Wood Back Panel																
Bottom	0.017	0.01	0.024	0.146	0.019	0.277	0.015	0.238	0.019	0.251	0.023	0.293	0.017	0.009	0.019	0.008
Center	0.022	0.012	0.022	0.164	0.027	0.281	0.024	0.257	0.024	0.279	0.018	0.289	0.022	0.009	0.020	0.008
Top	0.018	0.003	0.023	0.047	0.017	0.078	0.021	0.057	0.017	0.076	0.018	0.072	0.021	0.003	0.017	0.002
Chamber Walls																
Left (Closest to TM–1)	0.024	0.001	0.014	0.007	0.011	0.009	0.013	0.010	0.025	0.025	0.014	0.016	0.010	0.001	0.012	0.001
Right (Closest to TM–4)	0.011	0.001	0.010	0.005	0.016	0.013	0.026	0.025	0.012	0.010	0.009	0.009	0.015	0.001	0.022	0.001
Ceiling	0.015	0.001	0.011	0.006	0.013	0.010	0.016	0.013	0.013	0.012	0.01	0.013	0.012	0.001	0.013	0.001
Floor	0.210	0.008	0.189	0.078	0.188	0.138	0.224	0.182	0.210	0.170	0.209	0.148	0.198	0.005	0.221	0.005

The spectrum of the quartz lamps was taken to be that of a black body operating at 2230°K. The ordinate of the corresponding blackbody curve was adjusted so that the area under the curve was the same as the flux measured by the pyranometer. Following the computational sequence outlined in Section 6.3 of reference 3, this spectrum was divided into twenty equal-energy intervals which correspond to twenty wavelength bands of unequal size. These intervals are listed in Table 7-10. Optical properties were evaluated at the midpoint of each wavelength band. The energy absorbed in the cell and in each layer of the encapsulation system (Q_c, Q_1, Q_2) is evaluated for each wavelength band and summed over all bands. These values of Q_1, Q_2, and Q_c are then input to the thermal model to calculate the corresponding temperatures.

TABLE 7-10. EQUAL ENERGY WAVELENGTH BANDS FOR QUARTZ LAMPS* USED DURING THERMAL TEST

Energy Interval	Wavelength Band, μm	
	Endpoints	Midpoint
1	0.3, 0.86	0.58
2	0.86, 0.98	0.92
3	0.98, 1.10	1.04
4	1.10, 1.20	1.15
5	1.20, 1.32	1.26
6	1.32, 1.38	1.35
7	1.38, 1.54	1.46
8	1.54, 1.58	1.56
9	1.58, 1.76	1.67
10	1.76, 1.82	1.79
11	1.82, 2.02	1.92
12	2.02, 2.10	2.06
13	2.10, 2.36	2.23
14	2.36, 2.48	2.42
15	2.48, 2.84	2.66
16	2.84, 3.00	2.92
17	3.00, 3.68	3.34
18	3.68, 4.20	3.94
19	4.20, 5.94	5.07
20	5.94, 9.58	7.76

* Operated at 3.4 rated voltage

7.5.3 Results

Measured and predicted cell temperatures for test runs 1, 4, 5, and 8 are listed in Table 7-11. These results are for those tests performed at open circuit conditions. The power conversion efficiencies of the cells used in these modules were approximately 2.5 percent, and there was little overlap between the cell response curves and the spectrum of the quartz lamps. Thus, the cell temperature was not expected to differ significantly between open circuit and the maximum power generation conditions. This expectation was confirmed during the test (after adjusting for differences in air temperature); hence only predictions for open circuit conditions are reported here.

The average air speed between the glass and wood panels was found to be approximately 0.2 meter/sec. However, speed "pulses" were observed to occur about every 2 to 3 minutes; the maximum air speed during these pulses was about 0.4 meter/sec.

The pyranometer readings indicated that the nominal fluxes of 0.08 and 0.114 W/cm^2 were obtained along the dividing line between modules TM-2 and TM-3. However, the pyrheliometer readings indicated that the flux decreased by as much as 20 percent in going from the pyranometer to the spaces between modules TM-1 and TM-2 and between modules TM-3 and TM-4. Hence, the incident radiant energy fluxes used in the predictions correspond to those measured at positions B and E in Figure B-15 of Appendix B. This nonuniformity in radiant energy flux may be the reason for the 1 to 3°C difference between measured center cell and edge cell temperatures.

A comparison between predicted and measured cell temperature indicates that

1. The thermal, optical model overestimates the cell temperature
2. The thermal optical model shows best agreement for those situations where the module had a high emissivity back cover.

7.6 DISCUSSION

As mentioned above, the thermal model overpredicts the cell temperature. The two most probable causes of the overpredictions are the low value of emissivity (0.09) assumed for the chamber walls and a lateral temperature gradient in the glass front panel.

The emissivity of the chamber walls was probably closer to 0.2 (a value commonly used for the aluminum skin of an aircraft) than 0.09. A higher value of emissivity would lead to larger values for the script-F terms from the modules to the chamber walls and therefore to a higher prediction of radiant heat transfer from the modules to the chamber walls.

Although there were insufficient thermocouples to measure the lateral temperature differences in the front panel, the drop-off in radiant energy flux from the centerline of the test apparatus implies that the temperature in the glass panel decreased with distance from the centerline as well.

The measured cell temperatures in excess of the ambient air temperature for the present tests were about 15 to 20°C higher than those reported by Namkoong and Simons [11] for four different module designs operating in an outdoor environment. This difference is not surprising in that the outdoor environment is characterized by cooler radiation boundaries and forced convection cooling due to winds.

In test run No. 10, the modules were insulated such that none or very little of the absorbed radiant energy could be removed by convection and radiation from the module backsides. This configuration is typical of roof-top applications. Measured cell temperatures for this test run are listed in Table 7-12, which indicates that the cell temperatures for the insulated modules were about 5° to 11°C higher than those for the uninsulated modules. The cell temperatures in excess of the ambient air temperature compare with Namkoong's and Simon's data for insulated modules operating in an outdoor environment [11].

TABLE 7–11. COMPARISON OF MEASURED AND PREDICTED CELL TEMPERATURES

Test Run No.	Nominal Flux (W/cm^2)	Temperature, °C							
		TM1 (Glass)		TM2 (Steel)		TM3 (Wood)		TM4 (Wood)	
		Measured†	Predicted	Measured	Predicted	Measured†	Predicted	Measured	Predicted
1	0.08	72.1	78.5	63.7*	73.4	74.5	75.8	71.3*	76.7
4	0.114	85.1	93	75.6*	87	84.3	88	83.1*	89.1
5	0.114	80.1	80.2	69.4	79.4	84.2	92.7	82.9	94.1
8	0.08	69.1	69.4	64.5	68	74.6	79.4	71.2	80.8

* Questionable thermocouple reading for center cell. Switched to edge cell after test run No. 4.

† Center cell temperature

Note: Measured cell temperature is the higher of the central or edge cell temperatures for modules TM-1, TM-3, and TM-4.

TABLE 7–12. MEASURED CELL TEMPERATURES FOR MODULES WITH INSULATED BACKSIDES

Test Module No.	Description	Cell Temperature, °C	
		Uninsulated	Insulated
TM–1	Glass Superstrate Front Cover: 125 mil glass Pottant: 18 mil EVA/Craneglas Back Cover: Black tape	66.1	77.6
TM–2	Mild Steel Substrate Front Cover: 3 mil Tedlar Pottant: 18 mil EVA/Craneglas Substrate: 200 mil steel Back Cover: Silver tape	63.4*	70.2*
TM–3	Wood Substrate Front Cover: 3 mil Tedlar Pottant: 18 mil EVA/Craneglas Substrate: 125 mil wood Back Cover: Silver tape	76.1	—
TM–4	Wood Substrate Front Cover: 3 mil Tedlar Pottant: 36 mil EVA/Craneglas Substrate: 125 mil wood Back Cover: Silver tape	72.6	—

Environmental Conditions:

(1) Incident radiant energy flux $\cong$ 0.066 W cm^{-2}

(2) Air temperature $\cong$ 40°C

(3) Front (glass) panel temperatures = 52°C, 58°C, 69°C

(4) Chamber wall temperature = 41°C

(5) Chamber floor temperature = 44°C

(6) Air speed $\cong$ 0.2 meter/sec

* Thermocouple reading is doubtful

REFERENCES

1. Bechtel National, Inc., "Study of Curved Glass Photovoltaic Module and Module Electrical Isolation Design Requirements," DOE/JPL-954698-80/2, June 1980.
2. Dalley, James W. and William F. Riley, Experimental Stress Analysis, New York, McGraw-Hill, 1965.
3. Garcia, A. and C. Minning, "Design, Analysis, and Test Verification of Advanced Encapsulation Systems," DOE/JPL-955567-81/4, November 1981.
4. Griffith, John S., Mulchand S. Rathod and Joel Paslaski, "Some Tests of Flat Plate Photovoltaic Module Cell Temperatures in Simulated Field Conditions," Proceedings, Fifteenth Photovoltaic Specialists Conference, Kissimmee, Florida, 12-15 May 1981, pp. 822-830.
5. Holman, J. P., Heat Transfer, 4th ed., McGraw-Hill, New York,1976.
6. Hovel, Harold J., "Solar Cells", in R. K. Willardson and A. C. Bear (eds.), Semiconductors and Semimetals, Vol. II, Academic Press, New York, 1975.
7. LSA Engineering Area, "Low-Cost Solar Array Project: Photovoltaic Module Design, Qualification and Testing Specification," JPL Report 5101-65, 24 March 1978.
8. LSA Engineering Area, "Low-Cost Solar Array Project: Block IV Solar Cell Module Design and Test Specification for Residential Applications," JPL Report 5101-83, 1 November 1978.
9. Minning, C. P., "Encapsulation Systems Design Letter Report for April 1981," HAC IDC 704220/1121, 12 May 1981.
10. Moore, D. M., "Low-Cost Solar Array Project: Proposed Method for Determining the Thickness of Glass in Solar Collector Panels," JPL Report 5101-148, 1 March 1980.
11. Namkoong, David and Frederick F. Simon, "Comparison of Photovoltaic Cell Temperatures in Modules Operating with Exposed and Enclosed Back Surfaces," NASA TM-81769, May 1981.
12. Rauschenbach, Hans S., Solar Cell Array Design Handbook, Van Nostrand Reinhold Co., New York, 1980.
13. Roark, Raymond J. and Warren C. Young, Formulas for Stress and Strain, 5th ed., McGraw-Hill, New York, 1975.

APPENDIX A

TEST EQUIPMENT INFORMATION

APPENDIX A. TEST EQUIPMENT INFORMATION

A.1 OPTICAL TEST EQUIPMENT

A.1.1 Equipment Description, Test Function, and Nameplate Data

The test equipment and support instrumentation used in the optical test are listed in Table A-1.

TABLE A-1. TEST EQUIPMENT AND SUPPORT INSTRUMENTATION USED IN OPTICAL TESTS

Item No.	Description	Test Function	Nameplate Data
1	Xenon illumination source	Radiant energy source	Spectrosun Model No. 1206 Spectrolab, Inc. Sylmar, Calif.
2	Standard cell	Calibration of xenon source	Standard Cell No. 1039 Spectrolab, Inc. Sylmar, Calif.
3	Tungsten illumination source	Radiant energy source	Tungsten Solar Simulator, SN2 Spectrolab, Inc. Sylmar, Calif.
4	Standard cell	Calibration of tungsten source	Standard Cell No. I-3 Spectrolab, Inc. Sylmar, Calif.
5	Color temperature meter	Set-point instrumentation for tungsten source	Heliotek Color Temperature Meter Model HTA 159, Serial No. 122 Spectrolab, Inc. Sylmar, Calif.
6	Automatic load adjustment	Set voltage across terminals of solar cell	Electronic Load Model 279-1, SN2 Spectrolab, Inc. Sylmar, Calif.
7	Thermocouples (copper/constantan, 30 gauge)	Measure temperatures of cooling fixture and solar cell	Fabricated at Hughes Aircraft Co.
8	Digital temperature readout	Convert voltage output from thermocouples to temperature units	Model 2176A Digital Thermometer Serial No. 1860054 John Fluke Mfg. Co. Burbank, Calif.

A.1.2 Calibration Data

Calibrated photovoltaic cells were used to determine the radiant energy fluxes in the illumination sources. Standard cell 1039 was used for adjusting the xenon source; the current versus voltage characteristics of this cell, for an energy flux of 0.135 W/cm^2 (i.e. air mass zero) are shown in Figure A-1. Standard cell I-3 was used for determining the energy flux in the tungsten source; this cell was accidentally broken at conclusion of the optical tests and is no longer available. The dimensions of standard cell 1039 are 0.25 inch × 0.25 inch, and the dimensions of standard cell I-3 were 2.1 inch × 2.1 inch.

Each of the cells was inserted in a vacuum chuck and placed in the beam of each source. For the xenon source, the power to the lamp was adjusted such that cell 1039 produced a short-circuit current of 65 mA. The accuracy of this setting is ±2 percent. For the tungsten source, the power to the lamp was set to yield a color temperature at 2700°K (measured with a color temperature meter—see item 5, Table A-1). The vertical distance of the lamp above the vacuum chuck was then adjusted until the short circuit current produced by cell I-3 was 903 mA, which corresponds to a radiant energy flux of 0.100 W/cm^2.

A.2 ELECTRICAL TEST EQUIPMENT

A.2.1 Equipment Description, Test Function, and Nameplate Data

A hipot tester was used to measure breakdown voltage and leakage current through the test coupons. Nameplate data for the hipot tester are listed below:

Model HD 125 AC/DC Hipot Tester
Hipotronics, Inc.
Brewster, N.Y.

A.2.2 Calibration Data

Calibration data were not required for these measurements.

A.3 THERMAL STRUCTURAL TEST EQUIPMENT

A.3.1 Equipment Description, Test Function, and Name-plate Data

The test equipment and support instrumentation used in the thermal structural test are listed in Table A-2.

A.3.2 Calibration Data

The readings obtained from the strain indicator (item 10, Table A-2) must be corrected to obtain the actual strains experienced by the test specimens. This correction is made by means of the following relation:

$$\text{actual strain} = \text{indicated strain} \left(\frac{\text{indicated gage factor}}{\text{actual gage factor}} \right)$$

The indicated gage factor in these tests was 1.99. The actual gage factors decrease with increasing temperature for each strain gage type as shown in Figures A-2 through A-5. Information on item 2 of Table A-2 has been misplaced. A standard resistor (item 12, Table A-2) was used to check calibration of the strain indicator during the test.

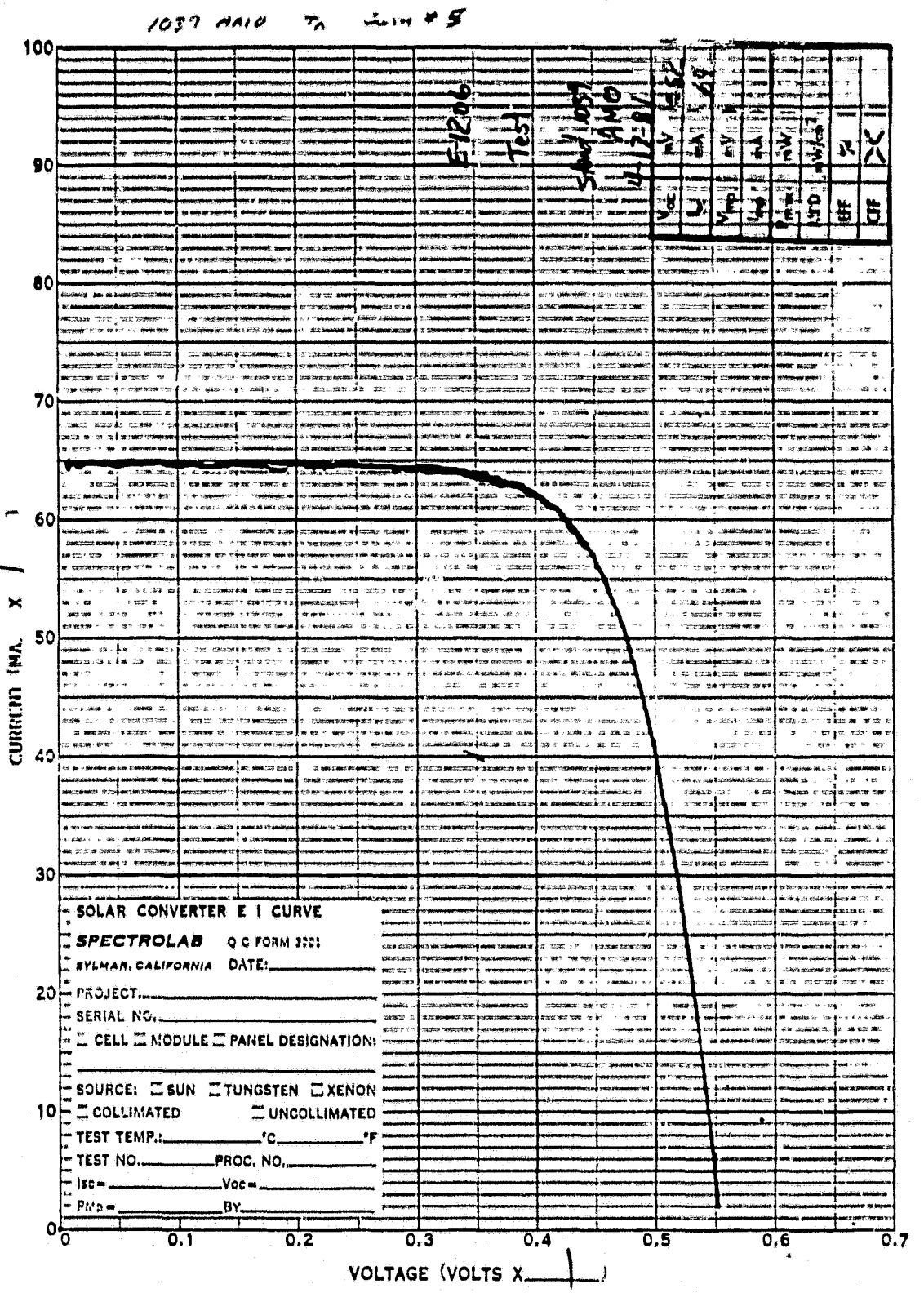

Figure A-1. Current/voltage characteristics for standard cell 1039.

TABLE A–2. TEST EQUIPMENT AND SUPPORT INSTRUMENTATION USED IN THERMAL STRUCTURAL TESTS

Item No.	Description	Test Function	Nameplate Data	Manufacturer
1	Strain gage	Measure strain in silicon (coupons TSC–1 thru TSC–12 and in unencapsulated cell)	Gage Type WK–03–250TM–350 Lot Number DG–K06FB12	Micro-Measurements Measurements Group Raleigh, NC
2	Strain gage	Measure strain in glass (coupon TSC–1)	Gage Type WK–06–250TM–350 Lot Number D–K06FD14	See item 1
3	Strain gage	Measure strain in glass (coupons TSC–2 thru TSC–5) and steel (coupons TSC–9 thru TSC–12)	Gage Type WK–06–250TM–350 Lot Number D–K14FD02	See item 1
4	Strain gage	Measure strain in aluminum (coupons TSC–6 and TSC–8 and in plain aluminum plate)	Gage Type WK–13–250TM–350 Lot Number DG–K14FF13	See item 1
5	Strain gage	Measure strain in steel (coupon TSC–8) plain steel plate and plain glass plate	Gage Type WK–06–250TM–350 Lot Number D–K06FD174	See item 1
6	Strain gage leads	—	26 gage stranded copper wire, teflon-coated	—
7	Thermocouples	Measure coupon temperature	Copper-constantan, 30 gage	
8	Potentiometer	Measure thermocouple voltage	Temperature Potentiometer Catalog No. 8695 (HAC S/N H–188286)	Leeds and Northrop Co. Philadelphia, PA
9	Selector switch	Select thermocouple for temperature reading	12–Position Thermocouple Switch Unit Type 20224–9, Serial No. 101	Baldwin-Lima-Hamilton Corp. Waltham, MA
10	Strain indicator	Convert resistance measurement from strain gage to units of strain	Digital Strain Indicator Model 205 (HAC No. H–210714)	W.T. Bean Detroit, MI
11	Selector switch	Select strain gage for reading	12–Channel Switching and Balancing Unit Type PSBA–12, Model No. 2 Serial No. 118	Baldwin-Lima-Hamilton Corp. Waltham, MA
12	Resistor	Standard resistance for calibration of item 10	Decade Resistor Type No. 1432–M, S/N 19573 (Primary Standard No. F720389)	General Radio Co. Cambridge, MA
13	Temperature chamber	Provide controlled temperature environment for test coupons	Stabil-Therm (Laboratory Oven) Model OV–490, S/N JP–1941 (HAC No. H71007)	Blue-M-Electric Co. Blue Island, IL

ENGINEERING DATA SHEET

THE INFORMATION APPEARING ON THIS SHEET HAS BEEN COMPILED SPECIFICALLY FOR THE GAGES CONTAINED IN THIS PACKAGE. THIS FORM IS PRODUCED WITH ADVANCED EQUIPMENT & PROCEDURES WHICH PERMIT COMPREHENSIVE QUALITY ASSURANCE VERIFICATION OF ALL DATA SUPPLIED HEREIN. SHOULD ANY QUESTIONS ARISE RELATIVE TO THESE GAGES, PLEASE MENTION GAGE TYPE, ITEM NUMBER, AND LOT NUMBER.

Item	Code	Check	Final QA
6	913215	J.R.	G.F.W.

MICRO-MEASUREMENTS
MEASUREMENTS GROUP
RALEIGH, NORTH CAROLINA

PRECISION STRAIN GAGES

GAGE TYPE	WK-03-250TM-350
RESISTANCE IN OHMS	350.0 ± 0.4%
LOT NUMBER	DG-K06FB12
QUANTITY	5 GAGES
OPTIONS	
GAGE FACTOR AT 75°F	
SECTION 1	1.96 ± 1.0%
SECTION 2	1.88 ± 1.0%
SECTION 3 NOMINAL (All Sections)	1.92 ± 3.0%
TCF	-4.6
	-6.0

WK-03-250TM-350

GENERAL INFORMATION: SERIES WK STRAIN GAGES

GENERAL DESCRIPTION WK Series gages are a family of fully encapsulated K-alloy strain gages used in both experimental stress analysis and transducer applications. These gages have integral high-endurance lead ribbons with a backing and encapsulation matrix consisting of a high temperature epoxy phenolic resin system reinforced with glass fiber.

TEMPERATURE RANGE -452°F (-269°C) to +550°F (+290°C) for continuous use in static measurements. Useful to +700°F (+370°C) for short term exposure.

SELF-TEMPERATURE COMPENSATION See data curve below.

STRAIN LIMITS ±1.5% at room temperature; ±1.0% at -320°F (-195°C); ±3% at +400°F (+205°C).

FATIGUE LIFE 10^7 cycles at ±2000μin/in (μm/m); 10^6 cycles at ±2200μin/in (μm/m). Longer gage lengths and lower resistances show greater endurance and less scatter in fatigue life.

BONDING AGENTS High temperature epoxy adhesives are recommended for best performance over the entire temperature range. Micro-Measurements M-Bond 610, 600 and M-Bond GA-60 are particularly compatible with WK Series gages. Refer to M-M Bulletin A-142 for information on bonding agents, and Bulletin B-130 for installation procedures.

LEADWIRE SYSTEM Two flat, high-endurance leads to each tab permit a 3-wire system to be carried directly to the gage, minimizing leadwire errors over the wide useful temperature range of the WK Series gages. Option B-87 WK Series gages are supplied with single 0.005 in (0.13 mm) diameter nickel-clad copper wire leads. Option B-129 gages have single 1/32 in (0.8 mm) x 0.002 in (0.05 mm) nickel-clad copper ribbon leads. Options B-87 and B-129 both reduce fatigue life of WK Series gages, and should not be selected where best cyclic endurance is required. Internal tab connections are +/- 70°F (+410°C) solder. Leadwires may be soft soldered, spot welded or silver soldered. Refer to M-M Bulletin B-132 for information on solders.

NOTE The backing of WK Series gages has been specially treated for optimum bond formation with all appropriate strain gage adhesives. No further cleaning is necessary if contamination of the prepared surface is avoided during handling.

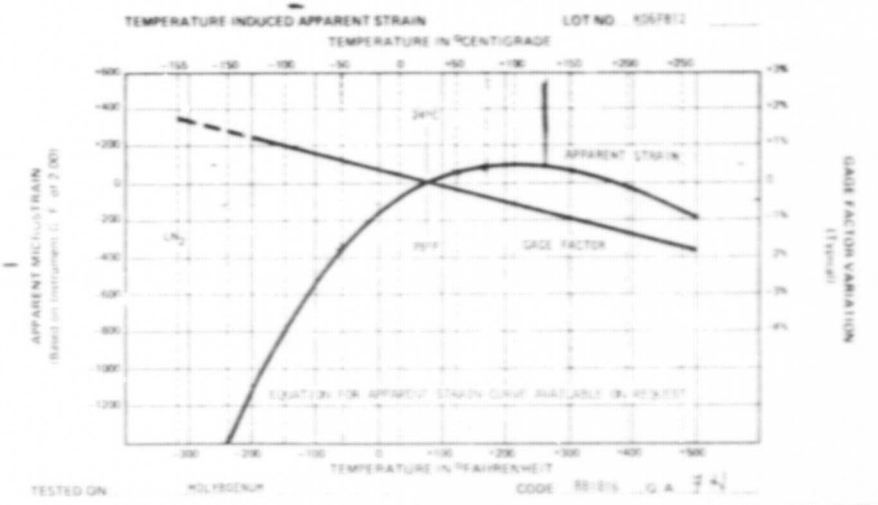

SPECIAL APPLICATION NOTE

FOR 90° T-ROSETTE PATTERNS

Since rolled foil exhibits superior mechanical properties in the direction of rolling, the grid section of a single gage or rosette which has been manufactured with parallel alignment to the rolling axis will possess somewhat improved fatigue characteristics. This section should therefore be aligned with the principal strain axis on the structure, particularly in transducer work. The gage section with most favorable fatigue life is identified below.

PATTERNS IN SECTION 1	062TT, 062TZ, 125TA, 125TB, 125TM, 125TQ, 125UT, 135TN, 250TA, 250TB, 250TC, M250UT, 121TN,
PATTERNS IN SECTION 2	044TP, 062T, 062U, 090TG, 090VA, 121TT, 125TG, 125UA, 125VB, 250TF, 250TG, 250VA, 250VB, 500TF, 062UT

QA MW JB

TEST PROCEDURES USED BY MICRO-MEASUREMENTS FOR STRAIN GAGE PERFORMANCE EVALUATION

OPTICAL DEFECT ANALYSIS	M-M Procedures and Standards
GAGE FACTOR AT 75°F	ASTM E251-67 (Constant Stress Cantilever Method) *
G.F. VARIATION WITH TEMPERATURE	ASTM E251-67 (Step Deflection Method)
APPARENT STRAIN VERSUS TEMPERATURE	ASTM E251-67 (Slow Heating Rate, Continuously Recorded)
TRANSVERSE SENSITIVITY	ASTM E251-67
INITIAL RESISTANCE	M-M Procedure, Direct NBS Traceability on Resistance Standards
FATIGUE LIFE	NAS 942 (Modified)
STRAIN LIMITS	NAS 942 (Modified)
GAGE THICKNESS	M-M Procedure
CREEP AND DRIFT	M-M Procedure (Similar to NAS 942 Method)

*Gage factor data are obtained in a uniaxial stress field with Poisson's ratio of approximately 0.285.

Figure A-2. Calibration data for item 1 (Table A-2) strain gages.

ENGINEERING DATA SHEET

THE INFORMATION APPEARING ON THIS SHEET HAS BEEN COMPILED SPECIFICALLY FOR THE GAGES CONTAINED IN THIS PACKAGE. THIS FORM IS PRODUCED WITH ADVANCED EQUIPMENT & PROCEDURES WHICH PERMIT COMPREHENSIVE QUALITY ASSURANCE VERIFICATION OF ALL DATA SUPPLIED HEREIN. SHOULD ANY QUESTIONS ARISE RELATIVE TO THESE GAGES, PLEASE MENTION GAGE TYPE, ITEM NUMBER, AND LOT NUMBER.

Item	Code	Check	Final QA
6774-2	913215	J.R.	G.F.M.

MICRO-MEASUREMENTS
MEASUREMENTS GROUP
RALEIGH, NORTH CAROLINA

PRECISION STRAIN GAGES

WK-06-250TM-350

GAGE TYPE: WK-06-250TM-350

RESISTANCE IN OHMS: 350.0 ± 0.4Ω

LOT NUMBER: D-K14FD02

QUANTITY: 5 GAGES

OPTIONS: Gages in pack

	GAGE FACTOR AT 75°F	NKL
SECTION 1	2.02 ± 1.0%	-4.4
SECTION 2	1.93 ± 1.0%	-6.2
NOMINAL (All Sections)	1.98 ± 3.5%	

GENERAL INFORMATION: SERIES WK STRAIN GAGES

GENERAL DESCRIPTION: WK-Series gages are a family of fully encapsulated K-alloy strain gages used in both experimental stress analysis and transducer applications. These gages have integral high-endurance lead ribbons with a backing and encapsulation matrix consisting of a high temperature epoxy phenolic resin system reinforced with glass fiber.

TEMPERATURE RANGE: -452°F (-269°C) to +550°F (+290°C) for continuous use in static measurements. Useful to +700°F (+370°C) for short term exposure.

SELF-TEMPERATURE COMPENSATION: See data curve below.

STRAIN LIMITS: ±1.5% at room temperature; ±1.0% at -320°F (-195°C); ±3% at +400°F (+205°C).

FATIGUE LIFE: 10^6 cycles at ±2000μin/in (μm/m); 10^7 cycles at ±2200μin/in (μm/m). Longer gage lengths and lower resistances show greater endurance and less scatter in fatigue life.

BONDING AGENTS: High-temperature epoxy adhesives are recommended for best performance over the entire temperature range. Micro-Measurements' M-Bond 610, 600 and M-Bond GA-60 are particularly compatible with WK-Series gages. Refer to M-M Bulletin A-142 for information on bonding agents, and Bulletin B-130 for installation procedures.

LEADWIRE SYSTEM: Two flat high-endurance leads to each tab permit a 3-wire system to be carried directly to the gage, minimizing leadwire errors over the wide useful temperature range of the WK-Series gages. Option B-87 WK-Series gages are supplied with single 0.005 in (0.13 mm) diameter nickel-clad copper wire leads. Option B-129 gages have single 1/32 in (0.8 mm) x 0.002 in (0.05 mm) nickel-clad copper ribbon leads. Options B-87 and B-129 both reduce fatigue life of WK-Series gages, and should not be selected where best cyclic endurance is required. Internal tab connections are +770°F (+410°C) solder. Leadwires may be soft soldered, spot welded or silver soldered. Refer to M-M Bulletin B-132 for information on solders.

NOTE: The backing of WK-Series gages has been specially treated for optimum bond formation with all appropriate strain gage adhesives. No further cleaning is necessary if contamination of the prepared surface is avoided during handling.

FORM B-301B

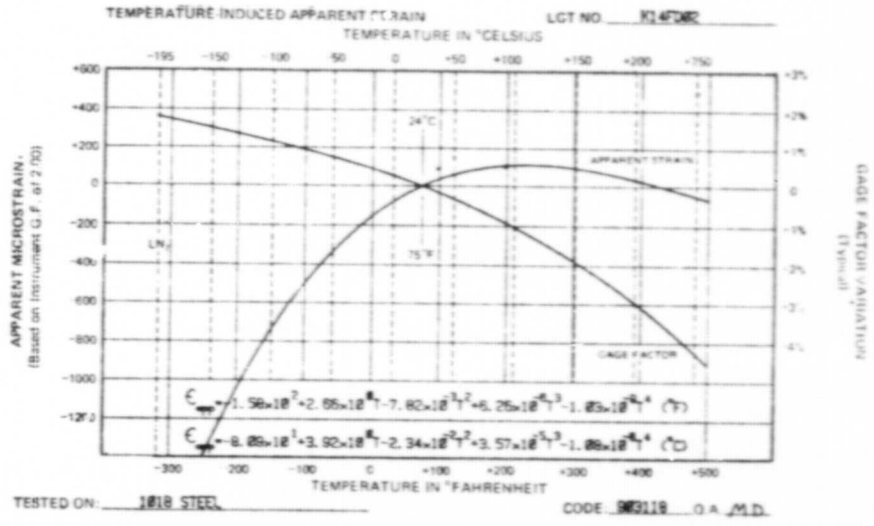

SPECIAL APPLICATION NOTE

FOR 90° T-ROSETTE PATTERNS

Since rolled foil exhibits superior mechanical properties in the direction of rolling, the grid section of a single-plane rosette which has been manufactured with parallel alignment to the rolling axis will possess somewhat improved fatigue characteristics. This section should therefore be aligned with the principal strain axis on the structure, particularly in transducer work. The gage section with most favorable fatigue life is identified below.

PATTERNS IN SECTION 1	062TT	062TZ	125TP	125TB	125TM	125TQ	125UT	135TN	250TA	250TB	250TM	250UT	270TN	
PATTERNS IN SECTION 2	044TP	062TJ	100TU	100VA	125TF	125TG	125VA	125VB	250TF	250TG	250VA	250VB	500TF	
	062UT													

Form 03-462
Date Printed

QA MM JB

TEST PROCEDURES USED BY MICRO-MEASUREMENTS FOR STRAIN GAGE PERFORMANCE EVALUATION

OPTICAL DEFECT ANALYSIS	M-M Procedures and Standards
GAGE FACTOR AT 75°F	ASTM E251-67 (Constant Stress Cantilever Method) *
G.F. VARIATION WITH TEMPERATURE	ASTM E251-67 (Step Deflection Method)
APPARENT STRAIN VERSUS TEMPERATURE	ASTM E251-67 (Slow Heating Rate, Continuously Recorded)
TRANSVERSE SENSITIVITY	ASTM E251-67
INITIAL RESISTANCE	M-M Procedure, Direct NBS Traceability on Resistance Standards
FATIGUE LIFE	NAS 942 (Modified)
STRAIN LIMITS	NAS 942 (Modified)
GAGE THICKNESS	M-M Procedure
CREEP AND DRIFT	M-M Procedure (Similar to NAS 942 Method)

*Gage factor data are obtained in a uniaxial stress field with Poisson's ratio of approximately 0.285.

Figure A-3. Calibration data for item 3 (Table A-2) strain gages.

ENGINEERING DATA SHEET

THE INFORMATION APPEARING ON THIS SHEET HAS BEEN COMPILED SPECIFICALLY FOR THE GAGES CONTAINED IN THIS PACKAGE. THIS FORM IS PRODUCED WITH ADVANCED EQUIPMENT & PROCEDURES WHICH PERMIT COMPREHENSIVE QUALITY ASSURANCE VERIFICATION OF ALL DATA SUPPLIED HEREIN. SHOULD ANY QUESTIONS ARISE RELATIVE TO THESE GAGES, PLEASE MENTION GAGE TYPE, ITEM NUMBER, AND LOT NUMBER.

Item	Code	Check	Final QA
6088 (K2)	881516	N.J.W.	M.T.

MICRO-MEASUREMENTS
ROMULUS, MICHIGAN

PRECISION STRAIN GAGES

ITEM NUMBER	WK-13-250TM-350
GAGE TYPE	WK-13-250TM-350
RESISTANCE IN OHMS	350.0 ± 0.4%
LOT NUMBER	DG-K14FF13
QUANTITY	5 GAGES
OPTIONS	
GAGE FACTOR AT 75°F	
SECTION 1	2.17 ± 1.0%
SECTION 2	2.02 ± 1.0%
SECTION 3 (NOMINAL, All Sections)	2.10 ± 4.5%
%R.*	-5.2
%R.*	-7.1

TEMPERATURE-INDUCED APPARENT STRAIN — LOT NO. K14FF13

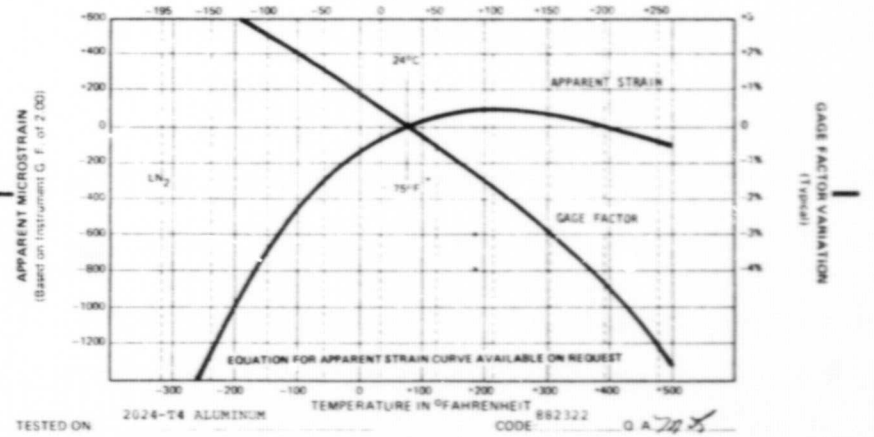

TESTED ON 2024-T4 ALUMINUM — CODE 882322 — Q.A.

GENERAL INFORMATION: SERIES WK STRAIN GAGES

GENERAL DESCRIPTION: WK Series gages are a family of fully encapsulated K alloy strain gages used in both experimental stress analysis and transducer applications. These gages have integral high-endurance lead ribbons with a backing and encapsulation matrix consisting of a high-temperature epoxy phenolic resin system reinforced with glass fiber.

TEMPERATURE RANGE: -452°F (-269°C) to +550°F (+290°C) for continuous use in static measurements. Useful to +700°F (+370°C) for short term exposure.

SELF-TEMPERATURE COMPENSATION: See data curve below.

STRAIN LIMITS: ±1.5% at room temperature; ±1.0% at -320°F (-195°C); ±3% at +400°F (+205°C).

FATIGUE LIFE: 10^7 cycles at ±2000μin/in (μm/m); 10^6 cycles at ±2200μin/in (μm/m). Longer gage lengths and lower resistances show greater endurance and less scatter in fatigue life.

BONDING AGENTS: High temperature epoxy adhesives are recommended for best performance over the entire temperature range. Micro-Measurements M-Bond 610, 600 and M-Bond GA-60 are particularly compatible with WK Series gages. Refer to M-M Bulletin A-142 for information on bonding agents, and Bulletin B-130 for installation procedures.

LEADWIRE SYSTEM: Two flat high-endurance leads to each tab permit a 3-wire system to be carried directly to the gage, minimizing leadwire errors over the wide useful temperature range of the WK Series gages. Option B-87 WK Series gages are supplied with single 0.005 in (0.13 mm) diameter nickel-clad copper wire leads. Option B-129 gages have single 1/32 in (0.8 mm) x 0.002 in (0.05 mm) nickel-clad copper ribbon leads. Options B-87 and B-129 both reduce fatigue life of WK Series gages, and should not be selected where best cyclic endurance is required. Internal tab connections are +770°F (+410°C) solder. Leadwires may be soft soldered, spot welded or silver soldered. Refer to M-M Bulletin B-132 for information on solders.

NOTE: The backing of WK Series gages has been specially treated for optimum bond formation with all appropriate strain gage adhesives. No further cleaning is necessary if contamination of the prepared surface is avoided during handling.

FORM 86318

SPECIAL APPLICATION NOTE

FOR 90° T-ROSETTE PATTERNS

Since rolled foil exhibits superior mechanical properties in the direction of rolling, the grid section of a single-plane rosette which has been manufactured with parallel alignment to the rolling axis will possess somewhat improved fatigue characteristics. This section should therefore be aligned with the principal strain axis on the structure, particularly in transducer work. The gage section with most favorable fatigue life is identified below:

PATTERNS IN SECTION 1	062TT	062TZ	125TA	125TB	125TM	125TQ	125UT	135TN	250TA	250TB	250TM	250UT	270TN
PATTERNS IN SECTION 2	044TP	062TJ	100TG	100VA	125TF	125TG	125VA	125VB	250TF	250TG	250VA	250VB	500TF

Form B1-462
Code B41021

TEST PROCEDURES USED BY MICRO-MEASUREMENTS FOR STRAIN GAGE PERFORMANCE EVALUATION

OPTICAL DEFECT ANALYSIS	M-M Procedures and Standards
GAGE FACTOR AT 75°F	ASTM E251-67 (Constant Stress Cantilever Method)*
G.F. VARIATION WITH TEMPERATURE	ASTM E251-67 (Step-Deflection Method)
APPARENT STRAIN VERSUS TEMPERATURE	ASTM E251-67 (Slow Heating Rate, Continuously Recorded)
TRANSVERSE SENSITIVITY	ASTM E251-67
INITIAL RESISTANCE	M-M Procedure, Direct NBS Traceability on Resistance Standards
FATIGUE LIFE	NAS 942 (Modified)
STRAIN LIMITS	NAS 942 (Modified)
GAGE THICKNESS	M-M Procedure
CREEP AND DRIFT	M-M Procedure (Similar to NAS 942 Method)

NOTE: This data is obtained in an uniaxial stress field with Poisson's ratio of approximately .285.

Figure A-4. Calibration data for item 4 (Table A-2) strain gages.

ENGINEERING DATA SHEET

THE INFORMATION APPEARING ON THIS SHEET HAS BEEN COMPILED SPECIFICALLY FOR THE GAGES CONTAINED IN THIS PACKAGE. THIS FORM IS PRODUCED WITH ADVANCED EQUIPMENT & PROCEDURES WHICH PERMIT COMPREHENSIVE QUALITY ASSURANCE VERIFICATION OF ALL DATA SUPPLIED HEREIN. SHOULD ANY QUESTIONS ARISE RELATIVE TO THESE GAGES, PLEASE MENTION GAGE TYPE, ITEM NUMBER, AND LOT NUMBER.

Final QA	Check	Code	Item
M.T.	N.J.W.	901819	6408

MICRO-MEASUREMENTS
ROMULUS, MICHIGAN

PRECISION STRAIN GAGES

WK-06-250TM-350

GAGE TYPE	RESISTANCE IN OHMS	LOT NUMBER	QUANTITY	OPTIONS	GAGE FACTOR AT 75°F		
WK-06-250TM-350	350.0 ± 0.4%	D-K06FD174	5 GAGES				

SECTION 3	SECTION 2	SECTION 1	GAGE FACTOR AT 75°F	
NOMINAL (All Sections)				
1.94 ± 3.5%	1.89 ± 1.0%	1.99 ± 1.0%	-5.2	NAL
	-6.6			

GENERAL INFORMATION: SERIES WK STRAIN GAGES

GENERAL DESCRIPTION: WK Series gages are a family of fully encapsulated K-alloy strain gages used in both experimental stress analysis and transducer applications. These gages have integral high endurance lead ribbons with a backing and encapsulation matrix consisting of a high temperature epoxy phenolic resin system reinforced with glass fiber.

TEMPERATURE RANGE: -452°F (-269°C) to +550°F (+290°C) for continuous use in static measurements. Useful to +700°F (+370°C) for short term exposure.

SELF-TEMPERATURE COMPENSATION: See data curve below.

STRAIN LIMITS: ±1.5% at room temperature, ±1.0% at -320°F (-195°C), ±3% at +400°F (+205°C).

FATIGUE LIFE: 10^7 cycles at ±2000μin/in (μm/m), 10^6 cycles at ±2200μin/in (μm/m). Longer gage lengths and lower resistances show greater endurance and less scatter in fatigue life.

BONDING AGENTS: High temperature epoxy adhesives are recommended for best performance over the entire temperature range. Micro-Measurements M-Bond 610, 600 and M-Bond GA-60 are particularly compatible with WK Series gages. Refer to M-M Bulletin A-142 for information on bonding agents, and Bulletin B-130 for installation procedures.

LEADWIRE SYSTEM: Two flat high-endurance leads to each tab permit a 3-wire system to be carried directly to the gage, minimizing leadwire errors over the wide useful temperature range of the WK Series gages. Option B-87 WK Series gages are supplied with single 0.005 in (0.13 mm) diameter nickel-clad copper wire leads. Option B-129 gages have single 1/32 in (0.8 mm) x 0.002 in (0.05 mm) nickel-clad copper ribbon leads. Options B-87 and B-129 both reduce fatigue life of WK Series gages, and should not be selected where best cyclic endurance is required. Internal tab connections are +770°F (+410°C) solder. Leadwires may be soft soldered, spot welded or silver soldered. Refer to M-M Bulletin B-132 for information on solders.

NOTE: The backing of WK Series gages has been specially treated for optimum bond formation with all appropriate strain gage adhesives. No further cleaning is necessary if contamination of the prepared surface is avoided during handling.

FORM 888018

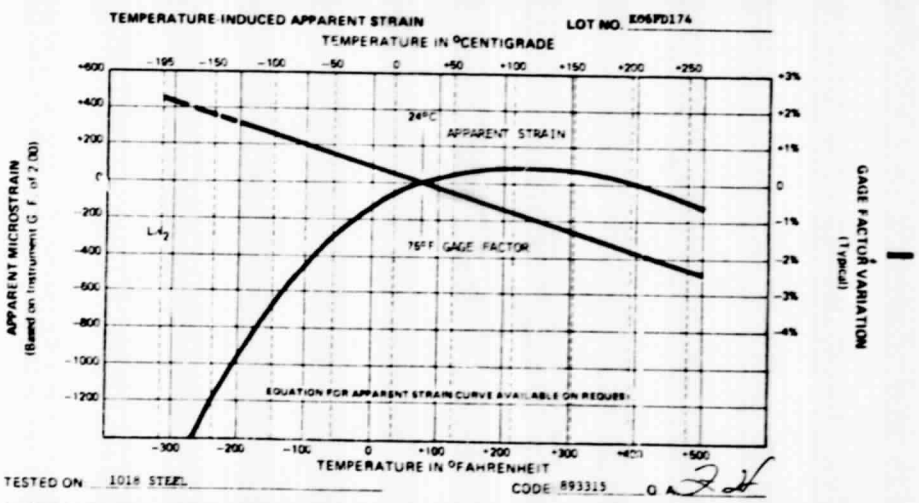

SPECIAL APPLICATION NOTE

FOR 90° T-ROSETTE PATTERNS

Since rolled foil exhibits superior mechanical properties in the direction of rolling, the grid section of a single-plane rosette which has been manufactured with parallel alignment to the rolling axis will possess somewhat improved fatigue characteristics. This section should therefore be aligned with the principal strain axis on the structure, particularly in transducer work. The axial section with most favorable fatigue life is identified below.

PATTERNS IN SECTION 1	062TT	062TZ	125TA	125TB	125TM	125TQ	125UT	135TN	250TA	250TB	250TM	250UT	270TN
PATTERNS IN SECTION 2	044TP	062TJ	100TG	100VA	125TF	125TG	125VA	125VB	250TF	250TG	250VA	250VB	500TF

Form 81-482
Code 841021

QA MM JB

TEST PROCEDURES USED BY MICRO-MEASUREMENTS FOR STRAIN GAGE PERFORMANCE EVALUATION

OPTICAL DEFECT ANALYSIS	M-M Procedures and Standards
GAGE FACTOR AT 75°F	ASTM E251-67 (Constant Stress Cantilever Method) *
G.F. VARIATION WITH TEMPERATURE	ASTM E251-67 (Step Deflection Method)
APPARENT STRAIN VERSUS TEMPERATURE	ASTM E251-67 (Slow Heating Rate, Continuously Recorded)
TRANSVERSE SENSITIVITY	ASTM E251-67
INITIAL RESISTANCE	M-M Procedure, Direct NBS Traceability on Resistance Standards
FATIGUE LIFE	NAS 942 (Modified)
STRAIN LIMITS	NAS 942 (Modified)
GAGE THICKNESS	M-M Procedure
CREEP AND DRIFT	M-M Procedure (Similar to NAS 942 Method)

*Gage factor data are obtained in a uniaxial stress field with Poisson's ratio of approximately 0.285.

Figure A-5. Calibration data for item 5 (Table A-2) strain gages

A.4 STRUCTURAL DEFLECTION TEST EQUIPMENT

A.4.1 Equipment Description, Test Function, and Nameplate Data

The test equipment and support instrumentation used in the structural deflection test are listed in Table A-3.

A.4.2 Calibration Data

Calibration data for the strain gages (item 1, Table A-3) are shown in Figure A-6. A standard resistor (item 4, Table A-3) was used to check calibration of the strain indicator (item 2, Table A-3) during the test.

TABLE A–3. TEST EQUIPMENT AND SUPPORT INSTRUMENTATION USED IN STRUCTURAL DEFLECTION TEST

Item No.	Description	Test Function	Nameplate Data	Manufacturer
1	Strain gage	Measure strain in all test specimens	Gage Type EA-05-250AE-350 Lot Number R-A38AC07	Micro-Measurements Measurements Group Raleigh, NC
2	Strain indicator	Convert resistance measurement from strain gage to units of strain	Digital Strain Indicator Model 205 (HAC No. H-210714)	W. T. Bean Detroit, MI
3	Selector switch	Select strain gage for reading during test	12-Channel Switching and Balancing Unit Type PSBA-12, Model No. 2 Serial No. 118	Baldwin-Lima-Hamilton Corp. Philadelphia, PA
4	Resistor	Standard resistance for calibration of item 2	Decade Resistor Type No. 1432-M, S/N 19573 (Primary Standard No. F720389)	General Radio Co. Cambridge, MA
5	X-Y plotter	Plot load versus deflection at center of each test specimen	Omnigraphic Plotter Model 2000 Recorder (HAC No. H323339)	Bausch and Lomb Houston Instrument Div. Houston, TX
6	Transducer	Measure deflection at center and mid-diagonal positions of test specimens	Displacement Transducer Model 406 (serial no. 764 at center position and serial no. 765 at mid-diagonal position) (3.5-inch maximum displacement)	Research, Inc. Controls Div. Minneapolis, MN
7	Dial indicator	Measure deflection at mid-diagonal and corner positions of test specimens	Dial Indicator Model No. 656-341 (HAC No. H-906336 at mid-diagonal position and HAC No. H-906346 at corner position)	L. S. Starrett Co. Athol, MA
8	Load cell	Meas weight of water in test apparatus	Load Cell Serial No. LC3-1000 (Primary Standard No. F437097)	Hughes Aircraft Co. Culver City, CA
9	Strain gage leads	Electrical connection between strain gages and selector switch	Flat-ribbon strain gage wire, 26-gage, vinyl coated	—

ENGINEERING DATA SHEET

THE INFORMATION APPEARING ON THIS SHEET HAS BEEN COMPILED SPECIFICALLY FOR THE GAGES CONTAINED IN THIS PACKAGE. THIS FORM IS PRODUCED WITH ADVANCED EQUIPMENT & PROCEDURES WHICH PERMIT COMPREHENSIVE QUALITY ASSURANCE VERIFICATION OF ALL DATA SUPPLIED. HOWEVER, SHOULD ANY QUESTIONS ARISE RELATIVE TO THESE GAGES, PLEASE MENTION GAGE TYPE, ITEM NUMBER, AND LOT NUMBER.

Final QA	Check	Date	Item
G.F.W.	J.R.	911415	[illegible]

MICRO-MEASUREMENTS
ROMULUS, MICHIGAN

PRECISION STRAIN GAGES

GAGE TYPE	EA-05-250AE-350
RESISTANCE IN OHMS	350.0 ± 0.15%
GAGE FACTOR AT 75°F	2.06 ± 0.5%
K_t	-0.5%
LOT NUMBER	R-A38AC07
QUANTITY	5 GAGES
OPTION	

EA-05-250AE-350

GENERAL INFORMATION: SERIES EA STRAIN GAGES

GENERAL DESCRIPTION: EA Series Gages are a general purpose family of constantan strain gages widely used in experimental stress analysis. These gages are of open faced construction with a 1 mil (0.03mm) tough, flexible polyimide film backing.

TEMPERATURE RANGE: -100°F (-75°C) to +350°F (+175°C) for continuous use in static measurements. -320°F (-195°C) to +400°F (+205°C) for special or short term exposure.

SELF TEMPERATURE COMPENSATION: See data curve below.

STRAIN LIMITS: Approximately 5% for gage lengths 1/8" (3.2mm) and larger, and approximately 3% for gage lengths under 1/8" (3.2mm).

FATIGUE LIFE: 10^6 cycles at ±1200μ"/" (μm/m); 10^7 cycles at ±1500μ"/" (μm/m); 10^7 cycles at ±1800 μ"/" (μm/m); 10^8 cycles at 2800μ"/" (μm/m) unidirectional, tension or compression only. Longer gage lengths and lower resistances result in greater endurance and less scatter in fatigue life.

CEMENTS: Compatible with M-M Certified M-Bond 200 but it will normally not provide the greatest fatigue life. Micro-Measurements' M-Bond AE 10/15, M-Bond GA-2, M-Bond 600, and M-Bond 610 are excellent. M-Bond 610 is the best choice over the entire operating range. Refer to M-M Bulletin A-142 for information on bonding agents, and Bulletins B-127, B-130, and B-137 for installation procedures.

SOLDER: If operating temperature will not exceed +300°F (+150°C), M-Line solder type 361 (63-37) tin-lead solder may be used for lead attachment. M-Line solder type 450 (95-5) tin-antimony is satisfactory to +400°F (+205°C). When solder turrets (Option S) are supplied on these gages, they are formed with +570°F (+300°C) lead-tin-silver solder alloy. Refer to M-M Bulletin A-132 for further information on solder, and Bulletin TT-127 and TT-128 for lead attachment techniques.

PROTECTIVE COATINGS: These EA open faced gages should always be protected with a suitable coating that is applied as soon as possible after gage installation. Refer to M-M Bulletin A-134 for information on Strain Gage Protective Coatings.

BACKING: The backing of EA Series Gages has been specially treated for optimum bond formation with all appropriate strain gage adhesives. No further cleaning is necessary if contamination of the prepared surface is avoided during handling.

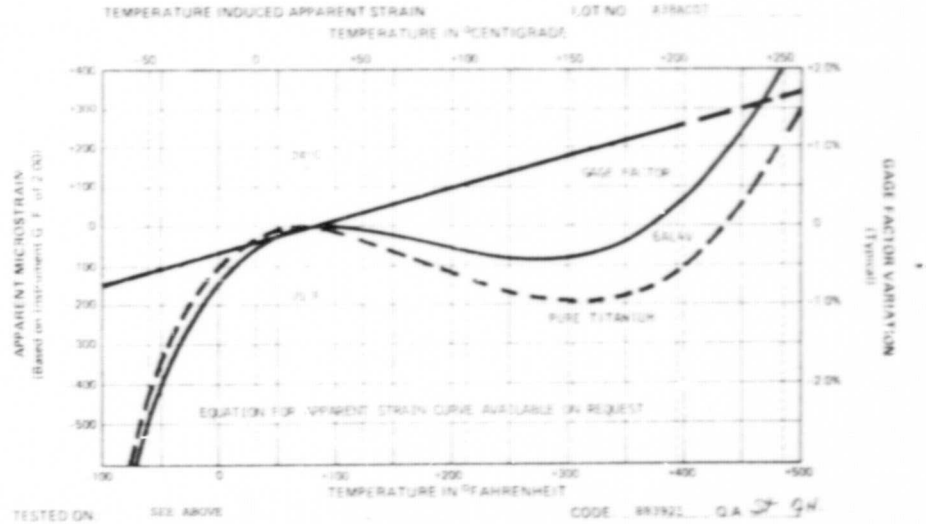

TEST PROCEDURES USED BY MICRO-MEASUREMENTS FOR STRAIN GAGE PERFORMANCE EVALUATION

OPTICAL DEFECT ANALYSIS	M-M Procedures and Standards
GAGE FACTOR AT 75°F	ASTM E251-67 (Constant Stress Cantilever Method) *
G.F. VARIATION WITH TEMPERATURE	ASTM E251-67 (Step Deflection Method)
APPARENT STRAIN VERSUS TEMPERATURE	ASTM E251-67 (Slow Heating Rate, Continuously Recorded)
TRANSVERSE SENSITIVITY	ASTM E251-67
INITIAL RESISTANCE	M-M Procedure, Direct NBS Traceability on Resistance Standards
FATIGUE LIFE	NAS 942 (Modified)
STRAIN LIMITS	NAS 942 (Modified)
GAGE THICKNESS	M-M Procedure
CREEP AND DRIFT	M-M Procedure (Similar to NAS 942 Method)

*Gage factor data are obtained in a uniaxial stress field with Poisson's ratio of approximately 0.285.

Figure A-6. Calibration data for item 1 (Table A-3) strain gages.

A.5 THERMAL TEST EQUIPMENT

A.5.1 Equipment Description, Test Function, and Nameplate Data

The test equipment and support instrumentation used in the thermal test are listed in Table A-4.

A.5.2 Calibration Data

The pyrheliometer (item 1, Table A-4) and the pyranometer (item 2, Table A-4) were used to measure the radiant energy flux in the plane of the test modules. The conversion constants are 0.0184 W cm^{-2} mV^{-1} and 0.0092 W cm^{-2} mV^{-1} for the pyrheliometer and pyranometer, respectively. The accuracies of these instruments are ±3 percent and ±1 percent, respectively.

TABLE A–4. TEST EQUIPMENT AND SUPPORT INSTRUMENTATION USED IN THERMAL TESTS

Item No.	Description	Test Function	Nameplate Data	Manufacturer
1	Pyrheliometer	Determine level and uniformity of radiant heat flux in front plane of modules	Pyrheliometer Model P–800–J–50–120	Hy-Cal Engineering Santa Ana, CA
2	Pyranometer	Determine radiant heat flux in front plane of modules	Pyranometer Spectrosun Model SR–75 Serial No. 78–129	Spectrolab, Inc. Sylmar, CA
3	Hot-wire anemometer	Determine air velocity at selected locations inside test chamber	TSI Air Velocity Meter Model 1646 Serial No. 902	TSI, Inc. St. Paul, MN
4	Multimeter	Measure voltage outputs from items 1, 2, and 10	Multimeter Model 8020A Serial No. 2026633 (HAC No. H973360)	John Fluke, Inc. Seattle, WA
5	Test chamber	Provide controlled thermal environment	Chamber Model 740H Serial No. G0397	Bally Case and Cooler, Inc. Bally, PA
6	Lamps	Source of radiant heat flux impinging on module surface	Lamp Model No. 1000 T3/CL (1000 Watt @ 240 Volt)	General Electric Co. Cleveland, OH
7	Holding fixture	Provide mounting support and reflectors for lamps (item 6)	Radiant Heater Assembly Model No. AU8–612	Research, Inc. Hopkins, MN
8	Thermocouples	Measure temperature of solar cells	Copper-constantan Cat. No. COCO–.010 (10 mil diam., 12 inches long)	Omega Engineering, Inc. Stamford, CT
9	Thermocouples	Measure temperatures other than those of solar cell	Copper-constantan, 30 Gage	Hughes Aircraft Co. Culver City, CA
10	Adjustable transformer	Provide constant line voltage to lamps	Variac Type 50–A (115 Volt, 5KVA, 60 cycle) (HAC No. 974000)	General Radio Co. Cambridge, MA

(Continued next page)

TABLE A–4. TEST EQUIPMENT AND SUPPORT INSTRUMENTATION USED IN THERMAL TESTS (Concluded)

Item No.	Description	Test Function	Nameplate Data	Manufacturer
11	Air temperature conditioning unit	Provide constant-temperature air to test chamber	Air Temperature Conditioning Unit Model P-CH-810-LN2 Serial No. 6696 (HAC No. H-340071)	Thermotron Corp. Holland, MI
12	Digital thermometer	Monitor air temperature measured by thermocouple No. 82	Digital Thermometer Model 2165A Serial No. 2110003 (HAC No. H-384476)	John Fluke, Inc. Seattle, WA
13	Data manager	Display thermocouple data and send data to storage	Data Manager Model 9845B (HAC No. 368745)	Hewlett Packard Palo Alto, CA
14	Remote data scanner	Transmit thermocouple data to control room	Remote Scanner Chassis Model 2202A Serial No. 2016003 (HAC No. 376279)	John Fluke, Inc. Seattle, WA
15	Test data aquisition system (TDAS)	Aquire thermocouple data from remote data scanner and send to data manager	TDAS Model 9835A (HAC No. 374336)	Hewlett Packard Palo Alto, CA
16	Datalogger	Collect thermocouple data and display each channel (one at a time) on a continuous updating basis	Datalogger Model 2240B Serial No. 2155008	John Fluke, Inc. Seattle, WA
17	Data storage	Store thermocouple data on disk	Flexible Disk Drive Model 98855 (HAC No. H-371733)	Hewlett Packard Palo Alto, CA

APPENDIX B

RAW DATA

APPENDIX B. RAW DATA

B.1 OPTICAL TEST DATA

Raw data for the optical test consist of the following items, which were measured for all photovoltaic cells used in the specimens. Data were obtained for both xenon and tungsten illumination sources:

1. Open-circuit voltage before encapsulation
2. Open-circuit voltage after encapsulation
3. Short-circuit current before encapsulation
4. Short-circuit current after encapsulation
5. Cell current at 500 mv before encapsulation
6. Cell current at 500 mv after encapsulation

These data are listed in Table B-1.

In a second series of tests, cardboard frames were used to permit illumination of the cells only. These tests were performed for both xenon and tungsten sources, and the data are listed in Table B-2.

TABLE B–1. RAW DATA FOR OPTICAL TESTS (NO FRAMING)

Coupon ID	Cell Number	Xenon Light Source					Tungsten Light Source				
		V_{oc} Before/After	I_{sc} Before/After	I_{500} Before/After	I_{sc} Ratio	I_{500} Ratio	V_{oc} Before/After	I_{sc} Before/After	I_{500} Before/After	I_{sc} Ratio	I_{500} Ratio
OC-1	BC-11	596/598	635/768	561/468	1.21	0.83	585/584	521/721	450/420	1.38	0.93
	BC-15	596/598	618/805	577/715	1.31	1.24	586/588	514/756	454/653	1.47	1.44
OC-2	A	536/540	952/1160	506/649	1.22	1.28	530/530	787/952	367/455	1.21	1.24
	AA	539/547	862/1080	464/651	1.25	1.40	533/535	726/866	345/439	1.19	1.27
OC-3	BC-14	597/594	647/732	536/646	1.13	1.21	587/571	527/648	469/526	1.23	1.12
	BC-9	597/597	634/733	577/656	1.16	1.14	587/576	524/650	466/546	1.24	1.17
OC-4	BC-17	598/596	634/837	577/750	1.32	1.30	587/590	529/760	472/669	1.44	1.42
	BC-18	594/595	647/830	536/658	1.28	1.23	583/582	529/762	431/585	1.44	1.36
OC-5	BC-10	597/597	637/829	574/737	1.30	1.28	587/583	520/774	460/661	1.49	1.44
	BC-13	597/595	622/815	564/730	1.31	1.29	586/583	523/761	464/668	1.46	1.44
OC-6	I-16	591/593	632/779	550/674	1.23	1.23	582/585	592/714	502/605	1.21	1.21
	B-7	597/602	669/737	603/765	1.10	1.27	597/596	649/694	577/594	1.07	1.03
OC-7	I-17	592/592	619/755	552/650	1.22	1.18	580/588	529/716	440/613	1.35	1.39
	I-18	591/591	625/765	553/643	1.22	1.16	579/584	529/721	435/591	1.36	1.36
OC-8	I-7	590/592	622/759	508/674	1.22	1.33	578/585	507/722	446/619	1.42	1.39
	I-6	592/595	619/762	556/674	1.23	1.21	578/587	517/727	435/610	1.41	1.40
OC-9	B-5	602/597	857/853	762/748	1.00	0.98	593/587	788/796	692/665	1.01	0.96
	B-14	603/598	857/852	780/784	0.99	1.01	594/588	784/797	705/689	1.02	0.98
OC-10	No. 15	590/590	701/737	578/597	1.05	1.03	580/582	642/673	511/534	1.05	1.05
	No. 16	580/587	703/740	569/581	1.05	1.02	578/578	644/670	503/512	1.04	1.02
OC-11	I-4	591/594	614/766	511/682	1.25	1.24	579/585	510/731	441/638	1.43	1.45
	I-12	590/591	618/754	542/658	1.22	1.21	578/583	504/715	423/622	1.42	1.47
OC-12	B-18	602/596	863/806	786/717	0.93	0.91	594/582	789/762	710/652	0.97	0.92
	B-19	602/596	857/815	770/718	0.95	0.93	594/584	781/765	694/648	0.98	0.93
OC-13	No. 23	589/589	756/739	570/552	0.98	0.97	581/571	696/681	505/465	0.98	0.92
	No. 24	595/592	751/742	609/571	0.99	0.94	589/578	693/684	550/489	0.99	0.89

Notes: 1. V_{oc} = open-circuit voltage, mv
I_{sc} = short-circuit current, ma
I_{500} = cell current at 500 mv, ma

2. Before/After refers to before encapsulation and after encapsulation of the cells

3. Current ratios refer to current measured after encapsulation divided by current measured before encapsulation.

TABLE B–2. DATA FOR OPTICAL TESTS WITH FRAMING

Coupon ID	Cell Number	Tungsten				Xenon			
		I_{sc}, ma		I_{500}, ma		I_{sc}, ma		I_{500}, ma	
		No Frame	With Frame	No Frame	With Frame	No Frame	With Frame	No Frame	With Frame
OC–1	BC–11	C	C	C	C	C	C	C	C
	BC–15	748	740	659	650	794	788	683	673
OC–2	A	NF	NF	NF	NF	NF	NF	NF	NF
	AA	NF	NF	NF	NF	NF	NF	NF	NF
OC–3	BC–14	654	652	558	552	728	725	619	612
	BC–9	643	642	549	545	720	717	618	610
OC–4	BC–17	C	C	C	C	C	C	C	C
	BC–18	766	753	613	602	819	807	623	604
OC–5	BC–10	C	C	C	C	C	C	C	C
	BC–13	758	745	671	655	798	786	700	686
OC–6	I–16	724	722	606	602	780	780	632	632
	B–7	C	C	C	C	C	C	C	C
OC–7	I–17	NA	NA	NA	NA	NA	NA	NA	NA
	I–18	NA	NA	NA	NA	NA	NA	NA	NA
OC–8	I–7	724	721	627	625	793	790	644	642
	I–6	729	727	625	611	790	785	635	632
OC–9	B–5	C	C	C	C	C	C	C	C
	B–14	C	C	C	C	C	C	C	C
OC–10	No. 15	677	664	527	525	736	726	526	521
	No. 16	682	678	517	516	730	723	503	503
OC–11	I–4	733	720	645	633	785	769	639	627
	I–12	719	709	595	586	778	766	625	599
OC–12	B–18	804	800	707	705	855	854	700	700
	B–19	808	805	706	704	856	854	692	688
OC–13	No. 23	679	665	488	402	737	720	460	455
	No. 24	C	C	C	C	C	C	C	C

C = cracked cell
NF = fixture not available at time of test
NA = coupon destroyed before test

B.2 ELECTRICAL ISOLATION TEST DATA

Raw data for the electrical isolation test consist of electrical breakdown voltage and current for 25 samples each of four types of test coupons. Data were obtained for both sides of each sample. These data are listed in Tables B-3 through B-6.

TABLE B-3. ELECTRICAL ISOLATION TEST DATA FOR COUPON TYPE A

	Front Side			Back Side		
	Breakdown Conditions		kV at 1 μA	Breakdown Conditions		kV at 1 μA
Coupon ID	Voltage, kV	Current μA	Leakage Current	Voltage, kV	Current, μA	Leakage Current
A-1	19	10.5	3	6	8.0	5
A-2	18	14.5	5	8	1.3	7
A-3	17	32.0	3	7	1.0	6
A-9	14	7.5	5	9	1.2	7
A-10	14	10.5	4	11	2.0	6
A-11	15	11.0	4	8	1.5	7
A-12	19	20.0	4	9	11.0	9
A-13	12	8.0	4	5	1.0	5
A-14	15	19.0	4	9	2.5	5
A-15	19	25.0	3	10	3.0	6
A-16	18	22.5	4	9	1.0	8
A-17	10	7.0	4	1	—	—
A-18	13	27.0	3	3	2.0	3
A-19	17	24.0	3	6	1.5	6
A-20	12	22.0	3	1	—	—
A-21	10	7.0	3	6	1.0	5
A-22	17	23.0	4	2	—	—
A-23	16	20.0	3	8	1.5	5
A-24	18	31.0	4	8	1.8	6
A-25	17	32.0	3	7	1.0	6
A-26	15	23.0	3	2	—	—
A-27	17	29.0	3	10	2.2	5

Total coupons = 22
Average breakdown voltage = 15.6 kV (front), 6.8 kV (back)
Standard deviation for breakdown voltage = 2.8 kV (front), 3.1 kV (back)

TABLE B–4. ELECTRICAL ISOLATION TEST DATA FOR COUPON TYPE B

Coupon ID	Front Side			Back Side		
	Breakdown Conditions		kV at 1 μA Leakage Current	Breakdown Conditions		kV at 1 μA Leakage Current
	Voltage, kV	Current, μA		Voltage, kV	Current, μA	
B-1	13	30.0	2	8	1.2	6
B-2	12	19.5	3	5	0.4	—
B-3	18	44.0	2	9	1.3	7
B-4	14	28.0	2	6	0.8	—
B-5	17	35.0	3	7	0.5	—
B-6	15	28.0	3	9	1.0	8
B-7	15	28.0	2	7	0.7	—
B-8	15	26.0	3	9	1.0	8
B-9	17	31.0	2	10	1.2	8
B-10	15	19.0	3	9	1.0	8
B-11	19	24.0	4	12	1.5	9
B-12	15	19.0	3	8	0.9	—
B-13	17	20.0	4	7	0.6	—
B-14	15	19.0	3	8	0.7	—
B-15	15	21.0	3	9	0.9	—
B-16	15	19.0	3	12	1.5	9
B-17	12	17.0	2	9	0.8	—
B-18	17	36.0	3	13	1.2	10
B-19	15	39.0	2	7	0.6	—
B-20	13	24.0	2	10	1.2	9
B-21	16	35.0	3	9	0.9	—
B-22	13	32.0	2	5	0.5	—
B-23	17	45.0	2	10	1.2	8

Total coupons = 23
Average breakdown voltage = 15.2 kV (front), 8.6 kV (back)
Standard deviation for breakdown voltage = 1.9 kV (front), 2.1 kV (back)

TABLE B–5. ELECTRICAL ISOLATION TEST DATA FOR COUPON TYPE C

Coupon ID	Front Side			Back Side		
	Breakdown Conditions		kV at 1 μA Leakage Current	Breakdown Conditions		kV at 1 μA Leakage Current
	Voltage, kV	Current, μA		Voltage, kV	Current, μA	
C-1	14	27.0	3	25	3.0	12
C-2	11	21.0	3	25*	6.0	15
C-4	15	29.0	3	25	11.0	14
C-5	18	40.0	3	25	10.0	13
C-7	16	45.0	3	23	4.0	11
C-8	14	37.5	3	21	4.8	12
C-9	15	31.0	3	21	6.5	11
C-10	16	35.0	3	25*	8.0	13
C-11	17	1.0	3	19	1.0	17
C-12	17	43.0	3	22	9.0	11
C-13	12	23.0	3	25	7.5	9
C-14	21	43.0	3	19	4.0	11
C-15	16	42.0	3	25	7.2	11
C-16	15	29.0	4	25	7.0	16
C-17	15	39.0	3	25	10.0	9
C-18	15	41.0	3	25	10.0	11
C-19	6	6.0	3	21	8.0	11
C-20	9	17.0	3	25	10.0	12
C-21	9	7.8	3	20	5.5	13
C-22	9	9.0	3	24	12.0	12
C-23	11	27.0	3	24	8.0	14
C-24	7	6.5	3	20	2.0	14
C-25	12	15.0	3	23	8.0	12
C-26	16	27.0	3	23	7.0	12
C-27	5	3.8	3	25*	8.5	12
C-28	13	23.2	3	25*	10.5	11
C-29	12	17.5	3	9	6.2	4
C-30	15	2.2	3	8	3.0	4
C-31	15	42.0	3	20	4.0	13
C-32	12	19.0	3	25*	10.0	10
C-33	11	20.5	3	23	6.7	13

Total coupons = 31
Average breakdown voltage = 13.2 kV (front), 22.3 kV (back)
Standard deviation for breakdown voltage = 3.6 kV (front), 4.2 kV (back)

*No breakdown—these samples were included at 25 kV for statistical purposes

TABLE B–6. ELECTRICAL ISOLATION TEST DATA FOR COUPON TYPE D

Coupon ID	Front Side**			Back Side		
	Breakdown Conditions		kV at 1 μA Leakage Current	Breakdown Conditions		kV at 1 μA Leakage Current
	Voltage, kV	Current, μA		Voltage, kV	Current, μA	
D-1	14	6.0	5	25*	2.3	17
D-2	25*	17.0	9	25*	2.3	18
D-3	12	4.0	7	25*	2.3	14
D-4	16	12.0	6	25	10.0	10
D-5	17	10.5	7	25*	4.0	15
D-6	14	6.5	7	25*	5.5	15
D-9	17	13.5	5	22	12.5	10
D-10	14	7.8	6	22	7.0	11
D-11	12	7.5	5	21	7.0	6
D-12	16	9.2	6	24	7.9	9
D-13	10	1.8	7	24	14.2	8
D-14	18	7.5	6	25*	7.5	10
D-15	22	18.0	7	23	7.5	10
D-16	21	17.0	7	25*	10.5	9
D-17	19	19.0	6	25	13.0	9
D-18	17	18.0	6	24	15.0	7
D-19	18	10.5	6	22	5.5	10
D-20	15	7.0	6	25	8.0	11
D-21	18	11.0	6	25*	10.0	11
D-22	23	24.0	6	23	10.0	9
D-23	16	9.5	6	25	7.5	11
D-26	22	10.2	8	24	5.5	15
D-27	16	3.8	10	25*	7.5	10
D-28	21	12.5	8	25*	8.5	11
D-29	12	3.5	8	24	6.5	10
D-30	21	11.0	8	24	5.8	11

Total coupons = 26
Average breakdown voltage = 18.1 kV (front, with Craneglas), 15.8 kV (front without Craneglas), 24 kV (back)
Standard deviation for breakdown voltage = 3.7 kV (front, with Craneglas), 4.0 kV (front without Craneglas), 1.2 kV (back)

*No breakdown—these samples were included at 25 kV for statistical purposes.
**Coupons D-1 through D-6 and D-9 through D-12 were fabricated with Craneglas in the front pottant layer. No coupons had Craneglas in the back pottant layer.

B.3 THERMAL STRUCTURAL TEST DATA

Raw data for the thermal structural test consist of temperature and biaxial strain (i.e., strain measured along perpendicular axes) measurements obtained with the coupons listed in Table 5-3 and with samples of plain steel, glass, silicon, and aluminum. For each coupon, temperature measurements were recorded for the silicon cell as well as the underlying structural material.

The plain silicon samples were approximately four inches square, and the plain steel, glass, and aluminum samples were approximately five inches square. Strain versus temperature data obtained from these samples were used to calculate "apparent" strain curves which were then used in subsequent strain calculations for the test coupons. The strain data for the plain samples are shown in Tables B-7 through B-11.

Strain data for the coupons are shown in Tables B-12 through B-23 for the normal test sequence. Strain data for overstress tests are shown in Tables B-24 through B-26.

Thermal structural test measurements were begun on 1 July 1981 and completed on 14 July 1981.

TABLE B–7. PLAIN GLASS AND PLAIN STEEL APPARENT STRAIN DATA (HEATING)

Date	Time	Temperature, °C		Strain, μinch/inch			
				Glass		Steel	
		Glass	Steel	Ch. 7	Ch. 8	Ch. 1	Ch. 2
7/1/81	2:10	23	23	+0007	0000	+0006	−0003
7/1/81	2:25	40	41	−16	−6	+68	+60
7/1/81	2:30	42	41	−25	−20	+54	+44
7/1/81	2:35	40	40	−25	−9	+44	+40
7/1/81	3:00	60	60	−61	−40	+94	+92
7/1/81	3:00	60	59	−63	−42	+89	+93
7/1/81	3:30	81	80	−50	−18	+189	+200
7/1/81	3:36	80	79	−45	−15	+190	+195
7/1/81	3:40	80	79	−41	−12	+191	+200
7/1/81	4:12*	101	100	−97	−53	+226	+244
7/1/81	4:20*	101	99	−102	−59	+221	+236
7/1/81	4:50*	122	119	−169	−112	+245	+262
7/1/81	4:55*	122	120	−162	−106	+247	+263

*Pressed "zero check" about six times

Notes: (1) Strain gage information

Item	Glass	Steel
Gage type	WK-06-250TM-350	WK-06-250TM-350
Sec. 1 gage factor	1.99 (Chan. 7)	1.99 (Chan. 1)
Sec. 2 gage factor	1.89 (Chan. 8)	1.89 (Chan. 2)

(2) Indicated gage factor = 1.99

(3) Test performed by J. Pimentel, R. Huebschen, and D. Gillaspy

TABLE B-8. PLAIN SILICON AND PLAIN ALUMINUM APPARENT STRAIN DATA (HEATING)

Date	Time	Temperature, °C		Strain, μinch/inch			
				Silicon		Aluminum	
		Silicon	Aluminum	Ch. 5	Ch. 6	Ch. 3	Ch. 4
7/1/81	2:10	23	23	0000	−0005	+0004	+0003
7/1/81	2:25	41	41	+20	+51	+53	+39
7/1/81	2:30	41	41	+4	+27	+38	+26
7/1/81	2:35	40	40	+5	+18	+40	+34
7/1/81	3:00	60	59	+15	+55	+89	+51
7/1/81	3:05	60	59	+22	+51	+83	+54
7/1/81	3:30*	82	79	+79	+151	+177	+125
7/1/81	3:36	80	78	+81	+155	+185	+128
7/1/81	3:40	81	78	+85	+154	+183	+131
7/1/81	4:12*	102	99	+77	+218	+213	+139
7/1/81	4:20*	101	99	+68	+220	+206	+135
7/1/81	4:50*	122	118	+50	+277	+220	+129
7/1/81	4:55*	124	120	+55	+276	+221	+133

*Pressed "zero check" about six times

Notes: (1) Strain gage information

Item	Silicon	Aluminum
Gage type	WK-03-250TM-350	WK-13-250TM-350
Sec. 1 gage factor	1.96 (Chan. 5)	2.17 (Chan. 3)
Sec. 2 gage factor	1.88 (Chan. 6)	2.02 (Chan. 4)

(2) Indicated gage factor = 1.99

(3) Test performed by J. Pimentel, R. Huebschen, and D. Gillaspy

TABLE B-9. PLAIN STEEL AND PLAIN ALUMINUM APPARENT STRAIN DATA FOR HEATING AND COOLING

Date	Time	Temperature, °C		Strain, μinch/inch			
				Steel		Aluminum	
		Steel	Aluminum	Ch. 1	Ch. 2	Ch. 3	Ch. 4
7/2/81	10:30	26	26	−0003	−0003	+0003	−0007
7/2/81	10:45	59	59	76	90	81	39
7/2/81	11:00	60	60	68	80	77	36
7/2/81	11:30	100	100	147	162	136	53
7/2/81	11:35	100	100	144	161	134	54
7/2/81	12:30	139	139	166	202	155	37
7/2/81	12:40	139	139	168	201	156	37
7/2/81	12:55	118	118	161	183	158	53
7/2/81	1:00	120	120	162	189	158	51
7/2/81	1:15	100	100	146	162	140	59
7/2/81	1:20	100	100	138	153	134	53
7/2/81	1:35	80	80	116	128	118	53
7/2/81	1:45	80	80	116	124	122	53
7/2/81	1:52	59	60	73	78	93	39
7/2/81	2:00	60	60	64	75	82	37
7/2/81	2:15	42	42	29	35	49	21
7/2/81	2:25	42	42	+35	+43	+59	+23
7/2/81	2:47	21	21	−18	−27	−05	−16
7/2/81	2:55	21	22	−11	−21	−03	−12
7/2/81	3:20	−5	−4	−122	−134	−102	−90
7/2/81	3:25	0	0	−95	−103	−78	−70
7/2/81	3:36	−19	−20	−186	199	−172	−148
7/2/81	3:45	−20	−20	−197	−211	−180	−156
7/2/81	4:00	−40	−40	−307	−323	−286	−248
7/2/81	4:15	−41	−41	−322	−347	−314	−272
7/2/81	4:26	−60	−60	−463	−493	−462	−398
7/2/81	4:30	−60	−60	−491	−516	−488	−423

(Continued next page)

TABLE B-9. PLAIN STEEL AND PLAIN ALUMINUM APPARENT STRAIN DATA FOR HEATING AND COOLING (Concluded)

Date	Time	Temperature, °C		Strain, μinch/inch			
				Steel		Aluminum	
		Steel	Aluminum	Ch. 1	Ch. 2	Ch. 3	Ch. 4
7/2/81	4:40	−41	−41	−322	−343	−320	−271
7/2/81	4:45	−20	−20	−186	−199	−174	−145
7/2/81	4:51	0	−2	−97	−106	−84	−76
7/6/81	8:50	22	22	+14	+04	+02	−05

Notes: (1) Strain gage information

Item	Steel	Aluminum
Gage type	WK-06-250TM-350	WK-13-250TM-350
Sec. 1 gage factor	1.99 (Chan. 1)	2.17 (Chan. 3)
Sec. 2 gage factor	1.89 (Chan. 2)	2.02 (Chan. 4)

(2) Indicated gage factor = 1.99

(3) Test performed by J. Pimentel, R. Huebschen, and D. Gillaspy

TABLE B–10. PLAIN STEEL AND PLAIN GLASS APPARENT STRAIN DATA FOR HEATING AND COOLING

Date	Time	Temperature, °C		Strain, μinch/inch			
				Silicon		Glass	
		Silicon	Glass	Ch. 5	Ch. 6	Ch. 7	Ch. 8
7/2/81	10:30	26	26	−0001	+0001	−0005	0000
7/2/81	10:45	60	60	+0007	65	−62	−42
7/2/81	11:00	60	60	+0007	48	−62	−44
7/2/81	11:30	104	102	+0004	128	−178	−129
7/2/81	11:35	103	102	+7	134	−170	−126
7/2/81	12:30	145	142	−52	+231	−312	−239
7/2/81	12:40	146	143	−52	+235	−316	−241
7/2/81	12:55	125	122	−27	190	−231	−172
7/2/81	1:00	127	123	−27	+195	−241	−178
7/2/81	1:15	106	102	−04	+143	−157	−114
7/2/81	1:20	104	101	−06	+134	−163	−118
7/2/81	1:35	86	82	+11	+110	−112	−74
7/2/81	1:45	84	82	+09	+103	−110	−76
7/2/81	1:52	65	60	+06	+61	−60	−34
7/2/81	2:00	65	61	−02	+63	−74	−54
7/2/81	2:15	45	42	−04	+21	−33	−23
7/2/81	2:25	45	42	−04	+28	−31	−20
7/2/81	2:47	22	21	−23	−35	−07	−16
7/2/81	2:55	22	22	−21	−33	−07	−15
7/2/81	3:20	−4	−5	−65	−136	−11	−31
7/2/81	3:25	0	0	−52	−118	−07	−25
7/2/81	3:36	−18	−20	−120	−211	−30	−64
7/2/81	3:45	−20	−22	−129	−221	−35	−65
7/2/81	4:00	−39	−41	−211	−342	−83	−118
7/2/81	4:15	−41	−43	−230	−366	−95	−131
7/2/81	4:26	−60	−62	−351	−543	−164	−214
7/2/81	4:30	−68	−64	−394	−617	−193	−241

(Continued next page)

TABLE B–10. PLAIN STEEL AND PLAIN GLASS APPARENT STRAIN DATA FOR HEATING AND COOLING (Concluded)

Date	Time	Temperature, °C		Strain, μinch/inch			
				Silicon		Glass	
		Silicon	Glass	Ch. 5	Ch. 6	Ch. 7	Ch. 8
7/2/81	4:40	−41	−41	−231	−385	−88	−127
7/2/81	4:45	− 20	−19	−126	−236	−30	−60
7/2/81	4:51	+2	+1	−58	−142	−04	−27
7/6/81	8:50	20	20	−57	−51	+11	+19

Notes: (1) Strain gage information

Item	Steel	Aluminum
Gage type	WK-03-250TM-350	WK-06-250TM-350
Sec. 1 gage factor	1.96 (Chan. 5)	1.99 (Chan. 7)
Sec. 2 gage factor	1.88 (Chan. 6)	1.89 (Chan. 8)

(2) Indicated gage factor = 1.99

(3) Test performed by J. Pimentel, R. Huebschen, and D. Gillaspy

TABLE B–11. PLAIN SILICON AND PLAIN ALUMINUM APPARENT STRAIN DATA FOR HEATING AND COOLING

Date	Time	Temperature, °C		Strain, μinch/inch			
				Silicon		Aluminum	
		Silicon	Aluminum	Ch. 1	Ch. 2	Ch. 3	Ch. 4
7/13/81	3:00	24	24	+03	+07	+06	−01
7/13/81	3:15	40	40	+36	+40	+46	+30
7/13/81	3:18	40	40	+32	+35	+46	+24
7/13/81	3:25	60	60	+42	+50	+80	+47
7/13/81	3:30	60	60	+38	+46	+81	+36
7/13/81	3:45	80	80	+27	+48	+118	+44
7/13/81	3:55	80	80	+19	+38	+113	+43
7/13/81	4:10	100	100	+17	+48	+126	+37
7/13/81	4:20	100	100	+09	+46	+125	+36
7/13/81	4:36	120	120	+05	+48	+133	+29
7/13/81	4:50	120	120	+07	+48	+125	+22
7/13/81	4:58	100	100	+08	+42	+127	+38
7/14/81	8:40	100	100	+11	+49	+126	+38
7/14/81	8:50	80	80	+03	+24	+104	+41
7/14/81	9:00	80	80	+06	+24	+108	+43
7/14/81	9:10	60	60	−09	−07	+85	+37
7/14/81	9:25	60	60	−09	−07	+90	+38
7/14/81	9:55	41	41	−36	−45	+43	+22
7/14/81	10:00	40	40	−36	−45	+41	+17
7/14/81	10:20	20	20	−82	−100	−09	−21
7/14/81	10:25	20	20	−79	−96	−05	−19
7/14/81	10:35	0	0	−162	−171	−88	−76
7/14/81	10:45	0	0	−154	−163	−85	−78
7/14/81	11:00	−20	−20	−240	−265	−194	−160
7/14/81	11:10	−20	−20	−239	−263	−191	−158
7/14/81	11:17	−40	−40	−349	−383	−318	−265
7/14/81	11:25	−40	−40	−347	−386	−320	−268
7/14/81	11:35	−60	−60	−470	−535	−473	−402
7/14/81	11:40	−60	−60	−480	−530	−472	−403

(Continued next page)

TABLE B-11. PLAIN SILICON AND PLAIN ALUMINUM APPARENT STRAIN DATA FOR HEATING AND COOLING (Concluded)

Date	Time	Temperature, °C		Strain, μinch/inch			
				Silicon		Aluminum	
		Silicon	Aluminum	Ch. 1	Ch. 2	Ch. 3	Ch. 4
7/14/81	11:50	−40	−40	−340	−384	−312	−259
7/14/81	11:55	−40	−40	−339	−385	−317	−265
7/14/81	12:10	−20	−20	−227	−262	−182	−152
7/14/81	12:25	−20	−20	−223	−259	−184	−154
7/14/81	1:05	0	0	−124	−147	−86	−74
7/14/81	1:10	0	0	−117	−139	−85	−74
7/14/81	1:30	20	20	−33	−56	−19	−20
7/14/81	1:35	20	20	−33	−54	−15	−25
7/14/81	1:40	22	22	−17	−34	−29	−21
7/14/81	1:45	22	22	−09	−21	−06	−10

Notes: (1) Strain gage information

Item	Silicon	Aluminum
Gage type	WK-03-250TM-350	WK-13-250TM-350
Sec. 1 gage factor	1.96 (Chan. 1)	2.17 (Chan. 3)
Sec. 2 gage factor	1.88 (Chan. 2)	2.02 (Chan. 4)

(2) Indicated gage factor = 1.99

(3) Test performed by J. Pimentel, R. Huebschen, and D. Gillaspy

TABLE B-12. THERMAL STRUCTURAL TEST DATA FOR COUPON TSC-1 NORMAL TEST

Date	Time	Temperature, °C		Strain, μinch/inch			
				Silicon		Aluminum	
		Silicon	Aluminum	Ch. 1	Ch. 2	Ch. 3	Ch. 4
7/10/81	9:15	27	27	−04	−08	−06	−04
7/10/81	9:20	40	40	+10	+18	−22	−10
7/10/81	9:30	40	40	+06	+12	−20	−14
7/10/81	9:50	60	60	+15	+36	−71	−48
7/10/81	9:55	60	60	+15	+39	−71	−49
7/10/81	10:30	80	80	+4	+41	−128	−95
7/10/81	10:40	80	80	−2	+21	−133	−99
7/10/81	10:55	100	100	−18	+25	−194	−155
7/10/81	11:05	100	100	−14	+25	−190	−149
7/10/81	11:30	81	80	−01	+26	−131	−98
7/10/81	11:45	80	80	−01	+25	−128	−97
7/10/81	12:10	60	60	−02	+10	−76	−55
7/10/81	12:21	60	60	+04	+10	−73	−54
7/10/81	12:42	40	40	−06	−16	−46	−35
7/10/81	12:50	40	40	−06	−07	−43	−32
7/10/81	1:05	21	21	−39	−56	−29	−27
7/10/81	1:15	21	21	−48	−63	−31	−30
7/10/81	1:25	0	0	−101	−126	−31	−42
7/10/81	1:35	0	0	−103	−125	−30	−43
7/10/81	1:50	−20	−20	−168	−208	−57	−73
7/10/81	2:05	−20	−20	−164	−202	−51	−72
7/10/81	2:25	−40	−40	−276	−351	−121	−152
7/10/81	3:00	−41	−41	−289	−364	−141	−169
7/10/81	3:11	−20	−20	−176	−216	−63	−84
7/10/81	3:16	−20	−20	−169	−210	−58	−76
7/10/81	3:25	0	0	−89	−117	−21	−39
7/10/81	3:30	0	0	−100	−119	−28	−38
7/10/81	3:45	21	21	−34	−45	−17	−15

(Continued next page)

TABLE B–12. THERMAL STRUCTURAL TEST DATA FOR COUPON TSC–1 NORMAL TEST (Concluded)

Date	Time	Temperature, °C		Strain, μinch/inch			
				Silicon		Aluminum	
		Silicon	Aluminum	Ch. 1	Ch. 2	Ch. 3	Ch. 4
7/10/81	3:52	20	20	−33	−45	−14	−14
7/10/81	4:05	40	40	+02	+06	−23	−12
7/10/81	4:10	40	40	00	+08	−21	−09
7/10/81	4:50	27	27	−12	−22	−10	−04
7/13/81	8:30*	24	24	−16	−26	−09	00

*3513 Calibration Check

Notes: (1) Strain gage information

Item	Silicon	Glass
Gage type	WK-03-250TM-350	WK-06-250TM-350
Sec. 1 gage factor	1.96 (Chan. 1)	1.99 (Chan. 3)
Sec. 2 gage factor	1.88 (Chan. 2)	1.89 (Chan. 4)

(2) Indicated gage factor = 1.99

(3) Test performed by J. Pimentel, R. Huebschen, and D. Gillaspy

TABLE B–13. THERMAL STRUCTURAL TEST DATA FOR COUPON TSC–2 NORMAL TEST

Date	Time	Temperature, °C		Strain, μinch/inch			
				Silicon		Glass	
		Silicon	Glass	Ch. 5	Ch. 6	Ch. 7	Ch. 8
7/10/81	9:15	27	27	+08	+04	−02	−02
7/10/81	9:20	40	40	+53	+59	00	+08
7/10/81	9:30	40	40	+36	+51	−06	−04
7/10/81	9:50	60	60	+83	+107	−35	−25
7/10/81	9:55	60	60	+80	+101	−36	−26
7/10/81	10:35	80	80	+93	+133	−73	−48
7/10/81	10:42	80	80	+94	+130	−76	−54
7/10/81	10:57	100	100	+113	+170	−124	−98
7/10/81	11:07	100	100	+118	+174	−122	−90
7/10/81	11:33	80	80	+94	+133	−73	−55
7/10/81	11:46	80	80	+95	+127	−75	−57
7/10/81	12:10	60	60	+55	+86	−41	−28
7/10/81	12:21	60	60	+51	+80	−40	−29
7/10/81	12:42	40	40	+02	+29	−24	−20
7/10/81	12:50	40	40	+01	+17	−21	−20
7/10/81	1:10	21	21	−58	−51	−16	−22
7/18/81	1:18	21	21	−60	−65	−22	−26
7/10/81	1:30	0	0	−155	−158	−37	−46
7/10/81	1:37	0	0	−156	−159	−37	−49
7/10/81	1:55	−20	−20	−254	−262	−56	−85
7/10/81	2:15	−20	−20	−253	−262	−58	−81
7/10/81	2:30	−41	−41	−402	−412	−130	−159
7/10/81	2:55	−40	−40	−394	−408	−121	−156
7/10/81	3:10	−21	−21	−266	−280	−77	−99
7/10/81	3:16	−20	−20	−252	−263	−65	−87
7/10/81	3:26	0	0	−145	−150	−30	−47

(Continued next page)

TABLE B–13. THERMAL STRUCTURAL TEST DATA FOR COUPON TSC–2 NORMAL TEST (Concluded)

Date	Time	Temperature, °C		Strain, μinch/inch			
				Silicon		Glass	
		Silicon	Glass	Ch. 5	Ch. 6	Ch. 7	Ch. 8
7/10/81	3:36	0	0	−144	−148	−29	−44
7/10/81	3:50	21	21	−38	−33	−04	−12
7/10/81	3:53	20	20	−39	−34	+01	−04
7/10/81	4:05	40	40	+36	+55	−01	+08
7/10/81	4:12	40	40	+34	+52	−01	+11
7/10/81	4:50	27	27	−06	+08	+04	+09
7/13/81	8:30*	24	24	−15	−02	−04	−10

* 3513 Calibration check

Notes: (1) Strain gage information

Item	Silicon	Glass
Gage type	WK-03-250TM-350	WK-06-250TM-350
Sec. 1 gage factor	1.96 (Chan. 5)	2.02 (Chan. 7)
Sec. 2 gage factor	1.88 (Chan. 6)	1.93 (Chan. 8)

(2) Indicated gage factor = 1.99

(3) Test performed by J. Pimentel, R. Huebschen, and D. Gillaspy

TABLE B–14. THERMAL STRUCTURAL TEST DATA FOR COUPON TSC–3 NORMAL TEST

Date	Time	Temperature, °C		Strain, μinch/inch			
				Silicon		Glass	
		Silicon	Glass	Ch. 9	Ch. 10	Ch. 11	Ch. 12
7/10/81	9:15	27	27	+01	−03	00	00
7/10/81	9:20	40	40	+15	+18	−04	−02
7/10/81	9:30	40	40	+16	+18	+01	+04
7/10/81	9:50	60	60	+12	+37	−46	−38
7/10/81	9:57	60	60	+05	+35	−51	−36
7/10/81	10:35	80	80	−05	+42	−93	−77
7/10/81	10:42	80	80	−14	+26	−97	−77
7/10/81	11:00	100	100	−28	+28	−146	−126
7/10/81	11:08	100	100	−28	+29	−149	−127
7/10/81	11:38	80	80	−08	+30	−93	−76
7/10/81	11:48	80	80	−09	+28	−97	−77
7/10/81	12:15	63	63	−03	+20	−55	−44
7/10/81	12:23	61	61	−03	+24	−51	−42
7/10/81	12:42	41	41	−13	−09	−24	−22
7/10/81	12:50	40	40	−13	−10	−22	−15
7/10/81	1:12	21	21	−40	−51	−18	−16
7/10/81	1:20	21	21	−41	−57	−16	−12
7/10/81	1:30	0	0	−100	−135	−38	−40
7/10/81	1:40	0	0	−91	−126	−25	−34
7/10/81	2:00	−20	−20	−148	−196	−57	−64
7/10/81	2:20	−20	−20	−138	−187	−47	−57
7/10/81	2:35	−40	−40	−225	−300	−106	−124
7/10/81	2:50	−40	−40	−243	−309	−113	−130
7/10/81	3:10	−20	−20	−159	−212	−65	−81
7/10/81	3:15	−20	−20	−153	−206	−61	−73
7/10/81	3:30	0	0	−87	−122	−27	−33

(Continued next page)

TABLE B–14. THERMAL STRUCTURAL TEST DATA FOR COUPON TSC–3 NORMAL TEST (Concluded)

Date	Time	Temperature, °C		Strain, μinch/inch			
				Silicon		Glass	
		Silicon	Glass	Ch. 9	Ch. 10	Ch. 11	Ch. 12
7/10/81	3:33	0	0	−83	−117	−22	−30
7/10/81	3:50	21	21	−26	−45	−02	−03
7/10/81	3:54	20	20	−26	−43	0000	−01
7/10/81	4:08	40	40	+11	+11	+05	+11
7/10/81	4:13	40	40	+11	+11	+11	+04
7/10/81	4:50	27	27	−04	−15	+22	+08
7/13/81	8:30*	24	24	−06	−16	−01	+01

* 3513 Calibration check

Notes: (1) Strain gage information

Item	Silicon	Glass
Gage type	WK-03-250TM-350	WK-06-250TM-350
Sec. 1 gage factor	1.96 (Chan. 9)	2.02 (Chan. 11)
Sec. 2 gage factor	1.88 (Chan. 10)	1.93 (Chan. 12)

(2) Indicated gage factor = 1.99

(3) Test performed by J. Pimentel, R. Huebschen, and D. Gillaspy

TABLE B-15. THERMAL STRUCTURAL TEST DATA FOR COUPON TSC-4 NORMAL TEST

Date	Time	Temperature, °C		Strain, μinch/inch			
				Silicon		Glass	
		Silicon	Glass	Ch. 1	Ch. 2	Ch. 3	Ch. 4
7/6/81	1:35*	23	23	−0000	−0003	+0006	+0003
7/6/81	1:55	40	40	+13	+28	−40	−16
7/6/81	2:00	40	40	+14	+36	−42	−14
7/6/81	2:20	59	59	+22	+39	−78	−44
7/6/81	2:30	60	60	+22	+38	−87	−47
7/6/81	2:55	78	78	+13	+45	−128	−78
7/6/81	3:07	79	79	+05	+48	−136	−85
7/6/81	3:40	98	98	−06	+37	−189	−124
7/6/81	3:45	99	99	+01	+39	−191	−130
7/6/81	4:05	80	80	+10	+45	−134	−81
7/6/81	4:10	80	80	+09	+42	−130	−81
7/6/81	4:25	60	60	+10	+38	−85	−46
7/6/81	4:30	60	60	+11	+38	−86	−45
7/6/81	4:40	40	40	+02	+13	−54	−27
7/6/81	4:45	40	40	+07	+20	−51	−19
7/7/81	8:50**	20	20	−29	−40	−26	−20
7/7/81	9:20†	20	20	−01	+03	+05	+03
7/7/81	9:37	0	0	−61	−75	−09	−10
7/7/81	9:42	0	0	−65	−76	−11	−23
7/7/81	9:48	20	20	−01	−04	+18	+23
7/7/81	9:55	20	20	−01	+05	+11	+12
7/7/81	10:00	22	22	−01	00	+09	+08

*3500 Calibration check

**3512 Calibration check

†All Channels rezeroed

Notes: (1) Strain gage information

Item	Silicon	Glass
Gage type	WK-03-250TM-350	WK-06-250TM-350
Sec. 1 gage factor	1.96 (Chan. 1)	2.02 (Chan. 3)
Sec. 2 gage factor	1.88 (Chan. 2)	1.93 (Chan. 4)

(2) Indicated gage factor = 1.99

(3) Test performed by J. Pimentel, R. Huebschen, and D. Gillaspy

TABLE B–16. THERMAL STRUCTURAL TEST DATA FOR COUPON TSC–5 NORMAL TEST

Date	Time	Temperature, °C		Strain, μinch/inch			
				Silicon		Glass	
		Silicon	Glass	Ch. 5	Ch. 6	Ch. 7	Ch. 8
7/6/81	1:35	23	23	+0005	+0004	+0006	−0005
7/6/81	1:55	40	40	+34	+28	−37	−30
7/6/81	2:00	40	40	+38	+37	−33	−25
7/6/81	2:20	59	59	+35	+48	−78	−63
7/6/81	2:30	60	60	+40	+52	−86	−68
7/6/81	2:55	78	78	+37	+56	−129	−103
7/6/81	3:07	79	79	+32	+48	−132	−100
7/6/81	3:40	98	98	+43	+50	−190	−157
7/6/81	3:45	100	100	+25	+50	−185	−154
7/6/81	4:05	80	80	+34	+57	−132	−102
7/6/81	4:10	80	80	+39	+55	−129	−101
7/6/81	4:25	60	60	+44	+43	−83	−63
7/6/81	4:30	60	60	+38	+48	−83	−60
7/6/81	4:40	40	40	+17	+27	−49	−36
7/6/81	4:45	40	40	+32	+23	−38	−35
7/7/81	8:50	20	20	−23	−45	−22	−26
7/7/81	9:20*	20	20	+04	+04	+03	+02
7/7/81	9:37	0	0	−56	−54	−05	−15
7/7/81	9:42	0	0	−60	−67	−06	−15
7/7/81	9:48	20	20	+08	+06	+22	+07
7/7/81	9:55	20	20	+11	+11	+10	+10
7/7/81	10:00	22	22	+12	+24	+07	+08

*Channels rezeroed

Notes: (1) Strain gage information

Item	Silicon	Glass
Gage type	WK-03-250TM-350	WK-06-250TM-350
Sec. 1 gage factor	1.96 (Chan. 5)	2.02 (Chan. 7)
Sec. 2 gage factor	1.88 (Chan. 6)	1.93 (Chan. 8)

(2) Indicated gage factor = 1.99

(3) Test performed by J. Pimentel, R. Huebschen, and D. Gillaspy

TABLE B–17. THERMAL STRUCTURAL TEST DATA FOR COUPON TSC–6 NORMAL TEST

Date	Time	Temperature, °C		Strain, μinch/inch			
				Silicon		Aluminum	
		Silicon	Aluminum	Ch. 1	Ch. 2	Ch. 3	Ch. 4
7/8/81	2:25	22	22	+0003	−0002	−0002	−0003
7/8/81	2:40	40	40	+48	+50	+67	+49
7/8/81	2:45	41	41	+40	+35	+62	+46
7/8/81	3:00	62	62	+44	+56	+105	+66
7/8/81	3:10	62	62	+33	+56	+99	+58
7/8/81	3:30	80	80	+23	+52	+123	+67
7/8/81	3:43	80	80	+24	+57	+119	+65
7/8/81	4:00	100	100	+10	+50	+136	+70
7/8/81	4:18	100	99	+09	+54	+139	+75
7/8/81	4:45	80	80	+23	+58	+128	+72
7/9/81	8:40	80	80	+23	+55	+131	+69
7/9/81	9:00	60	60	+18	+34	+98	+63
7/9/81	9:15	60	60	+18	+33	+91	+50
7/9/81	9:40	40	40	+02	−03	+61	+21
7/9/81	9:45	40	40	+09	+08	+51	+22
7/9/81	10:05	20	20	−15	−35	+04	−19
7/9/81	10:10*	20	20	−08	−36	+05	−19
7/9/81	11:03	0	0	−90	−110	−105	−80
7/9/81	11:15	0	0	−105	−110	−104	−103
7/9/81	11:35	−20	−20	−204	−192	−226	−211
7/9/81	11:44	−20	−20	−186	−192	−227	−183
7/9/81	12:05	−40	−40	−411	−369	−434	−386
7/9/81	12:12	−40	−40	−406	−370	−436	−386
7/9/81	12:35	−20	−20	−202	−215	−239	−202

(Continued next page)

TABLE B–17. THERMAL STRUCTURAL TEST DATA FOR COUPON TSC–6 NORMAL TEST (Concluded)

Date	Time	Temperature, °C		Strain, μinch/inch			
				Silicon		Aluminum	
		Silicon	Aluminum	Ch. 1	Ch. 2	Ch. 3	Ch. 4
7/9/81	12:42	−20	−20	−196	−200	−229	−199
7/9/81	12:48	0	0	−105	−120	−114	−104
7/9/81	1:05	0	0	−104	−128	−113	−104
7/9/81	1:21	+20	+20	−108	−140	−01	−20
7/9/81	1:40	+20	+20	−05	−19	−02	−03
7/9/81	2:10	+23	+23	+02	−17	+06	−06

*Changed temperature recorders

Notes: (1) Strain gage information

Item	Silicon	Aluminum
Gage type	WK-03-250TM-350	WK-13-250TM-350
Sec. 1 gage factor	1.96 (Chan. 1)	2.17 (Chan. 3)
Sec. 2 gage factor	1.88 (Chan. 2)	2.02 (Chan. 4)

(2) Indicated gage factor = 1.99

(3) Test performed by J. Pimentel, R. Huebschen, and D. Gillaspy

TABLE B-18. THERMAL STRUCTURAL TEST DATA FOR COUPON TSC-7 NORMAL TEST

Date	Time	Temperature, °C		Strain, μinch/inch			
				Silicon		Aluminum	
		Silicon	Aluminum	Ch. 5	Ch. 6	Ch. 7	Ch. 8
7/8/81	2:25	22	22	+0002	−0001	+0001	−0003
7/8/81	2:40	40	40	+36	+69	+58	+42
7/8/81	2:45	41	41	+29	+53	+63	+36
7/8/81	3:00	62	62	+50	+85	+107	+56
7/8/81	3:10	61	61	+27	+78	+92	+49
7/8/81	3:32	80	80	+26	+99	+121	+57
7/8/81	3:45	80	80	+25	+97	+120	+57
7/8/81	4:10	100	100	+12	+101	+143	+60
7/8/81	4:25	100	100	+08	+103	+153	+61
7/8/81	4:50	80	80	+18	+91	+131	+63
7/9/81	8:42	80	80	+21	+91	+127	+57
7/9/81	9:03	60	60	+12	+57	+93	+39
7/9/81	9:17	60	60	+22	+59	+92	+42
7/9/81	9:45	40	40	+04	+21	+51	+15
7/9/81	9:45	40	40	+03	+25	+48	+26
7/9/81	10:12	20	20	−21	−28	−17	−21
7/9/81	10:20*	20	20	−18	−17	−14	−17
7/9/81	11:04	0	0	−76	−89	−107	−90
7/9/81	11:15	0	0	−84	−100	−100	−86
7/9/81	11:35	−20	−20	−154	−189	−197	−155
7/9/81	11:45	−20	−20	−163	−186	−199	−179
7/9/81	12:05	−40	−40	−260	−300	−342	−291
7/9/81	12:12	−40	−40	−266	−302	−344	−295
7/9/81	12:35	−20	−20	−156	−187	−213	−170

(Continued next page)

TABLE B-18. THERMAL STRUCTURAL TEST DATA FOR COUPON TSC-7 NORMAL TEST (Concluded)

Date	Time	Temperature, °C		Strain, μinch/inch			
				Silicon		Aluminum	
		Silicon	Aluminum	Ch. 5	Ch. 6	Ch. 7	Ch. 8
7/9/81	12:43	−20	−20	−150	−185	−207	−158
7/9/81	12:48	0	0	−84	−98	−120	−104
7/9/81	1:05	0	0	−85	−97	−106	−87
7/9/81	1:22	+20	+20	−18	−11	−17	−230
7/9/81	1:40	+20	+20	00	+07	−13	−06
7/9/81	2:10	+23	+23	+06	+08	+07	−06

*Changed temperature recorders

Notes: (1) Strain gage information

Item	Silicon	Aluminum
Gage type	WK-03-250TM-350	WK-13-250TM-350
Sec. 1 gage factor	1.96 (Chan. 5)	2.17 (Chan. 7)
Sec. 2 gage factor	1.88 (Chan. 6)	2.02 (Chan. 8)

(2) Indicated gage factor = 1.99

(3) Test performed by J. Pimentel, R. Huebschen, and D. Gillaspy

TABLE B–19. THERMAL STRUCTURAL TEST DATA FOR COUPON TSC–8 NORMAL TEST

Date	Time	Temperature, °C		Strain, μinch/inch			
				Silicon		Steel	
		Silicon	Steel	Ch. 9	Ch. 10	Ch. 11	Ch. 12
7/8/81	2:25	22	22	0000	0000	0000	+0001
7/8/81	2:40	40	40	+55	+69	+58	+64
7/8/81	2:45	41	41	+44	+57	+51	+60
7/8/81	3:00	62	62	+66	+89	+104	+103
7/8/81	3:10	61	61	+51	+70	+86	+91
7/8/81	3:35	80	80	+59	+81	+121	+125
7/8/81	3:47	80	80	+62	+85	+121	+127
7/8/81	4:12	100	100	+62	+97	+145	+151
7/8/81	4:30	100	100	+73	+98	+148	+159
7/8/81	4:50	80	80	+50	+76	+130	+142
7/9/81	8:45	80	80	+50	+83	+117	+130
7/9/81	9:05	60	60	+15	+30	+77	+78
7/9/81	9:20	62	62	+26	+35	+82	+84
7/9/81	9:45	40	40	−10	−18	+27	+37
7/9/81	9:50	40	40	−05	−13	+48	+35
7/9/81	10:12	20	20	−62	−67	−28	−29
7/9/81	10:20	20	20	−60	−62	−23	−20
7/9/81	11:05*	0	0	−170	−180	−146	−145
7/9/81	11:18	0	0	−150	−146	−121	−135
7/9/81	11:36	−20	−20	−247	−243	−212	−213
7/9/81	11:45	−20	−20	−255	−251	−216	−228
7/9/81	12:07	−40	−40	−396	−368	−366	−360
7/9/81	12:14	−40	−40	−410	−370	−381	−377
7/9/81	12:36	−20	−20	−253	−253	−229	−229
7/9/81	12:44	−20	−20	−254	−254	−224	−225
7/9/81	12:49	0	0	−145	−152	−130	−130

(Continued next page)

TABLE B-19. THERMAL STRUCTURAL TEST DATA FOR COUPON TSC-8 NORMAL TEST (Concluded)

Date	Time	Temperature, °C		Strain, μinch/inch			
				Silicon		Steel	
		Silicon	Steel	Ch. 9	Ch. 10	Ch. 11	Ch. 12
7/9/81	1:06	0	0	−135	−144	−120	−125
7/9/81	1:23	+20	+20	−46	−38	−26	−42
7/9/81	1:41**	+20	+20	−24	−900	−17	−16
7/9/81	2:10	+23	+23	−18	−23	−01	−07

* Changed temperature recorders

** Drop of condensation fell from chamber ceiling onto Channel 10 leads. This caused erroneous readings for Channel 10.

Notes: (1) Strain gage information

Item	Silicon	Steel
Gage type	WK-03-250TM-350	WK-06-250TM-350
Sec. 1 gage factor	1.96 (Chan. 9)	1.99 (Chan. 11)
Sec. 2 gage factor	1.88 (Chan. 10)	1.89 (Chan. 12)

(2) Indicated gage factor = 1.99

(3) Test performed by J. Pimentel, R. Huebschen, and D. Gillaspy

TABLE B-20. THERMAL STRUCTURAL TEST DATA FOR COUPON TSC-9 NORMAL TEST

Date	Time	Temperature, °C		Strain, μinch/inch			
				Silicon		Steel	
		Silicon	Steel	Ch. 1	Ch. 2	Ch. 3	Ch. 4
7/7/81	2:30*	25	25	+05	−05	+07	+08
7/7/81	2:40	44	44	+50	+29	+55	+65
7/7/81	2:50	42	42	+28	+24	+48	+49
7/7/81	2:55	62	62	+45	+51	+92	+104
7/7/81	3:00	60	60	+35	+49	+80	+90
7/7/81	3:25	80	80	+29	+48	+114	+128
7/7/81	3:35	80	80	+28	+43	+120	+132
7/7/81	4:00	100	100	+18	+53	+137	+165
7/7/81	4:05	100	100	+15	+49	+139	+165
7/7/81	4:15	80	80	+32	+43	+117	+137
7/7/81	4:24	81	81	+27	+45	+123	+133
7/7/81	4:34	60	60	+15	+17	+80	+96
7/7/81	4:40	61	61	+20	+18	+82	+96
7/7/81	4:45	40	40	+07	−17	+36	+47
7/8/81	8:15**	25	25	+06	−20	−01	+01
7/8/81	9:10	26	26	+05	−22	−03	+02
7/8/81	9:30	−1	−1	−62	−115	−108	−119
7/8/81	9:40	−1	−1	−65	−121	−115	−120
7/8/81	10:08	−20	−20	−152	−203	−214	−237
7/8/81	10:20	−20	−20	−160	−215	−220	−233
7/8/81	10:35	−40	−40	−255	−322	−333	−354
7/8/81	10:40	−40	−40	−269	−333	−346	−374
7/8/81	10:50	−20	−20	−147	−202	−209	−228
7/8/81	11:10	−20	−20	−139	−192	−196	−214
7/8/81	11:20	−2	−2	−66	−121	−112	−121
7/8/81	11:25	0	0	−62	−109	−104	−120

(Continued next page)

TABLE B-20. THERMAL STRUCTURAL TEST DATA FOR COUPON TSC-9 NORMAL TEST (Concluded)

Date	Time	Temperature, °C		Strain, μinch/inch			
				Silicon		Steel	
		Silicon	Steel	Ch. 1	Ch. 2	Ch. 3	Ch. 4
7/8/81	11:40	+20	+20	−08	−40	−36	−45
7/8/81	11:45	+20	+20	−09	−39	−31	−41
7/8/81	12:00	+19	+19	−06	−38	−33	−43

* 3508 Calibration check

** 3509 Calibration check

Notes: (1) Strain gage information

Item	Silicon	Steel
Gage type	WK-03-250TM-350	WK-06-250TM-350
Sec. 1 gage factor	1.96 (Chan. 1)	2.02 (Chan. 3)
Sec. 2 gage factor	1.88 (Chan. 2)	1.93 (Chan. 4)

(2) Indicated gage factor = 1.99

(3) Test performed by J. Pimentel, R. Huebschen, and D. Gillaspy

TABLE B-21. THERMAL STRUCTURAL TEST DATA FOR COUPON TSC-10 NORMAL TEST

Date	Time	Temperature, °C		Strain, μinch/inch			
				Silicon		Steel	
		Silicon	Steel	Ch. 5	Ch. 6	Ch. 7	Ch. 8
7/7/81	2:30*	25	25	+02	−03	−07	−01
7/7/81	2:40	43	43	+42	+48	+44	+54
7/7/81	2:50	42	42	+23	+23	+41	+46
7/7/81	2:55	62	62	+48	+55	+88	+88
7/7/81	3:00	60	60	+33	+50	+76	+83
7/7/81	3:25	80	80	+33	+48	+94	+106
7/7/81	3:35	80	80	+25	+45	+103	+112
7/7/81	4:00	100	100	+28	+61	+133	+156
7/7/81	4:05	100	100	+25	+53	+133	+141
7/7/81	4:15	80	80	+25	+40	+107	+124
7/7/81	4:24	81	81	+34	+37	+109	+124
7/7/81	4:34	60	60	0	+16	+68	+84
7/7/81	4:40	61	61	+04	+22	+74	+80
7/7/81	4:45	40	40	−22	−17	+27	+36
7/8/81	8:15	25	25	−11	−19	−07	−05
7/8/81	9:10	26	26	−06	−23	−07	+02
7/8/81	9:30	−1	−1	−93	−119	−105	−116
7/8/81	9:40	−1	−1	−101	−122	−115	−125
7/8/81	10:08	−20	−20	−187	−214	−220	−228
7/8/81	10:20	−20	−20	−196	−225	−227	−237
7/8/81	10:35	−40	−40	−305	−330	−341	−353
7/8/81	10:40	−40	−40	−307	−334	−347	−356
7/8/81	10:50	−20	−20	−172	−207	−215	−223
7/8/81	11:10	−20	−20	−168	−194	−203	−211
7/8/81	11:20	−2	−2	−98	−120	−120	−126
7/8/81	11:25	0	0	−91	−113	−116	−120
7/8/81	11:40	+20	+20	−22	−42	−37	−56

(Continued next page)

TABLE B–21. THERMAL/STRUCTURAL TEST DATA FOR COUPON TSC–10 NORMAL TEST (Concluded)

Date	Time	Temperature, °C		Strain, μinch/inch			
				Silicon		Steel	
		Silicon	Steel	Ch. 5	Ch. 6	Ch. 7	Ch. 8
7/8/81	11:45	+20	+20	−12	−31	−30	−64
7/8/81	12:00	+19	+19	−12	−30	−32	−47

* 3508 Calibration check

Notes: (1) Strain gage information

Item	Silicon	Steel
Gage type	WK-03-250TM-350	WK-06-250TM-350
Sec. 1 gage factor	1.96 (Chan. 5)	2.02 (Chan. 7)
Sec. 2 gage factor	1.88 (Chan. 6)	1.93 (Chan. 8)

Notes: (2) Indicated gage factor = 1.99

(3) Test performed by J. Pimentel, R. Huebschen, and D. Gillaspy

TABLE B–22. THERMAL/STRUCTURAL TEST DATA FOR COUPON TSC–11 NORMAL TEST

Date	Time	Temperature, °C		Strain, μinch/inch			
				Silicon		Steel	
		Silicon	Steel	Ch. 9	Ch. 10	Ch. 11	Ch. 12
7/7/81	2:30*	25	25	−04	−03	−01	−04
7/7/81	2:40	44	44	+32	+27	+49	+56
7/7/81	2:50	42	42	+20	+26	+39	+46
7/7/81	2:55	62	62	+25	+52	+90	+92
7/7/81	3:00	60	60	+20	+36	+78	+86
7/7/81	3:25	80	80	+8	+41	+113	+114
7/7/81	3:35	80	80	+9	+53	+120	+126
7/7/81	4:00	102	102	−3	+47	+161	+161
7/7/81	4:05	102	102	−05	+55	+152	+150
7/7/81	4:15	82	82	+20	+48	+122	+128
7/7/81	4:24	82	82	+07	+51	+126	+130
7/7/81	4:34	63	63	0	+33	+89	+80
7/7/81	4:40	62	62	+14	+35	+91	+85
7/7/81	4:45	42	42	−03	−01	+40	+49
7/8/81	8:15**	25	25	−08	−09	−06	−08
7/8/81	9:10	26	26	−08	−18	−02	−10
7/8/81	9:30	−1	−1	−93	−94	−119	−125
7/8/81	9:40	−1	−1	−108	−118	−132	−136
7/8/81	10:08	−20	−20	−264	−267	−257	−265
7/8/81	10:20	−20	−20	−281	−291	−278	−285
7/8/81	10:35	−40	−40	−450	−457	−434	−437
7/8/81	10:40	−40	−40	−463	−460	−427	−435
7/8/81	10:50	−20	−20	−254	−259	−254	−260
7/8/81	11:10	−19	−19	−237	−249	−239	−253
7/8/81	11:20	−2	−2	−104	−120	−133	−135
7/8/81	11:25	0	0	−94	−108	−125	−130
7/8/81	11:40	+20	+20	−29	−34	−39	−38

(Continued next page)

TABLE B-22. THERMAL STRUCTURAL TEST DATA FOR COUPON TSC-11 NORMAL TEST (Concluded)

Date	Time	Temperature, °C		Strain, μinch/inch			
				Silicon		Steel	
		Silicon	Steel	Ch. 9	Ch. 10	Ch. 11	Ch. 12
7/8/81	11:45	+20	+20	−25	−27	−28	−30
7/8/81	12:00	+19	+19	−14	−22	−28	−33

* 3508 Calibration check

** 3509 Calibration check

Notes: (1) Strain gage information

Item	Silicon	Steel
Gage type	WK-03-250TM-350	WK-06-250TM-350
Sec. 1 gage factor	1.96 (Chan. 9)	2.02 (Chan. 11)
Sec. 2 gage factor	1.88 (Chan. 10)	1.93 (Chan. 12)

(2) Indicated gage factor = 1.99

(3) Test performed by J. Pimentel, R. Huebschen, and D. Gillaspy

TABLE B–23. THERMAL STRUCTURAL TEST DATA FOR COUPON TSC–12 NORMAL TEST

Date	Time	Temperature, °C		Strain, μinch/inch			
				Silicon		Steel	
		Silicon	Steel	Ch. 9	Ch. 10	Ch. 9	Ch. 10
7/6/81	1:35	23	23	−0005	+0004	+0004	0000
7/6/81	1:55	42	42	+08	+47	+59	+59
7/6/81	2:00	41	41	+09	+43	+56	+69
7/6/81	2:20	62	62	+01	+56	+81	+102
7/6/81	2:30	64	64	+11	+59	+86	+107
7/6/81	2:55	84	84	−8	+77	+114	+134
7/6/81	3:07	84	85	−16	+66	+117	+131
7/6/81	3:40	104	104	−37	+62	+123	+151
7/6/81	3:45	104	104	−33	+67	+127	+153
7/6/81	4:05	84	84	−16	+68	+119	+136
7/6/81	4:10	84	84	−12	+76	+127	+137
7/6/81	4:25	64	65	+01	+62	+99	+101
7/6/81	4:30	64	65	−01	+63	+102	+108
7/6/81	4:40	44	44	00	+28	+70	+67
7/6/81	4:45	43	44	−02	+38	+65	+68
7/7/81	8:50	20	20	−34	−32	−32	−32
7/7/81	9:20*	20	20	+06	+02	00	−02
7/7/81	9:37	0	0	−58	−82	−80	−83
7/7/81	9:42	0	0	−59	−86	−84	−84
7/7/81	9:48	20	20	+16	−04	+05	+13
7/7/81	9:55	20	20	+09	+08	+07	+07
7/7/81	10:00	22	22	+11	+12	+07	+07

* Rezero

Notes: (1) Strain gage information

Item	Silicon	Steel
Gage type	WK-03-250TM-350	WK-06-250TM-350
Sec. 1 gage factor	1.96 (Chan. 9)	1.99 (Chan. 11)
Sec. 2 gage factor	1.88 (Chan. 10)	1.89 (Chan. 12)

(2) Indicated gage factor = 1.99

(3) Test performed by J. Pimentel, R. Huebschen, and D. Gillaspy

TABLE B-24. THERMAL STRUCTURAL TEST DATA FOR COUPON TSC-1 OVERSTRESS TEST

Date	Time	Temperature, °C		Strain, μinch/inch			
				Silicon		Glass	
		Silicon	Glass	Ch. 1	Ch. 2	Ch. 3	Ch. 4
7/13/81	9:30	24	24	−02	+02	+09	−03
7/13/81	9:50	60	60	+37	+69	−46	−33
7/13/81	9:55	60	60	+31	+66	−52	−33
7/13/81	10:55	120	120	−19	+64	−240	−193
7/13/81	10:35	120	120	−15	+63	−237	−190
7/13/81	11:10	61	61	+14	+59	−58	−46
7/13/81	11:25	60	60	+15	+48	−58	−43
7/13/81	12:15	0	0	−88	−105	−21	−37
7/13/81	12:25	0	0	−89	−95	−18	−37
7/13/81	12:40	−60	−60	−418	−520	−224	−261
7/13/81	12.45	−60	−60	−406	−521	−211	−258
7/13/81	1:05	0	0	−83	−89	−14	−32
7/13/81	1:15	0	0	−83	−89	−12	−39
7/13/81	1:35	24	24	−06	+08	+02	−05

Notes: (1) Strain gage information

Item	Silicon	Glass
Gage type	WK-03-250TM-350	WK-06-250TM-350
Sec. 1 gage factor	1.96 (Chan. 1)	1.99 (Chan. 3)
Sec. 2 gage factor	1.88 (Chan. 2)	1.89 (Chan. 4)

(2) Indicated gage factor = 1.99

(3) Test performed by J. Pimentel, R. Huebscher, and D. Gillaspy

TABLE B–25. THERMAL STRUCTURAL TEST DATA FOR COUPON TSC–2 OVERSTRESS TEST

Date	Time	Temperature, °C		Strain, μinch/inch			
				Silicon		Glass	
		Silicon	Glass	Ch. 5	Ch. 6	Ch. 7	Ch. 8
7/13/81	9:30	24	24	−02	+05	−09	−07
7/13/81	9:50	60	60	+105	+124	−34	−20
7/13/81	9:56	60	60	+91	+121	−41	−25
7/13/81	10:27	120	120	+136	+203	−167	−138
7/13/81	10:38	120	120	+148	+206	−173	−133
7/13/81	11:15	61	61	+61	+95	−41	−30
7/13/81	11:25	60	60	+59	+82	−43	−20
7/13/81	12:15	0	0	−156	−167	−43	−53
7/13/81	12:25	0	0	−148	−158	−39	−49
7/13/81	12:40	−60	−60	−560	−572	−237	−270
7/13/81	12:45	−60	−60	−552	−563	−232	−260
7/13/81	1:05	0	0	−142	−154	−36	−49
7/13/81	1:15	0	0	−141	−153	−35	−57
7/13/81	1:35	24	24	−14	−10	+05	−04

Notes: (1) Strain gage information

Item	Silicon	Glass
Gage type	WK-03-250TM-350	WK-06-250TM-350
Sec. 1 gage factor	1.96 (Chan. 5)	2.02 (Chan. 7)
Sec. 2 gage factor	1.88 (Chan. 6)	1.93 (Chan. 8)

(2) Indicated gage factor = 1.99

(3) Test performed by J. Pimentel, R. Huebschen, and D. Gillaspy

TABLE B–26. THERMAL STRUCTURAL TEST DATA FOR COUPON TSC–3 OVERSTRESS TEST

Date	Time	Temperature, °C		Strain, μinch/inch			
				Silicon		Glass	
		Silicon	Glass	Ch. 9	Ch. 10	Ch. 11	Ch. 12
7/13/81	9:30	24	24	−01	−04	+03	+01
7/13/81	9:50	60	60	+27	+53	−38	−29
7/13/81	9:57	60	60	+21	+54	−46	−35
7/13/81	10:30	120	120	−42	−52	−209	−184
7/13/81	10:40	120	120	−38	−49	−207	−176
7/13/81	11:20	62	62	+23	+40	−53	−42
7/13/81	11:30	60	60	+25	+40	−36	−32
7/13/81	12:15	0	0	−75	−103	−27	−25
7/13/81	12:25	0	0	−71	−99	−24	−28
7/13/81	12:40	−60	−60	−350	−420	−200	−220
7/13/81	12:45	−60	−60	−351	−430	−208	−228
7/13/81	1:05	0	0	−61	−95	−21	−26
7/13/81	1:15	0	0	−67	−97	−20	−23
7/13/81	1:35	24	24	−03	−08	+05	+11

Notes: (1) Strain gage information

Item	Silicon	Glass
Gage type	WK-03-250TM-350	WK-06-250TM-350
Sec. 1 gage factor	1.96 (Chan. 9)	2.02 (Chan. 11)
Sec. 2 gage factor	1.88 (Chan. 10)	1.93 (Chan. 12)

(2) Indicated gage factor = 1.99

(3) Test performed by J. Pimentel, R. Huebschen, and D. Gillaspy

B.4 STRUCTURAL DEFLECTION TEST DATA

Raw data for the structural deflection test consists of: (a) total load on the module versus structural member deflection at the center, mid-diagonal, and corner cell locations, and (b) strain in both structural member and cell at the central, mid-diagonal, and corner cell locations. Results from the overstress tests are included in these data. The load versus deflection data for the center cell position are shown in Figures B-1 through B-14. The decreasing-load versus deflection curves were intentionally displaced horizontally from the increasing-load versus deflection curves. The strain data are summarized in Table B-28 through B-41.

The time span for these tests is summarized in Table B-27.

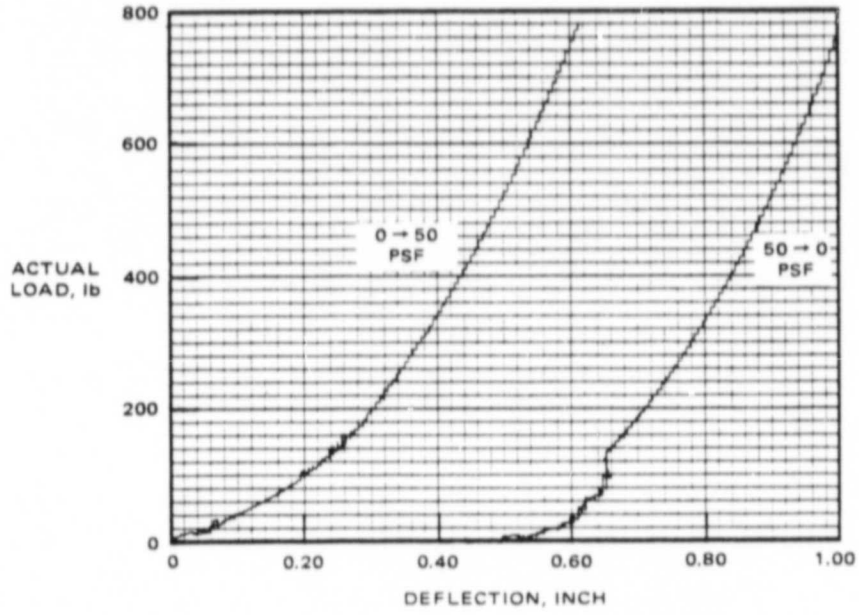

Figure B-1. Module SDM-1 load versus deflection data (glass side up) for normal (0→50→0 psf) test.

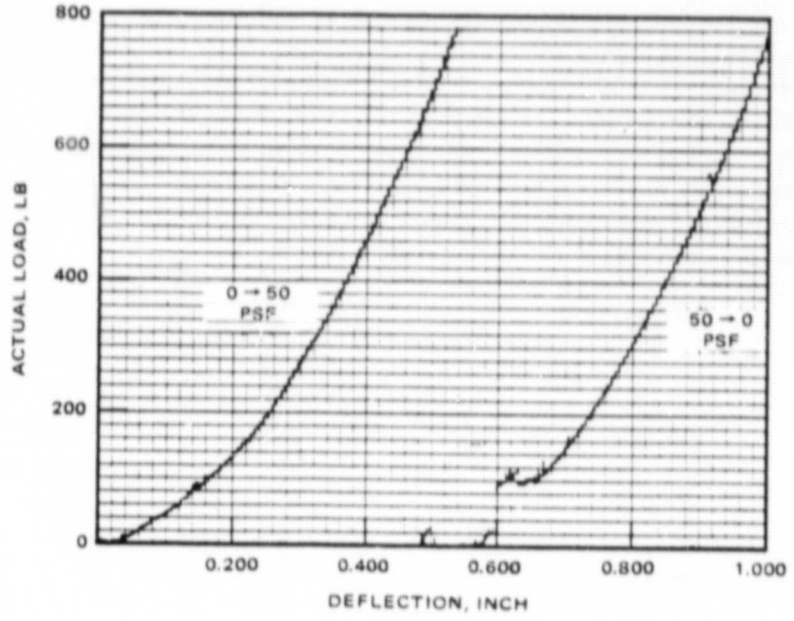

Figure B-2. Module SDM-2 load versus deflection data (glass side up) for normal (0→50→0 psf) test.

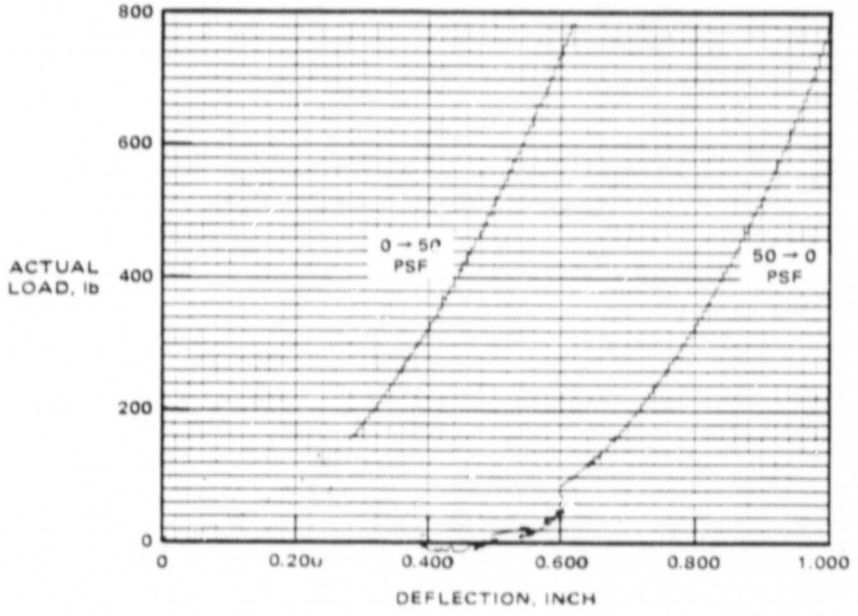

Figure B-3. Module SDM-2 load versus deflection data (glass side down) for normal (0→50→0 psf) test.

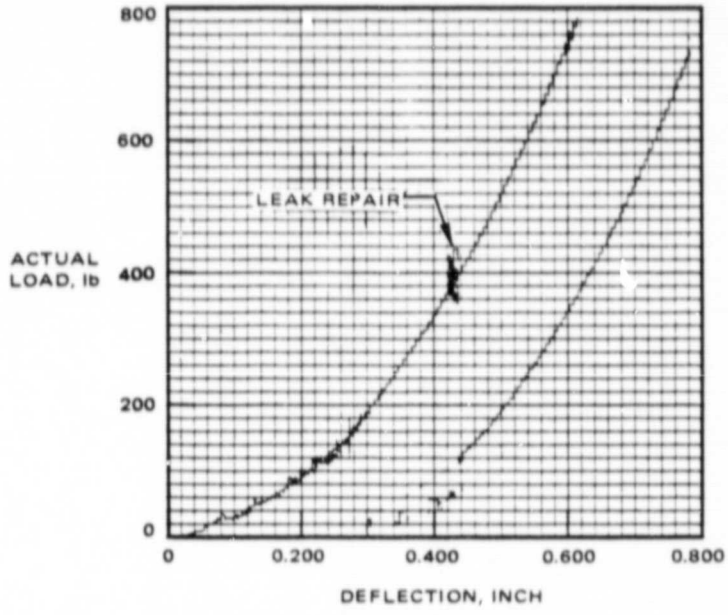

Figure B-4. Module SDM-3 load versus deflection data (glass side up) for normal (0→50→0 psf) test.

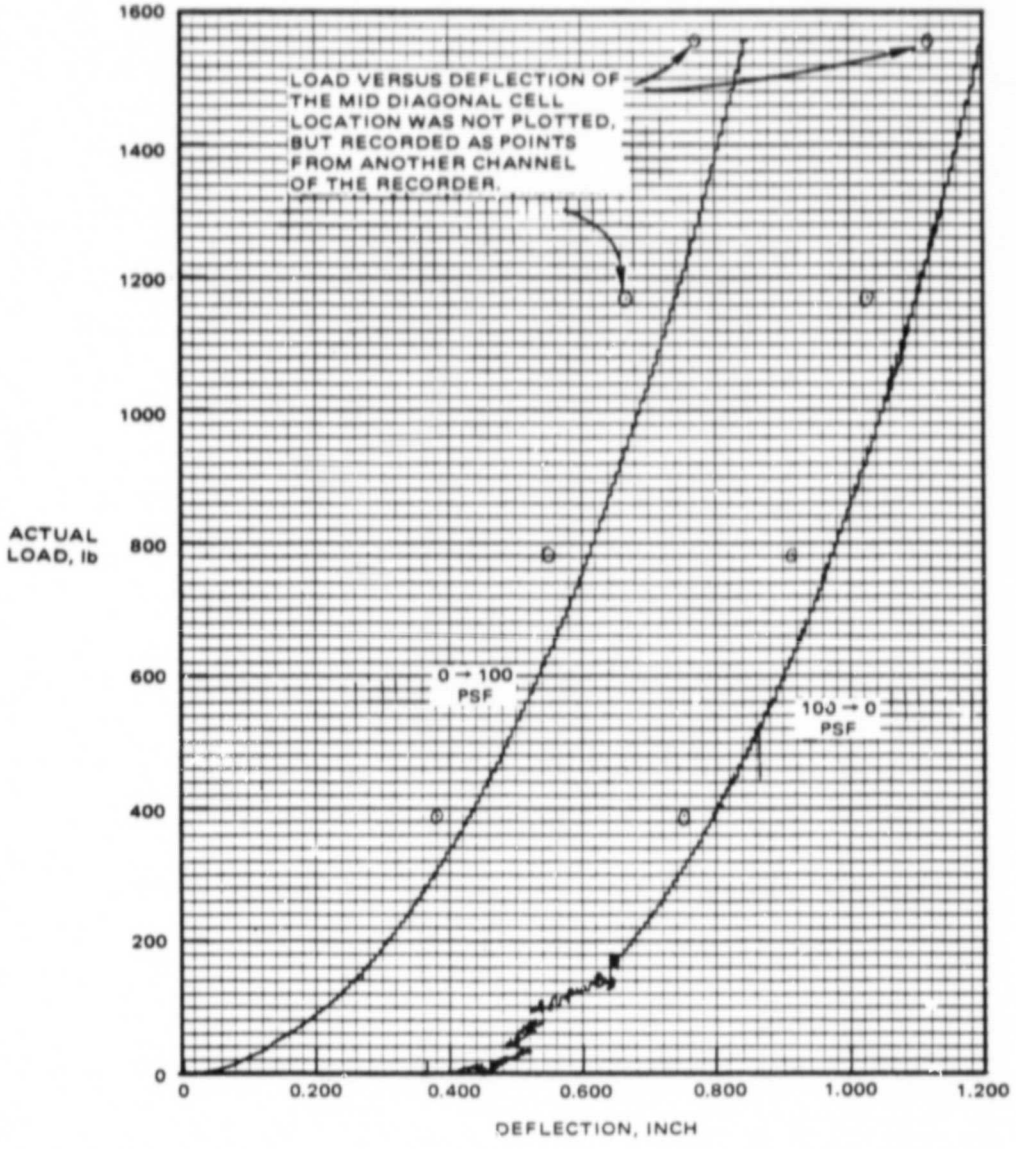

Figure B-5. Module SDM-3 load versus deflection data (glass side up) for overstress (0→100→0 psf) test.

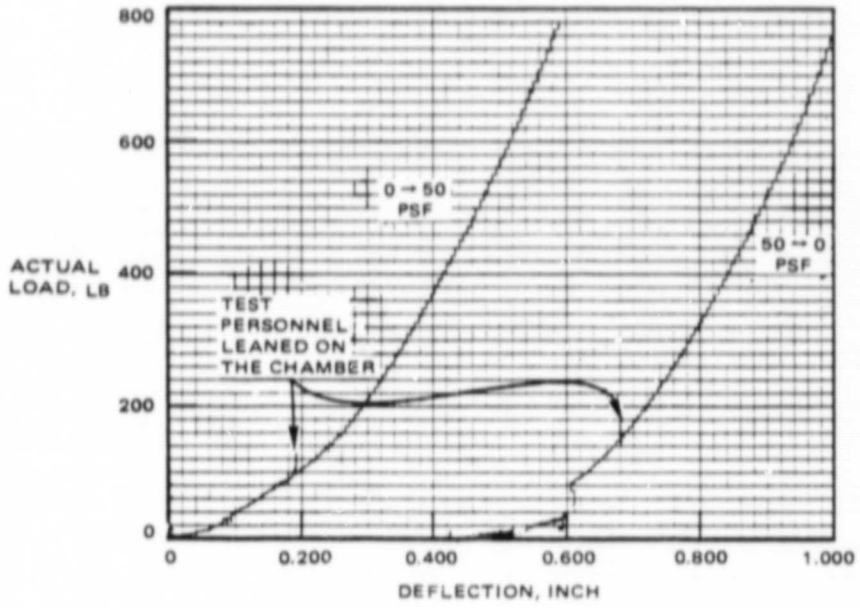

Figure B-6. Module SDM-4 load versus deflection data (glass side up) for normal (0→50→0 psf) test.

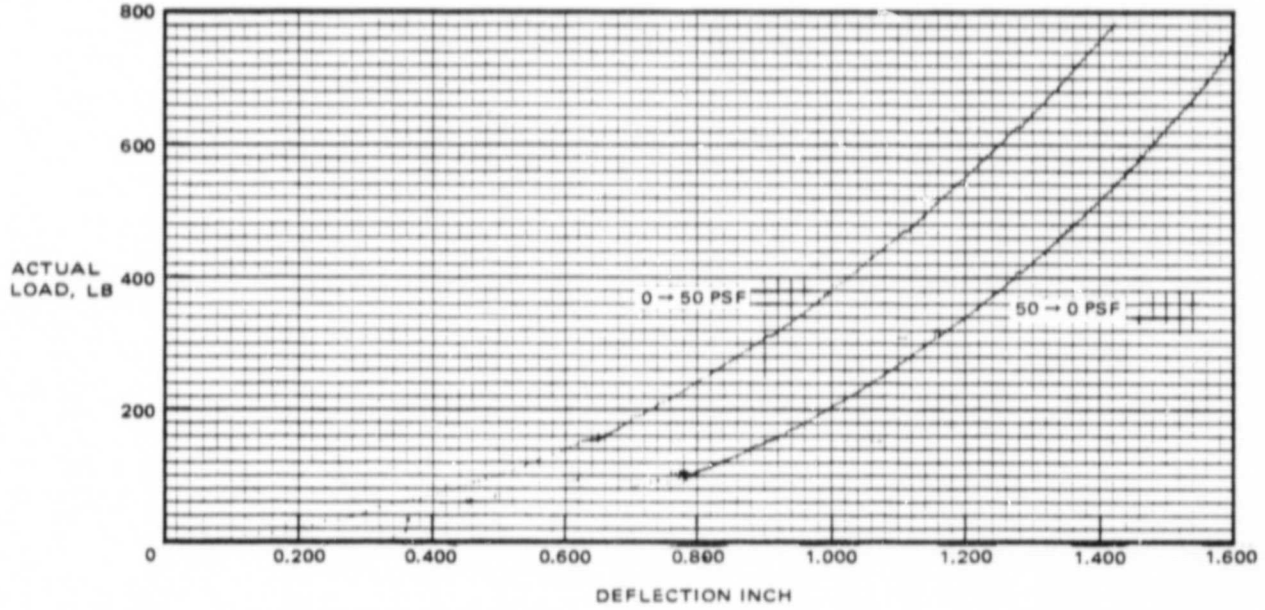

Figure B-7. Module SDM-5 load versus deflection data (bare wood side down) for normal (0→50→0 psf) test.

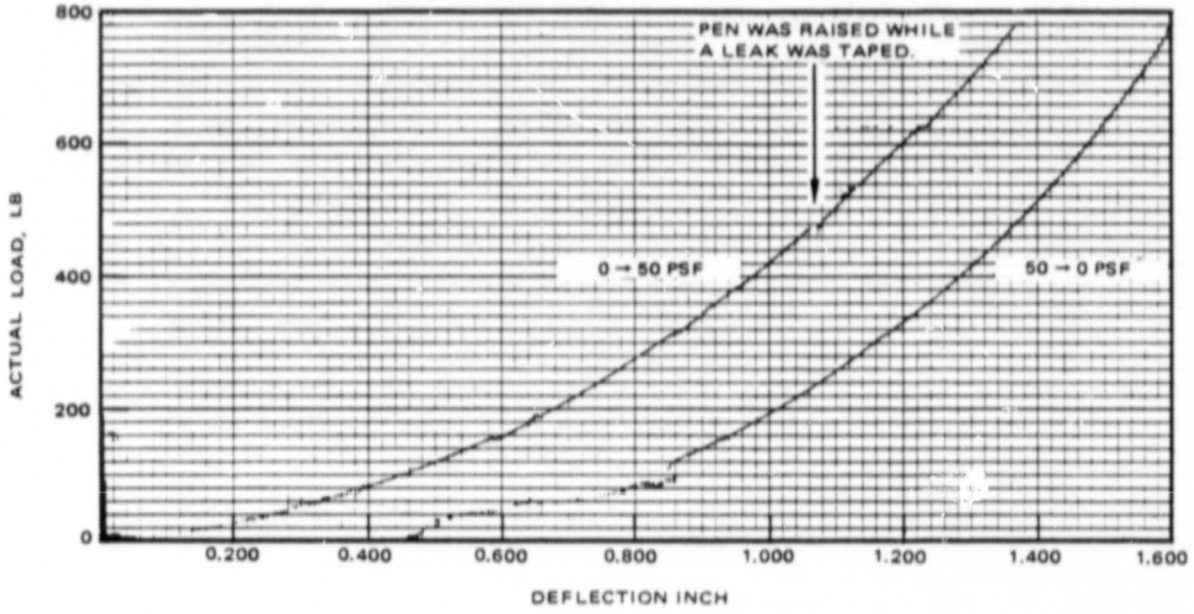

Figure B-8. Module SDM-6 load versus deflection data (bare wood side down) for normal (0→50→0 psf) test.

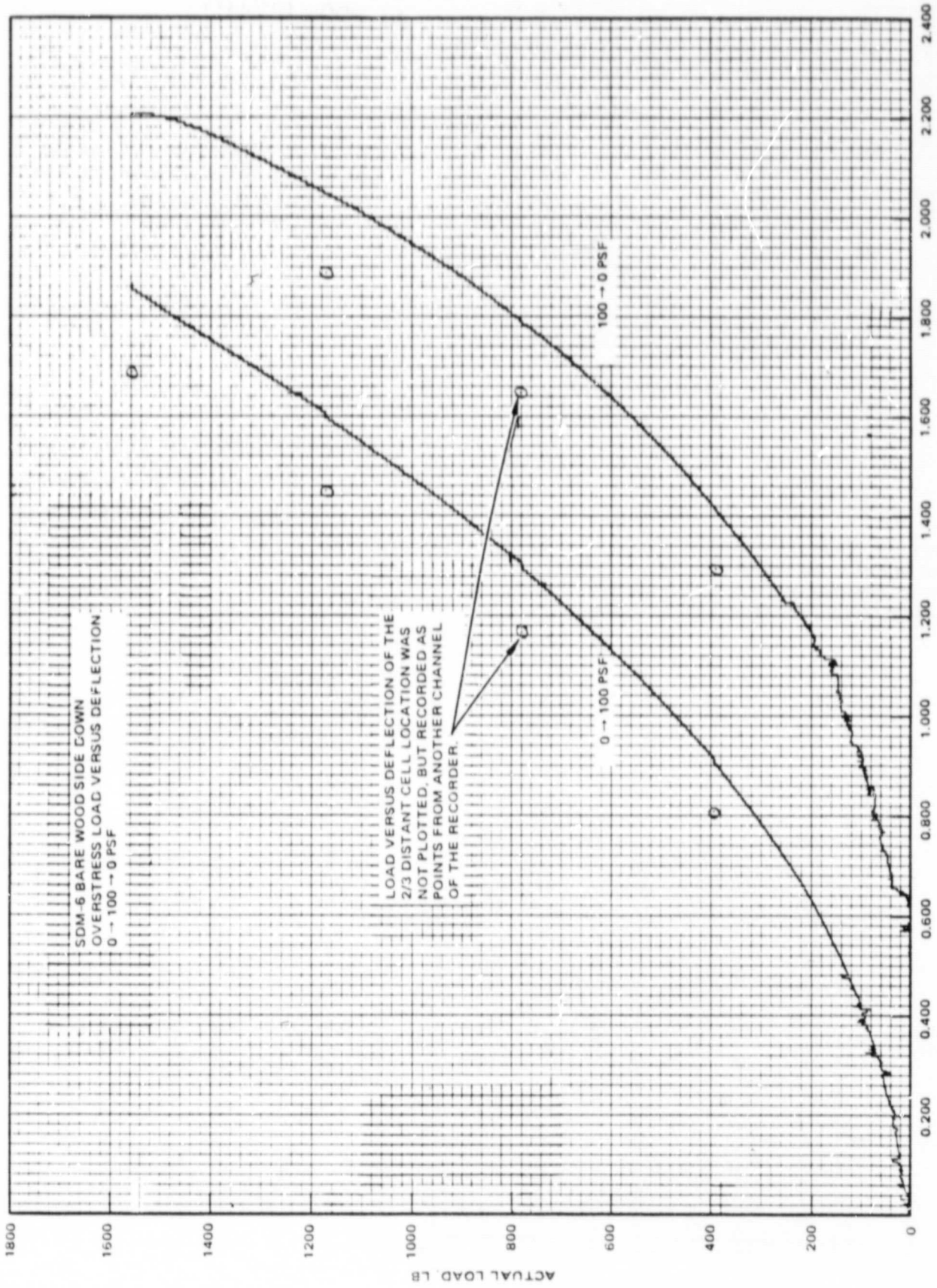

Figure B-9. Module SDM-6 load versus deflection data (bare wood side down) for overstress (0 → 100 → 0 psf) test.

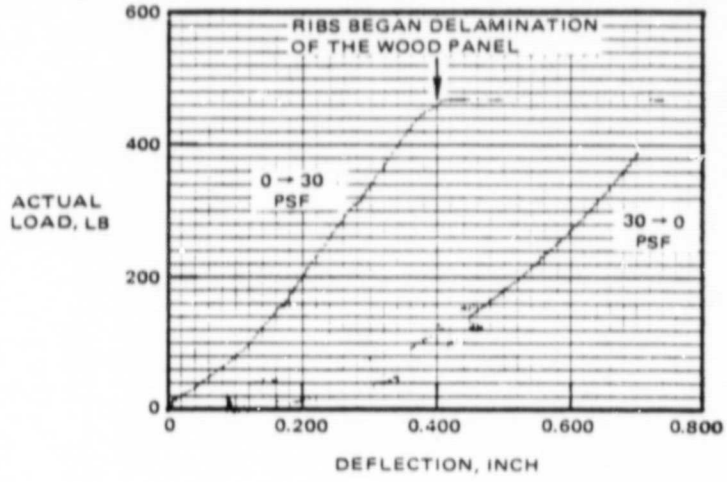

Figure B-10. Module SDM-7 load versus deflection data (ribbed side down, ribs untapered and rib ends are unsupported) for normal (0→50→0 psf) test.

Figure B-11. Module SDM-7 load versus deflection data (ribbed side down, rib ends tapered and unsupported) for normal (0→50→0 psf) test.

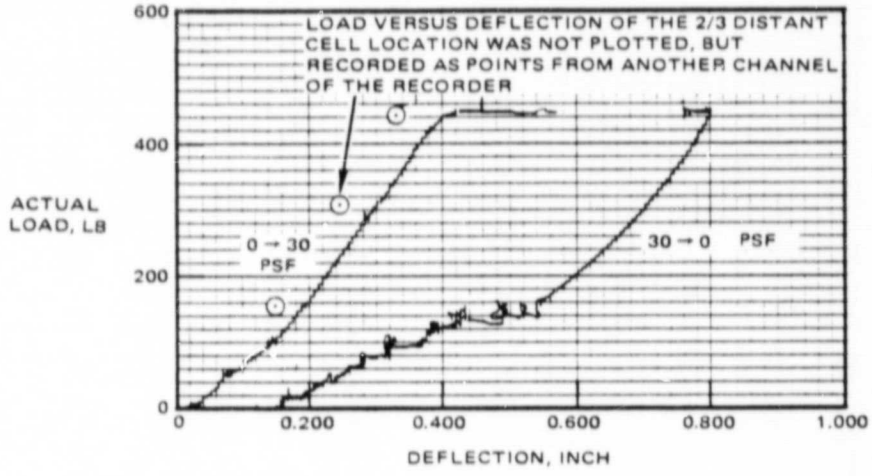

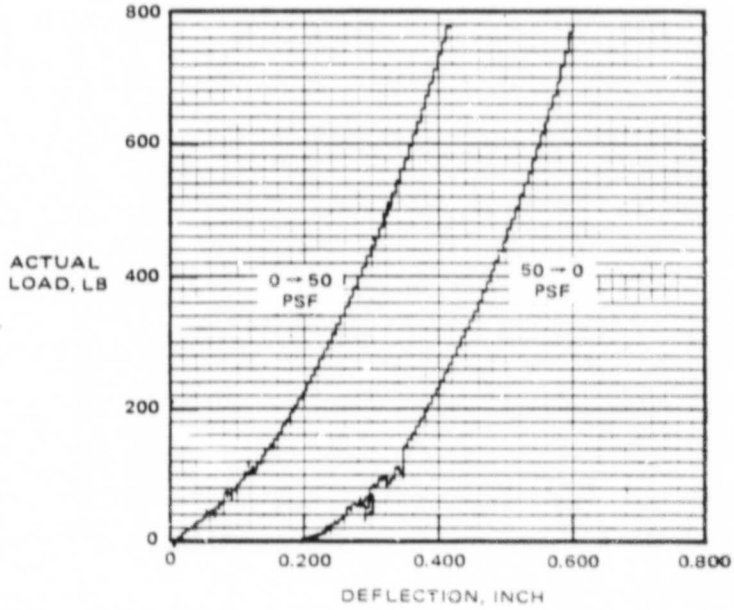

Figure B-12. Module SDM-8 load versus deflection data (bare steel side down) for normal (0→50→0 psf) test.

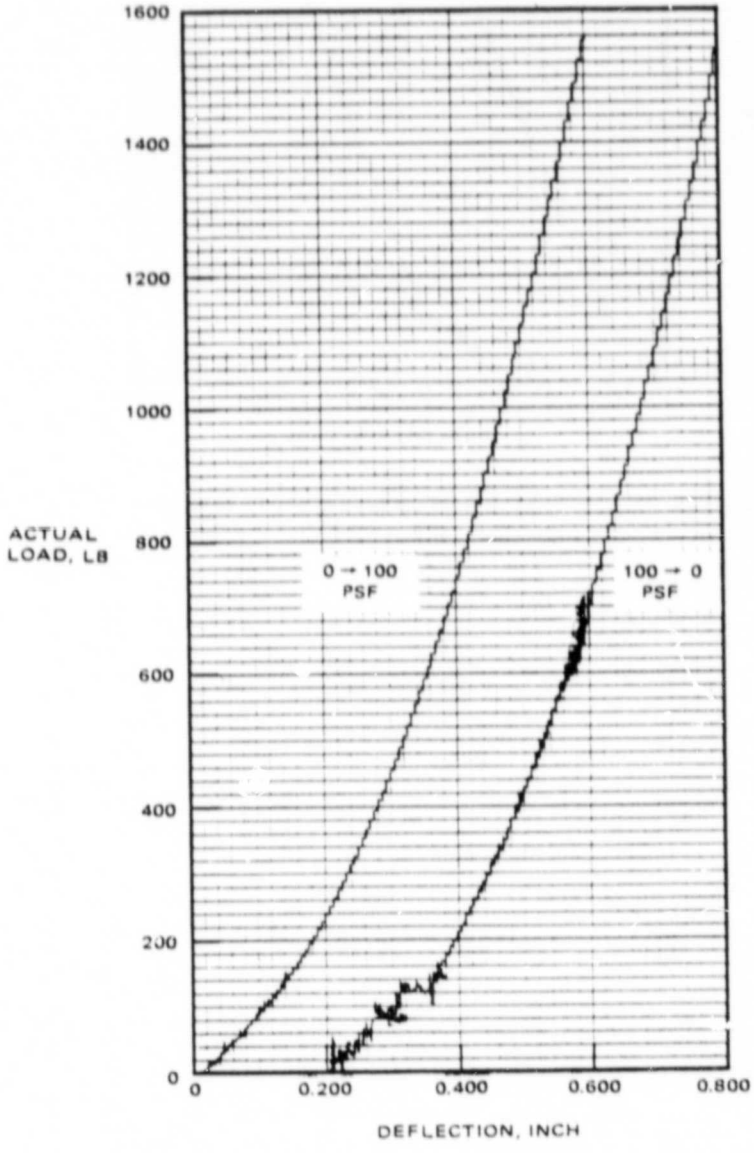

Figure B-13. Module SDM-8 load versus deflection data (bare steel side down) for overstress (0 → 100 → 0 psf) test.

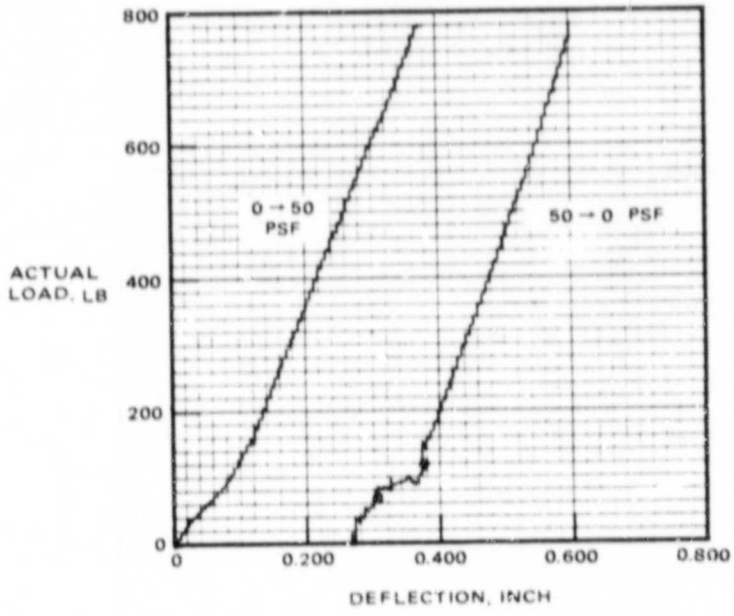

Figure B-14. Module SDM-9 load versus deflection data (ribbed side down, rib ends supported) for normal (0→50→0 psf) test.

TABLE B-27. TIME LINE FOR STRUCTURAL DEFLECTION TEST

Date	Module No.	Comments*
17 July 1981	SDM-2	Normal test—glass side up
20 July 1981	SDM-2	Normal test—glass side down
20 July 1981	SDM-1	Normal test—glass side up
21 July 1981	SDM-3	Normal test—glass side up
22 July 1981	SDM-4	Normal test—glass side up
22 July 1981	SDM-5	Normal test—bare wood side down
23 July 1981	SDM-6	Normal test—bare wood side down
24 July 1981	SDM-7	Normal test—ribbed side down (failure)
27 July 1981	SDM-8	Normal test—bare steel side down
28 July 1981	SDM-9	Normal test—supported rib side down
29 July 1981	SDM-8	Overstress test—bare steel side down
30 July 1981	SDM-7	Normal test—tapered, unsupported rib side down (failure)
30 July 1981	SDM-6	Overstress test—bare wood side down
31 July 1981	SDM-3	Overstress test—glass side up

*Normal test cycle: 0→50→0 psf in 10 psf steps
Overstress test cycle: 0→100→0 psf in 20 psf steps

TABLE B–28. STRAIN AND VERTICAL DEFLECTION DATA FOR MODULE SDM–1 (GLASS SIDE UP) NORMAL TEST

Load, lb	Pressure, psf	Time	Cell Strain, μ inch/inch						Glass Strain, μ inch/inch						Vertical Position, in.	
			CH. 1	CH. 2	CH. 3	CH. 4	CH. 5	CH. 6	CH. 7	CH. 8	CH. 9	CH. 10	CH. 11	CH. 12	Corner Position	Mid-Diagonal Position
0	0	3:35	+02	+02	−09	−10	+08	+02	−03	+03	+01	+06	+09	−01	0.067	0.009
156	10	3:45	+07	+04	−03	+02	+02	+06	+28	+45	−06	−30	−07	−28	0.103	0.283
312	20	3:50	+06	+02	+10	+03	+05	+08	+39	+61	+03	−31	−41	−66	0.125	0.398
468	30	3:54	+07	+04	+10	+08	+15	+16	+57	+79	+24	−27	−102	−108	0.147	0.491
624	40	3:57	+08	+07	+14	+14	+23	+24	+74	+92	+29	−23	−161	−152	0.167	0.566
780	50	4:01	+12	+05	+18	+20	+26	+25	+81	+100	+37	−17	−230	−209	0.184	0.629
624	40	4:10	+17	+08	+20	+26	+24	+30	+73	+95	+30	−23	−163	−161	0.170	0.572
468	30	4:17	+20	+08	+14	+15	+22	+27	+59	+79	+18	−27	−105	−114	0.150	0.500
312	20	4:25	+17	+16	+15	+15	+18	+28	+44	+68	+08	−28	−46	−68	0.129	0.408
156	10	4:35	+17	+07	+13	+12	+09	+20	+28	+43	−05	−30	−06	−29	0.107	0.293
0	0	4:45	+16	+07	+08	+02	+14	+13	−06	−04	+01	−10	+08	−03	0.070	0.020

Notes: (1) Relative humidity = 50%
(2) All gage factors (for strain gages) set at 2.06
(3) Date of test: 20 July 1981
(4) Test performed by R. Huebschen and D. Gillaspy

LOCATION AND DIRECTION OF STRAIN MEASUREMENTS
(6 STRAIN GAGES PER MODULE, 2 DATA CHANNELS PER STRAIN GAGE)

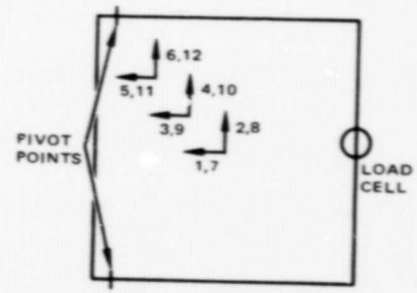

TABLE B–29. STRAIN AND VERTICAL DEFLECTION DATA FOR MODULE SDM–2 (GLASS SIDE UP) NORMAL TEST

Load, lb	Pressure, psf	Time	Cell Strain, μ inch/inch						Glass Strain, μ inch/inch						Vertical Position, in.	
			CH. 1	CH. 2	CH. 3	CH. 4	CH. 5	CH. 6	CH. 7	CH. 8	CH. 9	CH. 10	CH. 11	CH. 12	Corner Position	Mid-Diagonal Position
0	0	2:15	00	00	−02	+04	+02	−02	+02	+06	−02	−05	00	+09	0.037	0.069
156	10	2:25	+08	+02	+05	+20	+10	+02	+28	+33	−01	−29	−59	−54	0.069	0.275
312	20	2:35	+06	+05	+10	+28	+20	+10	+42	+47	+06	−38	−117	−109	0.088	0.369
468	30	2:40	+06	+10	+10	+28	+26	+14	+56	+58	+06	−54	−193	−184	0.106	0.450
624	40	2:50	00	00	+05	+26	+23	+16	+59	+62	+14	−55	−254	−250	0.122	0.515
780	50	3:00	+04	+06	+10	+33	+34	+24	+71	+75	+22	−55	−320	−315	0.136	0.573
624	40	3:35	+06	+06	+09	+27	+28	+22	+62	+65	+12	−55	−258	−257	0.125	0.523
468	30	3:45	+06	+10	+09	+27	+24	+16	+53	+56	+07	−50	−189	−191	0.111	0.460
312	20	3:55	+08	+08	+05	+21	+21	+14	+38	+44	−04	−46	−128	−131	0.094	0.383
156	10	4:05	+06	+04	+04	+17	+10	+07	+22	+26	−08	−37	−70	−70	0.076	0.288
0	0	4:15	+03	+04	−01	+08	+04	+02	−03	00	−10	−14	−05	−06	0.042	0.081

Notes: (1) Relative humidity = 50%
(2) All gage factors (for strain gages) set at 2.00
(3) Date of test: 17 July 1981
(4) Test performed by R. Huebschen and D. Gillaspy

LOCATION AND DIRECTION OF STRAIN MEASUREMENTS
(6 STRAIN GAGES PER MODULE, 2 DATA CHANNELS PER STRAIN GAGE)

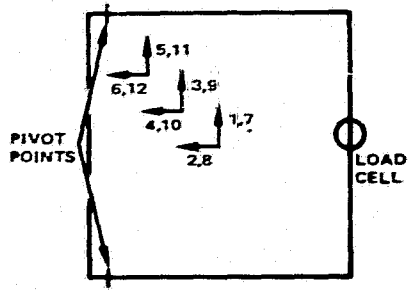

TABLE B–30. STRAIN AND VERTICAL DEFLECTION DATA FOR MODULE SDM–2 (GLASS SIDE DOWN) NORMAL TEST

Load, lb	Pressure, psf	Time	Cell Strain, μ inch/inch						Glass Strain, μ inch/inch						Vertical Position, in.	
			CH. 1	CH. 2	CH. 3	CH. 4	CH. 5	CH. 6	CH. 7	CH. 8	CH. 9	CH. 10	CH. 11	CH. 12	Corner Position	Mid-Diagonal Position
0	0	10:55	−02	+10	+12	−01	+07	−12	−06	−09	+07	−07	+09	+13	0.057	0.971
156	10	11:00	+10	+16	+16	+09	−01	−02	+39	+70	+93	+31	+23	+26	0.096	0.222
312	20	11:06	+06	+20	+19	+09	−06	−03	+64	+63	+127	+51	+47	+40	0.119	0.322
468	30	11:10	+20	+21	+10	+17	−15	−15	+90	+75	+156	+59	+71	+57	0.140	0.405
624	40	11:15	+11	+27	+16	+23	−25	−20	+109	+95	+179	+78	+109	+83	0.160	0.475
780	50	11:22	+09	+25	+11	+12	−40	−22	+121	+110	+203	+88	+173	+94	0.182	0.539
624	40	11:30	+11	+33	+06	+22	−26	−18	+101	+95	+179	+72	+137	+70	0.167	0.483
468	30	11:37	+04	+20	+08	+18	−19	−12	+90	+81	+159	+68	+104	+37	0.149	0.415
312	20	11:43	+15	+26	+11	+22	−06	−06	+66	+60	+134	+50	+69	+16	0.128	0.334
156	10	11:55	+13	+22	+17	+12	+02	+04	+51	+45	+97	+27	+50	−03	0.105	0.234
0	0	12:05	+11	+27	+26	+21	+05	+11	+12	+01	+17	+03	+40	−10	0.064	0.983

Notes: (1) Relative humidity = 50%
(2) All gage factors (for strain gages) set at 2.06
(3) Date of test: 20 July 1981
(4) Test performed by R. Huebschen and D. Gillaspy

LOCATION AND DIRECTION OF STRAIN MEASUREMENTS
(6 STRAIN GAGES PER MODULE, 2 DATA CHANNELS PER STRAIN GAGE)

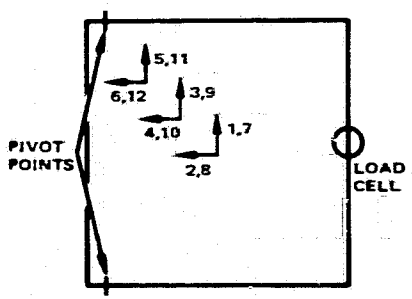

TABLE B–31. STRAIN AND VERTICAL DEFLECTION DATA FOR MODULE SDM–3 (GLASS SIDE UP) NORMAL TEST

Load, lb	Pressure, psf	Time	Cell Strain, μ inch/inch						Glass Strain, μ inch/inch						Vertical Position, in.	
			CH. 1	CH. 2	CH. 3	CH. 4	CH. 5	CH. 6	CH. 7	CH. 8	CH. 9	CH. 10	CH. 11	CH. 12	Corner Position	Mid-Diagonal Position
0	0	11:07	+02	−03	00	+01	−05	+01	−01	+02	−01	−04	−01	00	0.104	0.077
156	10	11:15	+07	+08	+20	+25	+06	−03	+31	+25	−01	−37	−19	−13	0.134	0.323
312	20	11:20	+13	+14	+20	+27	+01	+01	+53	+36	+01	−45	−49	−46	0.150	0.426
468	30	11:29	+20	+11	+26	+34	+05	+05	+58	+56	−08	−42	−91	−79	0.165	0.511
624	40	11:34	+17	+13	+34	+31	+08	+17	+74	+66	+03	−42	−137	−127	0.180	0.580
780	50	11:37	+17	+08	+31	+32	+08	+19	+80	+81	00	−31	−188	−174	0.194	0.642
624	40	11:50	+25	+07	+27	+29	+08	+11	+68	+65	+04	−38	−138	−129	0.182	0.581
468	30	1:10	+28	+26	+44	+48	+34	+33	+74	+66	+13	−27	−83	−76	0.169	0.516
312	20	1:21	+36	+26	+44	+47	+23	+29	+64	+53	+12	−28	−36	−38	0.153	0.432
156	10	1:30	+35	+27	+38	+43	+32	+23	+48	+40	+09	−22	−07	−04	0.137	0.324
0	0	1:40	+35	+23	+33	+31	+29	+17	+20	+05	+17	+06	+19	+21	0.108	0.087

Notes. (1) Relative humidity = 50%
(2) Slight pressure on the glass near Channel 9 caused 60–70 μ inch reading after test.
(3) Approximately one pint of water leaked into bottom of test fixture during lunch time.
(4) Date of test 21 July 1981
(5) Test performed by R. Huebschen and D. Gillaspy

LOCATION AND DIRECTION OF STRAIN MEASUREMENTS
(6 STRAIN GAGES PER MODULE, 2 DATA CHANNELS PER STRAIN GAGE)

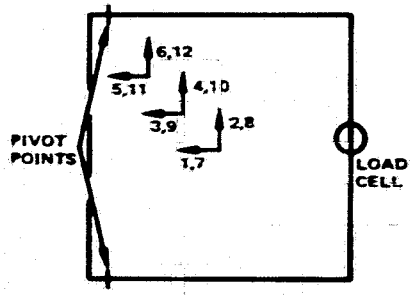

TABLE B–32. STRAIN AND VERTICAL DEFLECTION DATA FOR MODULE SDM–4 (GLASS SIDE UP) NORMAL TEST

Load, lb	Pressure, psf	Time	Cell Strain, μ inch/inch						Glass Strain, μ inch/inch						Vertical Position, in.	
			CH. 1	CH. 2	CH. 3	CH. 4	CH. 5	CH. 6	CH. 7	CH. 8	CH. 9	CH. 10	CH. 11	CH. 12	Corner Position	Mid-Diagonal Position
0	0	9:00	−06	−06	−09	00	−06	−06	−07	+01	−06	+03	−03	−06	0.105	0.114
156	10	9:08	−05	−08	−01	+04	−05	+05	+40	+43	+21	−26	−08	−39	0.136	0.346
312	20	9:14	−03	+05	−04	+12	+11	+10	+62	+58	+54	−32	−48	−80	0.153	0.447
468	30	9:17	−03	−06	−03	+21	+11	+10	+80	+78	+72	−32	−87	−123	0.171	0.531
624	40	9:23	+06	−08	−01	+25	+26	+10	+103	+91	+77	−29	−133	−171	0.186	0.600
780	50	9:28	+09	−05	+05	+29	+33	+20	+109	+107	+92	−25	−183	−224	0.199	0.658
780	50	9:50	−13	−18	−15	+11	+11	+05	+107	+97	+85	−38	−198	−240	0.199	0.658
624	40	10:00	−12	−15	−13	+07	−02	+05	+94	+80	+75	−42	−146	−185	0.189	0.605
468	30	10:10	−05	−17	−16	+09	−07	−01	+77	+62	+57	−38	−100	−139	0.174	0.538
312	20	10:17	−05	−05	−07	−04	−02	−11	+52	+57	+39	−40	−59	−97	0.157	0.555
156	10	10:25	−11	−05	−09	−01	00	−07	+39	+40	+25	−27	−17	−57	0.140	0.352
0	0	10:35	−11	−09	−09	−17	00	−03	+01	+11	+05	−05	−06	−22	0.109	0.123

Notes: (1) Relative humidity = 50%
(2) All gage factors (for strain gages) set at 2.06
(3) Lost power and restarted at 9:50 am
(4) Date of test 22 July 1981
(5) Test performed by R. Huebschen and D. Gillaspy

LOCATION AND DIRECTION OF STRAIN MEASUREMENTS
(6 STRAIN GAGES PER MODULE, 2 DATA CHANNELS PER STRAIN GAGE)

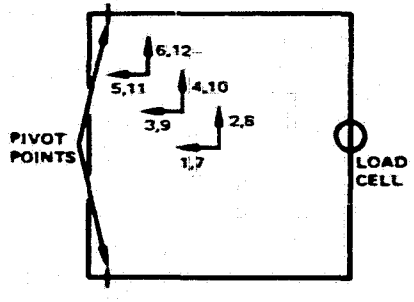

TABLE B–33. STRAIN AND VERTICAL DEFLECTION DATA FOR MODULE SDM–5 (WOOD SIDE DOWN) NORMAL TEST

Load, lb	Pressure, psf	Time	Cell Strain, μ inch/inch						Wood Strain, μ inch/inch						Vertical Position, in.	
			CH. 1	CH. 2	CH. 3	CH. 4	CH. 5	CH. 6	CH. 7	CH. 8	CH. 9	CH. 10	CH. 11	CH. 12	Corner Position	Mid-Diagonal Position
0	0	3:25	−01	−07	−03	−08	+02	−08	00	+02	+02	+01	+06	−01	0.093	0.088
156	10	3:37	−19	−21	−19	−25	−31	−19	+311	+264	−297	+334	+33	+100	0.164	0.658
312	20	3:45	−19	−23	−26	−33	−61	−33	+436	+372	+437	+504	+102	+201	0.204	—
468	30	3:52	−22	−25	−28	−35	−74	−60	+547	+470	+553	+630	+178	+378	0.240	—
624	40	3:56	−21	−25	−29	−34	−81	−84	+630	+554	+652	+735	+301	+590	0.271	—
780	50	4:00	−22	−30	−33	−35	−73	−49	+704	+620	+743	+814	+463	+859	0.303	—
624	40	4:10	−21	−27	−30	−36	−59	−34	+624	+557	+662	+745	+357	+681	0.284	—
468	30	4:18	−21	−24	−28	−34	−48	−25	+536	+476	+566	+650	+252	+498	0.258	—
312	20	4:27	−09	−19	−21	−28	−33	−15	+435	+384	+450	+528	+164	+337	0.227	—
156	10	4:35	−10	−14	−08	−20	−16	−01	+305	+278	+308	+371	+82	+201	0.188	—
0	0	4:50	+07	−02	+05	−02	+03	+07	+10	+27	+23	+41	+19	+62	0.116	

Notes (1) Relative humidity = 60%
(2) Dial indicator used to measure vertical displacement at mid-diagonal position removed at 3:45 pm
(3) Strain gage associated with channels 5 and 6 is mounted on a cracked cell
(4) Date of test 22 July 1981
(5) Test performed by R Huebschen and D Gillaspy

LOCATION AND DIRECTION OF STRAIN MEASUREMENTS
(6 STRAIN GAGES PER MODULE, 2 DATA CHANNELS PER STRAIN GAGE)

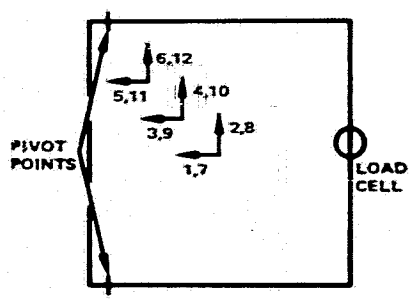

TABLE B–34. STRAIN AND VERTICAL DEFLECTION DATA FOR MODULE SDM–6 (WOOD SIDE DOWN) NORMAL TEST

Load, lb	Pressure, psf	Time	Cell Strain, μ inch/inch						Wood Strain, μ inch/inch						Vertical Position, in.	
			CH. 1	CH. 2	CH. 3	CH. 4	CH. 5	CH. 6	CH. 7	CH. 8	CH. 9	CH. 10	CH. 11	CH. 12	Corner Position	Mid-Diagonal Position
0	0	1:40	−05	−04	+03	+01	+01	+07	00	+01	−01	+07	+08	+03	0.138	—
156	10	1:45	−10	−13	−15	−11	−20	−08	+291	+210	+242	+317	+107	+95	0.187	—
312	20	1.51	−15	−23	−14	−23	−38	−28	+433	+304	+379	+474	+215	+220	0.220	—
468	30	1:56	−19	−19	−27	−31	−63	−54	+534	+381	+473	+608	+316	+377	0.250	—
624	40	2:01	−22	−19	−27	−31	−96	−88	+630	+445	+576	+704	+453	+546	0.275	—
780	50	2:07	−21	−15	−26	−32	−126	−124	+720	+504	+657	+792	+613	+754	0.300	—
624	40	2:50	−17	−14	−21	−26	−106	−108	+599	+437	+559	+716	+524	+687	0.291	—
468	30	3.11	−04	−08	−17	−23	−79	−80	+500	+374	+467	+620	+396	+553	0.270	—
312	20	3:20	+02	−02	−08	−13	−49	−45	+383	+293	+364	+503	+281	+398	0.244	—
156	10	3:30	−09	+03	+01	−03	−28	−25	+241	+203	+231	+354	+177	+257	0.211	—
0	0	3:38	+02	+03	+12	+06	−07	+01	−12	+35	+20	+87	+72	+152	0.160	—

Notes (1) Relative humidity = 54%
(2) Dial indicator used to measure vertical displacement at mid-diagonal position removed
(3) Date of test 23 July 1981
(4) Test performed by R. Huebschen and D. Gillaspy

LOCATION AND DIRECTION OF STRAIN MEASUREMENTS
(6 STRAIN GAGES PER MODULE, 2 DATA CHANNELS PER STRAIN GAGE)

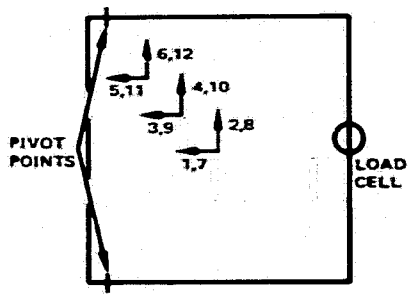

TABLE B–35. STRAIN AND VERTICAL DEFLECTION DATA FOR MODULE SDM–7 (RIBBED WOOD SIDE DOWN) NORMAL TEST

Load, lb	Pressure, psf	Time	Cell Strain, μ inch/inch						Wood Strain, μ inch/inch						Vertical Position, in.	
			CH. 1	CH. 2	CH. 3	CH. 4	CH. 5	CH. 6	CH. 7	CH. 8	CH. 9	CH. 10	CH. 11	CH. 12	Corner Position	Mid-Diagonal Position
0	0	10:40	−05	+04	00	00	+04	−03	00	−06	−03	+09	−05	+04	0.059	−0.006
156	10	10:46	+13	+07	+24	−16	00	00	−31	−88	−44	−62	+08	+18	0.074	0.136
312	20	10:50	+41	−11	+42	−14	−05	−14	−83	−156	−84	−127	+53	+39	0.091	0.228
468	30	10:56	+68	−14	+50	−27	−04	−23	—	—	—	—	—	—	—	—

Notes (1) Relative humidity = 56%
(2) Ribs started to tear away from substrate at 30 psf load condition
(3) Date of test 24 July 1981
(4) Test performed by R. Huebschen and D Gillaspy

LOCATION AND DIRECTION OF STRAIN MEASUREMENTS
(6 STRAIN GAGES PER MODULE, 2 DATA CHANNELS PER STRAIN GAGE)

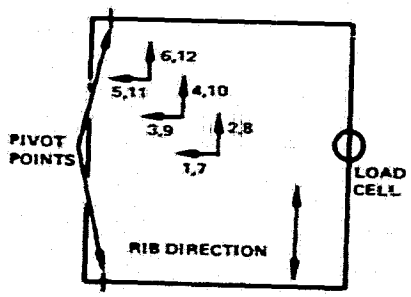

TABLE B–36. STRAIN AND VERTICAL DEFLECTION DATA FOR MODULE SDM–8 (STEEL SIDE DOWN) NORMAL TEST

Load, lb	Pressure, psf	Time	Cell Strain, μ inch/inch						Steel Strain, μ inch/inch						Vertical Position, in.	
			CH. 1	CH. 2	CH. 3	CH. 4	CH. 5	CH. 6	CH. 7	CH. 8	CH. 9	CH. 10	CH. 11	CH. 12	Corner Position	Mid-Diagonal Position
0	0	9:25	−04	+06	+08	+07	−01	+08	+01	+05	00	+06	+02	−05	0.048	0.213
156	10	9:30	00	+07	−05	+01	−06	−04	+24	+16	+24	+26	+46	−02	0.079	0.368
312	20	9:35	−02	−04	+06	+04	−17	00	+33	+25	+40	+36	+74	+10	0.098	0.452
468	30	9:40	+06	−04	−01	−11	−22	−13	+39	+48	+50	+51	+106	+39	0.115	0.518
624	40	9:45	+07	−03	−13	−14	−31	−22	+50	+44	+56	+64	+136	+55	0.129	0.573
780	50	9:51	−08	−07	−16	−17	−44	−35	+55	+55	+68	+77	+164	+88	0.140	0.617
624	40	10:02	−03	−04	−06	00	−30	−21	+52	+50	+67	+65	+145	+62	0.130	0.573
468	30	10:25	−03	+11	+06	−02	−20	−13	+49	+41	+53	+63	+100	+37	0.118	0.522
312	20	10:34	+08	−03	−04	−05	−16	−07	+32	+32	+40	+50	+81	+19	0.101	0.455
156	10	10:45	+11	+09	+09	−04	+06	−02	+22	+14	+24	+26	+43	+04	0.083	0.374
0	0	10:52	+07	+10	+07	−03	+05	−01	−03	+13	−07	−14	+06	−01	0.052	0.218

Notes: (1) Relative humidity = 50%
(2) Date of test: 27 July 1981
(3) Test performed by R. Huelsdonk and D. Gillaspy

LOCATION AND DIRECTION OF STRAIN MEASUREMENTS
(6 STRAIN GAGES PER MODULE, 2 DATA CHANNELS PER STRAIN GAGE)

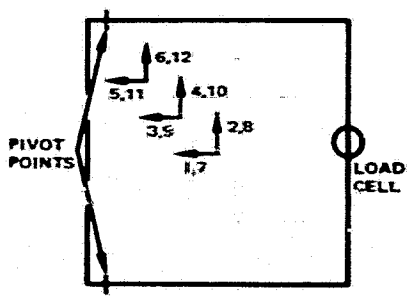

TABLE B–37. STRAIN AND VERTICAL DEFLECTION DATA FOR MODULE SDM–9 (RIBBED WOOD SIDE DOWN) NORMAL TEST

Load, lb	Pressure, psf	Time	Cell Strain, μ inch/inch						Wood Strain, μ inch/inch						Vertical Position, in.	
			CH. 1	CH. 2	CH. 3	CH. 4	CH. 5	CH. 6	CH. 7	CH. 8	CH. 9	CH. 10	CH. 11	CH. 12	Corner Position	Mid-Diagonal Position
0	0	1:55	+03	−03	—	—	+01	−03	−07	00	+04	−03	00	−03	0.076	0.001
156	10	2:00	−07	+16	—	—	−14	−01	+09	−70	−03	−60	+36	+23	0.103	0.114
312	20	2:05	−03	+27	—	—	−14	−01	+04	−137	−25	−110	+73	+46	0.118	0.170
468	30	2:09	−04	+37	—	—	−14	−16	+24	−199	−40	−157	+121	+60	0.131	0.226
624	40	2:14	−07	+38	—	—	−20	−20	+11	−264	−47	−210	+160	+76	0.143	0.280
780	50	2:18	−12	+63	—	—	−26	−27	−03	−335	−57	−248	+210	+96	0.154	0.334
624	40	2:25	−15	+54	—	—	−20	−20	+06	−282	−53	−212	+192	+77	0.148	0.295
468	30	2:35	−14	+40	—	—	−16	−17	+12	−212	−35	−168	+154	+52	0.141	0.249
312	20	2:45	−04	+39	—	—	−08	−05	+13	−154	−22	−139	+139	+25	0.132	0.200
156	10	2:55	+01	+33	—	—	−03	−13	+16	−93	−12	−94	+111	00	0.122	0.148
0	0	3:04	+01	+25	—	—	−04	+01	+08	−18	+14	−51	+87	−40	0.093	0.039

Notes (1) Relative humidity = 55%
(2) Ends of each rib have a 1-inch wide additional support at the frame edge
(3) Date of test: 28 July 1981
(4) Test performed by R. Huebschen and D. Gillaspy
(5) Strain gage associated with channels 3 and 4 is mounted on a cracked cell

LOCATION AND DIRECTION OF STRAIN MEASUREMENTS
(6 STRAIN GAGES PER MODULE, 2 DATA CHANNELS PER STRAIN GAGE)

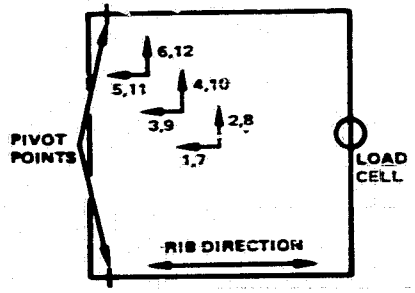

TABLE B–38. STRAIN AND VERTICAL DEFLECTION DATA FOR MODULE SDM–7 (TAPERED RIBS, RIBBED WOOD SIDE DOWN) NORMAL TEST

Load, lb	Pressure, psf	Time	Cell Strain, μ inch/inch						Wood Strain, μ inch/inch						Vertical Position, in.	
			CH. 1	CH. 2	CH. 3	CH. 4	CH. 5	CH. 6	CH. 7	CH. 8	CH. 9	CH. 10	CH. 11	CH. 12	Corner Position	Mid-Diagonal Position
0	0	2:22	+01	−07	−02	00	+07	+02	+02	+05	00	−03	−07	+09	0.077	—
156	10	2:27	+01	−15	+22	−03	+10	−02	−17	−84	−42	−63	+01	+48	0.093	—
312	20	2:32	+24	−17	+37	−10	−01	−14	−36	−155	−94	−115	+59	+78	0.114	—
450	29	2:38	+38	−24	+65	−08	−02	−16	+09	−197	−210	−171	+104	+107	0.131	—
450	29	2:42	+14	−12	−17	+03	−71	−240	+82	−44	+378	−20	+276	+973	—	—
0	0	3:00	−03	00	−03	+14	+19	−12	−03	+08	+67	−01	−15	+79	0.100	—

Notes: (1) Relative humidity = 50%
(2) Rib ends are unsupported
(3) Date of test: 30 July 1981
(4) Ribs began to separate from substrate at 2:38 p.m.
(5) Test performed by R. Huebscher and D. Gillaspy

LOCATION AND DIRECTION OF STRAIN MEASUREMENTS
(6 STRAIN GAGES PER MODULE, 2 DATA CHANNELS PER STRAIN GAGE)

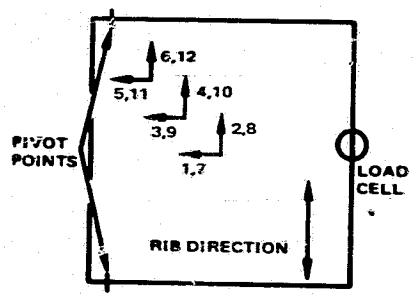

TABLE B-39. STRAIN AND VERTICAL DEFLECTION DATA FOR MODULE SDM-8 (STEEL SIDE UP) OVERSTRESS TES

Load, lb	Pressure, psf	Time	Cell Strain, μ inch/inch						Steel Strain, μ inch/inch						Vertical Position, in.	
			CH. 1	CH. 2	CH. 3	CH. 4	CH. 5	CH. 6	CH. 7	CH. 8	CH. 9	CH. 10	CH. 11	CH. 12	Corner Position	Mid-Diagonal Position
0	0	10:55	−05	−02	−04	−03	+07	−02	−04	−06	+01	00	−06	−02	0.066	−0.015
390	25	11:03	−01	+03	−07	−08	−04	+01	+36	+13	+54	+46	+77	+39	0.123	0.252
780	50	11:11	+01	−05	−06	−15	−29	−19	+63	+40	+87	+78	+157	+103	0.156	0.384
1170	75	11:20	−04	−02	−11	−17	−50	−38	+84	+56	+109	+100	+245	+178	0.185	0.482
1560	100	11:28	−04	+01	−09	−17	−73	−60	+103	+80	+133	+120	+337	+266	0.211	0.563
1170	75	11:41	−07	+05	−14	−29	−53	−41	+88	+58	+112	+103	+247	+187	0.189	0.486
780	50	11:55	+02	+03	−05	−14	−27	−17	+68	+47	+90	+84	+163	+114	0.162	0.390
390	25	12:07	+04	+01	−03	−14	−07	+02	+40	+29	+62	+52	+88	+48	0.130	0.261
0	0	12:25	+09	−05	−02	−04	−22	+14	+07	−04	+09	−17	−08	−06	0.073	−0.007

Notes (1) Relative humidity = 50%
(2) Date of test 29 July 1981
(3) Test performed by R. Huebschen and D. Gillaspy

LOCATION AND DIRECTION OF STRAIN MEASUREMENTS
(6 STRAIN GAGES PER MODULE, 2 DATA CHANNELS PER STRAIN GAGE)

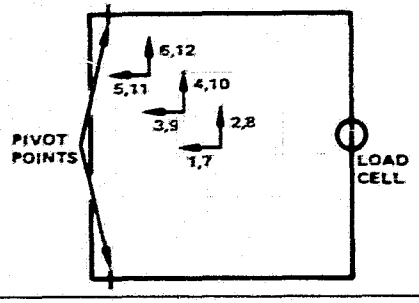

TABLE B–40 STRAIN AND VERTICAL DEFLECTION DATA FOR MODULE SDM–6 (BARE WOOD SIDE DOWN) OVERSTRESS TEST

Load, lb	Pressure, psf	Time	Cell Strain, μ inch/inch						Wood Strain, μ inch/inch						Vertical Position, in.	
			CH. 1	CH. 2	CH. 3	CH. 4	CH. 5	CH. 6	CH. 7	CH. 8	CH. 9	CH. 10	CH. 11	CH. 12	Corner Position	Mid-Diagonal Position
0	0	9:20	00	−02	−05	−03	+02	−03	−01	+03	−03	+07	+01	−08	0.010	—
390	25	9:30	−05	−02	−28	−29	−34	−49	+472	+337	+445	+526	+288	+276	0.117	—
780	50	9:38	−08	−15	−36	−38	−105	−129	+713	+506	+675	+760	+635	+682	0.185	—
1170	75	9:49	−16	−15	−41	−43	−186	−220	+910	+637	+850	+930	+1130	+1290	0.247	—
1560	100	9:58	−17	−17	−45	−48	−275	−311	+1080	+756	+990	+1071	+1817	+2162	0.312	—
1170	75	10:12	−16	−14	−39	−42	−229	−266	+912	+641	+869	+952	+1443	+1750	0.279	—
780	50	10:27	−16	−08	−39	−41	−163	−193	+711	+500	+689	+798	+993	+1206	0.227	—
390	25	10:44	−12	−05	−24	−26	−76	−99	+472	+354	+472	+570	+553	+696	0.157	—
0	0	11:01	00	−02	−05	−03	−08	−22	+37	+39	+61	+77	+111	+304	0.038	—

Notes: (1) Relative humidity = 50%
(2) Transducer instead of dial indicator, used to measure vertical deflection at the mid-diagonal position
(3) Test date 30 July 1981
(4) Test performed by R. Huebschen and D. Gillaspy

LOCATION AND DIRECTION OF STRAIN MEASUREMENTS
(6 STRAIN GAGES PER MODULE, 2 DATA CHANNELS PER STRAIN GAGE)

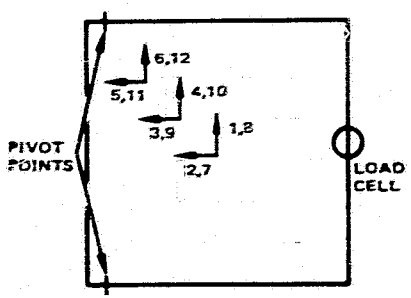

TABLE B–41. STRAIN AND VERTICAL DEFLECTION DATA FOR MODULE SDM–1 (GLASS SIDE UP) OVERSTRESS TEST

Load, lb	Pressure, psf	Time	Cell Strain, μ inch/inch						Glass Strain, μ inch/inch						Vertical Position, in.	
			CH. 1	CH. 2	CH. 3	CH. 4	CH. 5	CH. 6	CH. 7	CH. 8	CH. 9	CH. 10	CH. 11	CH. 12	Corner Position	Mid-Diagonal Position
0	0	8:55	+01	−06	−02	−03	−03	+04	+02	−02	00	−02	+02	−01	0.110	—
390	25	9:05	+03	−03	+07	+08	+01	+09	+54	+52	+10	−38	−83	−63	0.167	—
780	50	9:12	+06	−03	+15	+13	+05	+14	+79	+85	+11	−35	−211	−168	0.204	—
1170	75	9:20	+10	−02	+19	+14	+20	+20	+104	+114	+21	−28	−360	−295	0.234	—
1560	100	9:28	+14	+03	+31	+22	+35	+39	+123	+140	+26	−14	−516	−438	0.262	—
1170	75	9:39	+12	+06	+17	+15	+13	+24	+98	+114	+13	−29	−366	−308	0.237	—
780	50	9:50	+08	−04	+13	+10	00	+21	+79	+84	+09	−38	−223	−185	0.208	—
390	25	10:00	+02	−04	+12	+04	−06	+07	+49	+54	+08	−42	−88	−62	0.172	—
0	0	10:15	−03	−10	−02	−03	−06	+09	+06	+06	−03	−04	+05	−02	0.111	—

Notes: (1) Relative humidity = 50%
(2) Transducer, instead of dial indicator, used to measure vertical deflection at the mid-diagonal position
(3) Date of test: 31 July 1981
(4) Test performed by R. Huebschen and D. Gillaspy

LOCATION AND DIRECTION OF STRAIN MEASUREMENTS
(6 STRAIN GAGES PER MODULE, 2 DATA CHANNELS PER STRAIN GAGE)

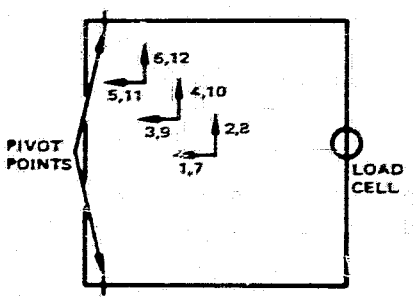

B.5 THERMAL TEST DATA

Raw data for the thermal test consist of temperatures measured in the modules, in the test apparatus, and at different locations in the chamber, center cell output voltage and current (when the modules were used to generate electric power), and millivolt readings on the radiometers. These data are summarized in Tables B-43 and B-44. Locations where the incident radiant energy flux was measured are shown in Figure B-15.

The time span for this test is summarized in Table B-42.

TABLE B-42. TIME LINE FOR THERMAL TEST

Test No.	Date	Time at Steady-State
1	8/20/81	12:09
2	8/20/81	14:09
3	8/21/81	9:18
4	8/21/81	9:36
5	8/21/81	11:35
6	8/21/81	12:37
7	8/21/81	14:04
8	8/21/81	14:29
9	9/14/81	10:27
10	9/14/81	12:45

TABLE B–43. FLUX MAP DATA FOR THERMAL TEST

Position	Measurement Device	0.08 W/cm^2 Nominal Flux		0.114 W/cm^2 Nominal Flux	
		mV	Radiant Flux, W/cm^2	mV	Radiant Flux, W/cm^2
A	Pyrheliometer (item 1, Table A–4)*	3.9	0.072	5.5	0.101
B	Pyrheliometer (item 1, Table A–4)*	3.6	0.066	4.9	0.09
C	Pyrheliometer (item 1, Table A–4)*	3.8	0.07	5.8	0.107
D	Pyrheliometer (item 1, Table A–4)*	4.3	0.079	6.3	0.116
E	Pyrheliometer (item 1, Table A–4)*	3.8	0.07	5.2	0.096
F	Pyrheliometer (item 1, Table A–4)*	4.2	0.077	6.5	0.12
G	Pyranometer (item 2, Table A–4)**	9.2	0.084	NA	NA

*Conversion constant for pyrheliometer = 0.0184 W cm^{-2} mV^{-1}

**Conversion constant for pyranometer = 0.0092 W cm^{-2} mV^{-1}

NA = not available

TABLE B–44. MEASURED TEMPERATURES FOR THERMAL TESTS

TC No.	Location	Temperature, °C									
		Test #1	Test #2	Test #3	Test #4	Test #5	Test #6	Test #7	Test #8	Test #9	Test #10
80	Chamber Air Inlet	26.3	26.3	26.2	26.1	25.9	26.0	26.1	26.2	25.3	25.3
81	Chamber Air Near Covered Circular Post	36.4	24.6	38.0	37.7	35.2	36.2	36.4	36.6	34.9	35.8
82	Chamber Air Below Glass Panel	41.3	41.9	40.1	40.3	38.7	39.4	38.1	39.3	38.9	39.1
83	Chamber Wall Adjacent to Module TM-1	41.8	41.9	40.5	40.7	39.1	40.2	41.3	41.4	41.0	42.0
84	Chamber Wall Adjacent to Module TM-4	43.4	43.6	42.1	42.2	40.2	41.9	43.1	43.2	41.0	42.2
85	Chamber Air Outlet (Directly Above Modules)	38.1	37.1	36.3	36.2	35.7	36.2	36.4	38.0	35.2	36.1
86	Chamber Floor	45.8	46.2	46.7	47.1	43.1	46.7	45.2	45.4	41.0	43.8
87	Edge Cell, Module TM-1	72.1	70.7	83.4	85.1	80.1	80.4	68.1	69.1	66.4	79.0
88	Center Cell, Module TM-1	69.4	68.4	79.5	80.6	78.4	79.4	67.4	68.1	66.1	77.6
89	Bottom of Frame, Module TM-1	53.5	53.3	57.1	56.9	55.9	57.1	52.1	52.3	50.5	55.7
90	Module TM-1 Back Surface	69.1	68.2	79.1	80.3	77.5	78.5	66.8	67.4	65.4	77.0
91 (91a)	Center (Edge) Cell, Module TM-2*	63.7	67.4	72.7	75.6	69.4	66.7	60.7	64.5	63.4	70.2
92	Side of Frame, Module TM-1	51.6	50.9	53.8	54.0	51.9	53.4	42.7	43.0	47.5	42.9
93	Module TM-2, Back Surface	65.1	65.3	70.8	71.5	70.7	71.9	64.3	64.8	65.8	72.0
94	Edge Cell, Module TM-3	74.5	75.6	84.5	84.8	83.9	85.7	74.1	74.1	77.0	81.9
95	Center Cell, Module TM-3	74.5	74.5	81.8	84.3	84.2	84.4	72.7	74.6	76.1	81.7
96	Side of Frame, Module TM-1	55.4	55.4	59.7	59.8	57.1	58.9	53.4	53.6	52.9	59.3
97	Module TM-3, Back Surface	68.1	68.7	75.6	77.3	77.7	78.2	68.6	69.1	71.2	79.0
98 (98a)	Center (Edge) Cell, Module TM-4*	71.3	47.6	61.1	83.1	82.9	84.3	71.2	71.2	72.6	76.9
99	Air Between Modules TM-3 & TM-4 (Rear)	39.4	39.7	39.4	39.7	38.4	39.5	40.0	39.6	38.8	39.5
100	Module TM-4, Back Surface	66.6	67.0	75.7	76.2	80.1	81.1	68.9	69.6	70.5	77.7
101	Center, Glass Front Panel	69.6	69.8	119.7	120.9	120.3	119.8	67.2	67.1	68.0	69.1
102	Top, Glass Front Panel	59.4	59.5	58.9	58.8	56.9	58.2	58.1	58.3	57.3	58.4
103	Bottom, Glass Front Panel	52.4	52.6	48.4	48.6	46.3	47.8	50.8	51.5	51.1	52.1
104	Center, Wood Back Panel	58.2	58.3	60.1	60.6	58.7	60.0	55.9	56.0	55.7	56.3
105	Top, Wood Back Panel	62.7	62.9	62.9	63.2	61.6	62.8	61.6	61.7	60.2	61.4
106	Bottom, Wood Back Panel	65.3	64.9	67.1	67.9	36.3	37.2	37.1	37.2	36.6	43.1
107	Air Between Modules TM-1 & TM-2 (Front)	42.3	41.7	41.6	42.1	39.7	41.0	40.5	40.3	40.2	40.9
108	Air Between Modules TM-1 & TM-2 (Rear)	40.9	40.6	40.2	41.1	39.4	40.0	39.6	39.4	38.8	38.9
109	Air Between Modules TM-3 & TM-4 (Front)	41.7	42.0	40.3	40.7	38.9	40.4	39.5	41.8	40.5	40.9
	Incident Radiant Heat Flux (nominal), w/cm^2	0.08	0.08	0.114	0.114	0.114	0.114	0.08	0.08	0.08	0.08
	Electric Power Production	No	Yes	No	Yes	Yes	No	No	No	No	No
	Module Back Side Condition	As Rec'd	As Rec'd	As Rec'd	As Rec'd	Taped	Taped	Taped	Taped	Taped	Insulated

* Temperature readings are for center cell (TC#91, #98) for test nos. 1-4 and for edge cell (TC#91a, #98a) for tests 5-10

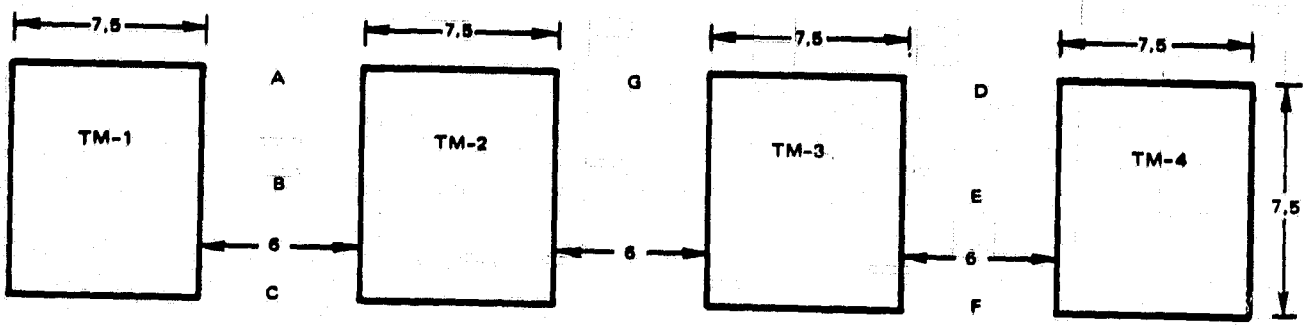

Figure B-15. Measurement locations for radiant energy flux (dimensions in inches).